Crystallization and melting behavior of phytosterol esters and their phase behavior in blends with palm oil

Eva DAELS

Supervisors:
Prof. dr. ir. I. Foubert
Prof. dr. B. Goderis

Members of the Examination Committee:
Prof. dr. ir. H. Ramon, Chair (KU Leuven)
Prof. dr. ir. I. Fraeye (KU Leuven)
Prof. dr. ir. W. Thielemans (KU Leuven)
Prof. dr. ir. S. Danthine (Université de Liège)
Dr. ir. B. Heyman (Vandemoortele)

Dissertation presented in partial fulfilment of the requirements for the degree of Doctor in Bioscience Engineering

June 2018

Doctoraatsproefschrift nr. 1514 aan de faculteit Bio-ingenieurswetenschappen van de KU Leuven

© 2018 Eva Daels
Uitgegeven in eigen beheer, Eva Daels, Kortrijk

Alle rechten voorbehouden. Niets uit deze uitgave mag worden vermenigvuldigd en/of openbaar gemaakt worden door middel van druk, fotokopie, microfilm, elektronisch of op welke andere wijze ook zonder voorafgaandelijke schriftelijke toestemming van de uitgever.

All rights reserved. No part of the publication may be reproduced in any form by print, photoprint, microfilm, electronic or any other means without written permission from the publisher.

DANKWOORD

November 2007, mijn eerste stappen op de Kulak. Zeer geboeid volgde ik in het kader van de open lesweek de les mechanica van prof. De Gersem mee in aula A350, met naast mij een toen nog onbekende persoon. Sindsdien zijn mijn hart voor de Kulak, mijn passie voor wetenschap en vooral mijn liefde voor die ene persoon alleen maar toegenomen. Ik ben heel dankbaar dat ik nu, 10 jaar later, op een geslaagd doctoraatsonderzoek aan de Kulak kan terugkijken.

In de eerste plaats wil ik prof. Paul Igodt bedanken om mij 5 jaar geleden de kans te geven een doctoraat te starten aan de Kulak. Maar ook om na 4 jaar de termijn van mijn doctoraat wat te verlengen zodat ik het maximale uit dit project zou kunnen halen.

Imogen, jou wil ik heel erg bedanken voor het vertrouwen dat je steeds in mij stelde en voor de goede begeleiding van mijn doctoraat. Ik kon steeds beroep doen op jou wanneer ik vast zat met mijn onderzoek, mijn resultaten wilde bespreken of feedback wou krijgen over een presentatie of een paper. Daarnaast wil ik je ook bedanken voor de kansen die je mij hebt gegeven om mezelf te ontplooien door onder andere het bijwonen van congressen en mijn verblijf in Denemarken. Ik ben zeer blij dat we onze goede samenwerking in de toekomst kunnen verder zetten.

Bart, ik prijs mezelf heel gelukkig dat jij in het derde jaar van mijn doctoraat toestemde om copromotor te worden van mijn onderzoek. Dankzij jou heb ik structuur kunnen brengen in mijn doctoraat en de data en verbanden van de verschillende delen kunnen linken. Jouw onuitputtelijke bron van kennis en ideeën hebben de kwaliteit van mijn doctoraat ongetwijfeld naar een hoger niveau gebracht. Bedankt ook voor jouw hulp bij de metingen in het ESRF en de intensieve dataverwerking achteraf. Deze data zijn van grote waarde gebleken voor mijn doctoraat.

Special thanks also to the members of the examination committee. Prof. Sabine Danthine, Bart Heyman, prof. Wim Thielemans and prof. Ilse Fraeye, thank you for the input and constructive feedback on my PhD manuscript. Voorzitters prof. Christophe Courtin en prof. Herman Ramon, bedankt om alles in goede banen te leiden tijdens de preliminaire en de publieke verdedigingen.

Er zijn ook een heel aantal personen die mij geholpen hebben bij de praktische kant van mijn doctoraat en het uitvoeren van experimenten. Annelien, jouw hulp bij het begin van mijn doctoraat was van onschatbare waarde. Bij jou kon ik steeds terecht

met inhoudelijke vragen over vetkristallisatie en praktische vragen over DSC, microscopie, statistiek, dataverwerking en nog zo veel meer. Valerie, bedankt voor onze goede samenwerking en het experimentele werk dat je hebt uitgevoerd voor mijn doctoraat. Het klikte al meteen tijdens onze eerste vergadering in Leuven waarop ik het thesisonderwerp aan jou voorstelde. Ik ben heel blij dat we naast collega's ook nog eens goeie vrienden zijn geworden. Francesca, thank you for doing some excellent experimental work for me. It was always fun working with you. Your enthusiasm works very contagious.

During my stay at Aarhus University I've met some wonderful and inspiring people. First, I want to thank Prof. Guo for letting me stay in his research group at Aarhus University for performing some enzymatic synthesis reactions and for the use of his lab facilities. Bianca, thank you very much for your daily advice on the optimization of the synthesis and purification. I very much enjoyed working with you. Also many thanks to Anette for her assistance in the lab and with administration and to Wei Wei, Jim and Marc for their hospitality and showing me around the lab, the campus and the city center of Aarhus.

Ik wil mijn dankwoord ook richten tot enkele collega's uit Leuven. Dorien, Olivier en Maarten C., bedankt voor jullie hulp bij de X-stralenmetingen en microscopie-analyses in jullie labo en de synchrotronmetingen in het ESRF. Daarnaast wil ik ook de collega's uit Gent bedanken, met name Liselot en Seline, voor hun hulp bij de hardheidsmetingen. Bedankt ook aan Wim, Jeroen en Peggy van Desmet Ballestra om hun labo ter beschikking te stellen en voor de begeleiding bij SFC-metingen en triglyceride-analyses. Many thanks also to the Renewable Materials and Nanotechnology Research Group of prof. Wim Thielemans and especially to Christina and Sabine R. for taking some of my samples to the ESRF and performing some of the synchrotron measurements for my PhD. Finally I want to thank Sam and Marianne for their advice on the purifications with the silica column and the revision of the language in the paper that is based on Chapter 3.

Enorm veel dank aan mijn collega's en ex-collega's van Food & Lipids (Lieselot, Lore, Valerie, Céline, Annelien, Charlotte L., Charlotte B. en Ali) voor de ontspannende momenten tijdens koffiepauzes, lunches, congressen en labo-activiteiten. Lieselot, Lore, Valerie en Annelien, dankzij de goede sfeer in de bureau kon er af en toe eens goed gelachen worden. Charlotte L., Charlotte D., Lore en Valerie, het was ook steeds een plezier om samen met jullie de labo's chemie en de oefenzittingen van fysische transportverschijnselen te verzorgen. Lieselot, na 10 jaar van samen studeren, thesissen en doctoreren scheiden helaas onze wegen. Op professioneel vlak dan toch, want hopelijk kunnen we nog geregeld eens afspreken om de laatste nieuwtjes uit te wisselen. Lore, ook jij bent al een heel eind deel van onze groep waarvoor je

steeds opnieuw een onevenaarbare inzet toont. Céline, jouw ondersteuning in het labo is een enorme bijdrage aan de onderzoeksgroep.

Bedankt ook aan alle collega's en ex-collega's van het IRF voor de gezellige babbels over de middag die zorgden voor de nodige afleiding van het doctoraatswerk. In het bijzonder bedankt aan Irina, bij jou kon ik altijd komen binnen vallen als ik er nood aan had om mijn hart eens te luchten. Willem en Martijn, bedankt voor het starten van de traditie van de Friday drinks met de gang waardoor we met de collega's regelmatig eens konden bijpraten buiten de context van het werk. Jonas V., Jonas B., Bert, Maarten M. en Valerie, merci dat jullie steeds van de partij zijn om deze traditie verder te zetten. Valerie en Jonas B., hopelijk kunnen we ook nog lang onze wekelijkse afspraak met de spinningfiets verder zetten om de extra glaasjes er weer af te fietsen.

Vrienden, dankzij jullie kon ik in *no time* het doctoraatswerk even vergeten. Elisa, Jenny, Judith, bedankt voor jullie onophoudelijke steun, jullie luisterend oor en niet te vergeten de vele, leuke *girls nights*. Dat er nog veel mogen volgen! Bedankt aan Team Jamie om samen de Schotse *Highlands* en Malta onveilig te maken. Ik kijk al enorm uit naar onze volgende avonturen in Slovenië en Kroatië. Dankjewel ook aan Team Kulak voor de fijne momenten op de vrijgezellen, trouwfeesten, bbq's, jaarlijkse weekendjes,… en aan Team Leuven voor de gezellige shoppingnamiddagen, *house warmings* en kerstmarkten.

Ik wil daarnaast ook mijn ouders in de bloemetjes zetten. Mama en papa, dankjewel om mij de mogelijkheid te geven om de studies bio-ingenieurswetenschappen te doen. Jullie gaven mij van bij het begin jullie vertrouwen in mijn studiekeuze en waren de beste coaches tijdens de lange blok- en examenperiodes. Ook tijdens mijn doctoraat kon ik steeds op jullie advies rekenen. Mijn broer Reinout wil ik bedanken voor zijn interesse in mijn onderzoek en de gezellige babbels op de familiebijeenkomsten. Bedankt ook aan mijn schoonouders voor de vele ontspannende momenten en de interessante discussies op zondagmiddag.

Tot slot gaat mijn grootste dank uit naar Ward. Mijn allerliefste schat, we zijn al samen van lang voordat ik dit doctoraatsonderzoek ben gestart. Motiverend zoals je altijd bent, stond je ook vanaf het begin van mijn doctoraat 100% achter mij om mij te steunen met raad en daad. Met alles van mijn doctoraat heb je heel erg hard meegeleefd, van de frustrerende crisismomentjes tot de gelukkigste topmomenten. Ik kon steeds alles met jou delen. Bedankt ook voor je eindeloze belangstelling voor mijn onderzoek en je kritische vragen over de concrete toepasbaarheid ervan die mij even uit de academische bubbel haalden. Je was ook begripvol wanneer in het voorbije jaar mijn doctoraatswerk voorrang kreeg en weekendjes of reisjes moesten

wijken. Bedankt voor al je liefde en de ontelbaar veel mooie momenten samen, ik kan er nooit genoeg van krijgen.

Eva,

Kortrijk, juni 2018

SAMENVATTING

Fytosterolen zijn plantaardige lipiden waarvan de chemische structuur vergelijkbaar is met die van cholesterol. Gedurende de laatste twee decennia hebben fytosterolen veel wetenschappelijke en commerciële belangstelling gekregen vanwege hun cholesterolverlagende activiteit. Om hun oplosbaarheid in lipidenrijke voedingsmiddelen zoals bijvoorbeeld margarines te verhogen worden fytosterolen veresterd met vetzuren om fytosterolesters (PEs) te verkrijgen. Fundamenteel onderzoek naar de invloed van PE-toevoeging op het kristallisatie- en smeltgedrag van lipidenrijke voedingsproducten is echter zeer schaars.

Het doel van dit doctoraatsonderzoek was daarom om een grondige kennis op te bouwen over het kristallisatie- en smeltgedrag van PEs en hun fasegedrag in mengsels met palmolie (PO). In een eerste deel (hoofdstukken 3, 4 en 5) werd een commercieel beschikbaar mengsel van PEs dat verschillende soorten fytosterolen bevat die veresterd zijn met verschillende soorten vetzuren, toegevoegd aan PO om het effect op het kristallisatie- en smeltgedrag van PO te onderzoeken. In een tweede deel (hoofdstukken 6 en 7) werden zuivere PEs gesynthetiseerd via enzymatische verestering om op een meer fundamentele wijze het effect van het type vetzuur te bestuderen op het kristallisatie- en smeltgedrag van de zuivere PEs als zodanig en indien toegevoegd aan PO.

In hoofdstuk 3 werd het niet-isotherme kristallisatie- en smeltgedrag van een commercieel PE-mengsel onderzocht in mengsels met PO op basis van differentiële scanningcalorimetrie (DSC) en synchrotron X-stralenverstrooiing (XRD). Er werden twee verschillende kristalstructuren geïdentificeerd in het commerciële PE-mengsel. De kristalstructuur benoemd als PE_x had een zeer grote onderkoeling nodig om kiemvorming te induceren en was samengesteld uit met stearine- en palmitinezuur veresterde PEs. De kristalstructuur aangeduid als PE_y was sterk verschillend, omdat deze zonder onderkoeling kristalliseerde, vloeibaar kristallijn was en overwegend met oliezuur veresterde PEs bevatte. In de PE-PO-mengsels, die eutectisch gedrag vertoonden, kristalliseerden de PEs en PO afzonderlijk van elkaar en werden geen nieuwe kristalstructuren gevormd.

Om te voorspellen of PE-toevoeging gewenste eigenschappen aan het eindproduct geeft en om directe informatie te verkrijgen over de microstructuur en de macroscopische eigenschappen zoals de hardheid werd in hoofdstuk 4 het effect van PE-toevoeging getest op PO die in een 'evenwichtstoestand' werd gebracht door middel van temperering op 10°C gedurende 48u. Er werd aangetoond dat

toevoeging van het commerciële PE-mengsel elk structureel niveau van de PO-kristallisatie beïnvloedde, zijnde primaire kristallisatie met inbegrip van polymorfisme, netwerkvorming en textuureigenschappen. Bij het toevoegen van tot 40% PEs kristalliseerde het commerciële PE-mengsel zelf niet, maar verdunde het de PO als een vloeibare olie waardoor het een negatief effect had op het vast vetgehalte, de smeltenthalpie, de netwerkstructuur en de hardheid. In het geval van een PE-concentratie van meer dan 40% kristalliseerden de PEs afzonderlijk van PO uit in de PE_x-vorm. Alleen vanaf 80% PEs werden naast de PE_x-kristallen ook de vloeibare kristallen van PE_y waargenomen. Bij deze hoge PE-concentraties ging de netwerkstructuur van PO echter verloren, wat samen met de daling in het vast vetgehalte leidde tot een grote afname van de hardheid.

Naast de effecten op de 'evenwichtstoestand', werd ook geverifieerd of PE-toevoeging de kristallisatiekinetiek van PO beïnvloedt. Hoofdstuk 5 onderzocht het isotherme kristallisatiegedrag van PO na toevoeging van 10-40% van het commerciële PE-mengsel bij een temperatuur van 20°C enerzijds en bij een constante onderkoeling van 18,7°C anderzijds. De DSC en synchrotron XRD-resultaten toonden aan dat met een toenemende PE-concentratie de PO-kristallisatie bij een isotherme temperatuur van 20°C later startte en langzamer was en bovendien werden er minder PO-kristallen gevormd. Verder werd een vertraging in de polymorfe transitie van α naar β' waargenomen. Wanneer de mengsels bij een constante onderkoeling van 18,7°C gekristalliseerd werden, was de vertraging van de polymorfe transitie bij een toenemende PE-concentratie het enige overblijvende effect.

In hoofdstuk 6 werden zuivere PEs gesynthetiseerd door verschillende types vetzuren (stearinezuur (C18:0), palmitinezuur (C16:0), laurinezuur (C12:0), oliezuur (C18:1) en linolzuur (C18:2)) te veresteren met β-sitosterol. Het niet-isotherme kristallisatie- en smeltgedrag van de zuivere PEs werd geanalyseerd om de invloed van ketenlengte en graad van onverzadiging van het veresterde vetzuur te onderzoeken. Er werd gevonden dat de smelttemperatuur en -enthalpie van de β-sitosterylesters toenamen met een stijgende vetzuurketenlengte terwijl deze afnamen met een stijgende graad van onverzadiging van de vetzuurketen. De microscopie-analyses toonden aan dat β-sitosteryloleaat (P-oleaat) veel kleinere sferulieten vormde dan de verzadigde β-sitosterylesters. Verder werd met behulp van de synchrotron XRD-resultaten aangetoond dat de verzadigde β-sitosterylesters en P-oleaat kristalliseerden in een dubbellaagstructuur waarvan de lamellaire afstanden daalden met een afnemende vetzuurketenlengte en met een toenemende graad van onverzadiging. De graad van onverzadiging van de vetzuurketen in de β-sitosterylesters bepaalde ook of er al dan niet een metastabiele of stabiele vloeibaar-kristallijne fase gevormd werd tijdens afkoeling.

In hoofdstuk 7 werden de verschillende types zuivere PEs toegevoegd aan PO om het effect op het kristallisatie- en smeltgedrag in de 'evenwichtstoestand' te bestuderen. Omdat de smelttemperaturen van de zuivere verzadigde β-sitosterylesters veel hoger waren dan die van PO, trad monotectisch fasegedrag op in hun binaire mengsels. De smelttemperatuur van zuiver P-oleaat was anderzijds zeer vergelijkbaar met die van PO wat leidde tot eutectisch fasegedrag in hun binaire mengsels. De microstructuur van de mengsels bevatte zowel gebieden met PO-kristallen als gebieden met β-sitosterylesterkristallen. Deze laatste waren grote sferulieten in het geval van de verzadigde β-sitosterylesters, maar kleine naaldvormige kristallen in het geval van P-oleaat.

ABSTRACT

Phytosterols are plant-based compounds with chemical structures similar to cholesterol. In the last two decades, phytosterols have gained much scientific and commercial interest due to their cholesterol-lowering activity. Phytosterols are esterified with fatty acids to obtain phytosterol esters (PEs) to enhance their solubility in lipid containing food products such as margarines and spreads. Fundamental research on how PE addition influences the crystallization and melting of lipid containing food products is however very scarce.

The objective of this PhD research was therefore to gain in-depth knowledge on the crystallization and melting behavior of PEs and their phase behavior in blends with palm oil (PO). In a first part a commercially available mixture of PEs containing different types of phytosterols, esterified to different types of fatty acids was added to PO to investigate the effect on the crystallization and melting behavior of their blends with PO. In a second part pure PEs were synthesized by enzymatic esterification to examine in a more fundamental way the effect of type of fatty acid in the pure PEs on the crystallization and melting behavior of the pure PEs as such and when added to PO.

In chapter 3 the non-isothermal crystallization and melting behavior of a commercial PE mixture was investigated in blends with PO based on differential scanning calorimetry (DSC) and time-resolved synchrotron X-ray diffraction (XRD) measurements. Two different crystal structures were identified in the commercial PE mixture. The crystal structure designated PE_X needed a very high degree of supercooling to induce nucleation and was composed of stearic and palmitic acid esterified PEs. The crystal structure designated PE_Y was quite different, since PE_Y crystallized without supercooling, was liquid crystalline and predominantly contained oleic acid esterified PEs. In the PE-PO blends, which showed eutectic behavior, the PEs and PO crystallized separately from each other and no new crystal structures were formed.

In order to predict whether or not PE addition gives any desired properties to the end product and to get direct information on microstructure and macroscopic characteristics such as the hardness, in chapter 4 the effect of PE addition was tested on PO that attained a kinetically stabilized state by tempering at 10°C for 48h, denoted as the ‘equilibrium’ state. It was shown that addition of the commercially available PE mixture influenced each structural level of the crystallization of PO being primary crystallization including polymorphism, network formation and textural

properties. When adding up to 40% PEs the commercial PE mixture itself did not crystallize but acted as a liquid oil diluting PO and thereby negatively affecting the solid fat content (SFC), melting enthalpy, network structure and hardness. In case of a PE concentration of more than 40% the PEs crystallized separately from PO in the PE_X form. Only from a concentration of 80% PEs also PE_Y liquid crystals were observed. At high PE concentrations the crystal network structure of PO was lost which together with the decrease in the SFC led to a drop in the hardness.

Next to the effects on the 'equilibrium' crystallization behavior, it was also verified whether PE addition influenced the crystallization kinetics of PO. Chapter 5 investigated the isothermal crystallization behavior of PO after adding 10-40% of the commercial PE mixture at a temperature of 20°C on the one hand and at a constant supercooling of 18.7°C on the other hand. The DSC and time-resolved synchrotron XRD results showed that with increasing PE concentrations PO crystallization at an isothermal temperature of 20°C started later and was slower and less crystals were formed. Furthermore, a delay in the polymorphic transition of PO from α to β' was observed. When the blends were isothermally crystallized at a constant supercooling of 18.7°C only the delay in the polymorphic transition with an increasing PE concentration remained.

In chapter 6 pure PEs were synthesized by esterification of different types of fatty acids (stearic (C18:0), palmitic (C16:0), lauric (C12:0), oleic (C18:1) and linoleic acid (C18:2)) to β-sitosterol. The non-isothermal crystallization and melting behavior of the pure PEs was analyzed to investigate the influence of chain length and degree of unsaturation of the esterified fatty acid. It was found that the melting temperature and enthalpy of the β-sitosteryl esters increased with an increasing fatty acid chain length while they decreased with an increasing degree of unsaturation. The microscopic analyses demonstrated that β-sitosteryl oleate (P-oleate) formed much smaller spherulites than the saturated β-sitosteryl esters. Furthermore it was proven by XRD that the saturated β-sitosteryl esters and P-oleate formed a bilayer crystal structure of which the lamellar spacings decreased with a decreasing fatty acid chain length and with an increasing degree of unsaturation. The degree of unsaturation of the fatty acid chain in the β-sitosteryl esters also influenced the type of subcell packing of the fatty acid moieties in the crystal structure and whether or not a metastable or stable liquid crystalline phase was formed during cooling.

In chapter 7 the pure PEs containing the different types of fatty acids were added to PO to monitor the effect on the 'equilibrium' crystallization and melting behavior. As the melting temperatures of the pure saturated β-sitosteryl esters were much higher than that of PO, monotectic phase behavior occurred in their binary blends. The melting temperature of pure P-oleate was very similar to that of PO leading to

eutectic phase behavior in their binary blends. The microstructure of the blends contained both regions with PO crystals and regions with β-sitosteryl ester crystals. The latter were large spherulites in case of the saturated β-sitosteryl esters, but small needle-shaped crystals in case of P-oleate.

LIST OF ABBREVIATIONS

2L	double chain length stacking
3L	triple chain length stacking
ABC	adenosine triphosphate binding cassette
ACAT	acyl-coenzyme A cholesterol acyl transferase
ATP	adenosine triphosphate
DSC	differential scanning calorimetry
ESRF	European Synchrotron Radiation Facility
HMF	high-melting fraction
HMG-CoA	3-hydroxy-3-methyl-glutaryl-coenzyme A
HPLC	high-performance liquid chromatograph
L	linoleic acid
La	lauric acid
LC	liquid crystals
LMF	low-melting fraction
LDL	low density lipoprotein
M	myristic acid
NMR	nuclear magnetic resonance
NPC1L1	Niemann-Pick C1-like 1
O	oleic acid
P	palmitic acid
P-laurate	β-sitosteryl laurate

P-linoleate	β-sitosteryl linoleate
P-palmitate	β-sitosteryl palmitate
P-oleate	β-sitosteryl oleate
P-stearate	β-sitosteryl stearate
PE(s)	phytosterol ester(s)
PLM	polarized light microscopy
PO	palm oil
Rf	retention factor
S	stearic acid
SAXS	small angle X-ray scattering
SFC	solid fat content
TLC	thin layer chromatography
WAXD	wide angle X-ray diffraction
XRD	X-ray diffraction

LIST OF SYMBOLS

a	maximal amount of crystallization in the Foubert model [J/g]
d	distance between the reflecting entities in XRD [Å]
ΔG_{crit}	Gibbs free energy barrier for nucleation [J/g]
ΔG_V	Gibbs free energy due to the formation of crystalline volume [J/g]
ΔG_S	Gibbs free energy barrier for nucleation [J/g]
ΔH_{melt}	melting enthalpy [J/g]
ΔH_α	melting enthalpy of the α polymorph [J/g]
ΔH_A [J/mol]	molar heat of fusion of component A in the Hildebrand equation
ΔH_B [J/mol]	molar heat of fusion of component B in the Hildebrand equation
ΔH_{tot}	total melting enthalpy after the isothermal crystallization [J/g]
ΔS_{melt}	melting entropy [J/g.K]
ΔT	difference between the onset temperature of crystallization and the onset temperature of melting [°C]
K	crystallization rate constant in the Foubert model [1/h]
λ	wavelength [Å]
n	reaction order in the Foubert model [-]
R	molar gas constant [J/mol.K]
r_{crit}	critical size to form stable nuclei
θ	diffraction angle (°)
$t_{\alpha\ peak}$	peak maximum of the α peak [h]

T_A melting point of component A in the Hildebrand equation [K]

T_B melting point of component B in the Hildebrand equation [K]

t_{ind} time needed to reach 1% of the a value in the Foubert model [h]

T_{c_max} peak maximum of the DSC crystallization curve [°C]

T_{c_onset} onset temperature of crystallization [°C]

T_{m_max} peak maximum of the DSC melting curve [°C]

T_{m_offset} offset temperature of melting [°C]

T_{m_onset} onset temperature of melting [°C]

$t_{transition}$ polymorphic transition time from α to β' [h]

X_A mole fraction of component A in the Hildebrand equation [-]

X_B mole fraction of component B in the Hildebrand equation [-]

TABLE OF CONTENTS

Dankwoord ..... **i**

Samenvatting ..... **i**

Abstract ..... **iv**

List of abbreviations ..... **vii**

List of symbols ..... **ix**

Table of contents ..... **xi**

Context and aim **1**

1. **Lipids and their crystallization and phase behavior** **7**

1.1. Nomenclature 7

1.2. General principles of crystallization behavior of lipids 8

1.2.1. Primary crystallization 10

1.2.1.1. Nucleation 10

1.2.1.2. Crystal growth 11

1.2.1.3. Crystal size and morphology 12

1.2.1.4. Crystal structures 12

1.2.1.5. Microstructure of lipid crystal networks 14

1.2.1.6. Mechanical and macroscopic properties 15

1.3. Phase behavior in lipid blends 16

1.3.1. General principles of phase behavior in binary blends of pure lipids 16

1.3.1.1. Eutectic systems 17

1.3.1.2. Binary systems with complete solid solution 18

1.3.1.3. Binary systems with partial solid solution 19

1.3.1.4. Binary systems with compound formation 21

1.3.2. Phase behavior in binary blends of real lipids 21

1.4. Techniques to monitor lipid crystallization and phase behavior 23

1.4.1. Pulsed nuclear magnetic resonance 24
1.4.2. Differential scanning calorimetry 24
1.4.3. X-ray diffraction 25
1.4.4. Polarized Light Microscopy 27
1.4.5. Mechanical and macroscopic properties 28
2. Palm oil and phytosterols and their esters 30
2.1. Palm oil 30
2.1.1. Sources 30
2.1.2. Chemical characteristics 31
2.1.3. Food applications 32
2.1.3.1. Spreadable fats 32
2.1.3.2. Other applications 33
2.1.4. Crystallization and phase behavior of palm oil 34
2.1.4.1. Polymorphism 34
2.1.4.2. Non-isothermal crystallization 34
2.1.4.3. Isothermal crystallization 35
2.1.4.4. Phase behavior of binary blends of palm oil with other lipids 35
2.2. Phytosterols and their esters 36
2.2.1. Chemical properties 36
2.2.2. Sources of phytosterols 38
2.2.2.1. Dietary sources and intake of phytosterols 39
2.2.2.2. Commercial sources of phytosterols 39
2.2.2.3. Synthesis of plant stanols 40
2.2.3. Cholesterol lowering activity of phytosterols 41
2.2.3.1. Metabolism 41
2.2.3.2. Cholesterol-lowering mechanism 43
2.2.3.3. Safety 45
2.2.4. Synthesis of phytosterol esters 45
2.2.5. Food applications of phytosterol esters 48

2.2.5.1. Regulatory status 48

2.2.5.2. Food categories and use levels 49

2.2.6. Crystallization and phase behavior of phytosterol esters 49

2.2.6.1. Crystallization behavior of pure phytosterol esters 50

2.2.6.2. Crystallization and phase behavior of binary mixtures of phystosterol esters 52

2.2.6.3. Crystallization behavior of binary mixtures of phytosterol esters and fats 53

3. Effect of adding a commercial phytosterol ester mixture on the non-isothermal crystallization and melting behavior of palm oil 57

3.1. Introduction 57

3.2. Materials and methods 57

3.2.1. Materials 57

3.2.2. Blend preparation 59

3.2.3. Differential scanning calorimetry 60

3.2.4. Time-resolved synchrotron X-ray diffraction 60

3.3. Results and Discussion 61

3.3.1. Differential scanning calorimetry 61

3.3.1.1. Palm oil 61

3.3.1.2. The commercial phytosterol ester mixture 63

3.3.1.3. Blends of palm oil with the commercial phytosterol ester mixture 64

3.3.2. Time-resolved synchrotron X-ray diffraction 64

3.3.2.1. Palm oil 64

3.3.2.2. The commercial phytosterol ester mixture 67

3.3.2.3. Blends of palm oil with the commercial phytosterol ester mixture 69

3.3.3. Modelling of the phase transitions and coupling to the DSC data 72

3.3.4. PE-PO phase diagram 75

3.4. Conclusion 75

4. Effect of adding a commercial phytosterol ester mixture on the 'equilibrium' crystallization behavior of palm oil 78

4.1. Introduction 78

4.2. Materials and methods 78

4.2.1. Materials 78

4.2.2. Blend preparation 79

4.2.3. Crystallization to the 'equilibrium' state 79

4.2.4. Solid fat content by NMR 79

4.2.5. Differential scanning calorimetry 79

4.2.6. X-ray diffraction 80

4.2.7. Polarized light microscopy 80

4.2.8. Hardness 80

4.2.9. Statistical analysis 81

4.3. Results and Discussion 81

4.3.1. Pure palm oil 81

4.3.1.1. Solid fat content by NMR 81

4.3.1.2. Melting profile by differential Scanning Calorimetry 81

4.3.1.3. X-ray diffraction 82

4.3.1.4. Polarized light microscopy 84

4.3.1.5. Hardness 85

4.3.2. Pure commercial phytosterol ester mixture 85

4.3.2.1. Solid fat content by NMR 85

4.3.2.2. Melting profile by differential scanning calorimetry 85

4.3.2.3. X-ray diffraction 85

4.3.2.4. Polarized light microscopy 86

4.3.2.5. Hardness 86

4.3.3. Blends of the commercial phytosterol ester mixture and palm oil 86

4.3.3.1. Solid fat content by NMR 86

4.3.3.2. Melting profile by differential scanning calorimetry 88

4.3.3.3. X-ray diffraction 90
4.3.3.4. Polarized light microscopy 91
4.3.3.5. Hardness 91
4.4. Conclusions 92
5. **Effect of adding a commercial phytosterol ester mixture on the isothermal crystallization kinetics of palm oil 95**
5.1. Introduction 95
5.2. Materials and methods 96
5.2.1. Materials 96
5.2.2. Blend preparation 96
5.2.3. Differential Scanning Calorimetry 96
5.2.4. Time-resolved Synchrotron X-ray Diffraction 98
5.2.5. Polarized light microscopy 100
5.2.6. Statistical analysis 100
5.3. Results and discussion 102
5.3.1. Isothermal crystallization at 20°C 102
5.3.1.1. Differential scanning calorimetry: qualitative analysis 102
5.3.1.2. Differential scanning calorimetry: quantitative analysis 104
5.3.2. Isothermal crystallization at a constant degree of supercooling of 18.7°C 108
5.3.2.1. Differential scanning calorimetry: qualitative analysis 108
5.3.2.2. Differential scanning calorimetry: quantitative analysis 109
5.3.2.3. X-ray diffraction 113
5.3.2.4. Polarized light microscopy 119
5.4. Conclusion 120
6. **Non-isothermal crystallization and melting behavior of pure phytosterol esters containing different types of fatty acids 124**
6.1. Introduction 124
6.2. Materials and methods 124
6.2.1. Materials 124

6.2.2. Enzymatic synthesis of the β-sitosteryl esters 125
6.2.3. Purification of the β-sitosteryl esters 126
6.2.4. Differential scanning calorimetry 127
6.2.5. X-ray diffraction 127
6.2.6. Polarized light microscopy 128
6.3. Results and discussion 129
6.3.1. Differential scanning calorimetry 129
6.3.2. Polarized light microscopy 132
6.3.3. X-ray diffraction 134
6.3.3.1. Cooling 134
6.3.3.2. Heating 137
6.3.4. Characterization of the bilayer structure 148
6.3.5. Link with crystallization and melting of triglycerides 149
6.4. Conclusion 150
7. Effect of adding phytosterol esters containing different types of fatty acids on the 'equilibrium' crystallization behavior of palm oil 152
7.1. Introduction 152
7.2. Materials and methods 152
7.2.1. Materials 152
7.2.2. Enzymatic synthesis of the β-sitosteryl esters 152
7.2.3. Purification of the β-sitosteryl esters 153
7.2.4. Blend preparation 153
7.2.5. Crystallization to the 'equilibrium' state 153
7.2.6. Melting profile by differential scanning calorimetry 153
7.2.7. X-ray diffraction 154
7.2.8. Polarized light microscopy 154
7.3. Results and discussion 154
7.3.1. Palm oil 154
7.3.2. Pure β-sitosteryl esters 156
7.3.2.1. Differential Scanning Calorimetry 156

7.3.2.2. X-ray diffraction 158

7.3.2.3. Polarized Light Microscopy 161

7.3.2.4. Link with the non-isothermal crystallization and melting behavior of the pure β-sitosteryl esters 162

7.3.3. Blends of palm oil with saturated β-sitosteryl esters 163

7.3.3.1. Differential scanning calorimetry 163

7.3.3.2. X-ray diffraction 167

7.3.3.3. Polarized light microscopy 171

7.3.4. Blends of palm oil with β-sitosteryl oleate 173

7.3.4.1. Differential scanning calorimetry 173

7.3.4.2. X-ray diffraction 174

7.3.4.3. Polarized light microscopy 174

7.4. Conclusion 175

General conclusions and perspectives for future work 177

Effect of adding a commercial phytosterol ester mixture on the crystallization and melting of palm oil 178

Crystallization and melting behavior of pure phytosterol esters and their phase behavior in blends with palm oil 179

Future work 184

References 186

List of publications 207

CONTEXT AND AIM

According to the European Heart Network, cardiovascular diseases are currently the main cause of death in Europe, killing 4.3 million people every year. Moreover these figures are expected to increase due to the increasing age of the baby boomer population and the high probability of an older population experiencing the disease[1]. It is estimated that a third of the cardiovascular diseases is attributable to raised serum cholesterol levels[2]. In the early 1950s it was discovered that phytosterols can reduce serum cholesterol levels by impairing the absorption of cholesterol in the gastrointestinal tract.

Phytosterols including plant sterols and their hydrogenation products plant stanols are plant based compounds with chemical structures similar to cholesterol. In the last two decades, phytosterols have gained much scientific and commercial interest due to their cholesterol-lowering activity. To increase their solubility in lipid containing food products and to increase their cholesterol-lowering activity in the body phytosterols are esterified with fatty acids to obtain phytosterol esters (PEs). Among the currently available PE enriched foods, margarines and spreads are by far the most common, followed by dairy foods and drinks.

Crystallization and melting behavior of lipids is of extreme importance in food products, such as butter, margarine and chocolates because their macroscopic properties, such as spreadability, hardness, appearance and mouth feel etc., strongly depend on it. Next to the processing conditions, the composition of the lipid phase is one of the main influencing factors for its crystallization and melting behavior. Therefore, addition of PEs to lipid (containing food products) may influence its crystallization and melting behavior and may thus lead to problems during the production process or with the macroscopic properties of the end product. Fundamental research on this topic is however very scarce.

Some publications have described the melting behavior of different types of pure PEs[3–8]. However, difficulties rise when trying to compare and use reported data on the melting behavior of different types of pure PEs because of various limitations. The purity of the PE used in the different studies was for example greatly divergent and it was also unclear how melting temperatures were extracted from the experimental data[3–8]. Furthermore, there is currently also no X-ray based crystallographic information available on PEs.

Only a few publications reported on the influence of the addition of PEs on the physical properties of edible fats. One study showed that pure PEs with a high lauric acid content added to liquid corn oil caused unwanted PE crystallization above a certain threshold concentration[5]. Another research investigated how the crystallization behavior of milk fat was changed by blending with a commercial mixture of PEs. The authors showed that adding PEs to milk fat induced a softer consistency and a lower solid fat content (SFC). These authors however did not report any information on the melting and polymorphic behavior of the pure substrates nor their blends since no differential scanning calorimetry (DSC) or X-ray diffraction (XRD) analyses were performed[9].

In this context, the objective of this PhD research was to gain in-depth knowledge on the effect of the addition of PEs on the crystallization and melting of edible fats, more specifically palm oil (PO). PO was selected as a 'host' fat for the PEs as it is the most consumed fat in the world because of its unique physical properties. Since PO is semi-solid at room temperature, it forms the ideal hard stock to be used in trans free food products such as margarines and spreads. Its small and stable crystals provide a smooth and glossy texture in these products.

This PhD thesis is divided into three parts which are represented in Figure 1. Part I comprises a literature review, while parts II and III include experimental work.

The literature review of **part I** is divided into two chapters. **Chapter 1** includes a brief literature review about the crystallization and phase behavior of lipids in general and gives an overview of the analyzing techniques to monitor the crystallization and phase behavior of lipids that were used in this PhD research. This chapter also defines some nomenclature that is used throughout the PhD thesis.

Chapter 2 deals with PO on the one hand and phytosterols and their esters on the other hand. More specifically their sources, chemical characteristics, food applications and phase behavior are discussed. In this chapter also the cholesterol-lowering properties of phytosterols and the synthesis of PEs are dealt with.

In **part II** (chapters 3, 4 and 5) a commercially available mixture of PEs containing different types of phytosterols, esterified to fatty acids which vary in chain length and chain saturation was used to investigate the effect of PE addition on the phase behavior of PO. The use of this commercial PE mixture allowed to already get a general insight in the crystallization and melting behavior of PEs during the time needed for the labor-intensive synthesis and purification of pure PEs as these are not commercially available. It was also necessary for the optimization and validation of the experimental protocols as the pure PEs were far too expensive to be used for optimization purposes. Another advantage of the commercial PE mixture was that

more different experimental techniques (also those needing a bigger sample size) could be used than possible with pure PEs.

In **chapter 3** the non-isothermal crystallization and melting behavior of the commercial PE mixture in blends with PO was investigated. Based on DSC and time-resolved synchrotron XRD measurements the occurrence of different crystal structures was mapped as a function of temperature and PE concentration.

These results enabled research on the impact of adding PEs to PO under industrially more relevant crystallization conditions in chapters 4 and 5. More specifically in **chapter 4** the influence of PE addition on the 'equilibrium' crystallization state at 10°C of PO was investigated in order to evaluate whether PE addition changes the desired properties of the end product. It was investigated if PE addition has a major influence on each level of the crystalline structural hierarchy (primary crystallization, polymorphism, network formation and textural properties) by using many different analyzing techniques (DSC, XRD, pulsed nuclear magnetic resonance, polarized light microscopy (PLM) and texture analysis).

Next to the effects related to the final 'equilibrium' state, it was verified whether PE addition also influenced the crystallization kinetics of PO. The objective of **chapter 5** was therefore to investigate the isothermal crystallization behavior of PO after addition of PEs in order to assess the potential impact in related food products under processing conditions. Isothermal crystallization of PE-PO blends was analyzed with DSC, time-resolved synchrotron XRD and PLM.

In **Part III** (chapters 6 and 7) pure PEs containing different types of fatty acids (stearic (C18:0), palmitic (C16:0), lauric (C12:0), oleic (C18:1) and linoleic acid (C18:2)) were synthesized by enzymatic esterification and used to obtain a more fundamental insight in the crystallization and melting behavior of PEs and their phase behavior in blends with PO. In **chapter 6** the pure PEs were used to investigate the influence of chain length and degree of unsaturation of the esterified fatty acid on the non-isothermal crystallization and melting behavior of the PEs by using DSC, time-resolved synchrotron XRD and PLM. In **chapter 7** the pure PEs were added to PO to monitor the effect on the 'equilibrium' crystallization behavior with the same analyzing techniques as in chapter 4.

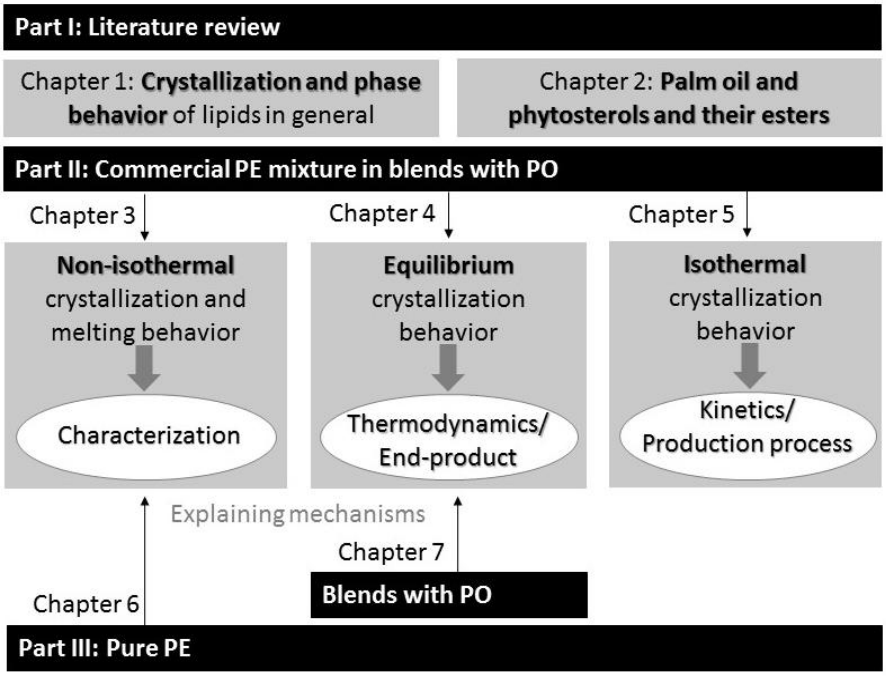

Figure 1. *Schematic overview of the research approach*

PART I
LITERATURE REVIEW

CHAPTER 1
LIPIDS AND THEIR CRYSTALLIZATION AND PHASE BEHAVIOR

1. LIPIDS AND THEIR CRYSTALLIZATION AND PHASE BEHAVIOR

Several commonly consumed food products, such as butter, margarine and chocolate contain an important amount of lipids, of which a substantial amount is present in the crystallized form. Crystallization of lipids is of ultimate importance in this type of food products. Insight in the different aspects of lipid crystallization behavior is extremely important to obtain products with the desired macroscopic properties, such as spreadability, appearance, mouthfeel, hardness, etc., which strongly depend on the underlying lipid crystal network[10]. This chapter presents a brief literature review about the crystallization and phase behavior of lipids. The first section comprises some definitions that are used throughout the PhD thesis. The second section deals with the crystallization behavior of lipid blends, while the third section focuses on the phase behavior of lipids. In a last part techniques to measure the crystallization and phase behavior of lipids are briefly discussed.

1.1. NOMENCLATURE

Lipids are a diverse range of compounds for which no widely accepted definition exists. In accordance with Christie (2003)[11] and the American Oil Chemists' Society[12] in this work the term 'lipids' refers to fatty acids and their naturally occurring derivatives and to compounds related closely through biosynthetic pathways or by function. This definition treats cholesterol and phytosterols as lipids, but it does not include steroids, fat-soluble vitamins or carotenoids.

By using this definition of lipids it is also necessary to define 'fatty acids'. Fatty acids are naturally-occurring compounds that are produced via condensation of malonyl coenzyme A units and contain an even number of carbon atoms in a straight chain with a carboxyl group at one extremity. Double bonds of the *cis* configuration often occur in the aliphatic chains and rarely also odd- and branched-chain fatty acids occur[11].

The main lipids of plant and animal origin consist of fatty acids linked by an ester bond to an alcohol such as glycerol, cholesterol or a phytosterol or by an amide bond to amines such as sphingoids. Lipids may also contain other components such as phosphoric acid and carbohydrates which can be released by various hydrolytic procedures. The most abundant lipids from animal and plant origin are triglycerides, which consist of glycerol of which each hydroxyl group is esterified to a fatty acid as shown in Figure 1.1[11].

In this work the term 'fat' refers to lipids of animal and plant origin that consist almost exclusively (> 90%) of triglycerides. This includes vegetable oils such as palm oil, olive oil and coconut oil as well as animal fats such as lard and milk fat. The lipids that are not fats are referred to as non-triglyceride lipids. These include phytosterols and their esters, but also diglycerides and monoglycerides, which respectively contain two moles and one mole of fatty acids per mole of glycerol[11].

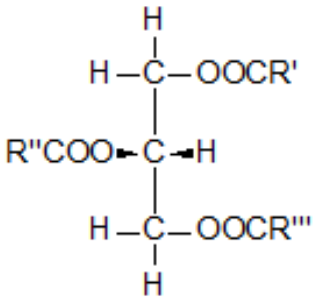

Figure 1.1. *The structure of a triglyceride (From Christie, 2003[11]).*

1.2. GENERAL PRINCIPLES OF CRYSTALLIZATION BEHAVIOR OF LIPIDS

The existing literature on the general principles of lipid crystallization is mainly focused on or even limited to fat crystallization. Crystallization behavior of non-triglyceride lipids is often not included in the reviews probably because it has much less been investigated than fat crystallization and because non-triglyceride lipids contain a wide variety of different components. The general principles of lipid crystallization discussed in this section are mainly described in literature about fat crystallization, but are also valid for lipids in general. Crystallization behavior of palm oil and phytosterol esters specifically is described in chapter 2.

When lipid molecules crystallize, they form nano-platelets composed of stacks of crystalline lamellae with a characteristic layer to layer distance and subcell packing of the fatty acid residues. The nano-platelets further associate into clusters. These clusters join through van der Waals attraction to form crystal aggregates, which interact further, resulting in the formation of a continuous three-dimensional crystal network. The number, size, shape and spatial distribution of crystals and clusters define the microstructure, which has an enormous influence on the macroscopic properties of fat products. Each step in this structural hierarchy is influenced by the processing conditions such as cooling rate, crystallization temperature, agitation speed and storage time[10]. The nomenclature used in this section is also applied in Figure 1.2.

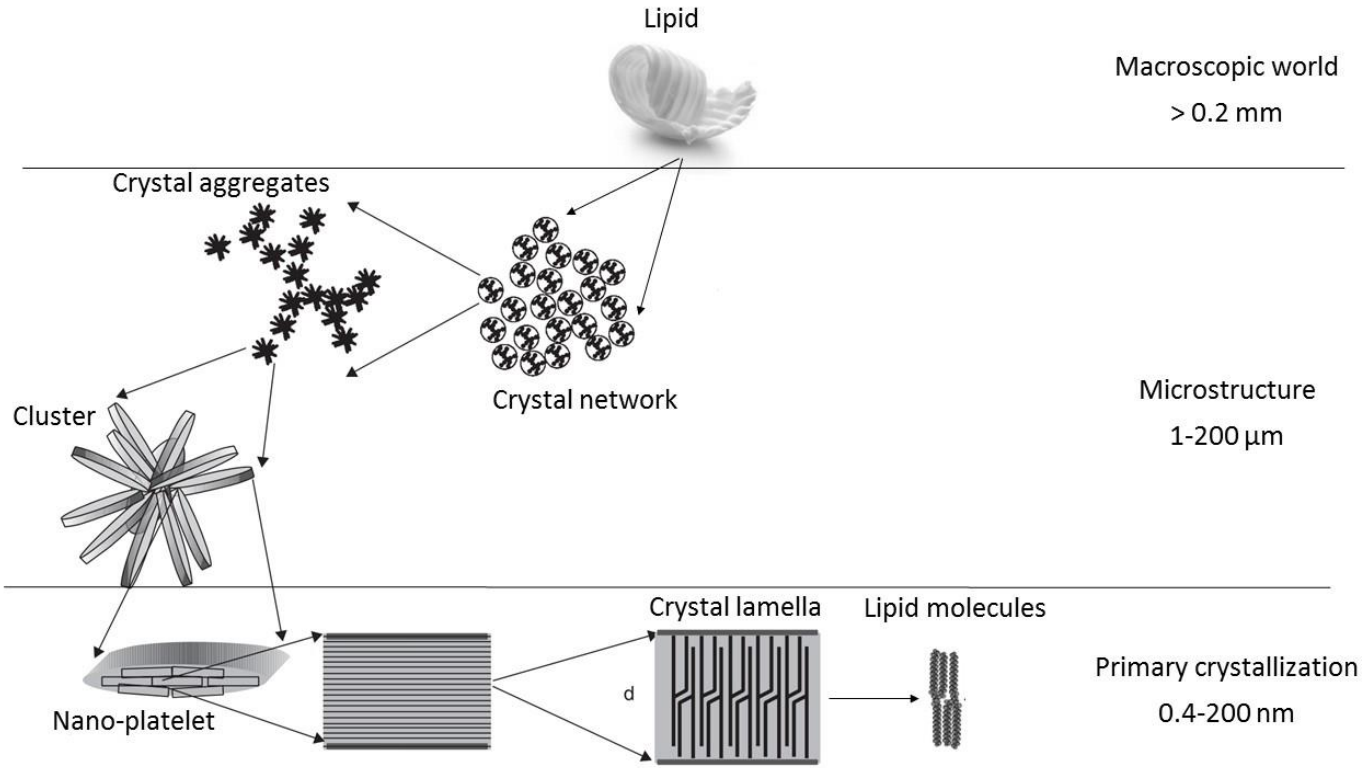

Figure 1.2. *Schematic overview of the structural hierarchy in a lipid crystal network (Adapted from Peyronel et al., 2010[13])*

1.2.1. PRIMARY CRYSTALLIZATION

1.2.1.1. *Nucleation*

According to the classical nucleation theory stable nuclei can only be formed when they reach a critical size (r_{crit}) which can be achieved if the Gibbs free energy barrier for nucleation (ΔG_{crit}) is overcome as is illustrated in Figure 1.3. This energy barrier results from a combination of a negative free energy due to the formation of crystalline volume (ΔG_V) and a positive free energy associated with the creation of a new interface (ΔG_S). Nuclei that reach r_{crit} continue to grow while subcritical nuclei tend to dissociate. In general crystals can be formed from the melt or from a solution. In practice, to overcome ΔG_{crit} sufficient supercooling (melt) or supersaturation (solution) must be applied to the liquid phase[14–19].

Three types of nucleation processes exist: primary nucleation which can be either homogeneous or heterogeneous, and secondary nucleation. Homogeneous primary nucleation is not catalyzed by lipid crystals or other solid surfaces and needs a relatively high supercooling or supersaturation. It has been proposed that homogeneous nucleation in lipid systems consists of two steps with first an ordering process of molecules into lamellae which then act as a precursor for the formation of solid crystalline nuclei[17,18,20].

When foreign impurities are present they catalyze primary heterogeneous nucleation, which needs a lower supercooling or supersaturation and is faster than homogeneous nucleation[14]. Natural lipids almost always undergo heterogeneous nucleation since they are normally impure[17]. Finally, secondary nucleation occurs after primary nucleation (so when crystals of the crystallizing material are already present) and is caused by fragments loosened from growing crystals or generated due to collision of crystals which act as new nuclei. Generally the kinetics of the nucleation process are determined by the diffusion rates of molecules in the liquid and solid phases and the arrangement and subsequent attachment of molecules onto the growing crystal nuclei[17].

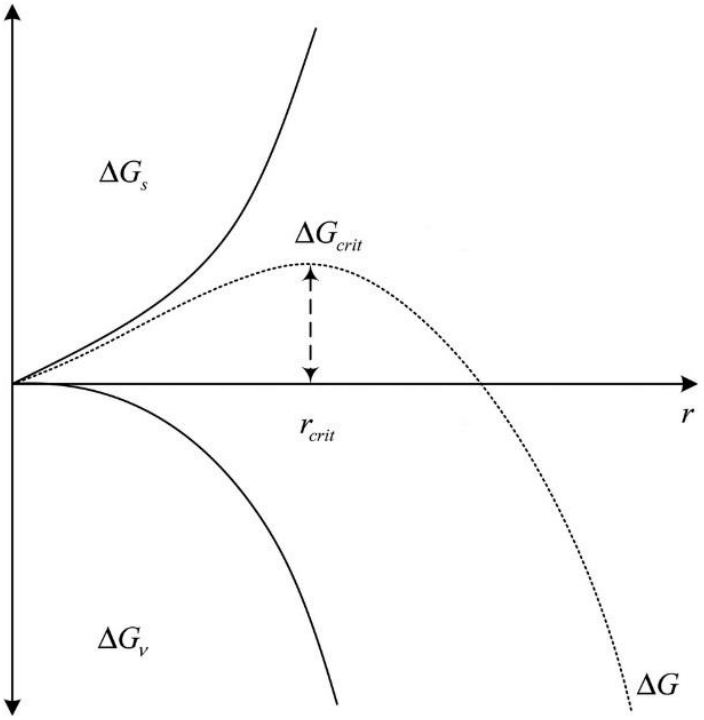

Figure 1.3. *Variation of the Gibbs free energy for nucleation (ΔG) as a function of nucleus size r [m] (Adapted from Wu et al. 2016*[21]*)*

1.2.1.2. *Crystal growth*

Once stable nuclei are formed, further growth occurs by attachment of molecules to the crystal surface[22]. Subsequently a great number of conformational changes are still needed before a molecule properly fits into the crystal lattice. This allows a chance for detachment of the molecule from the crystal surface in the meantime[17,23]. Diffusivity of molecules to the crystal surface can be decreased with an increasing viscosity. During crystal growth a substantial amount of latent heat is released at the surface which is subsequently transported to the bulk liquid. This heat transfer may significantly increase the interfacial temperature[17].

It is presumed that surface kinetics rather than heat and mass transport is the main controlling factor for the crystal growth rate. This is mainly evidenced by the fact that for the same driving force the crystal growth rates are usually orders of magnitude smaller than the dissolution or melting rates, which are proved to be limited by heat and mass transport, and not by surface kinetics[24].

1.2.1.3. *Crystal size and morphology*

Crystal size mainly depends on the nucleation rate, while crystal morphology is controlled by the rate of crystal growth. A high supercooling or supersaturation causes a high nucleation rate which leads to the formation of many nuclei and this results in many small crystals. On the other hand, a low supercooling or supersaturation leads to fewer and larger crystals[14]. In order to prevent an undesired mouth feel described as sandiness, crystal size in soft solid food products should not exceed 30 µm[23].

Crystal growth can occur in one, two or three dimensions resulting in the formation of crystals with a needle, disc or spherulite shape[23]. In most cases lipids crystallize in spherulites. Spherulites are near-spherical polycrystalline aggregates build up of many crystalline nano-platelets, which are in turn assembled from crystalline lamellae of lipid molecules (Figure 1.2)[19]. The nano-platelets are in many cases needle-like and grow radially from the same central nucleus. Differences in the magnitude of the driving force, which cause changes to the mechanism of the secondary nucleation can result in different morphologies of the spherulites. At a low driving force, the secondary nucleation is slow enough to allow the progression of the crystallization front to occur layer by layer. At higher driving forces secondary nucleation occurs simultaneously in different layers before a layer is completed resulting in a more diffuse structure[17].

1.2.1.4. *Crystal structures*

Crystals are built up of regular structures of atoms in three dimensions that are often represented by a repeat unit called the unit cell. The unit cell is defined as the smallest repeating unit which shows the full symmetry of the crystal structure. All necessary crystal structure information is contained in data on the unit cell such as the dimension and the positions or atomic coordinates of atoms inside the unit cell[25].

The existing literature on the general principles of lipid crystal structures is mainly focused on polymorphism of fats. Polymorphism is the ability of molecules with long aliphatic chains like triglycerides to pack in different subcell structures which exhibit different melting temperatures but yield identical liquid phases upon melting[14,17,23,26,27]. In a fat the subcell is determined by the cross-sectional packing mode of the aliphatic chains in the triglycerides (Figure 1.4)[28]. The subcell is thus different from the unit cell as it only describes the packing of the fatty acid chains of two lipid molecules, while the unit cell describes the packing of the entire lipid molecules and often contains more than two molecules. The unit cell packing of a lipid can thus be different from the subcell packing. For triglycerides three main polymorphs named α, β' and β were described based on the subcell structure. In the α form, which is the least stable form, the chains are arranged in a hexagonal

structure with no angle of tilt. The β' form has an orthorhombic and perpendicular packing which means the adjacent zigzag chains are not in the same plane. In this polymorphic form the chains have an angle of tilt between 50° and 70°. Finally, the β form is the most stable polymorph and is characterized by a triclinic and parallel packing with the same angle of tilt as the β' form. In this structure the adjacent chains are in the same plane[17,29].

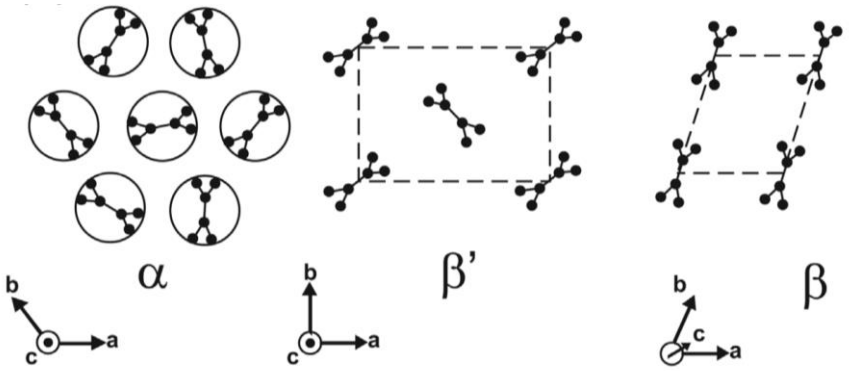

Figure 1.4. *Subcell structures of the three major polymorphic forms of triglycerides (From Idziak, 2012)*[30]

The three different subcell packings lead to different properties of the crystals. With an increasing stability, the polymorphs have an increasing packing density, a higher melting point and an increasing activation free energy for nucleation[20,28]. Since the nucleation rate is governed by the activation free energy for nucleation, the latter implies that the nucleation rate increases most rapidly for α and most slowly for β with an increasing supercooling. The formation of the α polymorph may thus be kinetically favored, although from a thermodynamic point of view, it is not the most stable polymorph[20].

Metastable forms (like the α and β' polymorph) can irreversibly transform to more stable forms (β). Two types of such polymorphic transformations are described in literature. The solid-state transformation occurs if the metastable form is kept below its melting temperature, while the melt-mediated transformation occurs during heating when the temperature rises above the melting temperature of the metastable form[20].

Next to the subcell packing, crystallizing triglyceride molecules, which adopt the conformation of a chair, can also have two different stacking modes based on their lamellar stacking: the double (2L) or triple chain length (3L) structure (Figure 1.5). The α polymorph normally only exists in the 2L structure, while the β' and β polymorphs are found in both chain length structures. The 2L structure occurs when all fatty acid chains in the triglyceride molecules are the same or very similar, while

the 3L structure is formed in case of fatty acid chains being quite different from each other[17,23,29]. For example, in monoacid triglycerides such as PPP (P = palmitic acid), SSS (S = stearic acid) and OOO (O = oleic acid) and in mixed acid triglycerides containing saturated fatty acids (e.g. PSS, PSP) the stable form occurs in a 2L packing. In mixed acid triglycerides containing one or two unsaturated fatty acids (e.g. SOS, PPO) the 3L packing is preferred[29].

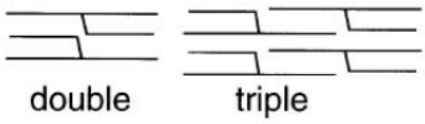

Figure 1.5. *Chain-length packing structures in triglycerides (From Sato, 2001[28])*

The factors controlling the rate and extent of crystallization of the different polymorphs were reviewed by Sato et al. (2013)[20]. Next to tempering, the presence of additives and application of shear, the cooling and heating rate are the main influencing factors. An increasing cooling rate increases the nucleation rate of the different polymorphic forms, but the effect is higher on less stable polymorphic forms. A decreasing heating rate may cause polymorphic transformation during heating[20].

Among the non-triglyceride lipids, some, like for example monoglycerides[31,32] and diglycerides[33], also crystallize in the α, β' and β polymorphs, while others such as cholesterol esters form other types of crystal structures[34].

1.2.1.5. *Microstructure of lipid crystal networks*

The microstructure is that level of the lipid crystal network with structures in the length range between 1 and 200 μm[19]. Figure 1.6 illustrates the various stages in the microstructure development (aggregation, network formation and sintering). The lipid crystals (often spherulites) that have grown from the nuclei grow up to dimensions of 1 to 4 μm and then join together attracted to each other due to van der Waals forces[23,27]. Brownian motion of the crystals makes them stick randomly to each other, leading to the formation of fractal aggregates (above 100 μm). The formation of these aggregates only takes between 10 and 100 seconds[23,35].

Subsequently the aggregates connect via a mass- and heat-transfer limited process to form a three-dimensional fractal network extending throughout the whole volume entrapping the liquid phase of the lipid[14,23,35]. Fractal systems are self-similar, which means they have a repeating pattern at various scales[36]. The continuous network or gel gives the mixture elastic properties at very small deformations (<< 1%). A solid fat content (SFC) of 1% is usually already sufficient to

achieve a gel. This means that at the time the primary network is formed, most of the lipid still has to crystallize[14]. The ongoing crystallization together with sintering (i.e. the formation of solid bridges between adjacent crystals in the network) leads to a compaction of the network thereby enhancing the strength of the bonds in the solid network in which the liquid phase of the lipid is trapped. Whether the network remains fractal at high SFC is a point of discussion[14,24,37].

The strength of the microstructural network depends on several parameters such as crystal size and morphology and agitation rate. An increasing crystal size leads to a weaker network and also polymorphism influences the network strength. Consequently, the degree of supercooling and cooling rate are also controlling factors since they influence crystal size and polymorphism. Finally, mild agitation may enhance aggregation of crystals, but high shear rates break up the formed network[37].

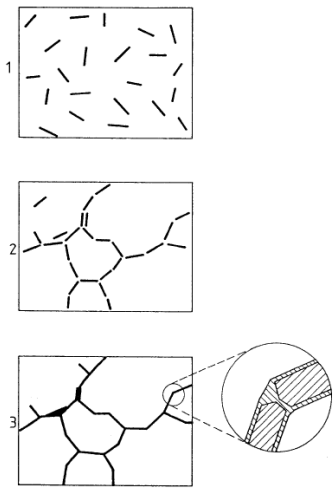

Figure 1.6. *Different stages in the microstructural development: aggregation (1), network formation (2) and sintering (3) (From Walstra, 1987[27])*

1.2.1.6. *Mechanical and macroscopic properties*

The mechanical and macroscopic properties of lipids are influenced by all the different structure levels as shown in Figure 1.2 and cannot be simply related to the molecular structure or composition of the lipid molecules. Rheological properties such as the linear visco-elastic region, the storage modulus and the loss modulus are influenced by the combination of SFC and the microstructure of the lipid crystal network including the shape, size and spatial distribution pattern of the crystal aggregates in the network[19].

Other macroscopic properties include textural properties such as hardness, brittleness and spreadability. Particularly for products like margarines, spreads and shortenings, the hardness is a very important asset[38]. A consumer desires a product that is spreadable both at refrigerator temperature and at room temperature and that completely melts in the mouth. This requires a specific melting profile of the lipid. In general a low SFC yields a soft, spreadable product, while a high SFC can lead to a hard, brittle product[39]. However Danthine (2012)[38] demonstrated that predicting the hardness based on the SFC alone leads to unreliable results since also polymorphism and size distribution of the crystal aggregates in the network structure have shown to be influencing factors. They stated it is important to take into account all of the structural levels when predicting the hardness of a lipid-based product.

1.3. PHASE BEHAVIOR IN LIPID BLENDS

The macroscopic properties of lipid blends are determined by the phase behavior of its components (different triglycerides in a fat, different fats in a fat blend or different lipids in a non-triglyceride lipid blend). A first part of this section focusses on the principles of phase behavior in binary blends of pure lipids. However, at the moment no literature exists reviewing the general principles of phase behavior in blends of pure lipids. Therefore, this part describes the principles of phase behavior in binary blends of pure components in general illustrated with examples of phase behavior in pure lipids such as pure triglycerides and pure cholesteryl esters from literature. A second part deals with the phase behavior in binary blends of naturally occurring, real lipids. Phase behavior of palm oil and phytosterol esters in lipid blends specifically is described in chapter 2.

1.3.1. GENERAL PRINCIPLES OF PHASE BEHAVIOR IN BINARY BLENDS OF PURE LIPIDS

A phase can be defined as a state of matter that is homogeneous and physically separated from other phases. A phase is fully determined by its composition, temperature and pressure, of which the latter can be ignored in food applications. A phase diagram describes the phase behavior of a binary mixture in the equilibrium state and plots the temperature as a function of the blend composition (at a constant pressure). It is used to get information on the solid phase behavior, especially with respect to the miscibility of components in the solid phase. The miscibility in the liquid phase is supposed to be ideal which means no heat or volume changes occur on mixing. If no ideal miscibility in the liquid phase would exist, phase separation would already occur in the liquid phase making the analysis of miscibility in the solid phase irrelevant[14].

In general, a phase diagram contains a liquidus line and a solidus line. The liquidus line is defined as the highest temperature at which crystals can exist, while the solidus line gives the lowest temperatures at which liquids can exist. So above the liquidus line, blends are completely molten, below the solidus line they are completely solid and in between partial melting occurs. The four main types of phase diagrams are discussed in more detail below[25].

1.3.1.1. *Eutectic systems*

The eutectic system as shown in Figure 1.7 occurs when two non-interacting components, A and B, are mixed and the blends melt at lower temperatures than the pure components. Above the liquidus line a single-phase liquid solution exists. Below the solidus line no compounds or solid solutions are formed, but only a mixture of two separate solid phases A and B. In the regions between the liquidus and the solidus lines, a two-phase region exists containing a crystalline phase and a liquid phase which both have a different composition [25].

The exact compositions of the two phases in the two-phase region at a specific temperature e.g. T_2 in Figure 1.7 (c) can be derived from drawing an isotherm on the phase diagram at that temperature. This isotherm is the horizontal dashed line from point h' to T_2. Point h' lies on the liquidus line and represents the liquid that is present in the two-phase mixture at temperature T_2. The composition of this liquid, h, is represented by the intersection of a vertical line through h' with the horizontal axis. In this example the liquid composition is 57% A and 43% B. The other phase that is present in the mixture is B, whose composition is fixed, being pure B[25].

Point y in Figure 1.7 (b) is the point at which three phases (liquid, solid A and solid B) coexist. This point is the eutectic point which is the minimum in the liquidus line. The eutectic point thus represents the lowest temperature at which the binary blend is completely liquid. In the eutectic system the eutectic point is also the intersection of the liquidus and the solidus lines[25].

Eutectic systems tend to occur in binary blends of pure triglycerides if the triglycerides differ in molecular volume, shape and polymorph, but not greatly in melting temperature (< 20°C)[17], like for example in POP/POO[40] and PSS/SSS[41] binary systems. Eutectic systems were also reported to occur in binary blends of pure cholesteryl esters, more specifically in blends of cholesteryl myristate with cholesteryl undecanoate[42].

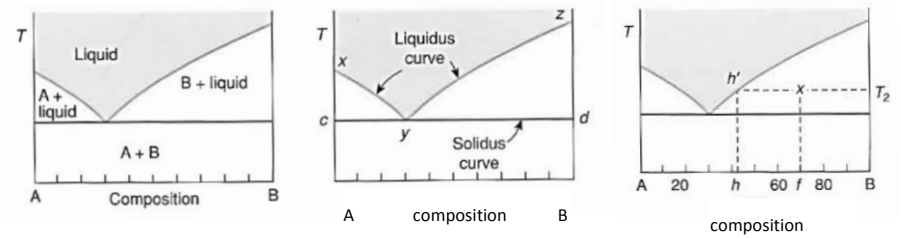

Figure 1.7. *Phase diagram of a simple eutectic system (From West, 2014[25])*

1.3.1.2. *Binary systems with complete solid solution*

The simplest binary system with solid solution is the one that shows complete miscibility in the solid phase as shown in Figure 1.8. In such system the melting temperature of component A is depressed by the addition of component B, while that of B is increased on addition of A. The liquidus and solidus line are both smooth curves which only meet at the compositions of pure component A and pure component B. Above the liquidus line single-phase liquid solution exists and below the solidus line a single-phase solid solution occurs. In between the liquidus and the solidus line, a two-phase region of solid solution and liquid exists[25].

The exact compositions of the two phases within the two-phase region at a specific temperature e.g. T_1 in Figure 1.8 can be derived from drawing isotherms on the phase diagram at that temperature. The intersection of the isotherm at T_1 with the solidus line gives the composition of the solid solution, a. The composition of the liquid, b, results from the intersection of the isotherm at T_1 with the liquidus[25].

Binary systems with complete solid solution were commonly observed in binary blends of pure triglycerides which are very similar in melting temperature, molecular volume and polymorphism[17]. This type of phase behavior was for example reported in PPP/SSS (α and β' forms)[43], SOS/SLS (α and γ forms, L = linoleic acid)[44] and LaLaLa/MMM (La = lauric acid, M = myristic acid)[45] binary systems. Also some binary blends of cholesteryl esters formed a complete solid solution like for example cholesteryl linoleate with cholesteryl oleate or cholesteryl undecanoate[42].

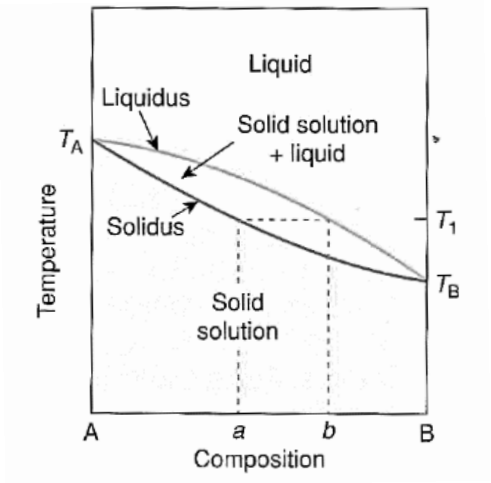

Figure 1.8. *Phase diagram of a binary system with complete solid solution (From West, 2014[25])*

1.3.1.3. *Binary systems with partial solid solution*

Binary systems with partial solid solution are extensions of existing phase diagrams including binary systems with complete solid solution or eutectic systems[25]. Figure 1.9 represents a eutectic system with partial solid solution. Crystals of B partially dissolve in crystals of A to form a solid solution represented by region A ss. Similarly, crystals of A partially dissolve in B crystals (region B ss). The extent of solid solution is maximal at the eutectic temperature (points m and n)[25]. An example of this type of phase behavior was reported in binary blends of cholesteryl myristate with cholesteryl stearate, palmitate or laurate[42].

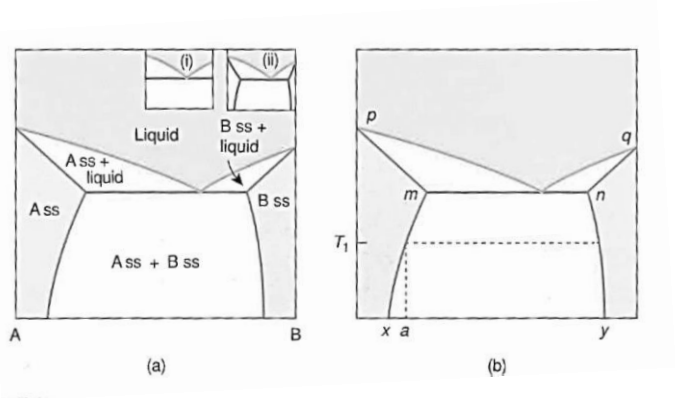

Figure 1.9. *Phase diagram of a eutectic system with partial solid solution (From West, 2014[25])*

Figure 1.10 shows two types of binary systems with partial solid solution, being the monotectic (a) and the peritectic (b) system[14]. In case of the monotectic system a limited amount of A crystals dissolve in crystals of B to form a solid solution represented by region B ss. By melting of B ss the two-phase region of liquid + B ss is entered. With an increasing temperature the B solid solution in equilibrium with the liquid becomes increasingly rich in B as shown by the solidus line[25].

In binary blends of pure triglycerides monotectic systems are formed preferably over eutectic systems if the difference in melting temperature of the triglycerides is increased (> 20°C)[17] and were for example reported in PPP/SSS (β form)[43], LaLaLa/PPP, LaLaLa/SSS[45], MSM/MMS[46] binary systems. Monotectic phase behavior was also reported in binary blends of cholesteryl palmitate with cholesteryl oleate or cholesteryl linoleate[42].

Similar to the monotectic system, in the peritectic system also a limited amount of B crystals dissolves in the A crystals, a region of A solid solution is formed (region A ss). Most of the A solid solution also melts in a similar way as the A solid solution by entering the two-phase region liquid + A ss. With an increasing temperature the A solid solution in equilibrium with the liquid becomes increasingly rich in B as shown by the solidus line. However at point d the A solid solution melts incongruently to give liquid + B ss with an associated peritectic point p[25].

Peritectic systems were reported to occur in binary blends of pure triglycerides that each contain saturated and unsaturated fatty acids and where at least one triglyceride has two unsaturated fatty acids[17], like for example the SOS/SOO binary system[47].

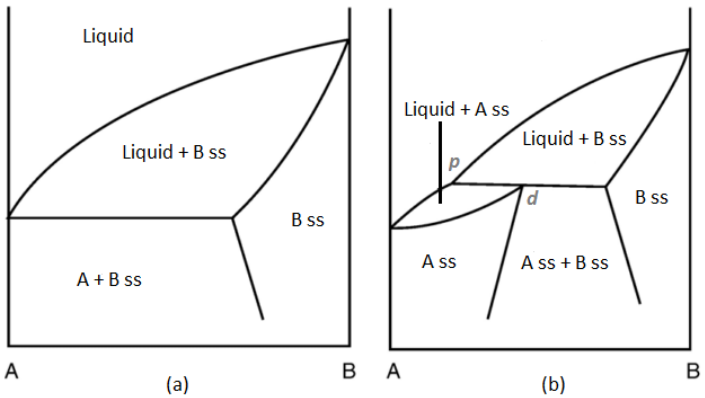

Figure 1.10. *Phase diagram of a monotectic (a) and a peritectic (b) binary systems with partial solid solution (Adapted from Himawan, 2006[17])*

1.3.1.4. *Binary systems with compound formation*

Figure 1.11 shows a binary system with the formation of a compound AB, which is represented by a vertical line. The line shows the range of temperatures over which compound AB is stable. At temperature T_3 compound AB changes from solid AB to a liquid of the same composition. The phase diagram may be conveniently divided into two parts that consist of the concentration ranges A-AB and AB-B each representing a phase diagram on its own. If the phase diagram is composed of two eutectic systems like in Figure 1.11 a characteristic feature is that the melting of AB represents a maximum in the liquidus line as is shown in Figure 1.11 since at either side of point y the liquidus line drops[25]. The phase diagram can also be composed of two binary systems with complete or partial solid solution. In that case the melting of the compound represents a minimum in the liquidus[48].

This type of phase behavior was already observed in some binary blends of pure triglycerides. For example, in the system SOS/SSO, there is clear evidence for the formation of a compound M. This system is composed of two eutectic systems, SOS/M and M/SSO[49]. On the other hand the system POP/PPO which also shows the formation of a compound is composed of two binary systems with partial solid solution[48].

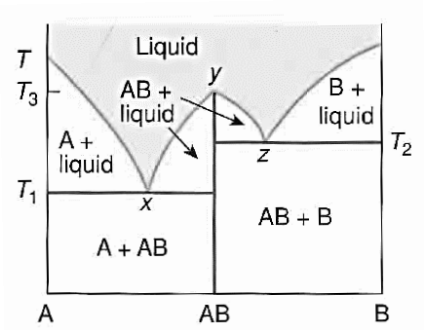

Figure 1.11. *Binary system showing formation of compound AB (From West, 2014[25])*

1.3.2. PHASE BEHAVIOR IN BINARY BLENDS OF REAL LIPIDS

Next to pure lipids, it is also possible to describe the phase behavior in binary blends of naturally occurring, real lipids by treating each lipid as a component on its own. Phase diagrams of binary blends of real lipids are different from phase diagrams of binary blends of pure components because a real lipid is not a single molecular component, but is already a blend itself. Essential differences between binary blends of real lipids and of pure components are[29]:

- A real lipid has a melting range instead of a melting temperature so in the phase diagram there is no unique temperature for a real lipid at 100% composition where liquidus and solidus line come together.
- Instead of a precise eutectic point where the liquidus and the solidus line come together, eutectic phase diagrams of real lipids have a eutectic minimum in the liquidus line.
- In the phase diagram of real lipids, the lines drawn horizontally in the two phase solid-liquid region cannot be used to determine the ratio of solid to liquid present in the blend.

From the different types of phase behavior in binary blends of pure components as described in section 1.3.1., Timms (1984)[29] deduced three types of phase behavior to be possible in binary blends of real lipids. Similar to blends of pure components, a system with complete solid solution would be obtained when the lipids show complete miscibility in the solid phase. This would result in a phase diagram such as that shown in Figure 1.12 (a), which is the equivalent of the phase diagram for two pure components shown in Figure 1.8. If the lipids are only partially or not at all miscible in the solid phase a eutectic or a monotectic system is formed. The phase diagram of the eutectic system formed by blends of real lipids is shown in Figure 1.12 (b) and is equivalent to the phase diagram of two pure components shown in Figure 1.9. Figure 1.12 (c) shows the phase diagram resulting from monotectic behavior in a binary blend of real lipids and is the equivalent of the phase diagram for two pure components shown in Figure 1.10(a)[29].

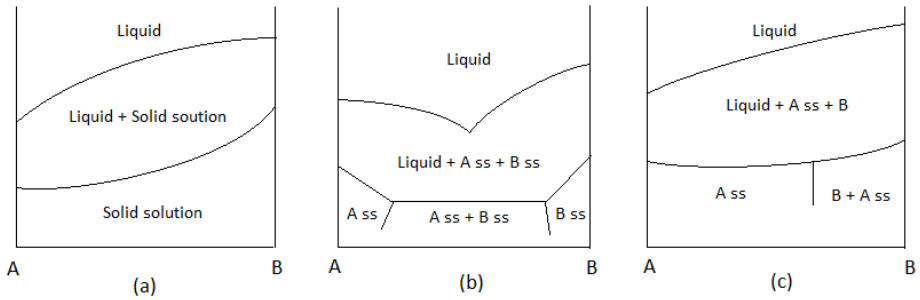

Figure 1.12. *Phase diagrams of binary blends of real lipids forming a (a) system with complete solid solution, (b) eutectic system, (c) monotectic system (From Timms, 1984[29])*

Experimental studies reported on the phase behavior of binary blends of real lipids are mainly, but not exclusively dealing with phase behavior of binary blends of real fats. A system with complete solid solution in a binary blend of real fats is only rarely reported, like for example in blends of a high-melting fraction of milk fat with a middle-melting fraction of milk fat[50].

Eutectic systems are the most commonly reported type of phase behavior for binary blends of real fats. They are for example formed in binary blends of cocoa butter with fractionated palm kernel oil, fractionated hydrogenated palm kernel oil, milk fat[51], or the high-melting[52] or middle-melting fractions of milk fat[51]. Milk fat and its fractions also formed eutectic systems with fractionated palm kernel oil or fractionated hydrogenated palm kernel[52].

When blending a low-melting fraction of milk fat with a high-melting or middle-melting fraction of milk fat monotectic systems were formed[50]. Monotectic phase behavior was also found in blends of low-erucic rapeseed oil with hydrogenated low-erucic rapeseed oil[53], blends of cocoa butter with hazelnut oil, almond oil, high-oleic sunflower oil or high-stearic high-oleic sunflower oil[54] and when blending a fat with a non-triglyceride lipid, more specifically in a blend of a confectionery fat blend with sorbitan monostearate[55].

As mentioned above Timms (1984) reported that in binary blends of pure triglycerides the eutectic system tends to shift to a monotectic system if the difference in melting temperature of the triglycerides is high (> 20°C)[29]. Based on the examples mentioned above, a similar rule seems valid in binary blends of real fats, but with considering the reported offset temperature of melting of both lipids instead of the melting temperature since unlike pure triglycerides, real fats have a melting range instead of one specific melting temperature. In the eutectic systems of real lipids mentioned above the difference in the offset temperatures of melting between the lipids is low (< 25°C), while in the monotectic systems of real lipids mentioned above the difference is high (> 25°C). The only exception to this rule are the blends of cocoa butter with high-oleic sunflower oil or high-stearic high-oleic sunflower oil where monotectic phase behavior was reported although the difference in offset temperature of melting of both fats was low (< 25°C)[54]. However this study did not cover the full concentration range of the binary blends, but only the blends with 50 to 100% cocoa butter, which may be insufficient to make conclusions about the phase behavior in the blends[54]. More examples of the different types of phase behavior observed in binary blends of real lipids containing palm oil or phytosterol esters are described in sections 2.1.4.4 and 2.2.5.3 respectively.

1.4. TECHNIQUES TO MONITOR LIPID CRYSTALLIZATION AND PHASE BEHAVIOR

Many different techniques exist to monitor lipid crystallization which all measure different aspects. Therefore, it is important to combine several techniques in order to monitor all structural levels of lipid crystallization from primary crystallization in a specific polymorphic form to microstructural development and macroscopic

properties. The same techniques as used to monitor lipid crystallization are also used to study phase behavior of lipid blends and construct binary phase diagrams. Rigolle et al. (2018)[56] made a complete overview of conventional and new techniques to monitor lipid crystallization, while this section is limited to the discussion of those techniques that are used in this PhD with special attention to which aspects of lipid crystallization are monitored and also taking into account the limitations of each technique.

1.4.1. PULSED NUCLEAR MAGNETIC RESONANCE

The SFC of a lipid sample is measured by pulsed nuclear magnetic resonance (pNMR). The lipid sample is put in a magnetic field and subjected to a short intense radio frequency pulse due to which the hydrogen protons in the sample become excited. When the radio frequency pulse is stopped the protons relax from their excited state and fall back to their initial state (in line with the magnetic field). The NMR signal observed after the radio frequency pulse decreases as a function of time due to the relaxation of the protons and is different for the solid and the liquid phase of the sample[57]. The NMR signal from protons in the solid phase declines faster (< 15 µs) than that of protons in the liquid phase (1 ms)[58].

There are two approaches to calculate the SFC from the NMR signal: the direct and the indirect method[57]. In the direct method the amplitude of the NMR signal is measured at two different time points: immediately after the radio frequency pulse and 70-150 µs after the pulse. These two NMR signals correspond to the total signal (solid and liquid) and the liquid signal respectively. The SFC is then calculated as the ratio between the solid signal, which is the difference between the total and the liquid signal, and the total signal[59]. The direct method is usually favored due to its speed and simplicity. On the other hand the indirect method determines the SFC by comparing the NMR signal obtained from the liquid phase at a certain temperature with the NMR signal of the fully melted sample[60]. The indirect method is to be used for lipid samples containing non-lipid solid particles (e.g. sugar, cocoa solids, nuts) which would otherwise contribute to the NMR signal of the solid phase and consequently result in an incorrect solid signal[57].

1.4.2. DIFFERENTIAL SCANNING CALORIMETRY

The thermal behavior of a lipid sample can be analyzed using differential scanning calorimetry (DSC). A DSC instrument measures the difference in heat input/output between the sample and a reference which are both subjected to a specific time-temperature profile. A substance is suitable as a reference if no phase transitions (crystallization or melting) occur in the specific time-temperature range. Consequently the measured difference in heat input/output between the sample

and the reference is only associated with phase transitions that occur in the sample[57].

The result of an experimental DSC run is a thermogram in which the heat flow is plotted as a function of time or temperature. Crystallization, which is an exothermic event, is observed in the thermogram as a peak. Melting, which is endothermic, results in a peak in the opposite direction. Several parameters can be calculated from the thermogram to describe the thermal behavior of the sample including the peak temperature of crystallization and melting, the onset temperature of crystallization, the offset temperature of melting and the enthalpy of crystallization and melting. The onset temperature of crystallization is the temperature at which the lipid starts to crystallize and corresponds to the temperature at which the baseline slope of the DSC cooling thermogram changes. Similarly, the offset temperature of melting is the temperature at which the lipid becomes fully liquid. The offset temperature of melting is often determined as the intersection of the baseline with the tangent line in the inflection point of the melting peak on its high temperature side. The enthalpy of a phase transition corresponds to the peak area and is calculated as the area between the thermogram and the baseline[57,61].

Furthermore, DSC can also be used to indirectly characterize the crystal structure present in a lipid by comparing the experimental peak temperature of melting with values reported in literature. It is recommended to use a high heating rate (≥ 5°C/min) to avoid structural changes such as polymorphic transformation and recrystallization during melting since such events will highly influence the melting properties[57].

DSC is also often used to study the crystallization kinetics of a lipid by monitoring the heat flow as a function of time at a constant temperature. In this case high cooling rates of 10°C/min or more are recommended for cooling the sample to the isothermal crystallization temperature to avoid that crystallization starts during the cooling stage. Otherwise the results reflect a dynamic crystallization process rather than isothermal crystallization[57,62].

1.4.3. X-RAY DIFFRACTION

Crystal structures in lipids can be identified with X-ray diffraction. X-rays are electromagnetic radiation with a wavelength of about 1 Å which are produced when accelerated high-energy charged particles such as electrons collide with matter. X-rays can be generated by laboratory sources or by synchrotron sources. In laboratory-based diffraction experiments a beam of electrons is accelerated by a voltage of about 30 kV and strikes a metal target, often Cu, causing ionization of some of the Cu electrons. The energy released when the ionized electrons relax to

their initial state appears as monochromatic X-rays with a characteristic wavelength, which is 1.5418 Å in case of Cu[25].

Synchrotron radiation is generated when electrons are accelerated to nearly the speed of light and are forced by bending magnets to deflect from their linear path and circulate in vacuum tubes called storage rings, which typically have diameters of 200 to 500 m. Figure 1.13 shows a schematic diagram of a synchrotron storage ring. Tangentially to the curved electron path the electrons emit the synchrotron radiation which form the beam lines for various diffraction and spectroscopic instruments. Synchrotron sources are large-scale facilities such as the European Synchrotron Radiation Facility (ESRF) in Grenoble (France). Compared to X-rays from conventional sources the intensity of synchrotron radiation is much higher and the beams are accurately parallel resulting in a much higher resolution[25]. Probing the crystalline structures directly, in-situ and in real time is only possible with the intensity provided by a synchrotron source. However the limited availability and extremely high cost of these time-resolved experiments make this technique not suitable for everyday use[63,64].

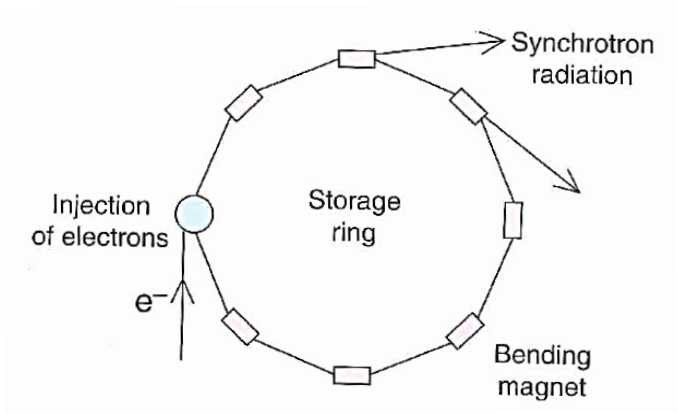

Figure 1.13. *Schematic diagram of a synchrotron storage ring (From West, 2014[25])*

Lipid crystals with their regularly repeating structures diffract incident X-rays because the interatomic spaces in the crystal are similar to the wavelength of the X-rays. The Bragg approach to diffraction considers the crystal lattice as a series of parallel atomic layers or planes (Figure 1.14). When two X-ray beams, 1 and 2, are reflected by adjacent planes, A and B, the distance between the adjacent planes d is related to the angle θ of the incident X-ray beams with wavelength λ by Bragg's law:

$$n\lambda = 2d \sin\theta$$

The integer 'n' refers to the order of reflection which refers to reflections from successive planes. When Bragg's law is satisfied, the reflected beams, 1' and 2', are in-phase and constructive interference leads to peak formation in the diffraction pattern. At other angles the reflected beams are out-of-phase and destructive interference or cancellation occurs [25,57].

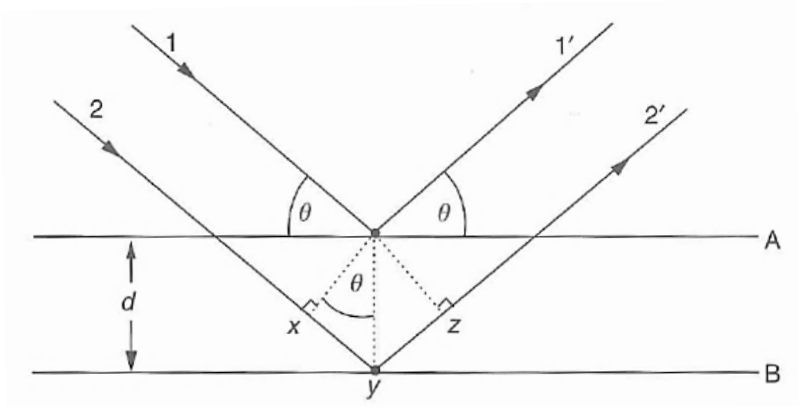

Figure 1.14. *Derivation of Bragg's law (From West, 2014).*

X-rays are scattered by lipid crystals into two main regions, the wide angle and the small angle region. Wide angle X-ray diffraction (WAXD) measures the characteristic short spacings of the subcell within the crystal lattice, providing for example information about the crystal structure of a lipid. On the other hand, small angle X-ray scattering (SAXS) measure the long spacings of the crystal structure, which provide insight in how the molecules stack together to form lamellar structures[17,29,57,65].

1.4.4. POLARIZED LIGHT MICROSCOPY

Many different microscopic techniques can be used to visualize the microstructure of lipid crystal networks, but polarized light microscopy (PLM) is probably the most popular one. A polarized light microscope is equipped with two polarizers: the first one is placed in the light path before the sample and the second (called the analyzer) is positioned in the optical path between the sample and the observation tube. Light is polarized by the first polarizer which means that the propagation of the light waves is restricted to a single, constant plane. Due to the analyzer which has its filters oriented perpendicular to those of the polarizer, no light passes through the analyzer and a dark field is visible. This changes when anisotropic material such as lipid crystals is placed between the crossed polarizers. When light passes through an anisotropic crystal it is refracted into two light rays polarized at right angles to each other and travelling at different speeds creating a phase difference between the two

rays. This phenomenon of double refraction is also called birefringence. The analyzer combines the two light rays so that the birefringent lipid crystals elucidate. Liquid oil on the other hand remains dark because it is an isotropic material meaning it only has one single refraction index[57].

Qualitative analysis of the microscopy images is possible when there are large differences in morphology or size of the crystals or crystal aggregates in the network structure or if there is a difference in presence or absence of certain features, but quantitative information cannot be obtained directly. Quantitative analysis can be performed using image analysis techniques such as those to determine the size and number of features, percent black which is related to the solid fraction of the network and the fractal dimension which is an indicator of the elastic properties of lipid crystal network[10,57]. The observed microstructure can also give an indication of the formed polymorph, although the same polymorph can lead to very different microstructures[10].

1.4.5. MECHANICAL AND MACROSCOPIC PROPERTIES

In general, mechanical properties are analyzed by testing how the lipids respond to applied forces or deformations. Small deformation rheology testing procedures do not cause structural damage to the sample and give information on viscoelastic properties of the substance such as the linear visco-elastic region, the storage modulus and the loss modulus[39,57,66–68]. In large deformation analyses the sample undergoes a deformation to the point where the force exceeds its structural capacity causing it to permanently deform or break. Methods such as cone penetrometry and parallel plate compression determine parameters such as yield force and compression modulus which can provide an index of hardness for lipids. These measurements have been successfully correlated to the hardness and spreadability of lipids obtained through sensory evaluation[57,67].

CHAPTER 2
PALM OIL AND PHYTOSTEROLS AND THEIR ESTERS

2. PALM OIL AND PHYTOSTEROLS AND THEIR ESTERS

Several food products that are rich in lipids, such as margarine, contain a substantial amount of palm oil or its fractions. Some of these food products may be enriched with phytosterols or their esters for their cholesterol-lowering properties. According to the definitions stated in section 1.1 palm oil is a fat, while phytosterols and their esters are non-triglyceride lipids. This chapter consists of two sections. The first section deals with the chemical characteristics, sources, food applications and crystallization and phase behavior of palm oil. In the second section chemical characteristics, sources and cholesterol-lowering mechanism of phytosterols are first discussed followed by the synthesis, food applications and crystallization and phase behavior of phytosterol esters.

2.1. PALM OIL

Palm oil has surpassed soybean oil to be the most consumed vegetable oil in the world because of its unique physical properties[69]. Because palm oil is semi-solid at ambient temperature, it is a very suitable trans-free main ingredient in e.g. margarines and shortenings to provide consistency, texture and structure[70].

2.1.1. SOURCES

Palm oil originates from the fruit of the oil palm tree (*Elaeis guineensis*). Because the oil palm tree is a tropical tree palm oil production occurs in countries which lie in tropical zones with hot and humid climates, mainly in Indonesia (36 million metric tons in 2017) and Malaysia (21 million metric tons in 2017). Other large producers are Thailand, Colombia and Nigeria, together producing 4.5 million metric tons in 2017[71].

Bunches of palm fruit can reach a weight of 10 to 40 kg and consist of 200 to 2000 smaller individual fruits each weighing around 6-20 g[72,73]. Three years after initial planting, the plant starts producing fruits and continues to do so throughout the year for approximately 25 consecutive years. The individual fruits produce two types of oils: the pulp (mesocarp) contains 55-70% orange-red crude palm oil, while the seeds in the central tissue (endocarp) consist of about 50% palm kernel oil[69,74]. After separation of the fruit from the seed, crude palm oil is obtained by pressing the fruit (so no chemical extraction is needed) and subsequently refined[75]. Under favorable conditions the oil palm tree produces 5 tons of oil/hectare/year, which is approximately ten times more than other leading oilseed crops like soybean[72]. The

objective of refining is to remove those components that have a negative effect on the overall quality (e.g. pigments, oxidation products, free fatty acids, partial glycerides, waxes, etc.) and at the same time retain the beneficial minor components such as vitamins and antioxidants as much as possible[76]. The refined palm oil can then also be fractionated, resulting in fractions of palm oil with different melting properties that can be used for diverse applications[74].

Although palm oil has a much higher yield per hectare than all other oilseed crops, the past decade has seen an on-going debate over the sustainability of palm oil production. While the palm oil industry has been a key driver for job creation and economic and social development in the producing countries it is accused of unsustainable practices for nature and local communities. The key sustainability challenges which the palm oil sector encounters are deforestation, biodiversity loss and social issues with regard to land ownership and rights of smallholders. As a reaction, several initiatives were taken to address the sustainability challenges such as the multi-stakeholder roundtable on sustainable palm oil (RSPO), which was formally established in 2004[77]. There are certain standards and criteria that must be met by the producers to be certified by RSPO. By February 2018 RSPO had members in more than 80 countries, although still only 19% of global production is currently certified[78].

2.1.2. CHEMICAL CHARACTERISTICS

Palm oil has a balanced fatty acid composition with the level of saturated fatty acids being almost equal to that of the unsaturated fatty acids, a unique property among vegetable oils and fats[74,79–82]. The primary fatty acids are palmitic acid (44%) and oleic acid (39%), along with linoleic acid (10%) and only a trace amount of linolenic acid (0.4%)[79].

Saturated fatty acids have important metabolic functions in the human body, but are not required in the diet. Already since the 1960s saturated fat intake has been investigated for its role in elevated levels of plasma total cholesterol which is associated with increased risk of coronary heart disease[83]. National and international dietary expert panels aiming to prevent coronary heart disease recommend that saturated fat consumption should not exceed 10% of the overall daily energy intake[84,85]. A recent regression analysis showed that reducing the saturated fatty acid intake by replacing them with cis-polyunsaturated fatty acids or cis-monounsaturated fatty acids (predominantly oleic acid) resulted in lower levels of total cholesterol and low density lipoprotein (LDL) cholesterol, while replacing with carbohydrates was not beneficial. Furthermore the authors showed that individual saturated fatty acids are not equally hypercholesterolemic: an increased intake of lauric, myristic or palmitic acid raised serum total and LDL-cholesterol levels, while

increased intake of stearic acid did not appear to have a significant effect on these or other serum lipid values[86].

Next to the fatty acid composition also the triglyceride composition of palm oil has been reported in many studies [32,74,80–82,87]. The major triglyceride species are POP (28%) and POO (24%) with also significant amounts of PLO, PLP (both around 10%), PPP (5%), POS and OOO (both 4-5%). Furthermore palm oil is also rich in tocopherols and carotenoids and is characterized by the presence of higher levels of diglycerides (5-8%) than in other vegetable oils[73,74,88].

2.1.3. FOOD APPLICATIONS

Many unique characteristics of palm oil allow its use in diverse food applications. Food industry uses about 90% of palm oil mainly for the manufacturing of spreadable fats, confectionery fats, deep frying oils, salad oils and ice cream, while the remaining 10% finds application in soap and oleochemical manufacturing[69,74].

The food use of palm oil is even more diversified by fractionation. This is a fully selective physical and/or thermo-mechanical process that utilizes the differences in the crystallization properties of TAGs to separate the palm oil into two major fractions: the low melting liquid fraction, palm olein, and the high melting solid fraction, palm stearin. Palm olein is more unsaturated than palm oil and with its melting point of 18-20°C it is liquid at room temperature. It expires less rapidly than many other liquid vegetable oils such as soybean, sunflower and canola oil. Double fractionation of palm olein can yield super olein and palm-mid fraction. Palm stearin has a higher amount of saturated fatty acids than palm oil leading to a melting point of 48-50°C. Double fractionation of palm stearin can also yield palm mid-fraction. The physicochemical properties of palm mid-fraction lie in between those of palm olein and palm stearin[88].

2.1.3.1. *Spreadable fats*

Spreadable fats include margarines and spreads and are water-in-oil emulsions that contain between 10% and 90% fat and that remain solid at 20°C. According to the European legislation spreadable fats obtained from vegetable and/or animal fats with a fat content between 80% and 90%, have to be labelled as margarine, while spreadable fats with less than 80% fat, are defined as fat spreads. Furthermore a reduced-fat spread contains between 41% and 60% fat, while a low-fat or light spread has a fat content of less than 39%[89].

Spreadable fats consist of a water phase and a fat phase. The fat phase usually contains a combination of three main types of ingredients: soft oil, semi-solid fat and hard fat[90]. The semi-solid and hard fats in a margarine play a key role in providing

the textural (e.g. hardness and spreadability) and sensorial (e.g. melt-in-mouth effect) characteristics of the product[91]. Palm oil can be used in the formulation of margarines as semi-solid fat, while palm olein can be applied as soft oil and palm stearin as hard fat[90].

The specific combination of one or more soft oils and hard fats in the formulation of a margarine depends on the desired SFC profile that is linked to the application. Table margarines are used as bread spread and must be spreadable both at room temperature and straight from the refrigerator. Pastry margarines usually require a higher SFC profile than table margarines because they need to withstand dough working[90].

2.1.3.2. *Other applications*

Other common applications of palm oil and its fractions are shortenings, cooking and frying oils, ice cream, salad oils and cocoa butter equivalents. The term shortening is used for blends of fats that have the same applications as bakery margarines (e.g. cakes, cookies and breads), but unlike bakery margarines, they do not contain water and are thus not defined as emulsions[90]. Palm oil and palm stearin are generally used for the preparation of shortenings in a concentration between 30 and 40%[88].

Furthermore, palm oil and its fractions are also very suitable for commercial deep frying because of their good resistance against foaming, oxidation and polymerization[74]. Deep frying is a very popular method for the preparation of food because it is easy, fast, and cheap and results in tasty foods. Frying temperatures range between 150°C and 190°C. During frying, heat and mass transfer processes occur between the oil and the food and therefore the quality of the fried food is a function of the oil quality. Palm oil, palm olein and palm stearin are widely used in large scale industrial frying of foods like French fries, snack food, fried chicken, chicken fillets and noodles. A large amount of palm oil is also used for frying in fast food restaurants[69].

Palm mid fraction is widely used in the confectionery industry as a cocoa butter equivalent ingredient. Cocoa butter is responsible for the crystallization and melting properties of chocolate that yield its characteristic macroscopic properties such as gloss, flavor release and “snap”. Shortage of the supply and fluctuations in the price of cocoa butter have encouraged the search for other vegetable oils that are suitable as replacers for cocoa butter. Blending palm mid fraction, which is rich in POP, with an SOS-rich tropical fat such as shea butter or mango kernel oil results in a cocoa butter equivalent with a composition and SFC profile similar to cocoa butter[92].

2.1.4. CRYSTALLIZATION AND PHASE BEHAVIOR OF PALM OIL

2.1.4.1. *Polymorphism*

The three main polymorphic forms described in fats (α, β' and β) were also detected in palm oil[29,38,74,87,93–97]. However in palm oil β' exhibits two sub forms being β_1' and β_2' which have a different thermodynamic stability and different melting temperature and are assigned with a subscript that increases with decreasing stability[29,38].. The diffraction pattern of the hexagonal α form generally shows one strong line at about 4.2 Å. The β_1' form is characterized by two strong diffraction lines at 4.19 Å and 4.35 Å and a medium strong line at 3.88 Å, while the β_2' can be distinguished by a strong diffraction line at 4.18 Å in combination with a medium strong one at 3.88 Å. Finally, the β form of palm oil features two weak lines at 3.75 Å and 3.83 Å and a medium strong line at 4.56 Å[74,87,93,95].

Mainly because of its high triglyceride diversity, palm oil is very stable in the β_1' polymorph and is therefore called a β' tending fat[93]. The β_1' stability of palm oil and its fractions has been repeatedly studied. It was reported that during storage at 5°C a small amount (about 5%) of β crystals were only formed in palm oil after 36 days, while at that time palm stearin contained already about 40% β crystals. Also after temperature cycling between 20°C and 5°C only 12% β crystals were present in palm oil, compared to 30% in palm stearin. The authors state that the β formation was due to partial melting of mixed triglycerides during the temperature cycling which caused some fractionation and the formation of palm stearin[93]. Furthermore also a low cooling rate to relatively high temperatures caused fractionation and the formation of trisaturated triglycerides (e.g. PPP and SSS) which promoted the formation of β crystals in palm oil[98].

2.1.4.2. *Non-isothermal crystallization*

The thermal profile of palm oil during cooling has been described many times before in literature[29,80,96,97,99–101]. A typical crystallization and melting profile of palm oil is shown in Figure 2.1. The crystallization profile of palm oil exhibits two well separated exothermic peaks due to the crystallization of a high-melting fraction and a low-melting fraction which are labelled as the stearin (or 'hard') and the olein (or 'soft') fraction respectively, as mentioned before. The stearin fraction is rich in di- and trisaturated triglycerides, while the olein fraction contains mainly di- and triunsaturated triglycerides[87]. Concerning polymorphism it was reported that during cooling to 0°C palm oil crystallizes in the α form[29,96,97], while when cooling to even lower temperatures also β_2' crystals were formed[29,97].

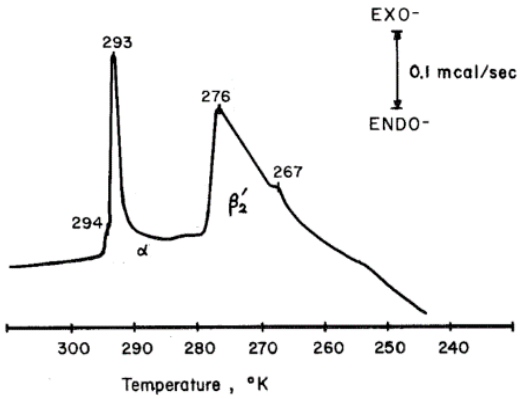

Figure 2.1. *Crystallization profile of palm oil (Adapted from Kawamura 1980[97]).*

2.1.4.3. *Isothermal crystallization*

Isothermal crystallization of palm oil has been extensively studied by several authors who reported that the isothermal crystallization mechanism of palm oil depends on the degree of supercooling[32,99,102–104]. At a high degree of supercooling, palm oil displays a two-step crystallization with the formation of α crystals in the first step, followed by a transformation into β_1' crystals and subsequently additional formation of β_1' crystals directly from the melt. At a lower degree of supercooling palm oil crystallizes directly into the β_1' polymorph without the prior formation of an α polymorph.

The reported value of the cut-off temperature between both mechanisms varies between 22°C and 25°C probably because of a difference in experimental conditions on the one hand and a difference in palm oil composition on the other hand[32]. One study analyzed isothermal palm oil crystallization at even higher temperatures and reported that when palm oil is kept isothermally between 34°C and 46°C it crystallizes directly in the β polymorph[74].

2.1.4.4. *Phase behavior of binary blends of palm oil with other lipids*

In literature on the phase behavior of palm oil in binary blends with other real lipids two types of phase behavior have been reported, being eutectic and monotectic phase behavior. Similarly to the general rule described for binary blends of real lipids (section 1.3.2.), the type of phase behavior of binary blends of palm oil with another real lipid seems to be dependent on the difference in the offset temperature of melting of between palm oil and the other lipid.

When the difference in offset temperature of melting between palm oil and the other real lipid was low (< 26°C), a eutectic system was formed. This was for example the case in blends of palm oil with hydrogenated low-erucic rapeseed oil[105,106], palm

kernel olein[81], anhydrous milk fat[38,106] or its low-melting, middle-melting or high-melting fractions[38].

In case the difference in offset temperature of melting between palm oil and the other real lipid was high (≥ 30°C), a monotectic system was formed. Monotectic phase behavior was for example reported in blends of palm oil with low-erucic rapeseed oil[105,106], rapeseed oil[94], the very low-melting fraction of anhydrous milk fat[38], soybean oil[106] and sunflower oil[81].

Furthermore, the phase behavior of hydrogenated and fractionated palm oil in binary blends with other fats has been studied mainly in the context of the search for suitable cocoa butter equivalents. Eutectic behavior was detected in binary blends of the palm mid fraction with sunflower hard stearin, shea stearin[107] and palm kernel oil[108], in blends of hydrogenated palm oil with cocoa butter or milk fat[52] and in blends of palm stearin with palm kernel oil[108]. In accordance with the eutectic systems of other lipids, the difference in offset temperature of melting of the lipids in these blends was also low (< 22°C). Monotectic behavior was reported in binary blends of hydrogenated palm oil with low-erucic rapeseed oil which have a high difference (> 30°C) in offset temperature of melting[105]. A complete solid solution was obtained when blending hydrogenated palm oil with hydrogenated low-erucic rapeseed oil[105].

2.2. PHYTOSTEROLS AND THEIR ESTERS

Phytosterol esters are currently already being used as a food ingredient in modern functional food formulations for their beneficial health effects in terms of reducing circulating cholesterol concentrations. This section first deals with the chemical properties and dietary and commercial sources of phytosterols and their cholesterol lowering activity. Next, the synthesis of phytosterol esters and their food applications are discussed. Addition of phytosterol esters to fat (containing food products) may however influence its crystallization behavior and may thus lead to problems occurring during the production process or with the macroscopic properties of the end product. Consequently, the last part of this section contains an overview of the scarce literature on this topic.

2.2.1. CHEMICAL PROPERTIES

Phytosterols are lipids with a chemical structure similar to cholesterol. As shown in Figure 2.2 they consist of a four-ring steroid nucleus with a hydroxyl group attached to the C-3 atom of the A-ring and an aliphatic side chain attached to the C-17 atom of the D-ring. Due to the junctures between the four rings (A, B, C, D), the steroid nucleus is a flat and rigid system and internal rotation about the C-C bonds in the nucleus is prohibited[34,109].

In this work the term phytosterols is used as a collective noun for plant sterols and plant stanols. Plant sterols mutually only vary in their side chain. Possible side chain variations include the presence of a branched methyl or ethyl group on the C-24 atom and the presence and position of a single double bond[109,110]. These side chain variations lead to differences in melting point and hydrophobicity[5,9,109]. In bulk the plant sterols are solid with high melting points (eg. 140°C for β-sitosterol and 170°C for stigmasterol). Their hydrophobicity is proportional with the number of carbon atoms in the side chain, while side chain double bonds make sterols more hydrophilic[109,111,112]. The most abundant naturally occurring phytosterols are β-sitosterol, stigmasterol, campesterol and brassicasterol (Fig. 2.2).

Plant stanols are the hydrogenation products of the sterols, in which the double bond in the ring and the potential double bond in the side chain are eliminated (Fig. 2.2). Because of the absence of the double bond(s) a stanol has a higher hydrophobicity and higher melting point than its sterol analogue[3,113].

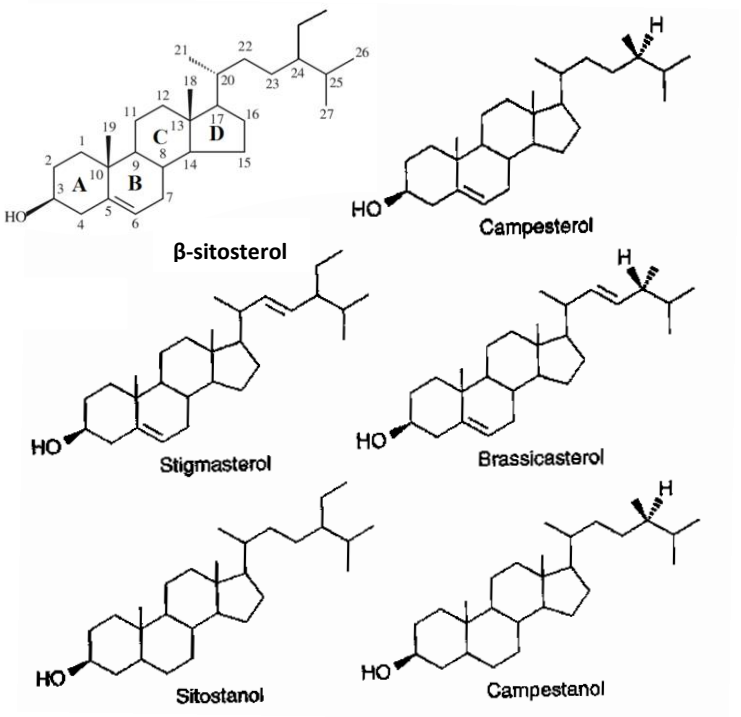

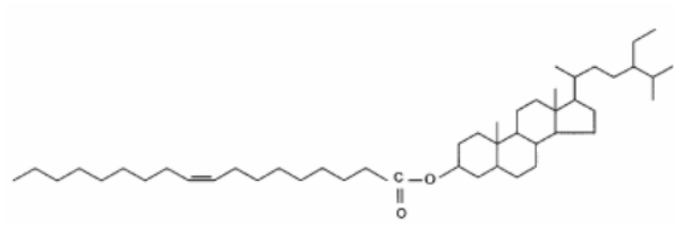

Sitostanol oleate

Figure 2.2. *Chemical structure of some phytosterols and a sterol ester (From Soupas et al., 2005[110] and Weber et al. 2006[114])*

2.2.2. SOURCES OF PHYTOSTEROLS

Phytosterols are not endogenously synthesized in the human body and are therefore obtained exclusively from dietary sources, which are listed in this section. The dietary intake of phytosterols is however not high enough to induce a significant decrease in serum cholesterol levels. One possible method to administer higher amounts of phytosterols is to incorporate commercially available phytosterols into a food matrix[115]. The main existing commercial sources of phytosterols and the synthesis of plant stanols are also discussed below.

2.2.2.1. *Dietary sources and intake of phytosterols*

Phytosterols are typical constituents of plant cells where they exist in free or esterified forms. Free phytosterols form a part of the cell membrane where they play a role in the stabilization of the phospholipid bilayer, whereas phytosterol esters are stored within the cell where they serve as a precursor for the biological production of plant hormones[116,117].

The main dietary sources of phytosterols in Western diets are vegetable oils, nuts and seeds and grains. The plant sterol content in vegetable oils usually ranges from 0.06 to 0.95 g/100 g. Corn and rapeseed oil contain high amounts of phytosterols, 0.69-0.95 g/100 g and 0.25-0.77 g/100g respectively. Palm oil contains a very low amount of plant sterols (0.06-0.08 g/100g). The plant sterol concentration in nuts such as peanuts and almond is about 0.14-0.32 g/100g, while that in cereals such as wheat grain is 0.04-0.18 g/100g. Only low amounts of plant sterols are found in fruit and vegetables (< 0.05 g/100g)[118]. Plant stanols are much less abundant than plant sterols and are mainly found in grains such as wheat, rye and corn in which they make up about 15-20% of the total phytosterol content[109,115,118].

The dietary intake of phytosterols in Western countries has been estimated by different studies and they reported that the average daily intake of phytosterols reaches between 0.20 and 0.40 g/day[119,120] of which the vast majority are sterols[115]. Higher phytosterol intakes are achieved with a vegetarian diet for which phytosterol intakes are almost doubled. However independent from the type of diet the daily dietary intake of phytosterols is not sufficient to benefit from their cholesterol lowering properties[119].

2.2.2.2. *Commercial sources of phytosterols*

On a commercial scale phytosterols can be derived from vegetable oils and from wood. Vegetable oil sterols are obtained as a by-product in the refining of vegetable oils. In the deodorization step of the refining process volatile compounds are distilled from the oil under reduced pressure (1-8 mbar) and steam injection at high temperature (180-270°C) to obtain a mild tasting vegetable oil with a good stability. The by-product of the steam distillation of vegetable oil is the deodorizer distillate (also called deodorizer sludge) and is composed of free fatty acids (30-85%), mono-, di- and triglycerides (5-30%), tocopherols (1-8%), free phytosterols (2-15%) and phytosterol esters (0-5%). The phytosterols are then obtained as a by-product of the isolation of natural tocopherols from the deodorizer distillates and are purified by crystallization from solvents. Among vegetable oils, corn oil, corn fiber oil and soybean oil are most commonly used as a source of phytosterols[116].

Another major source of phytosterols is tall oil, a by-product of the kraft process in which soft woods of the *Pinus* genus are converted into wood pulp ("Tall" is Swedish for "pine", but the term "pine oil" is already being used for the lighter volatile terpene fraction of wood extraction). The main goal of the kraft process is to remove lignin and hemicelluloses from the wood to obtain almost pure cellulose, the main component of paper. This is done by cooking wood chips in an alkaline aqueous solution in a steam heated digester. The pulping process yields paper pulp and a chemical mixture that is called black liquor. Due to the alkaline solution the fatty and resin acids contained in black liquor are converted into their sodium salts (also called soaps). The black liquor is concentrated until the soaps and unsaponifiables are skimmed off as they float to the surface. This skimmed material is known as tall oil soap. Acidulation of the tall oil soap with a mineral acid, usually sulfuric acid, yields an aqueous phase and crude tall oil which contains the unsaponifiables and free fatty acids and resin acids. The fatty and resin acids are separated from the unsaponifiables by distillation of the crude tall oil under high temperatures of at least 300°C. The distillation generates two phases: the so-called depitched phase, a light phase containing mostly volatile fatty and resin acids and the so-called pitch phase, a heavy phase containing the unsaponifiables and a minor amount of less volatile fatty and resin acids. Phytosterols are isolated from the tall oil pitch as well as from the crude tall oil and the tall oil soap. The phytosterol concentration in tall oil soap is 3-5% (w/w), while that in the tall oil pitch ranges from 8 to 20% (w/w)[115,116].

Other alternative, but minor sources of phytosterols are waste products of the fermentation and processing of sugarcane juice in rum factories and cocoa hulls, a by-product of the roasting of cocoa beans[116].

Many different methods have been suggested for phytosterol recovery from the phytosterol sources[116,121,122]. Most of the recovery processes involve separation processes such as supercritical fluid extraction, solvent crystallization, counter current chromatography or enzymatic esterification and have been reviewed by Kumar et al. (2017)[123]. The yearly commercially produced amount of phytosterols was 5000 metric ton in 2012 and is estimated to be 6400 metric ton in 2017[124]. The market price of phytosterols is 13-14€/kg[124], which is about 20 times as high as the market price of palm oil and its fractions, which cost about 0.6-0.8 €/kg[125].

2.2.2.3. *Synthesis of plant stanols*

Although plant stanols are naturally-occurring, the plant stanol concentration in the phytosterol blend obtained from vegetable oils or tall oil is limited to maximum 15%. Starting from the mainly unsaturated phytosterols obtained from the processes described in 2.2.2.2., saturated plant stanols are obtained by hydrogenation[126]. During hydrogenation the double bonds in the plant sterol molecules are saturated

by the addition of hydrogen. This reaction is catalyzed by a noble-metal based catalyst (e.g. Pd or Pt) and is performed under high hydrogen pressure in a suitable solvent[7,113,127]. Plant stanols produced from tall oil phytosterols typically contain about 90% β-sitostanol and 10% campestanol, whereas plant stanols synthesized from vegetable oil phytosterols contain 68-75% β-sitostanol and 25-32% campestanol[126].

2.2.3. CHOLESTEROL LOWERING ACTIVITY OF PHYTOSTEROLS

Cholesterol is a lipid which occurs naturally in our body where it is needed for example for the production of vitamin D, bile salts and different hormones such as testosterone. It is mainly produced in the liver, but is also absorbed from foods such as eggs, meat products and dairy products[128]. When the serum concentration of low density lipoprotein (LDL) cholesterol is too high, it can build up in the arteries, narrowing them and thereby increasing the risk of cardiovascular diseases such as cardial infarction and ischaemic stroke[118,129,130].

Globally a third of the cardiovascular diseases is attributable to raised serum LDL cholesterol levels[2]. According to the World Health Organization, cardiovascular diseases are the number one non-communicable disease causing deaths throughout the globe. Globally about 17.3 million people died in 2008 due to cardiovascular diseases, and this figure is estimated to rise to 23.6 million in 2030. According to the European Heart Network, cardiovascular diseases are the main cause of death in Europe, killing 4.3 million people every year. The American Heart Association reported that in the US in 2007 more than 150,000 people under the age of 65 died due to cardiovascular diseases. These figures are also expected to increase due to the increasing baby boomer population in the US and Europe and the high probability of an older population experiencing the disease[1]. The cholesterol lowering property of phytosterols was first recognized in the early 1950s[131]. Since phytosterols reduce serum cholesterol levels by impairing the absorption of cholesterol in the gastrointestinal tract, the first part of this section focusses on the metabolism of cholesterol and phytosterols, which is fairly similar. Next to the mechanism of action of phytosterols this section also deals with the phytosterol intake recommended to obtain the cholesterol lowering effect, the factors influencing the efficacy of phytosterols in reducing serum cholesterol levels and the safety issues regarding supplementation with phytosterols.

2.2.3.1. *Metabolism*

The absorption sequence of phytosterols is similar to that of cholesterol and is presented schematically in Figure 2.3. After take up potentially esterified phytosterols and cholesterol are hydrolyzed in the duodenum by a pancreatic ester

hydroxylase yielding free phytosterols and free cholesterol. Because the solubility of phytosterols and cholesterol in aqueous systems is low, the absorption depends on their incorporation in mixed micelles[117,118].

The mixed micelles have a hydrophilic surface due to the presence of bile salts and phospholipids and a hydrophobic core containing digestion products of fats such as free fatty acids, monoglycerides, diglycerides, fat-soluble micronutrients (vitamins), free cholesterol and free phytosterols. The mixed micelles carry the solubilized hydrophobic lipids through the aqueous digest medium into close proximity with the intestinal mucosal cells (enterocytes). The mixed micelles are not absorbed as such, but the various components are taken up in the enterocytes at different rates[117,129].

The precise mechanism of cholesterol and phytosterol transport from the mixed micelles into the enterocytes is not yet fully understood, but it probably involves both passive and active transport mechanisms. The latter involves the specific transport binding protein Niemann-Pick C1-like 1 (NPC1L1)[117,118].

From the point of uptake in the enterocytes the metabolism of phytosterols and cholesterol is distinctly different. In the enterocytes both the phytosterols and cholesterol are re-esterified by the enzyme acyl-coenzyme A cholesterol acyl transferase (ACAT) for incorporation in chylomicrons in which they are transported in the blood[118,132]. The intestinal esterification of phytosterols by ACAT is however much less efficient than that of cholesterol. This explains why the absorption of phytosterols from the diet is only between 0.04% and 4% depending on the type of phytosterol, whereas the absorption of cholesterol is about 55% to 60%. As a result, the plasma levels of phytosterols in humans are only about 0.3 – 1.0 mg/dL for plant sterols and 0.01 mg/dL for plant stanols[118], while that of cholesterol can be up to 190 mg/dL in normocholesteremic persons[132].

Unesterified phytosterols and cholesterol are secreted selectively from the enterocyte into the intestinal lumen by the adenosine triphosphate (ATP) binding cassette (ABC) transporters ABCG5 and ABCG8[117,118,132]. Unabsorbed phytosterols may undergo bacterial transformation by intestinal flora[132].

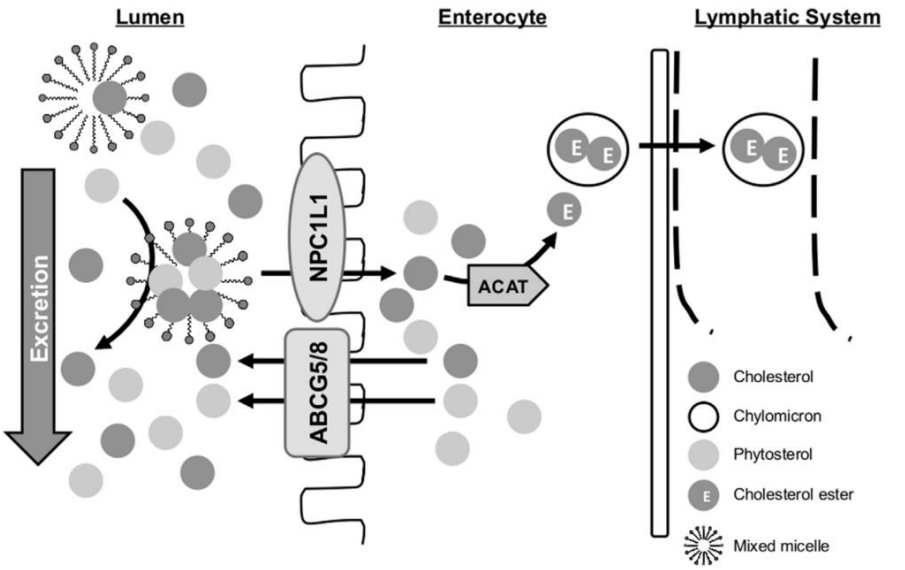

Figure 2.3. *Simplified model of the absorption mechanism of phytosterols and cholesterol. Abbreviations: ACAT: acyl-coenzyme A cholesterol acyl transferase, ABC: adenosine triphosphate binding cassette, NPC1L1: Niemann-Pick C1-like 1 (From Abumweis et al., 2014*[133]*)*

Absorbed cholesterol and phytosterols are transported to the liver via chylomicrons. Once taken up by the liver, phytosterols and cholesterol are incorporated into different types of lipoproteins. Phytosterols are mainly incorporated in high density lipoproteins (HDL) and thereby secreted via the bile, but they can also be secreted into the blood as constituents of LDL[117,129,132]. At the cellular level, phytosterols are stored in the cytoplasm or incorporated into the cell membrane where they play no known biological or functional role. Unlike phytosterols, cholesterol is also synthesized endogenously in the liver by the enzyme 3-hydroxy-3-methyl-glutaryl-coenzyme A (HMG-CoA) reductase[117,118].

2.2.3.2. *Cholesterol-lowering mechanism*

Of the 1.0-1.5 g cholesterol that daily enters the intestinal tract about one third is derived from the diet while the rest comes from the bile. Phytosterols reduce the serum cholesterol levels by interfering with the cholesterol absorption. The decrease in absorption applies to both dietary and endogenously synthesized biliary cholesterol, which explains why phytosterols also have an effect in vegan and vegetarian persons with a low-cholesterol diet[115,132].

Several mechanisms have been described by which phytosterols probably affect cholesterol absorption. The main mechanism is by reducing the incorporation of cholesterol into the mixed micelles due to competition for space in the mixed

micelles and co-precipitation of cholesterol and phytosterols. Furthermore phytosterols may also interfere in the expression of ABCG5/8 thereby increasing the transport of cholesterol from the enterocytes back into the intestinal lumen and in the activity of ACAT resulting in a decrease in chylomicron formation[118]. A decreased cholesterol absorption from the intestine is compensated by an upregulation in the liver which increases both the synthesis of cholesterol in the liver from its precursors and the uptake of cholesterol by increasing the expression of LDL receptors on the liver. This further reduces the amount of cholesterol in the blood[115,132].

Ras et al. (2014) performed a meta-analysis of 124 studies with various phytosterol doses and found that phytosterol intakes of 0.6-3.3 g/d gradually reduce LDL-cholesterol concentrations by 6-12%[119]. Although earlier meta-analyses concluded that the increasing effect on LDL-cholesterol-lowering with an increasing dose of phytosterols tapers off at doses of 2-3 g/d[115,133–135], no such effects were observed in the study of Ras et al. (2014)[119]. Like most other studies the one of Ras et al. (2014) observed comparable cholesterol-lowering effects of plant sterols and plant stanols, although the study of Musa-Veloso et al. (2011)[136] suggested that the maximal cholesterol-lowering effect was larger for plant stanols than for plant sterols.

It is suggested that each reduction in LDL-cholesterol of 1% corresponds to a 1-2% reduction in the relative risk of cardiovascular disease[136], especially for persons with a high cardiovascular risk, like those affected by type 2 diabetes[117]. This is larger than the effect that is expected by reducing the intake of saturated fat[137]. Phytosterols are effective in reducing cholesterol in hypercholesterolaemic patients, as well as in individuals with normal cholesterol levels. Furthermore phytosterol intake has no significant effect on serum HDL-cholesterol levels[118].

Several factors influence the efficacy of phytosterols in reducing the serum cholesterol levels. The optimal effect is achieved when phytosterols are consumed as part of a lipid rich meal as this is necessary to trigger the bile release allowing for optimal competition of the phytosterols with cholesterol for micellar incorporation. The type of food format also seems to have an effect as the cholesterol-lowering efficacy of phytosterols might be lower in liquid foods (drinks) than in solid foods due to a shorter transit time of drinks in the gastrointestinal tract[119].

Furthermore, the efficacy of phytosterols and their esters also depends on the duration and frequency of intake. The serum cholesterol reducing effect becomes apparent after two weeks of daily phytosterol intake but the optimal effect is obtained after 4 weeks[138]. When compared with single doses, multiple daily doses of phytosterols tend to have a greater cholesterol-lowering effect. Based on the mechanism of action, it is hypothesized that multiple daily intake of phytosterols ensures that a continuous supply of phytosterols is available to interact with and

facilitate the excretion of cholesterol. It is therefore recommended that phytosterol enriched products are consumed at least twice a day[133,134].

If phytosterols are combined with other cholesterol lowering medication such as statins, this leads to a greater reduction in serum cholesterol than statins alone because their mechanism of action is different. Statins lower serum cholesterol levels with up to 50% by blocking cholesterol synthesis in the liver by inhibition of HMG-CoA reductase[117,133,139], but they have several undesirable side effects such as muscle pain[140]. Phytosterols can therefore lower the statin dose while still obtaining the same high reduction in serum cholesterol[117,133,139].

2.2.3.3. *Safety*

No major safety concerns with the intake of phytosterols were discovered during clinical trials and meta-analyses. However some studies on phytosterol supplementation have observed a reduction of the levels of carotenoids in the blood (of about 10%) due to suppression of intestinal absorption[133].Therefore it is recommended that consumers of phytosterols eat at least five daily servings of fruit and vegetables to maintain the carotenoid levels within normal limits[117,141]. Although the effects of reduced carotenoid levels in the blood are largely unknown, there could be cause for concern during infancy, pregnancy and lactation, since these phases require higher carotenoid concentrations than normal. Children under the age of 5 years as well as pregnant and lactating women are therefore advised not to consume products with added phytosterols, although cholesterol-lowering is normally not a priority for these groups[142].

2.2.4. SYNTHESIS OF PHYTOSTEROL ESTERS

Phytosterol esters are produced via esterification of phytosterols with fatty acids. The main possible ways to perform this esterification reaction are explained below.

Phytosterol esters are produced via esterification of phytosterols with fatty acids. They consist of approximately 60% by weight of phytosterols and 40% by weight of fatty acids. If the fatty acids are derived from common vegetable oils, the fatty acid composition of the esters is similar to the parent vegetable oil used as a source of the fatty acids[126]. Esterification changes the physical properties of phytosterols from high-melting powders with low fat solubility into semi-liquid substances that are better soluble in fat and therefore easily incorporated in fat containing food products[143].

Phytosterols can be esterified with fatty acids by two different routes which are shown in Figure 2.4: the direct esterification route which uses free fatty acids and the trans-esterification route using fatty acid methyl esters[126]. For both reaction

types a catalyst is used to speed up the reaction and to force the equilibrium of the reversible reaction to the right resulting in a greater yield. Based on the type of catalyst that is used the synthesis methods can be divided into two main categories: the chemically catalyzed and the enzymatically catalyzed reactions.

Chemically catalyzed esterification has some downsides such as high reaction temperatures (170 to 250°C), high energy use and the formation of by-products due to side-reactions[144–146]. Chemically homogeneous catalyzed reactions require an acid or alkaline catalyst which both have their limitations concerning the formation of by-products. Acid catalysts such as sulfuric, phosphoric or p-toluenesulfonic acid may favor the dehydration of sterols to stigmastadienes, while alkaline catalysts like for example potassium hydroxide, sodium hydroxide, sodium methoxide or sodium ethoxide are well known to favor the formation of soaps. Moreover, homogeneous catalysts are difficult to separate from the products. Heterogeneous catalysts like for example lanthanum oxides, magnesium oxides and zinc oxides are known for their high activity, stability and easy recovery[147,148].

Generally, the enzymatic esterification is performed with a lipase (triacylglycerol acylhydrolase, E.C. 3.1.1.3) obtained from diverse kinds of microbial or plant sources. Microbial lipases give a better yield than plant lipases and among the former *Candida rugosa* lipase and *Candida antarctica* lipase A are most suitable for the esterification reaction[5,144–146]. In order to enhance the enzyme properties such as reusability, operational activity and stability and recovery the lipases can be immobilized on a solid carrier material[149]. The most important advantages of enzymatically catalyzed esterification are the mild and environmentally friendly reaction conditions. Large scale application of enzymatically catalyzed esterification is however still limited due to the high costs of the lipases, the lower yield of the reaction and the long reaction time (up to 48h)[148].

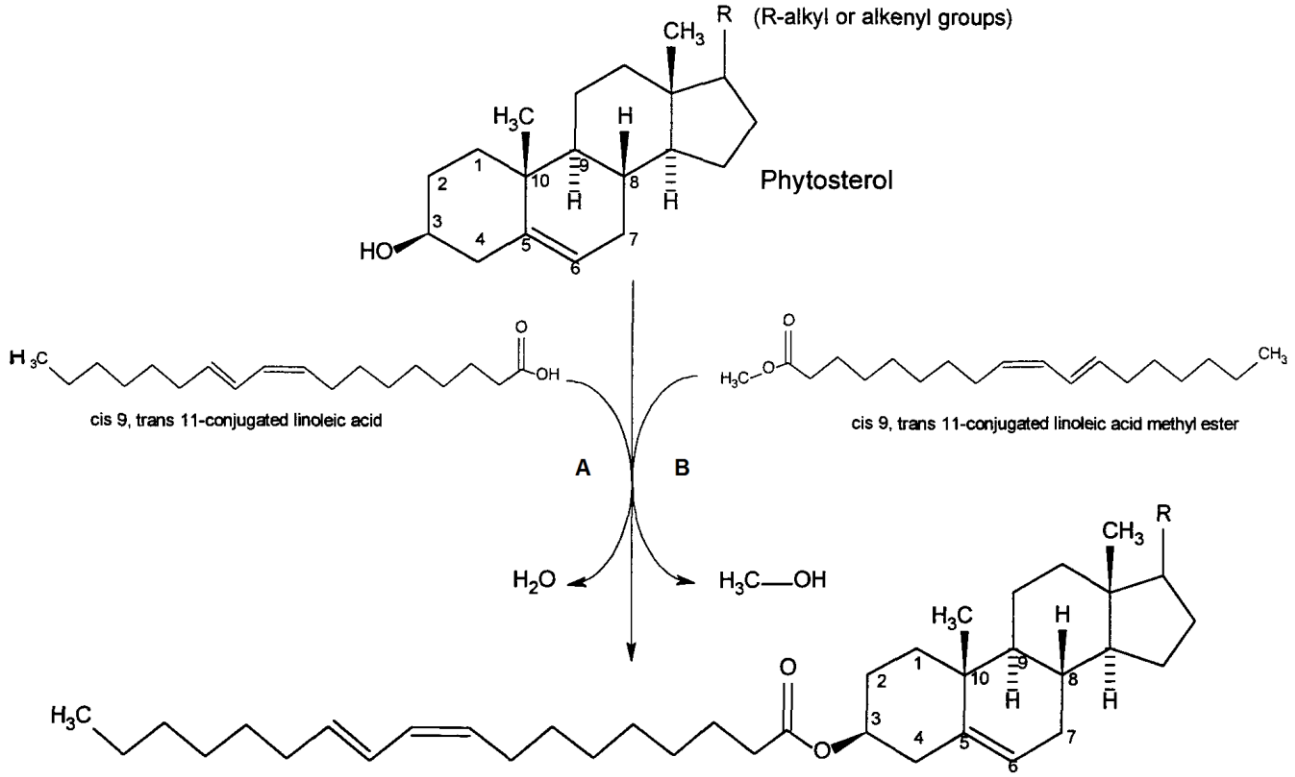

Figure 2.4. *The direct (A) and trans-esterification (B) route for the synthesis of phytosterol esters.*

If an excess of fatty acids or fatty acid methyl esters is used or if the yield of the esterification is not high enough the reaction product might need purification. Potentially present free fatty acids (in case of the direct esterification route) can be removed by distillation, while an excess of methyl esters (in case of the trans-esterification route) can be removed by deodorization[126]. If the yield of the esterification is not high enough fatty acids as well as phytosterols need to be removed from the product. This is mostly done by recrystallization in common organic solvents[3] or by separation by thin layer chromatography on a silica gel plate, although the latter technique is only used in a laboratory context and is not feasible on an industrial scale[5].

2.2.5. FOOD APPLICATIONS OF PHYTOSTEROL ESTERS

Various authorities have approved the use of phytosterols and their esters as a functional ingredient in food products. Details on EU regulations and legislation on the use of phytosterol esters as a functional food ingredient are reviewed in this section as well as the food categories and concentrations in which they are currently applied.

2.2.5.1. *Regulatory status*

The use of phytosterols and their esters as a functional ingredient in various food products has been evaluated globally by various authorities. Positive approval has been obtained in the European Union, the USA, Canada, Switzerland, Norway, Iceland, Turkey, Israel, Australia, New Zealand, Brazil, South Africa and Japan[126,142]. In the European Union sterol esters are only approved by the Novel Food Regulation for use in certain product types, being margarines, spreads, salad dressing, milk type products, fermented milk type products, yoghurt type products, milk based fruit drinks, milk based beverages, soy drinks, rice drinks, cheese type products, spicy sauces, cereal based products and rye bread[150–154]. Before sterol esters can be used in another product type, approval from the Novel Food Regulation will have to be obtained. A novel food or novel food ingredient has no history of significant consumption in the European Union prior to May 15 1997 and can only be placed on the market after a specific authorization procedure which involves a rigorous safety assessment[155,156]. Plant stanol esters and products containing them are excluded from the novel food regulation since they were already on the market before the law came into force.

Based on the advice of the European Food Safety Authority the European Commission has approved the health claim that 'Plant sterols have been shown to lower/reduce blood cholesterol. High cholesterol is a risk factor in the development of coronary heart disease' for several food products being fat spreads, dairy products

such as milk, yoghurt and cheese, mayonnaise and salad dressings. For other food products there is not enough proof of the cholesterol lowering effect[157,158].

Furthermore, in the EU strict labelling regulations are valid for phytosterol based ingredients. The labelling of foods with added sterol esters must contain the statements 'with added plant sterols', 'not intended for people who do not need to control their blood cholesterol level', 'patients under cholesterol lowering medication should only consume the product under medical supervision', 'the product may not be nutritionally appropriate for pregnant and breastfeeding woman and children under the age of five', 'the consumption of more than 3 g/day of added plant sterols should be avoided' and furthermore the amount of plant sterols present and a definition of a portion and the plant sterol amount that each portion contains[159]. The customer should also be informed that a beneficial effect is obtained with a daily intake of 1.5-3 g plant sterols and that the duration to obtain the effect is 2 to 3 weeks[157].

2.2.5.2. *Food categories and use levels*

Nowadays phytosterols and their esters are incorporated into various types of food products produced by a growing number of food manufacturers. The main product formats are fat spreads, yogurts and milk-based drinks[126]. The phytosterol ester concentration in these products is variable and ranges in fat spreads for example from 9 to 15 g/100g product. Fat spreads were the first products enriched with phytosterol esters and up to now they remain the main application. In 1995 Raisio Ltd launched Benecol margarine containing plant stanol esters in Finland. In 1999 Benecol products were also launched in the USA, the UK, Belgium, the Netherlands and Ireland[115]. Since then a number of different types of plant stanol ester enriched food products such as yogurts and salad dressings were also launched. In 2003 the first cereal based food containing plant stanols was Benecol dry pasta and was launched in Finland and later also instant oat meal was marketed[126].

Plant sterol ester enriched spreads were first launched by KKR (former Unilever) in 1999 in the USA under the brand of Take Control, but currently known as Promise active and one year later also in the EU as Pro.activ[115]. Next to KKR also other manufacturers launched sterol ester containing food products, for example Danone (Danacol brand), GFA Foods (Smart balance brand) and Bunge (PhytoBake brand).

2.2.6. CRYSTALLIZATION AND PHASE BEHAVIOR OF PHYTOSTEROL ESTERS

Phytosterol esters are already used as a functional ingredient in fat rich food products such as spreadable fats, cheese and salad dressings. However, addition of phytosterol esters to the fat phase of such food products may lead to problems during the production process or with the macroscopic properties of the end

product. Therefore, this section provides an overview of the scarce scientific and patent publications on the crystallization and phase behavior of phytosterol esters.

2.2.6.1. *Crystallization behavior of pure phytosterol esters*

Several publications described the crystallization and melting behavior of different types of pure phytosterol esters[3–8]. They all reported the melting temperature and melting enthalpy of the phytosterol esters except for Kuksis & Beveridge (1960)[3] who did not report the melting enthalpy since their only analyzing technique was polarized light microscopy. Next to the melting behavior Vu et al. (2004)[5] also described the crystallization behavior of β-sitosteryl laurate.

When comparing the publications, it is most remarkable that the different authors reported (in some cases very) different values for the melting temperatures and melting enthalpies of the same type of phytosterol ester. This can have several explanations. First the analyzing technique influences the measured melting temperature and enthalpy. Kuksis & Beveridge (1960) are the only authors who used polarized light microscopy as the only analyzing technique and they defined the melting point as the temperature at which the material became fully liquid and the field of polarized light turned dark[3]. All other authors used DSC to monitor the melting behavior of the phytosterol esters, but except for Panpipat et al. (2013)[6] they did not specify how they calculated the melting temperature from the DSC melting curve, e.g. if they determined the peak temperature or the offset temperature of melting. Furthermore, also differences in heating rate have a critical influence. Kuksis & Beveridge (1960) reported that upon increasing the heating rate the melting temperature of all the investigated phytosterol esters decreased[3]. Panpipat et al. (2013) used a heating rate of 2.5°C/min for phytosterol esters containing saturated fatty acids and 1°C/min for phytosterol esters containing unsaturated fatty acids, while the other authors used a heating rate of 10°C/min[6]. Next to the heating rate also the crystallization conditions prior to the heating, which influence the melting behavior are different in the different publications.

Secondly, next to the analyzing technique and conditions, also the purity of the phytosterol esters used in the different studies is greatly divergent. Since pure phytosterol esters are not commercially available the phytosterol esters used in the different studies were all synthesized on lab scale by enzymatic[5,6] or chemical[3,7,8] esterification reactions. Due to a varying yield of the esterification reaction the phytosterol esters comprise varying concentrations of reagents (free phytosterols and free fatty acids or fatty acid methyl esters) Kuksis & Beveridge (1960)[3] and Vu et al. (2004)[5] also performed a purification step after the enzymatic synthesis reaction. Leeson et al. (2002)[4] did not mention their synthesis method. The purity of the phytosterol esters is determined by the conversion of the esterification reaction and

the yield of an eventual following purification process. The phytosterol ester purity reported in the publications usually depends on the type of phytosterol ester and is sometimes very high (> 95%)[7,8], but it is rather low (50-99%) in the publication of Kuksis & Beveridge (1960)[3] and very low (8.5-40.3%) in the study of Vu et al. (2004)[5] or even not mentioned[4,6]. When the purity is not high enough the melting temperature of the phytosterol esters can be increased by the presence of free phytosterols as their melting temperature is much higher than that of phytosterol esters[160] or decreased by the presence of free fatty acids or fatty acid methyl esters since their melting temperature is significantly lower than that of phytosterol esters[161].

Despite the above described differences between the studies, some general trends can be deduced. Esterification of phytosterols with fatty acids results in a major decrease in melting temperature. The melting point of the most common phytosterols ranges between 138°C and 170°C[109]. The explanation for the high melting temperature of phytosterols is the intermolecular interaction between the planar cycloalkane rings which leads to a dense molecular packing. Esterification of the phytosterol with a fatty acid disturbs the proper packing between the intermolecular cycloalkane structures resulting in a decrease in melting temperature. For phytosterol esters containing saturated fatty acids the melting temperature decreases with an increasing fatty acid chain length, until a minimum is reached after which the melting points increases again. The reason for this increase is that the elongated fatty acid chain facilitates their molecular alignment and packing[6]. The minimum occurs in the hexanoate-palmitate region depending on the type of phytosterol to which the fatty acids are attached. The increasing trend in melting temperature continues up to phytosteryl stearate, but the melting temperature of the analyzed phytosterol esters is still lower than that of the free phytosterols. Phytosteryl oleate melts 34-64°C lower than the phytosteryl stearate and the introduction of additional double bonds brought about further lowering in the melting point[3,4,6]. It was stated that for phytosterol esters containing unsaturated fatty acids the fatty acid chain has more influence on the melting temperature than in phytosterol esters containing saturated fatty acids since the unsaturated fatty acid segment of the molecule seriously frustrates the crystal packing[6].

Next to the type of fatty acid, the melting temperature also depends on the type of phytosterol in the phytosterol ester. Khare (2002)[8] and Wester (1997)[7] showed that the melting temperature of stanol esters is higher than their corresponding sterol esters. The results of Kuksis & Beveridge (1960)[3] were contradictory with this, but due to the rather low purity of their phytosterol esters their results may be less reliable. Kuksis & Beveridge (1960) also reported that phytosterol esters containing

β-sitosterol had a slightly lower melting temperature than those containing stigmasterol.

The melting enthalpy of phytosterol esters generally decreases with an increasing degree of unsaturation of the fatty acid chain, but different trends are reported on the effect of fatty acid chain length[4,6]. As a function of an increasing fatty acid chain length Leeson et al. (2002)[4] observed an increase of the melting enthalpy, while Panpipat et al. (2013)[6] reported a parabolic curve of the melting enthalpy as a function of chain length with a maximum at phytosteryl myristate.

Finally, Leeson et al. (2002)[4] observed that phytosterol esters containing certain fatty acids formed liquid crystals. Liquid crystals are partially ordered, anisotropic fluids, with thermodynamic properties located between the three dimensionally ordered solid state and the isotropic liquid state. The liquid crystalline phase is often called "mesophase", derived from the Greek word *meso*, meaning "in between" (the crystalline and the liquid phase). In general the occurrence of a mesophase in lipids depends on the temperature[162]. They reported that they observed the formation of a mesophase in β-sitosteryl oleate and linoleate and in β-sitosteryl esters containing short-chain fatty acids. Unfortunately they do not mention at which temperature (range) the mesophases were observed nor do they describe how they detected the mesophases (in the DSC thermograms)[4]. The formation of mesophases has been described for other lipids which are comparable to phytosterol esters, for example in cholesteryl esters[34,42,163] and ergosteryl esters[164].

2.2.6.2. *Crystallization and phase behavior of binary mixtures of phystosterol esters*

The crystallization and phase behavior of binary mixtures of pure phytosterol esters was investigated twice up to now. Leeson et al. (2002) focused on the phase behavior of binary blends of pure phytosterol esters and constructed phase diagrams based on the melting temperatures and melting enthalpies calculated from the DSC thermograms. They reported that blends of β-sitosteryl esters containing short-chain fatty acids, blends of β-sitosteryl stearate with β-sitosteryl oleate and blends of β-sitosteryl stearate with β-sitosteryl esters containing short-chain fatty acids all show eutectic behavior. Only the blend of β-sitosteryl stearate with β-sitosteryl linoleate showed continuous solid solution phase behavior. Furthermore β-sitosteryl linoleate, β-sitosteryl oleate and β-sitosteryl esters containing short-chain fatty acids formed mesophases in their pure form and except for β-sitosteryl oleate oleate also after addition of 10% or more β-sitosteryl stearate[4].

Wester (1997)[7] synthesized plant sterol and plant stanol esters with fatty acids derived from real vegetable oils and fats. The phytosterol esters in their study were

therefore not pure but a mixture on their own containing different types of plant sterols or plant stanols esterified to different types of fatty acids. They focused on the melting behavior of phytosterol esters and binary blends thereof by determining the SFC using pNMR at different temperatures. Based on the SFC profile they stated that stanol esters and blends of sterol and stanol esters (15:85 and 25:75) with fatty acids derived from rapeseed oil are useful as a substitute for hardstock in spreadable fats. The sterol esters with fatty acids derived from rapeseed oil had too low SFC profiles to be used as a replacement for the hardstock. However, by optimizing the fatty acid composition of the sterol esters the desirable SFC profile could be obtained by using sterol esters with fatty acids derived from a fat blend of rapeseed oil with 10-30% palm oil or coconut oil.

2.2.6.3. *Crystallization behavior of binary mixtures of phytosterol esters and fats*

The influence of the addition of phytosterol esters on the physical properties of edible fats has been investigated only a few times before. Vu et al. (2004) showed that pure β-sitosteryl laurate added to liquid corn oil caused unwanted crystallization above a certain threshold concentration[5]. Rodrigues et al. (2007) investigated how the crystallization behavior of milk fat was changed by blending with a commercial mixture of phytosterol esters. They showed that adding phytosterol esters containing mainly linoleic acid to milk fat induces a softer consistency and a lower SFC[9]. Wester (1997) examined the SFC profiles of blends of rapeseed oil with stanol esters containing fatty acids of rapeseed oil. If less than 30% stanol esters were added to rapeseed oil the addition of extra hard stock was needed to obtain a fat blend with an SFC that is high enough for application in spreadable fats. The desirable SFC profile could also be obtained by adding sterol esters instead of stanol esters to rapeseed oil, but only if the fatty acids in the sterol esters were derived from a blend of rapeseed oil with 10-30% palm or coconut oil[7].

Based on this literature review it was decided to first investigate the effect of adding a commercial phytosterol ester (PE) mixture containing different types of phytosterols esterified to fatty acids which vary in chain length and chain saturation on the phase behavior of palm oil (PO) (Part II). The main reason to use a commercial PE mixture was to get a general insight in the phase behavior of PEs as the information in literature on this topic is very limited. Starting with a commercial PE mixture also allowed time to optimize and perform the labor-intensive synthesis and purification of pure PEs. For characterization of the blends of the commercial PE mixture with PO the non-isothermal phase behavior was investigated in chapter 3. The phase behavior of the blends was also investigated under industrially more relevant conditions. In chapter 4 it was studied how PE addition influences the phase behavior of PO that was brought in the 'equilibrium' crystallization state by tempering at 10°C for 48h. These results enabled to evaluate how PE addition

changes the properties of the end product. To assess the potential impact under processing conditions, the isothermal crystallization behavior of PO after addition of PEs was investigated in chapter 5. In Part III pure PEs containing different types of fatty acids were synthesized by enzymatic esterification. The pure PEs were used to obtain a more fundamental insight in the phase behavior of PEs as such and in blends with PO.

PART II
EFFECT OF ADDING A COMMERCIAL PHYTOSTEROL ESTER MIXTURE ON THE CRYSTALLIZATION, MELTING AND PHASE BEHAVIOR OF PALM OIL

CHAPTER 3
EFFECT OF ADDING A COMMERCIAL PHYTOSTEROL ESTER MIXTURE ON THE NON-ISOTHERMAL CRYSTALLIZATION AND MELTING BEHAVIOR OF PALM OIL

This chapter is based on the following publication:
Daels, E., Foubert, I & Goderis, B. (2017). The effect of adding a commercial phytosterol ester mixture on the phase behavior of palm oil. Food Research International, 100, 841-849.

3. EFFECT OF ADDING A COMMERCIAL PHYTOSTEROL ESTER MIXTURE ON THE NON-ISOTHERMAL CRYSTALLIZATION AND MELTING BEHAVIOR OF PALM OIL

3.1. INTRODUCTION

Based on the literature review in chapter 2 it was decided to investigate the non-isothermal crystallization and melting behavior of a commercial phytosterol ester (PE) mixture in blends with palm oil (PO). To our knowledge, the influence of the addition of PEs on the physical properties of edible fats has only been reported twice in the literature. Vu et al. (2004)[5] showed that self-made PEs with a high lauric acid content added to liquid corn oil caused unwanted PE crystallization above a certain threshold concentration. Rodrigues et al. (2007)[9] investigated how the crystallization behavior of milk fat was changed by blending with a commercial mixture of PEs. They showed that adding PEs to milk fat induced a softer consistency and a lower solid fat content (SFC). These authors however, did not report any information on the melting and polymorphic behavior of the pure substrates nor were their blends since no differential scanning calorimetry (DSC) or X-ray diffraction (XRD) analyses performed. Furthermore, PEs were only added in two different concentrations giving only a limited insight into the phase behavior of PE blends with milk fat.

In this chapter a commercially available mixture of PEs containing different types of phytosterols esterified to different types of fatty acids was added to PO in the full concentration range of 0 to 100% PEs to obtain insight into the phase behavior of the blends, although the concentration range of PEs that is applied in the fat phase of most of the existing cholesterol lowering fat rich food products is 10 to 50%. Based on DSC and time-resolved synchrotron XRD measurements the different crystal structures as a function of temperature and PE concentration were mapped. The results of this chapter were necessary to provide the necessary background to investigate and understand PE loaded PO systems in a more practical context in the next chapters.

3.2. MATERIALS AND METHODS

3.2.1. MATERIALS

The same PO and a commercial PE mixture donated by Unilever (Vlaardingen, The Netherlands) were used for the experiments in this PhD. The esterification oil used for the synthesis of the PE mixture was sunflower oil. The degree of esterification in

the commercial PE mixture was 97.7 ± 1.1% as was confirmed by solid phase extraction performed as described in Panpipat et al. (2013)[145]. Table 3.1 reports the sterol composition of the commercial PE mixture as measured by the method described in Ryckebosch, Bruneel et al. (2012)[165]. In general wood sterol esters have a higher β-sitosterol (up to 80%) and lower campesterol (up to 10%) content than vegetable oil sterol esters, which contain up to 60% sitosterol and up to 30% campesterol[117]. The high β-sitosterol composition (about 78%) of the commercial PE mixture indicates tall oil was probably the origin of the phytosterols used for its synthesis Table 3.2 shows the fatty acid composition of PO and the commercial PE mixture as determined by the method described in Ryckebosch, Muylaert, & Foubert (2012)[166]. The fatty acid composition of the commercial PE mixture was indeed very similar to that of sunflower oil as reported in literature[81]. Table 3.3 depicts the triglyceride composition of the PO used. It was analyzed in a high-performance liquid chromatograph (HPLC) (Waters, Belgium) on a NOVA-Pak C18 column (4 µm, 150 × 3.9 mm; Waters, Belgium) at 30°C with acetonitrile–acetone (37.5:62.5, v:v) as the mobile phase. The HPLC was coupled with a refractive index detector (Waters, Belgium) set at 40°C. PO was solubilized in a solvent mixture (1:1 methanol:chloroform) at a concentration of 20 mg/mL and injected in duplo (20 µL). The fatty acid profile and the triglyceride profile of PO were in good agreement with other studies[70].

Table 3.1. *Sterol composition (%) of the commercial phytosterol ester mixture. The values show the average of two measurements. The error is 0.2%.*

Sterol	
Brassicasterol	1.3
Campesterol	10.0
Stigmasterol	0.6
β-sitosterol	78.5
β-sitostanol	9.7

Table 3.2. *Fatty acid composition (%) of palm oil and the commercial phytosterol ester mixture. The values show the average of three measurements. The error is 0.2%.*

Fatty acid	Palm oil	Phytosterol ester mixture
C14:0	1.0	-
C16:0	45.4	6.6
C18:0	4.3	3.8
C18:1	39.6	29.8
C18:2	9.8	59.7

Table 3.3. *Triglyceride composition (%) of palm oil. The values show the average of two measurements. The error is 0.02%. Abbreviations: L: linoleic acid, O: oleic acid, P: palmitic acid, M: myristic acid, S: stearic acid.*

Triglyceride	
PLL	2.71
MLP	0.67
OOL	1.87
POL	10.97
PLP	10.54
OOO	3.62
POO	23.14
POP	31.42
PPP	5.15
SOO	2.49
POS	5.64
PPS	1.08
SOS	0.70

3.2.2. BLEND PREPARATION

Binary blends of PEs and PO were prepared with a PE concentration from 0 to 100% with intervals of 10% for the DSC measurements and 20% for the time-resolved synchrotron XRD analyses. The blends were prepared after complete melting of the pure substrates at 80°C for 30 min under continuous stirring. The blends were visually homogeneous and stable, indicating that no liquid-liquid phase separation occurred.

3.2.3. DIFFERENTIAL SCANNING CALORIMETRY

The DSC experiments were performed using a DSC Q2000 (TA Instruments, Brussels, Belgium) equipped with an autosampler and nitrogen as a purge gas. Sapphire and indium were used for the baseline and heating rate calibration and an empty pan was used as a reference. About 10-20 mg of melted lipids was sealed into a hermetic aluminum pan (TA Instruments, Brussels, Belgium). The following time-temperature program was used: equilibration at 80°C for 15 min to ensure complete melting and to erase the crystal memory, followed by cooling at 5°C/min to -55°C to induce crystallization, subsequently holding at -55°C for 5 min and finally heating at 5°C/min to 80°C to obtain the melting profile. Each measurement was repeated five times. The crystallization onset temperature (T_{c_onset}) of different peaks in the crystallization curve was determined by the intersection of the baseline of the crystallization curve with the absolute highest tangent at the high temperature side of the crystallization peak. The melting offset temperature (T_{m_offset}) of different peaks in the melting curve was determined as the intersection of the baseline in the melting curve with the absolute highest tangent at the high temperature site of the melting peak.

3.2.4. TIME-RESOLVED SYNCHROTRON X-RAY DIFFRACTION

Time-resolved synchrotron XRD experiments were performed at DUBBLE, the Dutch-Belgian beamline (BM26) at the European Synchrotron Radiation Facility (ESRF; Grenoble, France). SAXS and WAXD patterns were recorded simultaneously using a wavelength, λ, of 1.033 Å. The beamline was equipped with a two-dimensional Pilatus 1 M detector to capture the SAXS signals and a Pilatus 300 K detector to gather the WAXD data. The scattering angles were calibrated with silver behenate and high-density polyethylene standards.

About 10-20 mg of melted lipid was sealed into a hermetic aluminum pan (TA Instruments, Brussels, Belgium) and loaded onto a temperature-controlled sample stage (Linkam HFS 191, Tadworth, UK). The same time-temperature program was used as for the DSC measurements (section 2.3). During the cooling and heating period SAXS and WAXD patterns were collected simultaneously in consecutive 12 s time frames. Each time frame consisted of 11.985 s measuring time and 0.005 s data saving. The 2D SAXS and WAXD data were azimuthally averaged using the program ConeX[167], normalized to the intensity of the incoming beam measured by a photodiode placed downstream from the sample and corrected for the scattering of an empty setup, including the DSC pan scattering. The WAXD data were further corrected by subtracting a straight line connecting the scattered intensities around 6.5 and 22.0° 2θ. This extra correction approaches the background scattering. In a next step the WAXD data were normalized to their integrated intensity, which yields scattered intensities due to identical scattering masses. This approach compensates

for possible changes in scattering mass by e.g. melt flow at high temperatures which might lead to different amounts of material in front of the beam. The WAXD normalization factors were also used to normalize the SAXS patterns for the same effect. The scattering angle 2ϑ ranged from $0.48 < 2\vartheta < 7.29°$ for SAXS and $6.63 < 2\vartheta < 21.9°$ for WAXD. The observed SAXS and WAXD spacings were temperature dependent. The reported spacings of the different crystal structures are those observed at the end of the cooling stage (at -54.5°C). If crystal structures only formed during heating, spacings were read at 25.8°C.

3.3. RESULTS AND DISCUSSION

3.3.1. DIFFERENTIAL SCANNING CALORIMETRY

3.3.1.1. *Palm oil*

Figures 3.1 and 3.2 show the DSC cooling and heating runs of pure PO, the pure PEs and their blends. The results of pure PO were very similar to those reported in earlier studies that used the same cooling and heating rates[80,99,100]. The cooling run of pure PO exhibited two well separated exothermic peaks with the high and low-temperature peak due to the crystallization of a high-melting fraction (HMF) and a low-melting fraction (LMF) respectively. HMF and LMF are sometimes labelled as the stearin (or "hard") and the olein (or "soft") fraction since the former is rich in disaturated and trisaturated triglycerides, while the latter contains more diunsaturated and triunsaturated triglycerides[80,82,87,168]. T_{c_onset} of HMF and LMF were 19.9 ± 0.3°C and 7.7 ± 0.1°C respectively.

The bimodal crystallization behavior was also mirrored in the subsequent heating run, exhibiting two endothermic melting peaks with a clear exothermic event in between, suggesting recrystallization or additional crystallization of the HMF during the heating run. Although the high-temperature peak in the cooling run was very sharp, its melting endotherm in the heating run showed a severe amount of broadening over a temperature range of about 25°C. This could be expected since the composition of the melt is changing during the course of melting. The rather narrow high-temperature crystallization peak is a kinetic effect, as a result of nucleation being postponed to lower temperatures. Once triggered, the crystallization proceeds very rapidly, i.e. over a narrowed temperature interval. It is also clear that the enthalpy of the (broad) high-temperature melting peak was much larger compared with the high-temperature crystallization peak. This is likely due to how the HMF changed in nature or magnitude during the exothermic (re)crystallization during heating. The low-temperature endotherm also showed some broadening, as expected. T_{m_offset} of the HMF was 40.8 ± 0.4°C while that of the LMF was 16.7 ± 0.2°C indicating that the degree of supercooling was much higher for

the HMF compared to the LMF. Note that the actual T_{m_offset} for the LMF could be situated at somewhat higher temperatures because this part of the signal is obscured by the overlapping exothermic heat in this temperature range. Be that as it may, this effect would at most reduce the difference in supercooling and not eliminate it.

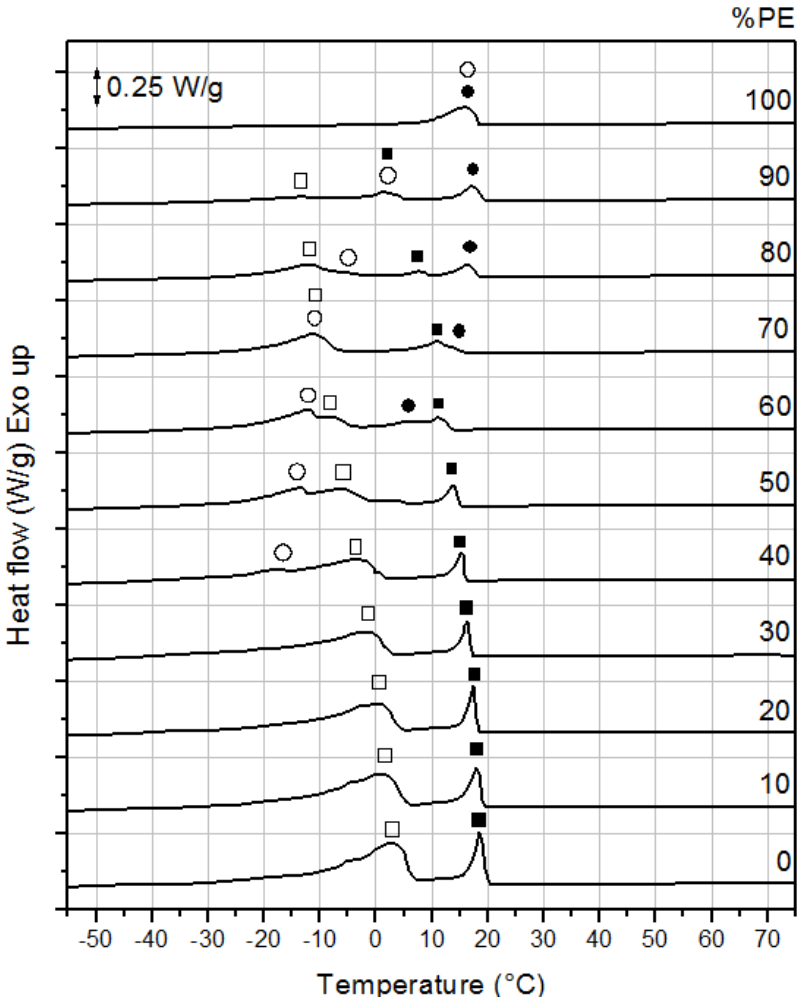

Figure 3.1. *DSC cooling runs of the blends of palm oil with the commercial phytosterol ester (PE) mixture. PE concentrations (%PE) are reported above each curve at the right-hand side of the figure. Peak maxima of the most likely polymorphic forms are indicated with different symbols above the peak: HMF_α (■), LMF_β2' (□), PE_x (●) and PE_y (○) based on the morphology map of cooling. Abbreviations: HMF = high-melting fraction and LMF = low-melting fraction.*

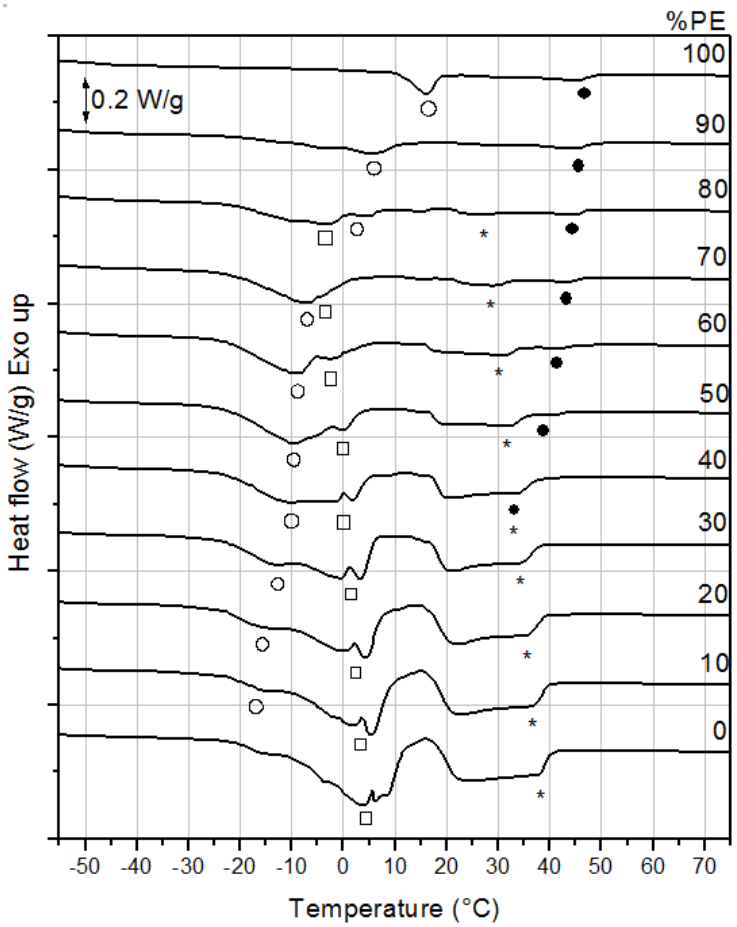

Figure 3.2. *DSC heating runs of the blends of palm oil with the commercial phytosterol ester (PE) mixture. PE concentrations (%PE) are reported above each curve at the right-hand side of the figure. Peak maxima of the most likely polymorphic forms based on the morphology map of heating are indicated with different symbols above the peak: HMF_ β₁′ (*), LMF_β₂′ (□), PEₓ (●) and PEᵧ (○). Abbreviations: HMF = high-melting fraction and LMF = low-melting fraction.*

3.3.1.2. *The commercial phytosterol ester mixture*

The DSC cooling run of the pure PEs contained one crystallization peak with an onset of 18.3 ± 0.0°C, while the heating profile contained two melting peaks, a sharper one with a peak maximum at 16.4 ± 0.1°C and a very broad, plateau-shaped one with a temperature range of about 30°C and an offset temperature of 48.7 ± 0.2°C. Whether or not an exothermic event occurs in between the endothermic signals cannot be determined from the DSC data. The fact that no such signal is clearly seen,

does not mean that it is absent. It could be that its magnitude is too small to overcome the endothermic heat with which it might overlap. XRD measurements are required to further explain the thermal behavior of this material. The plateau nature of the high-temperature melting peak reflects the fact that this product is a mixture, just like PO is.

3.3.1.3. *Blends of palm oil with the commercial phytosterol ester mixture*

For the PE-PO blends, it can be seen in Figure 3.1 that the DSC cooling runs of the blends with a low PE concentration (≤ 40%) were very similar to the cooling runs of pure PO. From a PE concentration of 50% the crystallization peaks of the HMF and the LMF of pure PO became less dominant since the PE crystallization peaks became more distinct and modified the shape of the cooling curve. Interpreting the data in terms of two PE crystallization peaks is justified because the XRD data (to be discussed in section 3.3.2) revealed that the single crystallization peak of the pure PEs in fact contained two overlapping transitions which split over the temperature domain in blends with PO. As the PE concentration increased, T_{c_onset} of the blends gradually decreased reaching a minimal value of 13.4 ± 0.2°C at a PE concentration of 60%. From a PE concentration of 70% T_{c_onset} gradually increased again to the T_{c_onset} value of the pure PEs. Correspondingly, Figure 3.2 shows that the DSC heating runs of the blends with a low PE concentration (≤ 40%) were very similar to the heating run of pure PO since the main peaks were those corresponding to the melting of the HMF and LMF of PO with an exothermic peak in between. From a PE concentration of 50% onwards other peaks started to occur and the high-temperature peak was stretched out at the high-temperature side. This plateau-shaped peak became bigger with increasing PE concentration and was most likely due to the melting of PEs (confirmed with XRD in section 3.3.2). The observed trend in T_{m_offset} of the PE-PO blends was analogous to that of T_{c_onset}, however the minimal value of T_{m_offset} was reached at a PE concentration of 40% and equaled 37.2 ± 0.4°C.

3.3.2. TIME-RESOLVED SYNCHROTRON X-RAY DIFFRACTION

3.3.2.1. *Palm oil*

The different polymorphic forms can only be unambiguously identified by XRD. The simultaneously collected SAXS and WAXD diffraction patterns of the pure PO and the pure PEs during cooling and heating are shown in Figure 3.3 together with the corresponding DSC cooling and heating runs. The XRD patterns of pure PO were similar to those described for non-isothermal crystallization of PO in literature.

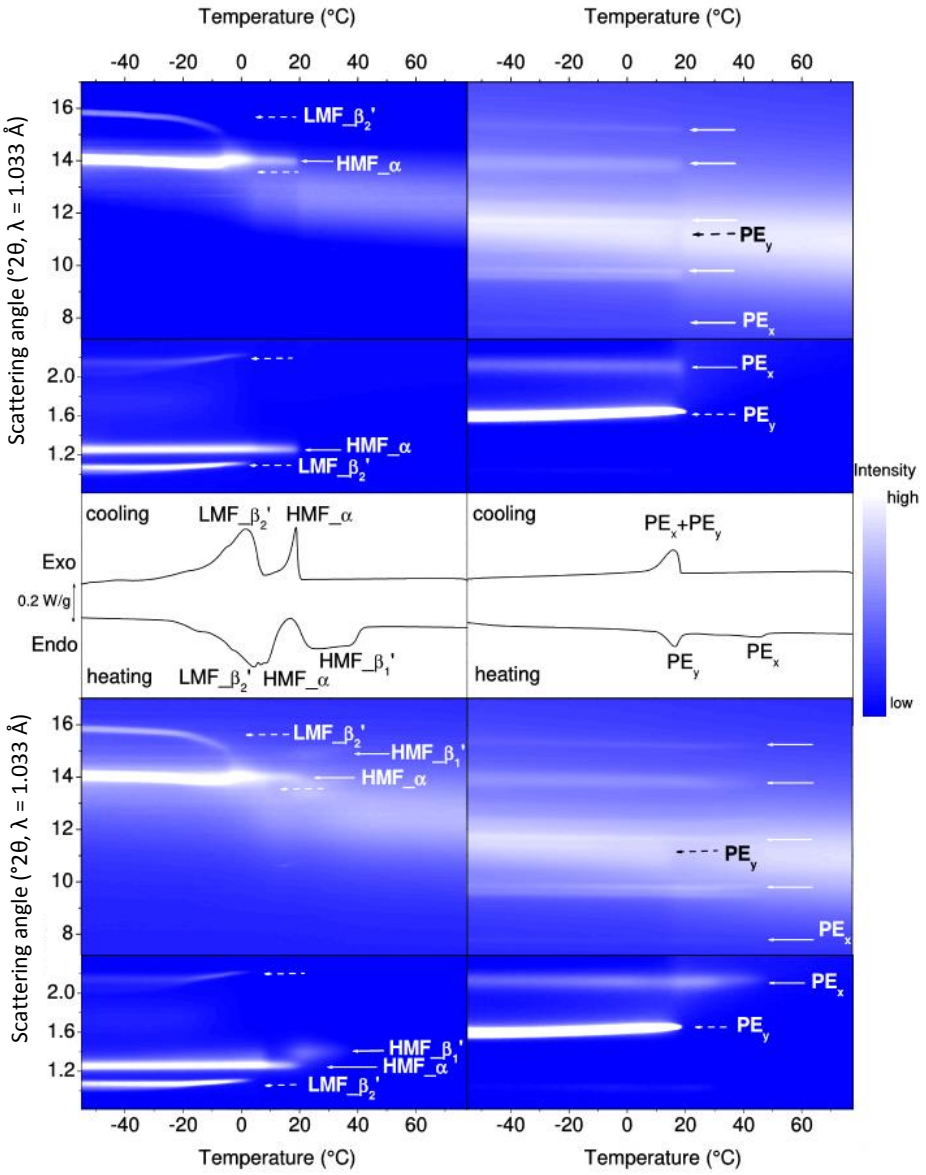

Figure 3.3. *WAXD, SAXS and DSC data for pure palm oil (PO, left) and the pure commercial phytosterol ester mixture (PE, right) during cooling (upper part) and heating (lower part). The WAXD and SAXS intensities are color coded. The DSC heat flow data are depicted upward for the cooling runs and downward for the heating runs. Different polymorphic forms are indicated on the WAXD and SAXS patterns with arrows and on the DSC runs. Abbreviations: HMF = high-melting fraction and LMF = low-melting fraction.*

During cooling, from 20.4°C the SAXS pattern showed one peak at 2θ = 1.27° (d = 46.7 Å) and the WAXD pattern had one peak at 2θ = 14.0° (d = 4.23 Å). This short spacing is characteristic for the hexagonal subcell packing of PO in the α-polymorph, while the long spacing corresponds to the first order reflection of a double chain length (2L) structure[87,169].

During further cooling, from a temperature of 4.5°C two extra peaks occurred in the SAXS pattern: a strong peak at 2θ = 1.08° (d = 54.6 Å) and a weak peak at 2θ = 2.17° (d = 27.3 Å). These peaks correspond to the first (54.6 Å) and second order (27.3 Å) reflections of a triple chain length (3L) structure. At the same temperature the WAXD pattern showed one strong peak at 2θ = 14.1° (d = 4.21 Å) coinciding with the short spacing of the α-polymorph and one medium peak at 2θ = 15.9° (d = 3.74 Å). These short spacings are characteristic for the orthorhombic subcell packing of PO in a β_2' polymorph[170]. In PO, β' exhibits two sub forms which have a different thermodynamic stability and different melting points and are labelled with a subscript number that increases with decreasing stability. β_2' is the low-melting and less stable form of β'[171], which is formed during cooling from about 5°C[97,171]. Another study labelled a crystal structure of PO with very similar spacings and formed below 0°C after rapid cooling at 25°C/min, the sub-α structure[87].

When comparing these XRD results with the DSC cooling run, the peaks of the 2Lα polymorph in the XRD patterns coincided with the crystallization peak of the HMF of PO in DSC, while the XRD peaks of the 3Lβ_2' polymorph corresponded to the crystallization of the LMF of PO in DSC. Therefore, in the remaining part of this chapter these two polymorphic forms of PO are referred to as HMF_α and LMF_β_2'.

The XRD patterns of pure PO during heating revealed that LMF_β_2' was fully melted at 5.8°C since the XRD peaks completely disappeared at this temperature. Furthermore, from 10.8°C HMF_α started to recrystallize in a 2Lβ_1' polymorphic form since emerging peaks were observed at 2θ = 1.4° (d = 42.4 Å) in the SAXS pattern and at 2θ = 13.4° (d = 4.41 Å), 2θ = 13.9° (d = 4.28 Å) and 2θ = 14.7° (d = 4.03 Å) in the WAXD pattern[87,93]. β_1' is the high-melting and more stable β' form and is referred to as HMF_β_1' in this study[87,103,171]. The polymorphic transition from HMF_α to HMF_β_1' was also visible as an exothermic signal in DSC and was complete at 20.8°C. The fact that this transition occurred at temperatures *below* the HMF_α crystallization temperature implies that this is a solid-solid transition rather than a process involving full melting and recrystallization[20]. Indeed, on thermodynamic grounds, a material cannot melt at temperatures below its crystallization temperature. Literature reported the same transition from HMF_α to HMF_β_1' when PO is kept isothermally at a temperature between 10°C and the HMF_α crystallization

temperature for a longer period of time[32,99,102,172]. Upon further heating HMF_β_1' melted and PO was fully liquid above 42.8°C.

Some authors also reported a partial transition from β_1' to β in PO during heating based on DSC melting points[103] or the occurrence of a very weak WAXD peak at d = 4.58 Å[87]. In this study no clear β1' to β transition could be observed in SAXS nor WAXD, maybe because the peak intensity associated with the β phase was below the detection limit. In summary, the XRD data relate well to the DSC heating run of pure PO with the first endotherm corresponding to the melting of LMF_β_2', the subsequent broad exothermic peak being related to the solid-solid polymorphic transition of HMF_α to HMF_β_1' and ultimately the high-temperature endothermic peak being due to the melting of HMF_β_1'.

3.3.2.2. *The commercial phytosterol ester mixture*

The right side of Figure 3.3 shows the XRD results for the pure PEs. In the SAXS pattern during cooling from 19.4°C two distinct peaks were observed: a weak peak at 2θ = 2.11° (d = 28.1 Å) and a very strong peak at 2θ = 1.60° (d = 37.0 Å). Figure 3.4A shows a more detailed SAXS pattern of the pure PE at -54.5°C. A further two weak peaks at 2θ = 1.05° (d = 56.2 Å) and 2θ = 3.21° (d = 18.5 Å) were present that are not visible in Figure 3.3 due to the very high intensity of the peak at 37.0 Å and the color scale used. In the WAXD pattern of the pure PEs during cooling (Figure 3.3) one weak broad peak at 2θ = 11.3° (d = 5.24 Å) and five weak to medium-strong sharper peaks at 2θ = 7.75° (d = 7.63 Å), 2θ = 9.69° (d = 6.10 Å), 2θ = 11.6° (d = 5.10 Å), 2θ = 13.9° (d = 4.29 Å) and 2θ =15.2° (d = 3.92 Å) emerged from 19.4°C. However, the peak at 4.29 Å was also less sharp and could be composed of two partially overlapping peaks. The more detailed WAXD pattern of the pure PEs plotted in Figure 3.4B shows four more peaks at 2θ = 9.51° (d = 6.23 Å), 2θ = 10.3° (d = 5.76 Å), 2θ = 12.1° (d = 4.89 Å) and 2θ = 12.7° (d = 4.65 Å) which were very weak and therefore not visible in Figure 3.3. Unlike most triglyceride fats, the PEs showed WAXD peaks at unusually low 2θ values which therefore, do not overlap with the WAXD peaks of PO and thus allow for an unambiguous PE identification in blends with PO.

During heating the SAXS peak in Figure 3.3 at 37.0 Å disappeared at 19.9°C, while the one at 28.1 Å disappeared at 48.9°C which indicated that the SAXS peaks were linked to two different crystal structures with different melting temperatures although during crystallization they occurred at the same temperature. For the identification of the WAXD and SAXS peaks of the pure commercial PE mixture, the triglyceride terminology cannot be applied since the molecular structure of PEs is too different from the triglyceride structure. Moreover, as far as we are aware, XRD data on PEs have not been reported before in literature. Therefore, the crystal structures linked to the SAXS peaks at 28.1 Å and 37.0 Å are referred to as PE_x and PE_Y respectively. It

is also clear that the SAXS peak at 28.1 Å in Figure 3.3 is actually a second order reflection of PE_x with a first order reflection at 56.2 Å as can be seen in the more detailed SAXS pattern in Figure 3.4A. Furthermore, based on the temperature at which the reflections disappeared during heating the single WAXD peak at 5.24 Å can be linked to PE_y, while the other five short spacings correspond to PE_x.

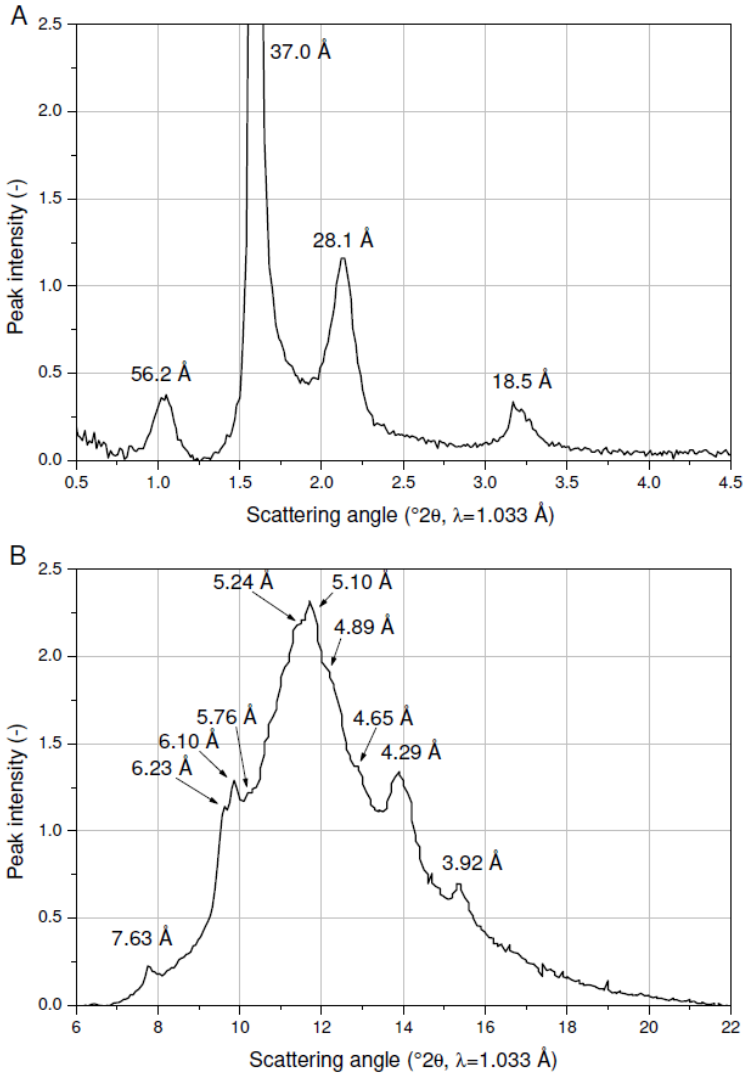

Figure 3.4. *SAXS (A) and WAXD (B) diffraction pattern of the pure commercial phytosterol ester mixture at -54.5°C with indicated d-spacings.*

When comparing these XRD results with the DSC runs, it is apparent that the single peak in the DSC cooling run coincides with the simultaneous crystallization of PE_x and PE_y, while the low-melting and high-melting peaks in the DSC heating run correspond

to the respective melting of PE_Y and PE_X. Relying on the melting points of pure PEs reported by Leeson et al. (2002)[4] combined with the fatty acid profile of the PEs (Table 3.2) our hypothesis is that PE_X contains mainly stearic and palmitic acid esterified to the phytosterols while phytosteryl oleate is the predominant PE in PE_Y. Linoleic acid based PE, although being predominantly present, most likely did not crystallize since according to Leeson et al. (2002)[4] pure β-sitosteryl linoleate already has a very low melting temperature (-5°C), falling below that of PE_Y.

From Figure 3.3 it could also be determined that the nature of PE_X and PE_Y is quite different. The nucleation of PE_Y seems to occur rather swiftly since its formation happened without any noticeable supercooling, while PE_X needed a high degree of supercooling to crystallize. Crystallization without supercooling and the presence of only one single broad WAXD reflection suggests that PE_Y is liquid crystalline, rather than truly crystalline[14]. It is of interest in future research to alter the cooling rate to verify whether or not the solidification into PE_X and PE_Y remain coincident or if one would precede the other. Without such information, discussing the potential influence of PE_X crystallization on PE_Y formation (or vice versa) would remain speculative. Their simultaneous formation might be a coincidence, specific to the cooling rate used.

Very clearly, the intensity of the PE_X peaks in the SAXS and WAXD patterns increased during melting of PE_Y (Figure 3.3). This was probably caused by a 'melting' (or 'clearing', if one wishes to adhere to the terminology of liquid crystals) of PE_Y and a partial recrystallization into PE_X. Given the high intensity of the PE_Y SAXS peak, it seems that quite a lot of material was involved in this phase. A high tolerance for molecules of different chemical nature is to be expected for liquid crystals while this is less so for true crystals. It can be envisaged that a fraction of high-melting stearic and palmitic acid esterified PEs was enclosed in the PE_Y liquid crystals during their cooling-induced formation and that these were liberated during melting and added to the PE_X crystals that were already created during the preceding cooling run.

3.3.2.3. *Blends of palm oil with the commercial phytosterol ester mixture*

For the PE-PO blends with a PE concentration of 20, 40, 60 and 80% time-resolved SAXS and WAXD diffraction patterns were also simultaneously collected and analyzed. In the patterns of the PE-PO blends only peaks with the same spacings as in the pure components occurred (although partially dependent on temperature and concentration). Since no new peaks at other spacings occurred in the XRD patterns, it can be concluded that no other (compound) crystal structures were formed in the PE-PO blends. As the plots are merely superpositions of the already discussed SAXS and WAXD patterns, plots of these five PE-PO blends are not reported in this manuscript. Instead, the occurrence of the different polymorphic forms as a function

of concentration and temperature is summarized in two morphology maps for cooling and heating in Figure 3.5 and Figure3.6 respectively.

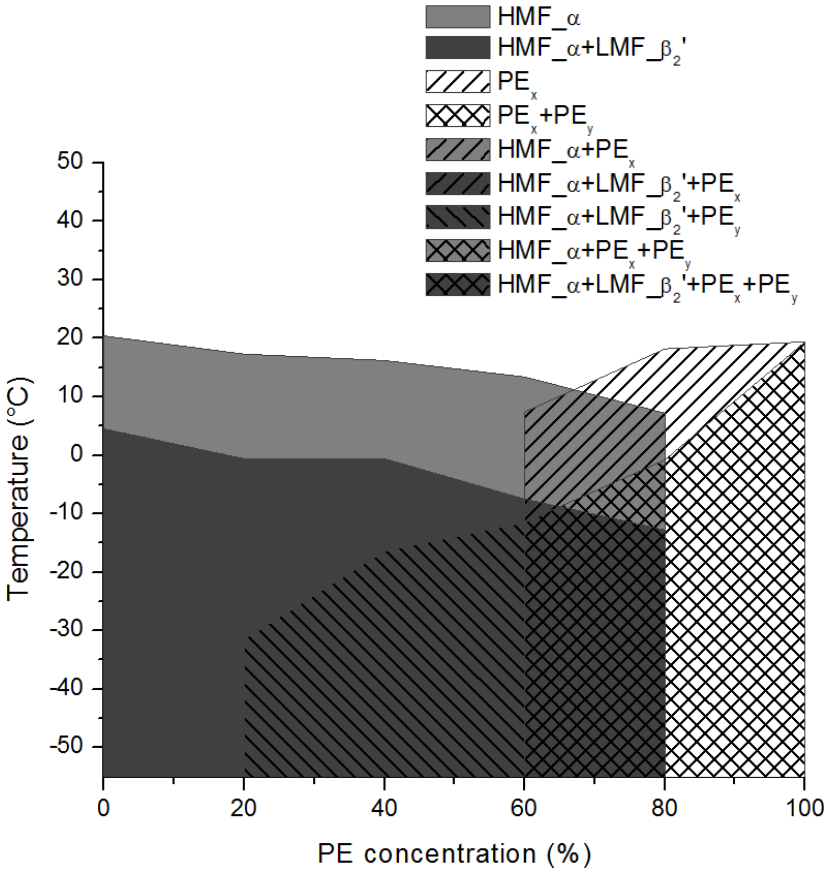

Figure 3.5. *Morphology map of cooling of the blends of palm oil with the commercial phytosterol ester (PE) mixture. Abbreviations: HMF = high-melting fraction and LMF = low-melting fraction.*

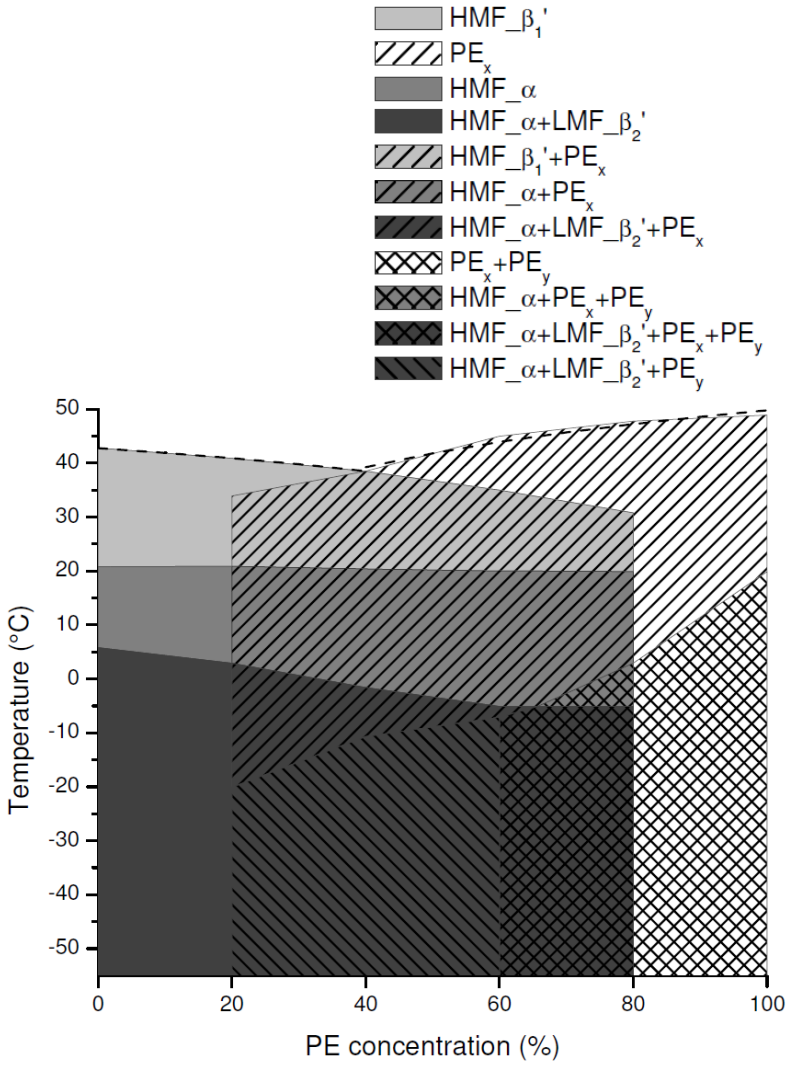

Fig. 3.6. *Morphology map of heating also representing the phase diagram of the blends of palm oil with the commercial phytosterol ester (PE) mixture. Dashed line represents the liquidus line of the phase diagram. Abbreviations: HMF = high-melting fraction and LMF = low-melting fraction.*

Upon cooling the 20% PE blend, first, HMF_α started crystallizing at a temperature of 17.3°C, followed by LMF_β_2' at -0.6°C and finally PE_y at -31.5°C. Typical PE_y peaks could be observed in SAXS, although with a low intensity, but not in WAXD likely due to being too weak. No PE_x typical peaks appeared during cooling. During subsequent heating of the 20% PE blend PE_y fully disappeared at -20.1°C. After PE_y was fully melted, PE_x typical peaks appeared in WAXD, clearly visible from a temperature of

- 5.1°C. Then, LMF_β_2' disappeared at 2.9°C, followed by a polymorphic transition from HMF_α to HMF_β_1' from 10.9°C to 20.9°C. Finally, PE_x completely melted at 33.9°C and HMF_β_1' at 40.9°C. During heating, no PE_x peaks were detected in SAXS probably due to being too weak.

The observations for the 40% PE blend were analogous to those for the 20% PE blend. When cooling the 40% PE blend, HMF_α started crystallizing first at 16.2°C, followed by LMF_β_2' at -0.6°C and finally, PE_y at -16.4°C. No PE_x peaks were observed. During subsequent heating of the 40% PE blend first PE_y disappeared at -10.7°C. From that temperature, PE_x typical peaks appeared in WAXD. Next, LMF_β_2' disappeared at -1.6 °C followed by a conversion from HMF_α to HMF_β_1' from 10.4°C to 20.4°C. Finally, PE_x and HMF_β_1' melted simultaneously and completely vanished at 38.5°C. For the 20% and 40% PE blends it is clear that PE_x crystals were only formed during heating by recrystallization of the high-melting PE molecules that were liberated from PE_y during its melting.

The order of crystal form (dis)appearance changed for the 60% PE blend. When cooling the 60% PE blend first, HMF_α started crystallizing at 13.4°C, followed by PE_x at 7.4°C, LMF_β_2' at -7.5°C and finally, PE_y at -11.5°C. During subsequent heating PE_y disappeared at -7.5°C and LMF_β_2' did at -5.1°C. From 10.0°C to 20.0°C, HMF_α converted into HMF_β_1' which ultimately disappeared fully at 35.0°C. Finally, PE_x was no longer observed beyond 45.0°C.

For the 80% PE blend the order of events changed again. In this case PE_x appeared first during cooling at 18.2°C, followed by HMF_α at 7.2°C. Then, PE_y started forming at -0.8°C. LMF_β_2' was only formed at -12.8°C. During subsequent heating, LMF_β_2' disappeared fully at -5.1°C, followed by PE_y at 2.9°C. HMF_α vanished at 19.9°C and at least partially transformed into HMF_β_1'. HMF_β_1' melted completely at 30.8°C, i.e. before PE_x just as in the 60% PE blend. PE_x was fully liquid above 47.8°C in the 80% PE blend.

Similar to in the pure PE sample, the intensity of the PE_x peaks in the 60% and 80% PE blends increased after melting of PE_y (mostly seen in WAXD) due to a partial recrystallization into PE_x. As was hypothesized before, it is most likely that high-melting PE molecules that were enclosed in the PE_y liquid crystals during cooling, were released again during melting and added to the PE_x crystals that were already formed during cooling.

3.3.3. MODELLING OF THE PHASE TRANSITIONS AND COUPLING TO THE DSC DATA

The Hildebrand equation was used to describe the liquid-solid boundaries in the morphology map of heating (Figure 3.6) in order to extrapolate and interpolate between the experimental data points (at intervals of 20% PEs). The Hildebrand

equation is based on thermodynamics and is commonly used to rationalize the phase behavior and miscibility of binary mixtures of chemically pure triglycerides[168,173,174] and sometimes – although theoretically less rigorous - also of binary mixtures of real, multi-component fats[175,176]. According to the Hildebrand equation the equilibrium liquidus line in the binary system composed of PO and PE can be described by the following two equations:

$$\ln X_{PO} = -\frac{\Delta H_{PO}}{R}\left(\frac{1}{T} - \frac{1}{T_{PO}}\right)$$

for the part of the liquidus line at the left side of the eutectic point and

$$\ln X_{PE} = -\frac{\Delta H_{PE}}{R}\left(\frac{1}{T} - \frac{1}{T_{PE}}\right)$$

for the part of the liquidus line at the right side of the eutectic point,

with R being the molar gas constant (J/mol.K), X_{PO} the concentration of PO in the melt (mole fraction), ΔH_{PO} the molar heat of fusion of PO in the β' polymorph (J/mol) and T_{PO} the melting point of PO in the β' polymorph (K). X_{PE}, ΔH_{PE}, $and\ T_{PE}$ are the same parameters but applied to the PEs (in the PE_x form). Both equations can only be used provided both components are ideally miscible in the liquid state and provided they do not cocrystallize into compound crystals. Furthermore, this equation can only explain the trends in melting offsets, because only in these cases the melt composition X_{PO} or X_{PE} can be approximated by the overall material composition since at the melting offset temperature it can be assumed that the melt surrounding the finally melting crystals is very close to that of the material as a whole. At temperatures below the melting offset temperature the blend is partially in the solid state, implying that the melt composition differs from the overall material composition[177,178]. Considering that both blend components in the present case are in fact already mixtures, a treatment in terms of the Hildebrand equation at most represents a convenient format to reveal trends.

The Hildebrand equation was fit most ideally to the experimental data points by a least squares procedure. The values of T_{PO} and T_{PE} used in the fitting procedure were the melting offset temperatures of pure PO and pure PE as measured with XRD. The mole fractions used in the fitting procedure were calculated via the mass fractions and the molar masses of pure PO and pure PE. The latter were determined by using their fatty acid composition as described in Table 3.2 and, only for the pure PE, also the sterol composition from Table 3.1, thereby assuming that PO fully consisted of triglycerides and the commercial PE mixture fully of PE. The as such determined molar mass of PO was 851.27 g/mol, while that of the pure PE was 676.66 g/mol. ΔH_A and ΔH_B, respectively the melting enthalpies of pure PO in the β' polymorph and pure PE in the PE_x form, were left as a variable in the fitting procedure. ΔH_{PO}

equaled 115.6 kJ/mol, which is very similar to the melting enthalpy of tripalmitin in the β' polymorph as reported in literature[179]. ΔH_{PE} was 59.4 kJ/mol, which is quite similar to the melting enthalpy of β-sitosteryl palmitate (the main component of PE_x) as reported by Panpipat et al. (2013)[6]. These enthalpy values correspond to melting enthalpies of fully crystalline material and are therefore not the same as the experimental values obtained by integrating the melting curves of pure PO and pure PE.

Clearly, approaching the experimental melting offset and crystallization onset of the blends with the Hildebrand formalism appears to be quite accurate as illustrated by the dashed lines in Fig. 3.6 and Fig. 3.7, despite the boundaries of its use clearly being violated. One thing, however, that can reliably be derived is that these transitions are (melt) composition dependent. The melting point depression with increasing dilution of the melting species as covered by the Hildebrand equation, is a result of the increased melting entropy, ΔS_{melt}, with increasing dilution. After all, the melting temperature, of a substance is given by the ratio $\Delta H_{melt}/\Delta S_{melt}$, with ΔH_{melt} the melting enthalpy[17]. The remixing of the crystalline species with the surrounding liquid during the melting process leads to an entropy increase, which is larger, the larger the dilution of the crystallizable species is. For that reason, ΔS_{melt} increases with increasing dilution and hence the melting temperature decreases. Other phase transitions, such as those at lower temperatures than the melting offset and the crystallization onset temperatures of the blends, were not simulated with the Hildebrand equation, but they also showed the same (melt) composition dependency, except for the melting of HMF_α. Such effects do not play a role if the transition happens within one single phase and remixing is not an issue, such as is the case for a solid-solid transition. The fact that the T_{m_offset} of HMF_α is composition independent, supports the idea that HMF_α disappears in favor of the creation of HMF_β_1' via a solid-solid transition.

The results on the morphology maps in Figures 3.5 and 3.6 can be transferred to the DSC experiments in Figures 3.1 and 3.2. The peak maxima in the DSC crystallization and melting curves corresponding to the most likely polymorphic forms are indicated with different symbols above and below the peaks respectively. For PE concentrations of 0-100% with 20% intervals this was done based on the morphology maps in Figures 3.6 and 3.7, while the peak maxima in the DSC crystallization and melting curves of the intermediate concentrations were assigned by interpolation. When focusing on the cooling runs of the PE-PO blends (Fig. 3.1), the crystallization peak maxima of HMF_α , LMF_β_2', PE_x and PE_y show the same trend as a function of the PE concentration as the T_{c_onset} of these polymorphic forms in the morphology map of cooling (Fig. 3.6). The DSC data show a minimal T_{c_onset} at a PE concentration of 60%, which is consistent with the morphology maps. PE_x and PE_y peaks are hidden

under the LMF_β_2' crystallization peak in the DSC runs of the mixtures with a PE concentration below 40% and 30% respectively. In the heating runs of the PE-PO blends (Fig. 3.2) the melting peak maxima of HMF_β_1', LMF_β_2', PE_x and PE_y show the same trend as a function of the PE concentration as T_{m_offset} of these polymorphic forms in the morphology map of heating (Fig. 3.6). The morphology map of heating showed a minimal T_{m_offset} at a PE concentration of 40%, analogous to the DSC data. For mixtures with a PE concentration below 40% the PE_x melting peak was hidden under the HMF_β_1' melting peak in the DSC runs and could thus not be distinguished. Also, for the mixture with a PE concentration of 90%, the HMF_β_1' peak could not be distinguished. Finally, the melting peak maximum of HMF_α was not indicated in Figure 3.2 because in this temperature range the signal is obscured by the overlapping exothermic peak of the polymorphic transition.

3.3.4. PE-PO PHASE DIAGRAM

The morphology map of heating (Fig. 3.6) can be considered as a kinetic phase diagram of the PE-PO blends[45,174,180]. Although the thermal protocol used in this study (constant cooling and heating rates) did not produce equilibrium states, the ensuing kinetic binary phase diagram allows analysis of the solubility of the two substrates and may be extrapolated to describe equilibrium states[180]. It can be seen that up to a concentration of 40% PEs the liquidus line decreased with an increasing PE concentration, while when more than 40% PEs were added the liquidus line increased again. A clear eutectic behavior with a eutectic point at the blend with 40% PE was thus observed. The eutectic behavior of the PE-PO blends indicates that the PEs and PO are immiscible in the solid state[17,181,182], most probably as a result of their highly different molecular shape[14]. In fact, the absence of compound crystals is a prerequisite for the use of the Hildebrand equation. Rodrigues et al. (2007)[9] also observed eutectic behavior in blends of a highly unsaturated commercial PE mixture with milk fat, but only based on solid fat content and consistency measurements.

3.4. CONCLUSION

Based on the time-resolved synchrotron XRD results, two different crystal structures were identified in the pure PEs. The crystal structure designated PE_x needed a very high degree of supercooling to induce nucleation and most likely is composed of stearic and palmitic acid esterified PEs. The nature of the crystal structure designated PE_y was quite different, since PE_y crystallized without supercooling and showed only one single broad WAXD reflection, suggesting that PE_y is liquid crystalline. PE_y is believed to predominantly contain phytosteryl oleate with a high tolerance for molecules of a different chemical nature, such as stearic and palmitic acid esterified PEs. In the PE-PO blends, the PEs and PO crystallized separately from each other and no new crystal structures were formed other than the typical PE and PO crystal

structures. Based on the analysis of the XRD measurements of the PE-PO blends, morphology maps were constructed which show the occurrence of the different polymorphic forms as a function of concentration and temperature. The peaks in the DSC runs of the PE-PO blends were also linked to the occurrence of the different polymorphic forms as a function of concentration and temperature. The morphology map of heating (Fig. 3.6) can be considered as a kinetic phase diagram of the PE-PO blends, representing a typical eutectic behavior with a eutectic point at the blend with 40% PEs. This observation implies that the PEs and PO were immiscible in the solid state, most likely as a result of their highly different molecular shape which does not allow for the formation of compound crystals.

CHAPTER 4
EFFECT OF ADDING A COMMERCIAL PHYTOSTEROL ESTER MIXTURE ON THE 'EQUILIBRIUM' CRYSTALLIZATION BEHAVIOR OF PALM OIL

This chapter is based on the following publication:
Daels, E., Goderis, B., Steen, L. & Foubert, I. (2018). Influence of adding a commercial phytosterol ester mixture on the 'equilibrium' phase behavior in palm oil. Food Structure, 17: 1-8.

4. EFFECT OF ADDING A COMMERCIAL PHYTOSTEROL ESTER MIXTURE ON THE 'EQUILIBRIUM' CRYSTALLIZATION BEHAVIOR OF PALM OIL

4.1. INTRODUCTION

In the previous chapter the non-isothermal crystallization and melting behavior of a commercial phytosterol ester (PE) mixture in blends with palm oil (PO) was investigated with differential scanning calorimetry (DSC) and time-resolved synchrotron X-ray diffraction (XRD) measurements. The occurrence of different polymorphic forms during cooling and heating of the PE-PO blends was mapped as a function of temperature and PE concentration on two morphology maps.

It is however hard to predict whether or not PE addition gives any desired properties to the end product based on the non-isothermal experiments of chapter 3. As no equilibrium conditions were obtained the results of chapter 3 did not give direct information on the microstructure or macroscopic assets of end products containing the lipid blends.

Therefore, in this chapter the influence of the addition of a commercially available mixture of PEs was analyzed at each structural level of the crystallization of PO being primary crystallization, polymorphism, network formation and textural properties. To do so many different experimental techniques were applied including DSC, XRD, pulsed nuclear magnetic resonance (pNMR), polarized light microscopy (PLM) and texture analysis. The effect of PE addition was tested on the properties of PO crystals in a kinetically stabilized state obtained after long-term isothermal crystallization and annealing. This kinetically stabilized state is from now on denoted as the 'equilibrium' state.

4.2. MATERIALS AND METHODS

4.2.1. MATERIALS

The same PO and commercial PE mixture as described in section 3.2.1 were used for the experiments in this chapter. The sterol and fatty acid composition of the commercial PE mixture as analyzed by the methods described in section 3.2.1 are shown in Table 3.1 and Table 3.2 respectively. The fatty acid composition and the triglyceride composition of PO obtained by the methods described in section 3.2.1 are presented in Table 3.2 and Table 3.3 respectively.

4.2.2. BLEND PREPARATION

Nine binary blends of PEs and PO were prepared with a PE concentration of 10 to 90% with composition intervals of 10%. The samples were prepared after complete melting of the pure lipids at 80°C for 30 min under continuous stirring and the blends were stored at -20°C. The blends were visually homogeneous and stable, indicating that no liquid-liquid phase separation occurred.

4.2.3. CRYSTALLIZATION TO THE 'EQUILIBRIUM' STATE

In this chapter the effect of PE addition on PO crystallization in the 'equilibrium' state was examined. First the blends were transferred in/on the recipient of the analyzing technique (DSC cup, NMR tube, glass slide with cover slide or plastic container) after which they were melted at 80°C during 15 min and subsequently put in a water bath at 10°C for rapid cooling (at about 5°C/min). In accordance with the existing literature[183], a time-temperature profile of 48h at 10°C was used to bring the samples in the 'equilibrium' state. It was observed (detailed results not shown) that the DSC melting enthalpy and the peak maximum of the melting curve of pure PO and PEs indeed did no longer change significantly when holding at that temperature for longer times. The described tempering of the samples was performed in a water bath.

4.2.4. SOLID FAT CONTENT BY NMR

The solid fat content (SFC) of the samples in the 'equilibrium' state was measured with a pulsed NMR spectrometer (Mini-spec mq20; Bruker, Germany) using the direct method as described by AOCS (1997)[59]. Calibration was performed by using three standards supplied by Bruker containing 0.0, 31.3, and 74.0% solids. The samples were not subjected to the often used standard tempering method described by AOCS (1997)[59], but were measured directly after they reached the 'equilibrium' state. Determinations were carried out in triplicate. For the pure PEs one extra SFC measurement was performed at 25°C, after the measurement at 10°C and subsequent heating to 25°C and holding at 25°C for 1h.

4.2.5. DIFFERENTIAL SCANNING CALORIMETRY

The blends were analyzed with DSC in a similar way as described in section 3.2.3, but by using a different time-temperature profile. After reaching the 'equilibrium' state (section 4.2.3), the samples were heated at 20°C/min to 80°C to obtain the melting profile. For each sample, at least five repetitions were evaluated. The melting enthalpy (ΔH), i.e. the amount of heat released during melting, was calculated by integration of the melting curve using a horizontal baseline. The offset temperature of melting (T_{m_offset}) of different peaks in the melting curve was determined as the

inflection point of the melting peak at the high temperature side of the peak, according to Timms (2003)[184].

4.2.6. X-RAY DIFFRACTION

A Xenocs Xeuss X-ray camera (Xenocs, Sassenage, France) equipped with a Mar345 image plate detector (MARresearch, Norder-stedt, Germany) was used for taking X-ray scattering patterns of a selection of samples in the 'equilibrium' state: the PE-PO blends with 20, 40, 60 and 80% PEs and pure PO and PEs. The GeniX 3D Molybdenum ultra-low divergence X-ray beam source had a power of 50 kV (1 mA) giving a constant intensity beam of 0.7107 Å. About 25-30 mg of melted sample was sealed into Tzero hermetic aluminum pans (TA Instruments, Brussels, Belgium). After reaching the 'equilibrium' state the samples were placed on a temperature-controlled Linkam DSC600 stage (Linkam Scientific Instruments, Surrey, UK) in front of the beam. Combined small-angle X-ray scattering (SAXS) and wide-angle X-ray diffraction (WAXD) patterns were recorded at a constant temperature of 10°C. All 2D X-ray patterns were azimuthally averaged with Conex software also using an empty DSC pan measurement and a calibration measurement with a silver behenate sample[167]. The XRD data were also corrected for the background scattering, the intensity of the incoming beam and were normalized to the area underneath the scattering patterns after a baseline correction. The scattering angle 2θ ranged from $0.31° < 2\theta < 14.99°$.

4.2.7. POLARIZED LIGHT MICROSCOPY

The microstructure of the samples was studied by means of a polarized light microscope Olympus BX51 (Olympus Optical Co. Ltd., Tokyo, Japan) equipped with a digital camera Infinity 2 (Lumenera corporation, Ontario, Canada). A drop of melted sample was transferred onto a glass slide using a capillary tube and covered with a pre-heated covering slide. After reaching the 'equilibrium' state the samples were placed on a temperature-controlled Linkam PE120 stage set at 10°C (Linkam Scientific Instruments, Surrey, UK). Images were taken at a magnification of 100x or 200x using the Infinity capture software (Lumenera Corporation, Ottawa, Canada).

4.2.8. HARDNESS

Texture analyses of the nine PE-PO blends and pure PO and PEs was performed using a Lloyd Texture Analyzer (Model LF plus, Lloyd Instruments Ltd, Fareham, Hampshire, UK). Plastic cans with diameter 30 mm and height 70 mm were filled with 16 g sample. Force-distance deformation curves of the samples in the 'equilibrium' state were obtained using a 100 N load cell and a cylindrical probe (diameter 6 mm). The probe penetrated the lipid at a constant speed of 10 mm/min to a distance of 10 mm.

The hardness is defined as the maximum force required to penetrate the sample 10 mm. For each sample, four repetitions were evaluated.

4.2.9. STATISTICAL ANALYSIS

The data were statistically analyzed by one-way ANOVA with SigmaPlot version 11.0 (Systat Software, Drunen, The Netherlands). Furthermore, Tukey tests were applied to determine significant differences between the mean values of the different blends. A significance level of 0.05 was used throughout.

4.3. RESULTS AND DISCUSSION

4.3.1. PURE PALM OIL

4.3.1.1. *Solid fat content by NMR*

The obtained value of the SFC of pure PO in the 'equilibrium' state was 52.5 ± 0.1%, which is within the typical range for SFC values of PO at 10°C reported in literature[70,88].

4.3.1.2. *Melting profile by differential Scanning Calorimetry*

The melting curve of pure PO in 'equilibrium' shown in Figure 4.1 had one, rather broad peak with a peak maximum at about 30°C and a small shoulder on the high temperature side. The calculated T_{m_offset} of the pure PO was 38.7 ± 0.2°C and ΔH_{melt} was 57.6 ± 0.5 J/g. The existence of one broad peak indicated that compound crystals, i.e. crystals with different types of triglycerides together[185], were formed, which is probably due to the high cooling rate (more than 5°C/min) obtained in the tempering procedure[186]. The melting range of the obtained crystals indicated the existence of β' crystals[26,32], which is according to literature the expected polymorphic form after tempering at 10°C since PO is a β'-tending lipid[90,98].

The small shoulder on the high temperature side of the melting curve was reported by several other authors[80,187] but their suggested explanations for the shoulder were never really proven. To be sure if the shoulder was caused by (i) a polymorphic transition of β' to β during heating, (ii) a polymorphic transition of β' to β during tempering or (iii) the melting of some compound crystals richer in high melting trisaturated triglycerides as was already suggested in literature[80,187] some extra tests were performed on the pure PO after it reached the 'equilibrium' state. A variation of the heating rate (0.5, 1, 5, 10 and 20°C/min) had no influence on the shape of the melting curve of pure PO demonstrating that the shoulder was not due to a polymorphic transition of β' to β during heating (detailed results not shown). Furthermore when the tempering of PO was interrupted after several different time intervals (2h, 4h, 16h and 48h) to melt the sample at a heating rate of 20°C/min, the

same shoulder was already present in the melting curves, which demonstrates that the shoulder could also not be related to the polymorphic transition of β' to β during tempering (detailed results not shown). Therefore the shoulder was most probably caused by the melting of some compound crystals richer in high melting trisaturated triglycerides (mainly PPP and PPS).

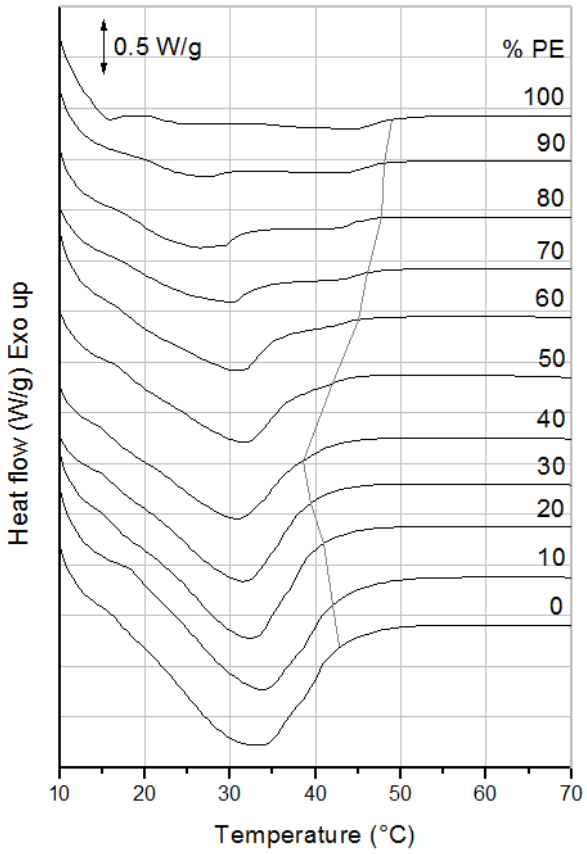

Figure 4.1. *Melting curves of phytosterol ester (PE) - palm oil (PO) blends in the 'equilibrium' state as a function of the PE concentration.*

4.3.1.3. *X-ray diffraction*

Figure 4.2 shows the wide angle X-ray diffraction (WAXD) and small angle X-ray scattering (SAXS) patterns of pure PO in the 'equilibrium' state. The SAXS pattern of pure PO showed one main peak at 2θ = 0.96° (d = 42.2 Å) and a second much smaller peak at 2θ = 2.9° (d = 14.6 Å). These peaks correspond to the first (42.2 Å) and third order (14.6 Å) reflections of a 2L packing[169]. The WAXD pattern showed one medium peak at 2θ = 10.53° (d = 3.91 Å) and two strong peaks at 2θ = 9.73° (d = 4.19 Å) and 2θ = 9.43° (d = 4.32 Å). These short spacings are characteristic for the orthorhombic

subcell stacking of PO in a β'-polymorph[32,93,169]. Based on the DSC and XRD results of pure PO reported in chapter 3 it can be stated that these β' crystals consist of disaturated and trisaturated triglycerides and that they compose the so-called high-melting fraction also called stearin fraction of PO and that they are formed by a polymorphic transition of α crystals during tempering.

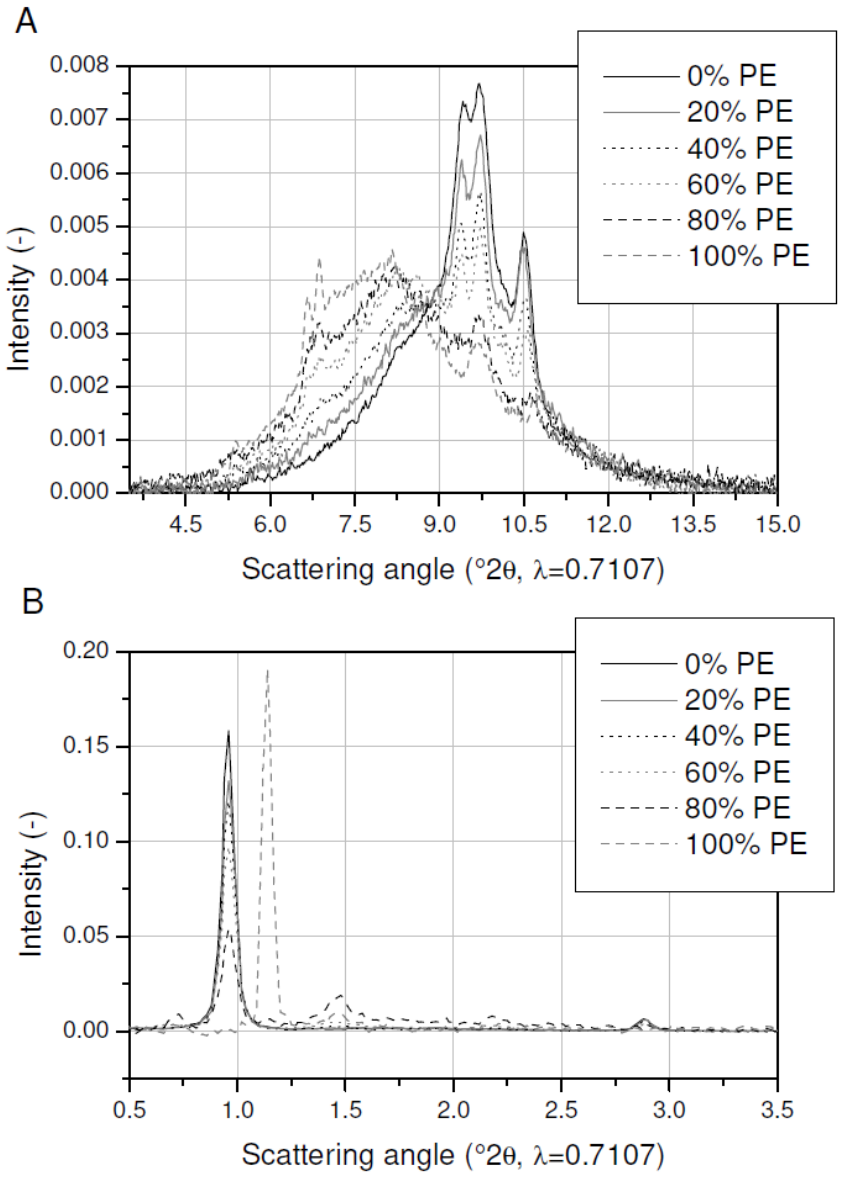

***Figure 4.2**. Wide angle X-ray diffraction (A) and small angle X-ray scattering (B) patterns of some phytosterol ester (PE) - palm oil (PO) blends in the 'equilibrium' state achieved by tempering at 10°C for 48h.*

4.3.1.4. *Polarized light microscopy*

As can be seen in Figure 4.3 the microstructure of pure PO showed the typical network of spherulites which are themselves aggregates of needle-shaped crystals[13,98,188]. As could be expected many small crystals were formed due to the rather high cooling rate[186].

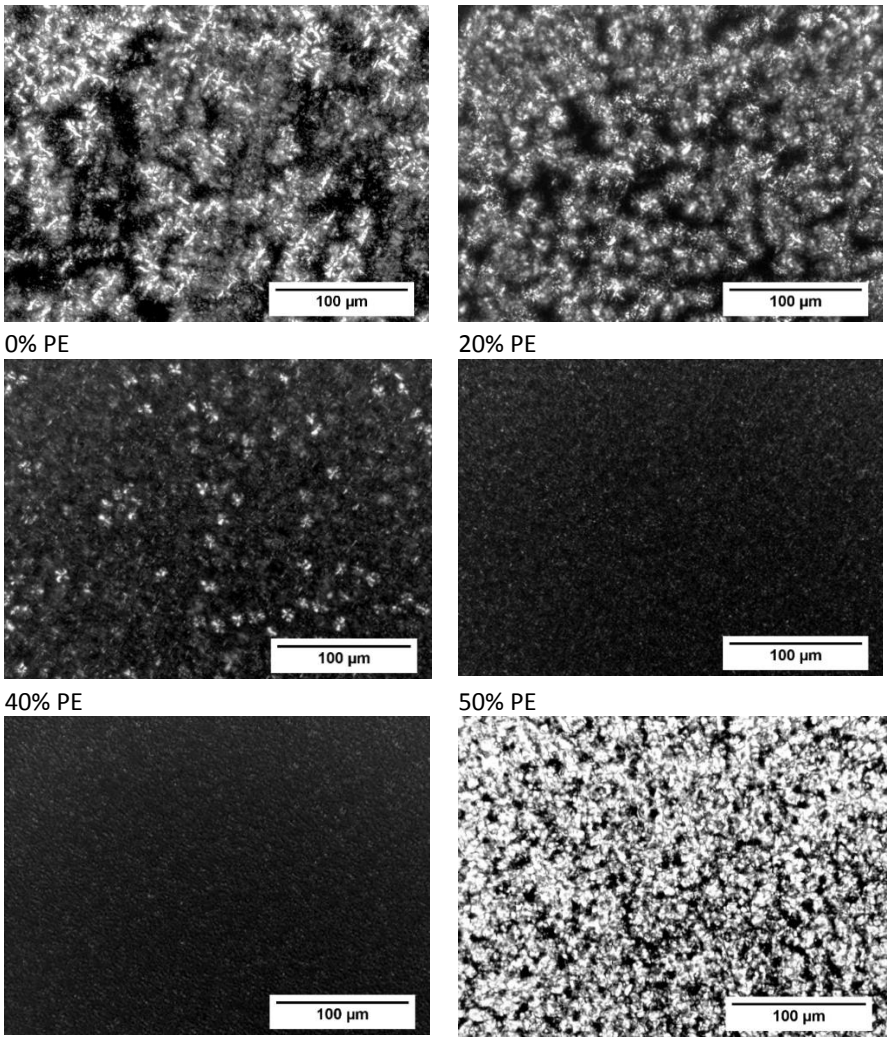

Figure 4.3. *Images of the lipid crystal networks of different phytosterol ester (PE) - palm oil (PO) blends in the 'equilibrium' state achieved by tempering at 10°C for 48h. Black bars represent 100 µm.*

4.3.1.5. *Hardness*

With the texture analysis a hardness of 27.0 ± 0.1 N was obtained for pure PO.

4.3.2. PURE COMMERCIAL PHYTOSTEROL ESTER MIXTURE

4.3.2.1. *Solid fat content by NMR*

The SFC of the pure PEs analyzed by NMR at 10°C was 62.3 ± 0.3%, which corresponds with the value reported by Rodrigues et al. (2007)[9] for a commercial PE mixture that was also highly unsaturated (more than 85% of the fatty acid were unsaturated). The SFC of the pure PEs at 25°C was 17.7 ± 0.1%, which is much lower than the SFC of the pure PEs at 10°C. This could be expected from the morphology map of heating reported in chapter 3 (section 3.3.2.3). The morphology map in Figure 3.6 shows that at 10°C the two ordered structures of PEs, being PE_x and PE_y, can be expected, while at 25°C only the PE_x form will remain. Therefore, it can be concluded that the high SFC value of the pure PEs at 10°C is dominated by the presence of PE_y liquid crystals, rather than of PE_x crystals. As was demonstrated in chapter 3 PE_y is liquid crystalline, instead of truly crystalline. However, since NMR measures mobility rather than true crystallinity, liquid crystals are taken for a solid phase during the NMR measurement leading to a high SFC value[59].

4.3.2.2. *Melting profile by differential scanning calorimetry*

The melting curve of the pure PEs shown in Figure 4.1 has two peaks: a sharp low-melting peak with a maximum at 16°C and a very broad high-melting peak between 25 and 45°C. Based on the morphology map of heating reported in chapter 3 (section 3.3.2.3), the low-melting and high-melting peaks could be attributed to the melting of respectively PE_y and PE_x.

The calculated T_{m_offset} of the pure PEs was 45.6 ± 0.5°C and ΔH_{melt} was 9.0 ± 0.8 J/g. In contrast to the observed SFC of the pure PEs being higher than that of pure PO, the ΔH_{melt} of the pure PEs was much lower than that of pure PO. The low ΔH_{melt} of the pure PEs is due to the structure of PE_y being liquid crystalline which generally leads to a low ΔH_{melt} value[34]. It was for example shown by Leeson et al. (2002)[4] that the mesophase of β-sitosteryl linoleate, which is the main constituent in the commercial PE mixture used in this study, also has a very low ΔH_{melt} of only 5.1 J/g.

4.3.2.3. *X-ray diffraction*

When looking at the XRD data of the pure PEs in Figure 4.2, the WAXD pattern showed a very broad peak at 2θ = 7.67° (d = 5.31 Å) and eight smaller peaks at 2θ = 5.36° (d = 7.60 Å) 2θ = 6.68° (d = 6.10 Å), 2θ = 6.86° (d = 5.94 Å), 2θ = 8.18° (d = 4.98 Å), 2θ = 8.68° (d = 4.70 Å), 2θ = 8.96° (d = 4.55 Å), 2θ = 9.71° (d = 4.19 Å) and 2θ =

10.72° (d = 3.82 Å). The peaks at 6.10 Å and 5.94 Å were very sharp, while the one at 4.19 Å was rather broad and was probably composed of two partially overlapping peaks. In the SAXS pattern one very intensive peak was observed at 2θ = 1.14° (d = 35.8 Å) and three rather small and broad peaks were detected at 2θ = 0.73° (d = 55.8 Å), 2θ = 1.46° (d = 27.5 Å) and 2θ = 2.23° (d = 14.1 Å). Based on chapter 3 (section 3.3.2.3) the SAXS peak at 35.8 Å and the WAXD peak at 5.31 Å could both be linked to the ordered structure of PE_γ, while the other short and long spacings corresponded to PE_x. It was already hypothesized in chapter 3 that PE_x crystals contained mainly stearic and palmitic acid esterified to the phytosterols while oleic acid esterified PEs were the predominant PEs in the PE_γ liquid crystals.

4.3.2.4. *Polarized light microscopy*

PLM of the pure PEs revealed a dense crystal structure, similar to that observed by Rodrigues et al. (2007) for a commercial PE mixture after storage at 10°C[9] (Figure 4.3). The network had an irregular structure which is different from what is normally seen in triglyceride lipids since the crystals were not needle-shaped or organized into spherulites. The remarkable microstructure was typical for the presence of liquid crystals and was therefore caused by the presence of PE_γ. In general mesophases are strongly birefringent and thus visible through PLM[14,34].

4.3.2.5. *Hardness*

The observed hardness of the pure PEs was 0.9 ± 0.1 N, which is very low compared to pure PO. The low hardness despite the high SFC and high density of the crystal network is caused by the presence of liquid crystals since they generally consist of two-dimensional layers of ordered molecules that can move over one another, negatively affecting the hardness[162]. A similar observation was reported by Rodrigues et al. (2007)[9] who also detected a low consistency in a commercial PE mixture with a high SFC and a dense crystal network. Different from what is generally observed in triglyceride lipids[53,90,189,190], hardness of the pure PEs is therefore not correlated with SFC, but only with ΔH_{melt} and this due to the presence of a liquid crystalline phase in the form of PE_γ.

4.3.3. BLENDS OF THE COMMERCIAL PHYTOSTEROL ESTER MIXTURE AND PALM OIL

4.3.3.1. *Solid fat content by NMR*

Figure 3.4 shows the SFC of the PE-PO blends as a function of the PE concentration. In general, when blending a solid fat (e.g. palm oil) with a liquid oil (e.g. rapeseed oil) three possible behaviors have been described. The SFC can decrease linearly as function of an increasing liquid oil concentration and in proportion to the reduced amount of crystallizable molecules in the system, i.e. a simple dilution effect.

However in other cases the SFC as function of the liquid oil concentration does not decline linearly but curved. Such a situation is indicative for interactions. On the one hand the SFC can be lower than expected from dilution effects due to solubilisation of solute triglycerides in the liquid oil resulting in less crystallization of solute triglycerides. On the other hand, the SFC can also be higher than expected from dilution effects due to complex formation and cocrystallization of solute and solvent triglycerides resulting in crystallization of more triglycerides[191].

In order to visualize the theoretical case of a simple dilution effect, a straight black solid line was added to Figure 4.4 representing the theoretical dilution effect on the SFC if PO would have been blended with a fully liquid oil, instead of PEs. In order to visualize the formation of PE_x crystals and make a distinction with the formation of PE_y liquid crystals a grey solid line was also added to Figure 4.4 representing the theoretical dilution effect on SFC if PE_x would have been blended with a fully liquid oil, instead of PO. A third line (the black dotted line) shows the theoretical value of the SFC of the PE-PO blends supposing the PE solids consist only of PE_x. The latter one is thus the sum of the two solid lines.

When adding less than 40% PEs to PO, the SFC was slightly lower than expected from a simple dilution effect, indicating the PEs acted as a liquid oil solubilizing the high-melting PO triglycerides from the stearin fraction. It was confirmed by XRD that the PEs indeed did not crystallize in these blends. The experimental SFC value of the blend with 40% PEs coincides with the black solid line. This does not indicate that at this concentration a simple dilution effect is in place. It most likely reflects a contribution from solid PEs in the form of PE_x to the SFC, as confirmed by XRD, compensating the loss in SFC due to solubilisation of the PO triglycerides in the PEs that remained liquid.

When more than 40% PEs were added to PO the decrease in SFC is function of the concentration became smaller due to a progressively increasing contribution of crystalline PE molecules, more specifically in the form of PE_x, as confirmed by XRD (section 4.3.3.3). The experimental data were however still located below the black dashed line indicating less PO and/or PE_x crystals were formed than expected based on the blend composition and the SFC values of pure PO and PE_x. This may be caused by solubilisation of high-melting PO triglycerides in the liquid part of the PEs or by solubilisation of high-melting PEs in the liquid part of PO (the olein fraction) or a combination of both. When more than 80% PEs were present the SFC values were positioned above the black dashed line because, as confirmed by XRD (section 4.3.3.3), in these blends also PE_y liquid crystals were formed next to PO and PE_x crystals. As demonstrated for pure PE (section 4.3.2.1) the presence of liquid crystals contributes to the SFC value.

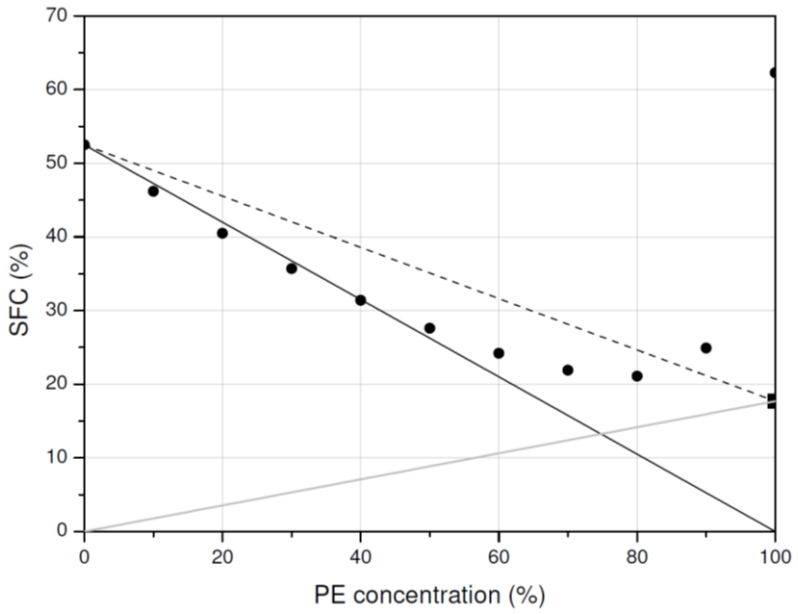

Figure 4.4. *Mean solid fat content (SFC) ± standard deviation (n = 5) of phytosterol ester (PE) - palm oil (PO) blends in the 'equilibrium' state (black dots) as a function of the PE concentration and of the pure PEs that was subsequently heated to 25°C and kept at 25°C for 1h after reaching the 'equilibrium' state (black square). The black solid line represents the theoretical dilution effect on SFC if PO would have been blended with a fully liquid oil, instead of PE. The grey solid line represents the theoretical dilution effect on SFC if PE_x would have been blended with a fully liquid oil, instead of PO. The black dotted line shows the theoretical value of the SFC of the PE-PO blends supposing they both crystallized, but the PE solids consisting only of PE_x.*

4.3.3.2. *Melting profile by differential scanning calorimetry*

In the melting curves of the PE-PO blends shown in Figure 4.1 it can be seen that when the PE concentration increased, the total peak area gradually decreased, while the peak maximum of the PO melting peak remained almost constant. From a PE concentration of about 50% onwards the endothermic peak was stretched out at the high temperature side. This extra plateau-shaped peak became bigger with an increasing PE concentration and was most probably due to the melting of PEs, since T_{m_offset} of the pure PEs is higher than that of pure PO.

In Figure 4.5 ΔH_{melt} of the PE-PO blends was plotted as a function of the PE concentration. As the SFC and melting enthalpy are both a measure of the amount of crystallization, SFC and the melting enthalpy are in theory linearly correlated.

Therefore three straight lines were added to Figure 4.5 which have a similar meaning as the lines in the plot of the SFC as function of the concentration (Figure 4.4). The black solid line represents the theoretical case if ΔH_{melt} of PO would decrease linearly with and proportional to the decreasing PO concentration. The grey solid line represents the theoretical case if ΔH_{melt} of the PE would increase linearly with and proportional to an increasing PE concentration. A third line (the black dotted line) shows the theoretical value of ΔH_{melt} of the PE-PO blends supposing both components crystallize proportionally to their concentration.

A linear (R^2 = 0.998) decrease in ΔH_{melt} of PO was observed when 10 up to 90% PEs were added. Moreover the decrease of ΔH_{melt} in the PE-PO blends was almost equal to the proportion of added PEs (as indicated with the black solid line in Fig. 4.5). Therefore it seems that ΔH_{melt} mainly measured the PO crystals and captured the PE crystals only to a much lesser extent. Indeed, there should be PE_x crystals present from a concentration of 40% PEs and PE_y crystals from a concentration of 80% PE as demonstrated by the XRD results (section 4.3.3.3), but unlike in the behavior of SFC, this did not lead to a significant increase in ΔH_{melt}. Concerning the PE_y crystals this can be explained by their liquid crystalline nature leading to a low ΔH_{melt} despite the high SFC as was demonstrated for the pure PEs. Concerning PE_x the sensitivity to detect these crystals seems to be lower for DSC than for NMR.

T_{m_offset} of the blends as in chapter 3 and measured by synchrotron XRD (section 3.3.2.3) are indicated by the grey solid line in Figure 4.1 and agree with the values of T_{m_offset} if they would have been visually determined based on the shape of the DSC curves. At some PE concentrations T_{m_offset} of the blends was clearly lower than both T_{m_offset} of pure PO and the pure PEs indicating eutectic behavior of the PE-PO binary system. The eutectic phase behavior was due to the PEs and PO being immiscible in the solid state because of their difference in molecular shape prohibiting the formation of compound crystals. Rodrigues et al. (2007)[9] also observed eutectic behavior in blends of a highly unsaturated commercial PE mixture with milk fat.

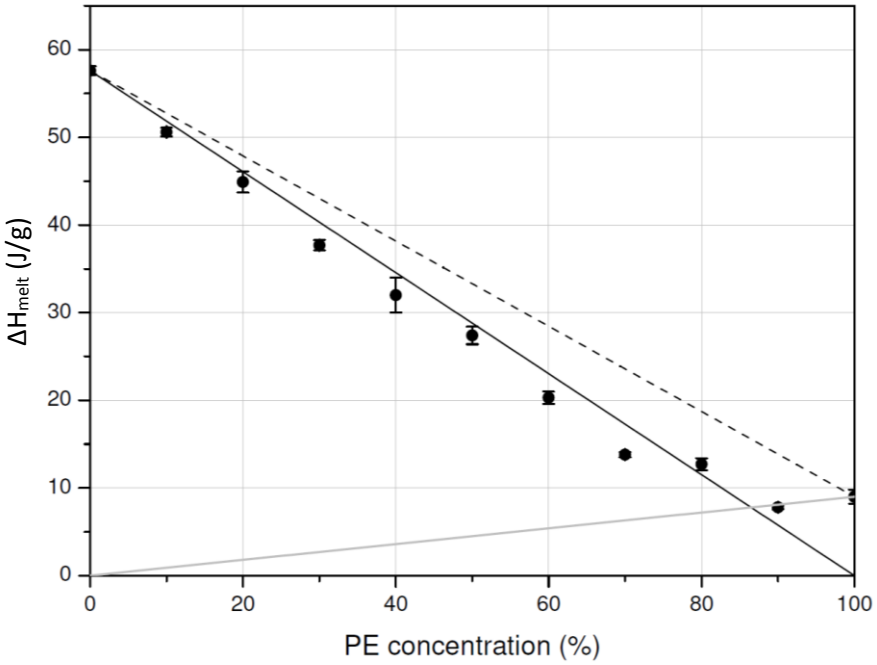

Figure 4.5. *Mean melting enthalpy (ΔH_{melt}) ± standard deviation (n = 5) as a function of the PE concentration of phytosterol ester (PE) - palm oil (PO) blends in the 'equilibrium' state after tempering at 10°C for 48h.* The black solid line represents the theoretical case if ΔH_{melt} of PO would decrease linearly with and proportional to an increasing PE concentration. The grey solid line represents the theoretical case if ΔH_{melt} of the PE would increase linearly with and proportional to an increasing PE concentration. A third line (the black dotted line) shows the theoretical value of ΔH_{melt} of the PE-PO blends supposing both components crystallize proportionally to their concentration.

4.3.3.3. *X-ray diffraction*

When looking at the XRD patterns of the PE-PO blends (Figure 4.2), only peaks with the same spacings as in the pure components were present. Since no new peaks at other spacings occurred in the XRD patterns, it can be concluded that no new crystal structures were formed in the PE-PO blends and the plots are thus superpositions of the already discussed SAXS and WAXD patterns of the pure substrates.

In the SAXS and WAXD patterns of the PE-PO blends with 20% PEs only the typical PO peaks appeared, although smaller indicating no PE crystals were formed. From a concentration of 40% PEs next to the typical PO peaks also PE_x peaks were detected in the WAXD patterns. However, in SAXS they were only found when zooming in very

closely since the intensity of the PE_x peaks was very low in this concentration range. Based on the morphology map of heating (section 3.3.2.3) it was expected that PE_x crystals would also be detected in the blend of PO with 20% PEs. This may indicate that the 'equilibrium' state was not yet reached in this blend after 48h at 10°C. Most probably because the supercooling was not large enough to induce PE_x nucleation within the allowed time frame.

At a PE concentration of 80% the typical PE_y peak was seen in SAXS, although with a very low intensity. The typical PE_y peak in WAXD was not observed since in general in WAXD patterns the noise is bigger compared to SAXS patterns and the PE_y WAXD peak is a small and broad peak anyway while the PE_y SAXS peak is very strong. So in this blend next to PO and PE_x crystals also PE_y liquid crystals were formed, however most probably in a very low amount because of the very low intensity of the SAXS peak and since the presence of PE_y was not reflected in the results of the NMR analyses (see section 4.3.3.1). The XRD results of the 80% PE blend also indicate that even at high PE concentrations PO could still form a small amount of crystals. The morphology map of heating reported in chapter 3 (section 3.3.2.3) shows that in the 80% PE blend PE_y has already fully cleared at a temperature of 2.9°C in contrast to our results which show that PE_y was present in that blend at 10°C. The slope of the curve of T_{m_offset} of PE_y as a function of the PE concentration is however rather steep around 80% PEs in the morphology map of heating, leading to a much higher T_{m_offset} of PE_y when the PE concentration is only slightly higher.

4.3.3.4. *Polarized light microscopy*

Figure 4.3 shows the PLM images of some of the PE-PO blends. The blends with 10 to 40% PEs presented a similar crystal structure as pure PO, although with less and smaller spherulites when the PE concentration was higher. In the blends with 50 to 90% PEs only very little and very small granular crystals were visible. From the previous results for the PE-PO blends it was demonstrated that in the 80% and 90% PEs blends liquid crystals in the form of PE_y were formed in a very small amount. Probably the amount of PE_y was too low for the formation of a dense crystal network structure as was observed for the pure PEs.

4.3.3.5. *Hardness*

PE addition had a major influence on the hardness of PO as is shown in Figure 4.6. The hardness of the blend with 50% PEs had a much larger standard deviation than the hardness of the other blends. The reason for this is not clear since the variables of the blend with 50% PEs tested with the other analyzing techniques did not have a larger standard deviation compared to the values of the other blends. When adding up to 70% PEs, the hardness of PO decreased strongly as a function of the PE

concentration. When adding more than 70% PEs the hardness of the PE-PO blends reached a more or less constant value which was very low and in the same order of magnitude as the hardness of the pure PEs. By comparing Figure 4.6 with Figure 4.4 it is clear that the behavior of the hardness as function of the PE concentration is much different from the SFC behavior indicating that the hardness has other influencing factors next to the SFC. The decrease of the hardness as a function of the PE concentration was much stronger than expected from the SFC behavior. Based on the previous results in this chapter this can be explained by the loss of the network structure of the PO crystals and by the presence of liquid crystals of the PEs giving no hardness, despite their high SFC.

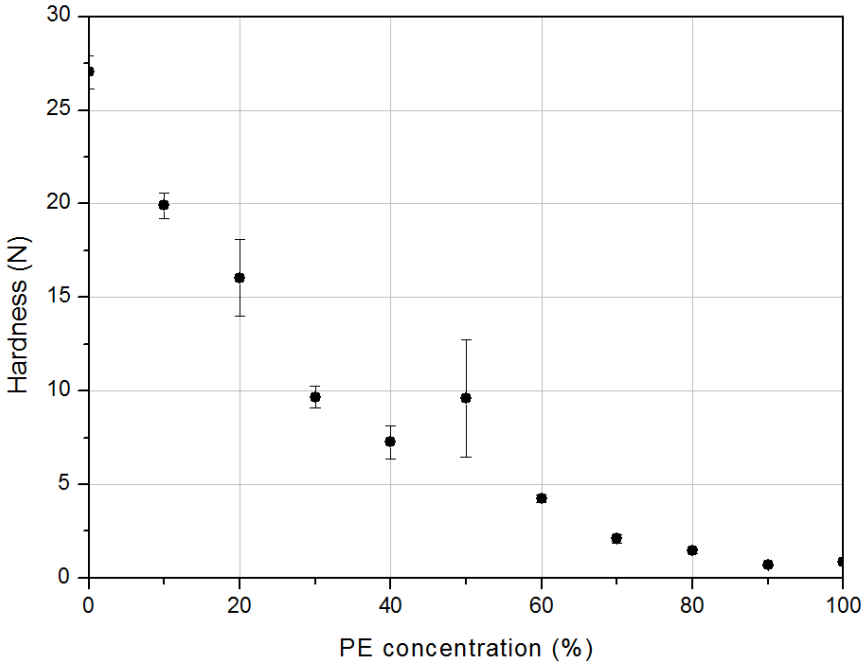

Figure 4.6. *Mean hardness ± standard deviation (n = 4) of phytosterol ester (PE) - palm oil (PO) blends in the 'equilibrium' state after tempering at 10°C for 48h.*

4.4. CONCLUSIONS

It could be concluded from this chapter that addition of PEs to PO (containing products) influences the crystallization and melting properties. In industry this may lead to problems occurring during the production process or with the macroscopic properties of the end product. In case of a low PE concentration the commercial PE mixture itself did not crystallize but acted as a liquid oil diluting PO. From a concentration of 40% PEs also PE_x crystals were observed in the blends and from a concentration of 80% PEs also PE_Y liquid crystals were formed. In the PE

concentration range that is usually applied in industrial applications (up to 40% PEs) the PEs negatively affected the solid fat content, melting enthalpy, network structure and hardness, one of the key factors that determine the macroscopic characteristics of the food product. The crystal network structure and solid fat content of PO was lost after PE addition which led to the drop in the hardness. When applying this commercial PE mixture in a product, additional adaptations on the composition level will have to be made in order to compensate for the loss in hardness.

Chapter 5
Effect of adding a commercial phytosterol ester mixture on the isothermal crystallization kinetics of palm oil

This chapter is based on the following publication:
Daels, E., Goderis, B., Matton, V. & Foubert, I. (2018). Isothermal crystallization kinetics of palm oil as influenced by addition of a commercial phytosterol ester mixture. Journal of Agricultural and Food Chemistry, 66(15): 3910-3921.

5. EFFECT OF ADDING A COMMERCIAL PHYTOSTEROL ESTER MIXTURE ON THE ISOTHERMAL CRYSTALLIZATION KINETICS OF PALM OIL

5.1. INTRODUCTION

In chapter 3 the effects of adding a commercial phytosterol ester (PE) mixture on the non-isothermal crystallization and melting behavior of palm oil (PO) was examined and morphology maps showing the different crystal structures as a function of temperature and PE concentration during cooling and heating were constructed. These results enabled research on the impact of adding PEs to PO under industrially more relevant crystallization conditions. More specifically in chapter 4 the influence of PE addition on the 'equilibrium' crystallization state of PO was investigated in order to evaluate whether PE addition gives desired properties to the end product. It was found that PE addition has a major influence on each level of the crystalline structural hierarchy (primary crystallization, polymorphism, network formation and textural properties).

Next to the effects related to the final 'equilibrium' state, it is also interesting to verify whether PE addition influences the crystallization kinetics of PO. Diluting PO with PE is expected to delay or slow down the PO crystallization. The extent of this delay and the impact on the rate of polymorphic transitions is however, less predictable. To the best of our knowledge the effect of adding PEs on the isothermal PO crystallization kinetics has not been reported in literature before.

More generally, the effect of addition of many other types of lipids like mono- and diglycerides on the crystallization kinetics of different edible oils and lipids has been studied, but mostly in low concentrations (< 10%) since these minor components can already influence the kinetics at a concentration <0.1%[192]. Also the isothermal crystallization behavior of PO without the addition of other lipids has been extensively studied by several authors[32,99,102–104] who reported that the isothermal crystallization mechanism of PO depends on the degree of supercooling. At a high degree of supercooling, PO displays a two-step crystallization with the formation of α crystals in the first step, followed by a transformation into β' crystals and additional formation of β' crystals directly from the melt. At a lower degree of supercooling PO crystallizes directly into the β' polymorph without the prior formation of an α polymorph. The reported value of the cut-off temperature between both mechanisms varies between 22 and 25°C probably because of a difference in

experimental conditions on the one hand and a difference in PO composition on the other hand[32].

In this chapter the crystallization kinetics of PO was investigated after addition of a commercial PE mixture in concentrations of 10 to 40% because that is the concentration range of PEs in the lipid phase of most of the existing cholesterol lowering lipid containing food products. Such information is required to assess the potential impact of adding high PE amounts to food products under processing conditions. The isothermal crystallization of the PE-PO blends was analyzed at a temperature of 20°C to examine the effect of PE addition on the two-step crystallization mechanism of PO. In a second set of experiments crystallization was studied at a constant supercooling of 18.7°C in order to eliminate effects on the crystallization kinetics related to differences in degree of supercooling of the blends. Differential scanning calorimetry (DSC) experiments were performed to get a first view on the isothermal crystallization mechanism and to provide quantitative data on the kinetic behavior by applying the Foubert model. The crystallization mechanism and the polymorphic behavior was examined with time resolved synchrotron X-ray diffraction (XRD) analyses for selected blends. Furthermore, polarized light microscopy (PLM) was used to study the microstructure of the blends.

5.2. MATERIALS AND METHODS

5.2.1. MATERIALS

The same PO and commercial PE mixture as described in section 3.2.1 were used for the experiments in this chapter. The sterol and fatty acid composition of the commercial PE mixture as analyzed by the methods described in section 3.2.1 are shown in Table 3.1 and Table 3.2 respectively. The fatty acid composition and the triglyceride composition of PO obtained by the methods described in section 3.2.1 are presented in Table 3.2 and Table 3.3 respectively.

5.2.2. BLEND PREPARATION

PEs were added to PO in concentrations of 10, 20, 30 and 40% by weight. The samples were prepared after complete melting of the lipids at 80°C for 30 min under continuous stirring to obtain a homogeneous, clear mixture.

5.2.3. DIFFERENTIAL SCANNING CALORIMETRY

The DSC experiments were performed using the same equipment as described in section 3.2.3. About 15 mg of melted lipids was sealed into hermetic aluminum pans (TA Instruments, Brussels, Belgium). Three different types of DSC experiments were performed on the pure PO and the PE-PO blends: isothermal crystallization experiments, stop-and-return experiments and determination of the melting curve

after reaching the 'equilibrium' state to determine T_{m_offset}. All measurements were carried out at least five times.

For the isothermal crystallization experiments the following time-temperature program was used: equilibration at 80°C during 15 min to ensure complete melting and to erase the crystal memory, followed by cooling at 10°C/min to the isothermal temperature (20°C or alternatively a degree of supercooling of 18.7°C) and holding at that temperature until crystallization had finished. The Universal Analysis 2000 software version 4.5A (TA Instruments, New Castle, USA) was used to determine the peak maximum of the α peak ($t_{\alpha\ peak}$) which corresponds to the first peak in the isothermal crystallization curve. The start point and the end point of the β' crystallization, which is the second step in the two-step crystallization of PO, were determined using an objective calculation algorithm described by Foubert et al. (2002)[193]. Next to the two peaks due to the α and β' crystallization of PO a third peak occurred in the isothermal crystallization curve of the 40% PE blend at a supercooling of 18.7°C indicating PE crystallization. This peak was however not further analyzed. For indicative purposes the isothermal crystallization experiments at a temperature of 20°C were also performed on the pure PEs, but this DSC crystallization curve was also not further analyzed.

Stop-and-return experiments were performed as described in detail in Foubert et al. (2008)[194] for the quantitative analysis of the α crystallization, which is the first step in the two-step crystallization of PO. In this technique the isothermal crystallization was interrupted after the α crystallization, followed by heating the sample at 20°C/min to obtain the melting curve. The end point of the α crystallization was defined as the start point of the β' crystallization which had been determined with the calculation algorithm of Foubert et al. (2002)[193]. Table 5.1 shows the isothermal stop-and-return times used for the different PE concentrations. The melting enthalpy of the α polymorph (ΔH_α) was calculated by integration of the melting curve using a horizontal baseline with a fixed end point at 50°C and the starting point being the intersection of the melting curve with the horizontal baseline.

Table 5.1. *Isothermal stop-and-return time (min) in case of isothermal crystallization at 20°C and isothermal crystallization at a constant degree of supercooling of 18.7°C for different phytosterol ester (PE) concentrations.*

PE concentration (%)	Isothermal at 20°C	Constant supercooling
0	4.7	4.7
10	5.2	5.9
20	8.7	6.3
30	20.2	6.7
40	30.7	20.1

A last type of DSC experiment was designed to determine the offset temperature of melting (T_{m_offset}) of pure PO and the PE-PO blends. As described in section 4.2.3 a time-temperature profile of 48h at 10°C was used to bring the samples in the 'equilibrium' (or kinetically stabilized) state. Then the samples were heated at 20°C/min to 80°C to obtain the melting profile. T_{m_offset} of the peak in the melting curve was determined as the inflection point of the melting peak at the high temperature side of the peak, according to Timms (2003)[184]. The degree of supercooling of the blends was calculated using this T_{m_offset}.

5.2.4. TIME-RESOLVED SYNCHROTRON X-RAY DIFFRACTION

Pure PO and PO with 20 and 40% of PEs added were analyzed by time-resolved synchrotron X-ray diffraction experiments conducted in the same way as described in section 3.2.4. In this chapter the following time-temperature program was used: equilibration at 80°C during 15 min to ensure complete melting and to erase the crystal memory, followed by cooling at 10 °C/min to the isothermal crystallization temperature which is at a degree of supercooling of 18.7°C and holding at that temperature until crystallization had finished. Also the same data processing steps as described in section 3.2.4 were performed. Identification of the polymorphs was done on the basis of literature data[32,103,104,195].

Furthermore, The WAXD data were quantitatively analyzed to obtain the fractions of the different polymorphic forms as a function of the isothermal time and this is further explained on the basis of Figure 5.1. For pure PO and PO with 20% PEs the same method was applied to extract the fractions of the α and β' polymorphs from WAXD. First a reference pattern of the liquid phase ('liquid reference'; Fig. 5.1A) was made by averaging the last ten WAXD patterns during the cooling because no crystallization occurred in that stage. The reference pattern of the α polymorph ('α reference') as shown in Figure 5.1A was obtained by first selecting the WAXD pattern where the intensity of the α peak was maximal and no peaks of other polymorphic forms were present (named 'α frame' in Figure 5.1A). The peak maximum of the α

peak in the 'α frame' was located at 2θ = 13.2° (d = 4.22 Å). Then the 'liquid reference' was scaled to fit in the 'α frame' (named 'scaled liquid reference' in Figure 5.1A, scaling factor = 0.91) and this 'scaled liquid reference' was subtracted from the 'α frame' to acquire the 'α reference'. As a final step the intensities to the left and right side of the peak in the 'α reference' were set to 0, resulting in the 'cleaned α reference'. The reference pattern of the β' polymorph was made analogously as shown in Figure 5.1B. The 'β' frame' contained three peaks at 2θ = 13.4° (d = 4.41 Å), 2θ = 13.9° (d = 4.27 Å) and 2θ = 15.0° (d = 3.95 Å). As can be seen on Figure 5.1B the scaling factor to fit the 'liquid reference' in the 'β' frame' was smaller than for the 'α frame' and equaled 0.85. Subsequently all WAXD patterns were fit with a linear combination of the 'liquid reference', the 'cleaned α reference' and the 'cleaned β' reference' with the intensities of the liquid phase and the different polymorphic forms as unknown parameters. The area below each of the constituting curves corresponds to the phase specific mass fractions. Via the Excel Solver the sum of the squared residuals of this fit was minimized. For each pattern the sum of the fractions equaled 1.

For the PE-PO blend with 40% PEs the method to extract the fractions of the different polymorphic forms differed a little because only in these crystallization conditions and at this PE concentration the PEs also crystallized separately from PO, more specifically in the form of PE_x. The formation of the PE_x crystals started after the α crystallization and before the polymorphic transition from α to β' crystals. Consequently, there were no WAXD patterns in which only the PE_x peaks occurred. Therefore to make the 'PE_x frame' for the PE_x reference (see Figure 5.1C), a WAXD pattern of pure PEs crystallized in the PE_x form at 27°C was used since this temperature is higher than the melting temperature of PE_Y, but lower than the melting temperature of PE_x[195]. The 'PE_x frame' contained nine peaks: a weak peak at 2θ = 7.81° (d = 7.58 Å), two strong sharp peaks at 2θ = 9.54° (d = 6.21 Å) and 2θ = 9.86° (d = 6.02 Å), again three weak peaks at 2θ = 10.2° (d = 5.81 Å), 2θ = 11.7° (d = 5.08 Å) and 2θ = 12.4° (d = 4.78 Å), a strong double peak at 2θ = 13.9° (d = 4.27 Å) and 2θ = 14.1° (d = 4.22 Å) and one stronger peak at 2θ = 15.2° (d = 3.91 Å). The scaling factor of the 'liquid reference' was 0.90 in this case. Furthermore because of overlapping peaks in the WAXD patterns, the fits of most of the WAXD patterns of PO with 40% PEs did not lead to unique solutions when more than one polymorphic form had crystallized. Therefore, determination of the fractions of the different polymorphic forms was done differently for this sample. First the α fraction at an isothermal time of 10 min was determined via the WAXD data using the above described method since at that time no peaks of other polymorphic forms occurred. Then the α fraction as a function of the isothermal time was calculated from the integral of the α peak in the SAXS region between 2θ = 3.74 and 2θ = 3.84 and scaling

of this (time dependent) integral to the WAXD based α fraction at 10 min. Subsequently all WAXD patterns were fitted again with the α phase fraction fixed to the scaled SAXS based value and with the fractions of the liquid phase, the β' and PE_x crystal form fractions left as adjustable parameters.

5.2.5. POLARIZED LIGHT MICROSCOPY

The microstructure of the samples was studied by the method described in section 4.2.7, but with a different time-temperature profile. In the Linkam PE120 stage (Linkam Scientific Instruments, Surrey, UK) the samples were heated at 80°C during 15 min to ensure complete melting and to erase the crystal memory, followed by cooling at 10°C/min to the isothermal temperature at a degree of supercooling of 18.7°C and holding at that temperature until crystallization had finished. Images of the microstructures were captured with a digital camera Infinity 2 (Lumenera corporation, Ontario, Canada) and the Infinity capture software (Lumenera Corporation, Ottawa, Canada) every minute during the isothermal crystallization.

5.2.6. STATISTICAL ANALYSIS

The obtained mean values of the crystallization parameters were statistically analyzed by one-way ANOVA with SigmaPlot version 11.0 (Systat Software, Drunen, The Netherlands). Furthermore, with the same software Tukey tests were applied to determine significant differences between the mean values at a significance level of 0.05.

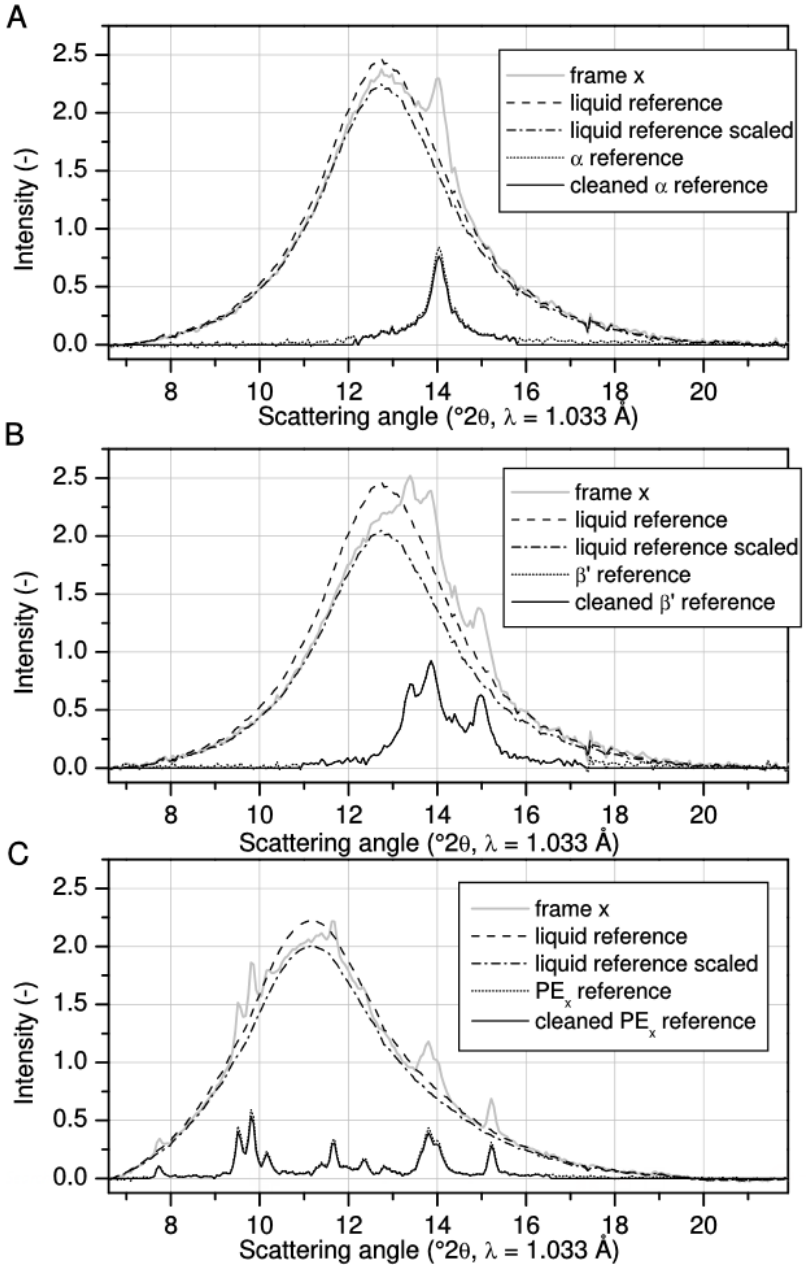

Figure 5.1. *Illustration of the method to make the cleaned reference patterns of the different polymorphic forms, being α (A), β' (B) and PE_x (C), of which a linear combination was used to fit the WAXD patterns of selected samples in order to quantitatively analyze the fractions of the different polymorphic forms as a function of the isothermal time.*

5.3. RESULTS AND DISCUSSION

5.3.1. ISOTHERMAL CRYSTALLIZATION AT 20°C

5.3.1.1. *Differential scanning calorimetry: qualitative analysis*

For each PE concentration (0, 10, 20, 30, 40 and 100%) Figure 5.2A shows an overlay of one representative DSC isothermal crystallization curve at 20°C. The isothermal crystallization curve of the pure PO showed two peaks which, according to the WAXD data discussed below (see section 5.3.2.3), correspond to the crystallization of PO in the α polymorph (indicated as Peak I) and the subsequent polymorphic transition to the β' form followed by additional crystallization of β' crystals directly from the melt (indicated as Peak II). Many other studies reported this two-step crystallization mechanism when PO was isothermally crystallized at 20°C[32,99,102–104]. Peak I started immediately after cooling and was therefore not fully separated from the cooling segment in the DSC curve. However, Peak I was fully separated from Peak II by the baseline.

The isothermal crystallization curve of the pure PEs consisted of one single crystallization peak that also started immediately after cooling. Based on the melting temperatures of PE_X (48.9°C) and PE_Y (19.9°C) as reported in chapter 3 (section 3.3.1.2) it is conceivable that this peak is dominated by the crystallization of PE_X. The DSC curve of the pure PEs is only shown for indicative purposes and, in contrast to the other curves, was not quantitatively analyzed.

The isothermal crystallization curves of the PE-PO blends showed the same two peaks (Peak I and Peak II) as the curve of the pure PO, although shifted to higher crystallization times with increasing PE concentration. No peaks due to PE crystallization could be distinguished, although PE_X crystallization might be hidden below the PO crystallization events for the blend containing 40% PE. Indeed, in the quantitative DSC analysis an unexpected increase of the PO β' share was detected (see section 5.3.1.2), which might be due to non-legitimately allocated exothermic heat from the PE_X crystallization.

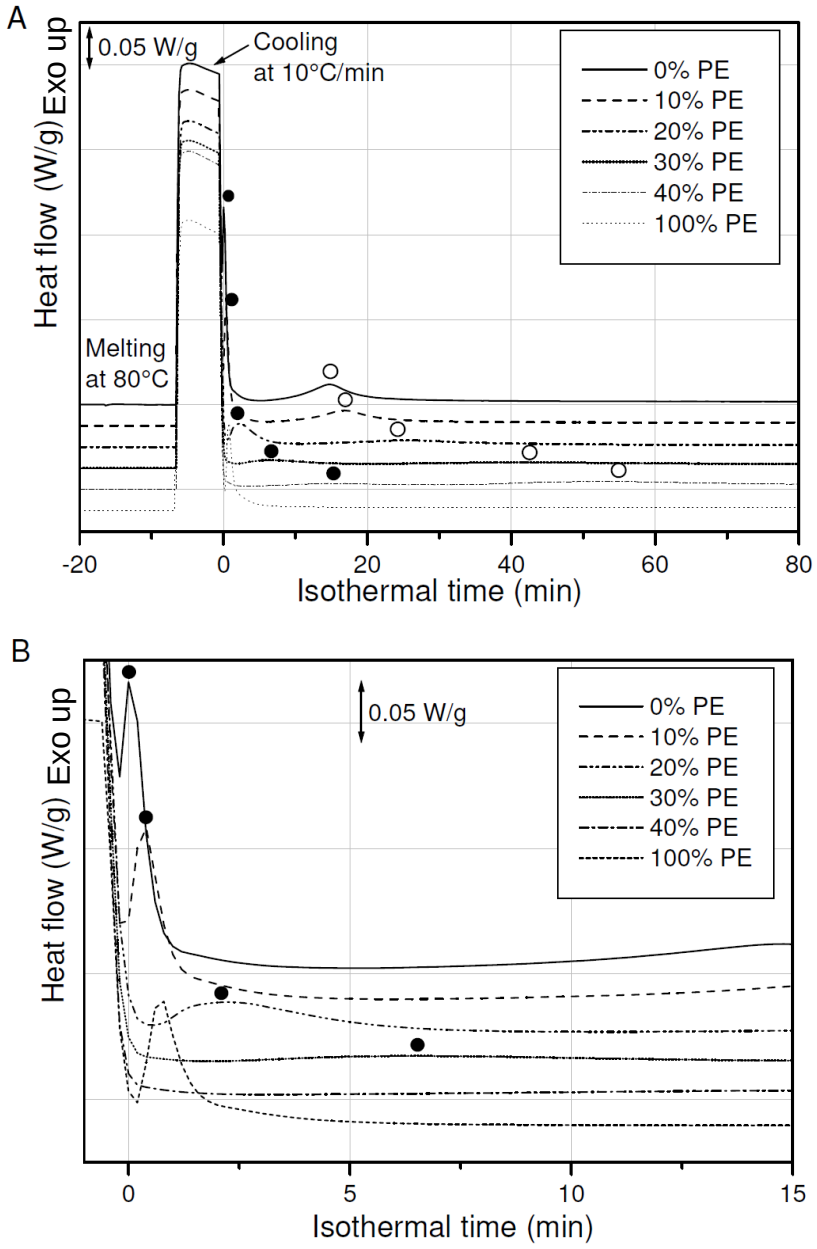

Figure 5.2. *Overlay plot of isothermal DSC crystallization curves of the pure palm oil and the pure phytosterol esters (PEs) and the blends containing 10%, 20%, 30% and 40% PEs at 20°C (Exo up) (A) and the same plot but zoomed in on Peak I (B). Peak maxima of Peak I (α crystallization) and Peak II (β' crystallization) are indicated with different symbols above the peak: Peak I (●) and Peak II (○).*

Relying on the morphology maps of PE-PO blends reported in chapter 3 (section 3.3.2.3) PE is expected to be at least partially in the PE_x crystalline state in the blends of PO with 10-40% PEs at 20°C. However, the same study reported that a large degree of supercooling is required for PE_x to crystallize, which might translate into a large induction time for isothermal crystallization at 20°C. This induction time seems to be longer than the isothermal crystallization time in the present study, except apparently for the sample with 40% PE.

Just as in the isothermal crystallization curve of pure PO, Peak I and Peak II were fully separated in time, irrespective of the PE concentration. For all samples, except for the 10% PEs sample, Peak I was also fully separated from the cooling run (Figure 5.2B). When looking at the isothermal crystallization curves of the PE-PO blends it can readily be observed that with an increasing PE concentration Peak I and Peak II shifted to longer crystallization times, broadened and became less intense. The lower intensity (i.e. the lower area covered by these peaks) obviously relates to the lower amount of PO present in these blends. However, areas should be calculated quantitatively to determine whether the reduced area simply follows the PO content or whether additional reducing effects are in place (see section 5.3.1.2). For Peak I, the shift and broadening effect can more clearly be seen in Figure 5.2B.

5.3.1.2. *Differential scanning calorimetry: quantitative analysis*

Because the isothermal crystallization curves of pure PO and the PE-PO blends showed the same peaks (Peak I and Peak II), they were quantitatively analyzed in the same way. Since Peak I was not fully separated from the cooling segment in the isothermal crystallization curves of pure PO and some of the PE-PO blends it could not be integrated and analyzed in terms of a crystallization model. Therefore Peak I was quantitatively analyzed by determining the time at its peak maximum in the isothermal crystallization curve (t_α) and the melting enthalpy (ΔH_α) obtained by integration of the endothermic melting peak obtained during heating in the stop-and-return experiments in which the isothermal crystallization was interrupted after the α crystallization. Both parameters are shown in Table 5.2. It was observed that t_α increased strongly as a function of the PE concentration (significant from 20% PE) which indicates the α crystallization was delayed upon PE addition. After addition of 10% PEs to PO t_α was already doubled and when adding 40% PEs t_α increased even more than 20 times. ΔH_α strongly decreased with increasing PE concentration showing that less α crystals were formed when adding an increasing amount of PE. For each PE concentration the decrease in ΔH_α was much larger than expected from the reduced PO amount by adding PE. For example when 40% PEs were added ΔH_α of PO became almost 10 times smaller.

The β' crystallization was analyzed using a model to describe fat crystallization kinetics that was introduced by Foubert et al. (2002)[196] and which obeys the following algebraic equation:

$$f(t) = a * \left[1 - \left(1 + (0.99^{1-n} - 1) * e^{(n-1)*K*(t-t_{ind})}\right)\right]^{\frac{1}{1-n}}.$$

When using DSC to follow the crystallization kinetics f is the released crystallization heat [J/g] at time t [h] and increases with time in a sigmoidal way. a is the value for f as t approaches infinity [J/g] which reflects the maximal amount of crystallization and K is the crystallization rate constant [h^{-1}]. t_{ind} [h] is defined as the time needed to reach 1% of the a value. It is a measure for the so-called induction time. n is the reaction order (dimensionless) and is related to the degree of curve asymmetry. A value of 2 for n means the sigmoidal curve is perfectly symmetric[196]. This model was fitted to the cumulative heat flow curve during the β' crystallization as a function of time. Because the parameters n and K are correlated, n was fixed at 5.2, which was the mean value of n of all measurements after the first fit and the fitting was subsequently redone with n fixed at 5.2. A value of n larger than 2 indicates that the beginning of the crystallization process is faster than the end[196].

Table 5.2 gives the parameters resulting from the Foubert model for the different blends. At higher PE fractions, a clearly decreased (significant from 10% PE) indicating that less β' crystals were formed. When adding 30% PEs the decrease in a was larger than the proportional amount of PE added. However, when adding 40% PEs a significantly increased relative to the value for the 30% PE blend. This was probably due to crystallization of PEs in the 40% PE blend as explained above in section 5.3.1.1.

The K value of the blends decreased up to 70% upon increasing the PE concentration, indicating a progressively slowing down β' crystallization. In case of the blend with 40% PEs a small (not significant) increase of K relative to the value obtained for the 30% PE blend was observed which could also be due to PE crystallization in the 40% PE blend.

Concerning t_{ind} a strong increase was noticed with increasing PE concentration for all the PE-PO blends demonstrating that the start of the β' crystallization was delayed. In the blend with 40% PEs t_{ind} was the highest being four times larger than t_{ind} of pure PO. This makes sense since in this two-step crystallization, β' crystals are formed by polymorphic transition of α crystals of which the crystallization also started later upon PE addition.

To verify whether the polymorphic transition itself was also effectively delayed, the polymorphic transition time from α to β' ($t_{transition}$) was calculated as the difference

between t_{ind} and t_{α} and the values are also represented in Table 5.2. Clearly $t_{transition}$ increased with an increasing PE concentration (significant from 20% PE) indicating β' crystallization started later not only due to the delayed α crystallization but also because of an increasingly delayed polymorphic transition. After adding 40% PEs $t_{transition}$ more than doubled compared to the value of pure PO.

Furthermore also the total melting enthalpy after the isothermal crystallization (ΔH_{tot}) was calculated as the sum of ΔH_{α} and a and is also represented in Table 5.2. As could be expected from the decreasing trends in ΔH_{α} and a also ΔH_{tot} decreased with an increasing PE concentration (significant from 10% PE). After adding 30% or more PEs ΔH_{tot} of PO was more than halved.

T_{m_offset} for each of the PE-PO blends was determined from the melting curves of the blends after reaching the 'equilibrium' state and are shown in Table 5.3. As T_{m_offset} of the PE-PO blends decreased with increasing PE concentration, the degree of supercooling during the isothermal measurements at 20°C also decreased with increasing PE concentration. Therefore, the observed effects as a result of PE addition during isothermal crystallization at 20°C could have been caused by the difference in supercooling rather than being provoked by differences in PE concentration.

Table 5.2. *Peak maximum of crystallization peak I (t_α) for isothermal crystallization, melting enthalpy (ΔH_α) of the stop-and-return melting profiles, parameters resulting from the Foubert model fit, transition time ($t_{transition}$) and total melting enthalpy after isothermal crystallization (ΔH_{tot}) for the pure PO and the blends containing 10%, 20%, 30% and 40% phytosterol esters at a crystallization temperature of 20°C. Values show mean ± standard deviation (n = 5)*

%PE	t_α (min)	ΔH_α (J/g)	*a* (J/g)	t_{ind} (min)	K (1/s)	$t_{transition}$ (min)	ΔH_{tot} (J/g)
0	0.7 ± 0.1 [a]	6.1 ± 0.2 [a]	9.4 ± 0.4 [a]	8.5 ± 0.2 [a]	10.9 ± 0.5 [a]	7.8 ± 0.2 [a]	15.5 ± 0.6 [a]
10	1.1 ± 0.2 [a]	4.7 ± 0.1 [b]	8.0 ± 0.0 [b]	10.0 ± 0.2 [b]	9.3 ± 0.9 [b]	8.9 ± 0.3 [a]	12.6 ± 0.2 [b]
20	2.4 ± 0.7 [b]	2.8 ± 0.2 [c]	5.7 ± 0.3 [c]	12.6 ± 1.1 [c]	5.3 ± 0.4 [c]	10.2 ± 1.3 [b]	8.5 ± 0.5 [c]
30	7.7 ± 0.6 [c]	1.8 ± 0.1 [d]	4.5 ± 0.2 [d]	22.4 ± 0.7 [d]	3.1 ± 0.2 [d]	14.7 ± 1.0 [c]	6.4 ± 0.2 [d]
40	17.1 ± 0.9 [d]	0.6 ± 0.1 [e]	7.1 ± 0.3 [e]	35.8 ± 1.2 [e]	3.5 ± 0.0 [d]	18.7 ± 1.5 [d]	7.7 ± 0.3 [c]

***Table 5.3**. T_{m_offset} of the pure PO and the blends containing 10%, 20%, 30% and 40% phytosterol esters (PEs) and the calculated isothermal temperature based on the average T_{m_offset} inducing a degree of supercooling of 18.7°C for all the blends. T_{m_offset} shows the average ± standard deviation (n=5).*

% PEs	T_{m_offset} (°C)	Isothermal temperature (°C)
0	38.7 ± 0.2 [a]	20.0
10	38.0 ± 0.3 [b]	19.3
20	36.7 ± 0.2 [c]	18.1
30	35.9 ± 0.2 [d]	17.3
40	35.0 ± 0.4 [e]	16.3

5.3.2. ISOTHERMAL CRYSTALLIZATION AT A CONSTANT DEGREE OF SUPERCOOLING OF 18.7°C

In order to eliminate the difference in degree of supercooling of the blends, isothermal crystallization was analyzed at a constant supercooling of 18.7°C. The isothermal temperature used for each blend was calculated based on T_{m_offset} and is shown in Table 5.3. The DSC data were used to get a first view on the isothermal crystallization mechanism and to provide quantitative data on the kinetic behavior by applying the Foubert model. This time also synchrotron XRD analyses were performed to examine the polymorphic behavior.

5.3.2.1. *Differential scanning calorimetry: qualitative analysis*

Figure 5.3A shows an overlay of representative isothermal crystallization curves of pure PO and PO with addition of different concentrations of PEs at a supercooling of 18.7°C. The curve of pure PO during isothermal crystallization at 20°C has already been discussed in section 5.3.1.1. The isothermal crystallization curves of the PE-PO blends with 10 to 30% PEs showed the same two peaks (Peak I and Peak II) as the curve of pure PO and no other peaks (due to PE crystallization) could be visually distinguished. For the blend with 20% PEs it was later confirmed by XRD that PEs did not crystallize during the isothermal crystallization at a supercooling of 18.7°C (see section 5.3.2.3). The isothermal crystallization curve of the blend with 40% PEs showed one extra peak between Peak I and Peak II which corresponded to the crystallization of PEs (later confirmed by XRD, see section 5.3.2.3). From Figure 5.3A and more clearly from the detailed picture of Peak I in Figure 5.3B it is clear that Peak I was sharp and started immediately after cooling in the isothermal crystallization

curves of each of the PE-PO blends. The intensity of Peak I became lower as a function of the PE concentration but there was no noticeable effect of the PE concentration on the width of Peak I. Concerning Peak II the effects of PE addition were clearer than for Peak I. With an increasing PE concentration Peak II became broader, was shifted to later times and its intensity became lower.

5.3.2.2. *Differential scanning calorimetry: quantitative analysis*

Since the isothermal crystallization curves at a supercooling of 18.7°C of the PE-PO blends with 10 to 30% PEs showed the same peaks (Peak I and Peak II) as the isothermal crystallization curve of pure PO at 20°C, their quantitative analysis was performed similarly. For the blend with 40% PEs, Peak I was not fully separated from the PE crystallization peak and therefore no stop-and-return analysis could be done on this sample and ΔH_α could not be determined. For the same blend Peak II was fully separated from the crystallization peak of the PEs and was therefore quantitatively analyzed in the same way as Peak II of pure PO during isothermal crystallization at 20°C.

The analyzed parameters for the α crystallization (t_α and ΔH_α) of the pure PO and the PE-PO blends during isothermal crystallization at a supercooling of 18.7°C are reported in Table 5.4. It can be seen that the α crystallization of PO only started later once 40% PEs was added (t_α increased). At lower PE concentrations, no difference was observed with respect to the value of pure PO. The increase of t_α was ten times less compared to when crystallization was executed at 20°C for the sample with 40% PEs. The observation that the α crystallization of the PE-PO blends during isothermal crystallization at 20°C was strongly delayed as a function of the PE concentration was therefore caused by the difference in the degree of supercooling of the PE-PO blends, since this delay is nearly absent when the isothermal temperature is corrected for this difference in the degree of supercooling. Furthermore, only when at least 20% PEs were added ΔH_α reduced significantly, indicating that besides a less outspoken increase of t_α with increasing PE concentration, also the decrease of ΔH_α is less pronounced at constant degree of supercooling.

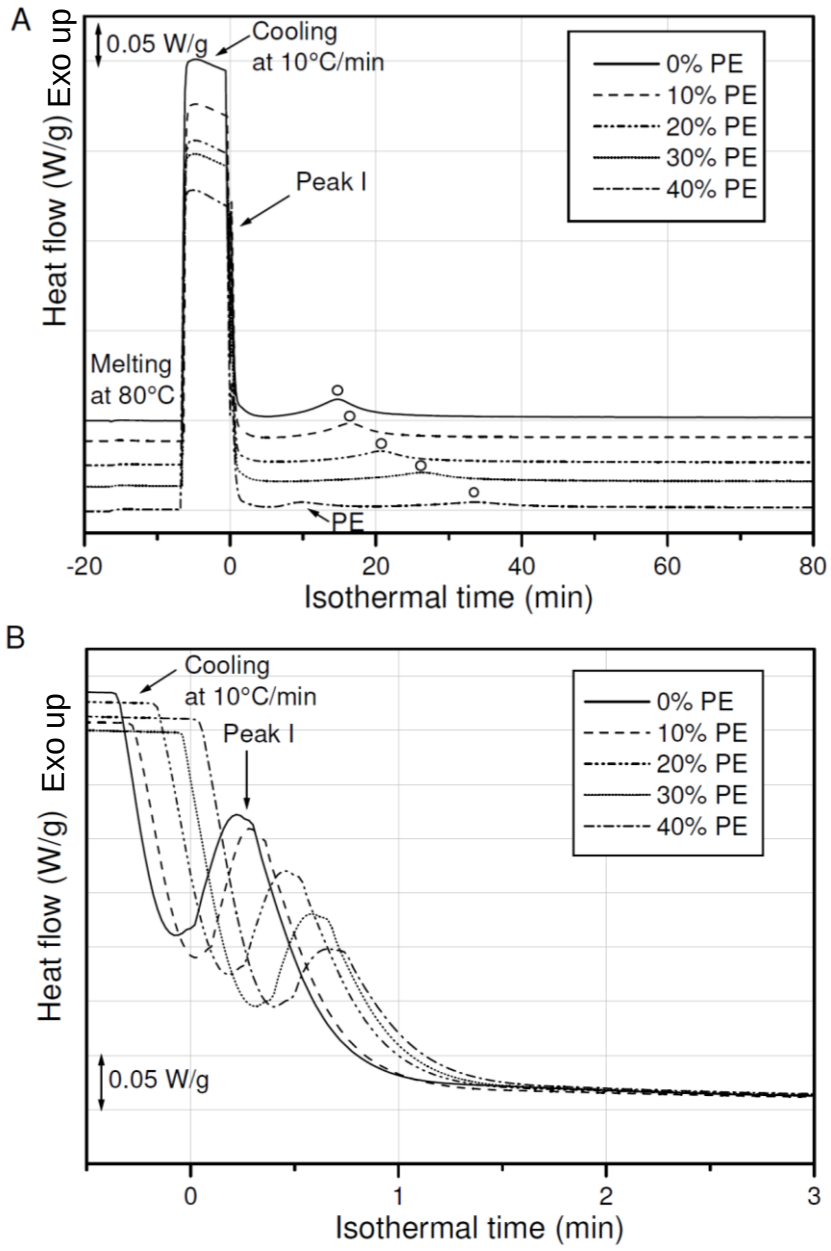

Figure 5.3. *Overlay plot of isothermal DSC crystallization curves of the pure palm oil and the blends containing 10%, 20%, 30% and 40% phytosterol esters (PE) at a constant degree of supercooling of 18.7°C (Exo up) (A) and an overlay plot of the same curves, zoomed in on Peak I (α crystallization) (B). Peak maxima of Peak II (β' crystallization) are indicated with a symbol (○) above the peak.*

Table 5.4. *Peak maximum of crystallization peak I (t_α) for isothermal crystallization, melting enthalpy (ΔH_α) of the stop-and-return melting profiles, Parameters resulting from the Foubert model fit, transition time ($t_{transition}$) and total melting enthalpy after isothermal crystallization (ΔH_{tot}) for the pure PO and the blends containing 10%, 20%, 30% and 40% PEs at a constant degree of supercooling of 18.7°C. Values show mean ± standard deviation (n = 5)*

%PE	t_α (min)	ΔH_α (J/g)	a (J/g)	t_{ind} (min)	K (1/s)	$t_{transition}$ (min)	ΔH_{tot} (J/g)
0	0.7 ± 0.1 [a]	6.1 ± 0.2 [a]	9.4 ± 0.4 [a]	8.5 ± 0.2 [a]	10.9 ± 0.5 [a]	7.8 ± 0.2 [a]	15.5 ± 0.6 [a]
10	0.7 ± 0.1 [a]	5.4 ± 2.2 [a,b]	7.9 ± 0.3 [b]	10.5 ± 0.6 [b]	12.1 ± 1.5 [a]	9.8 ± 0.6 [b]	13.3 ± 2.2 [a,b]
20	0.7 ± 0.1 [a]	3.4 ± 0.5 [b]	7.6 ± 0.5 [b]	11.7 ± 0.5 [c]	8.8 ± 0.8 [b]	11.1 ± 0.5 [c]	11.1 ± 0.3 [b]
30	0.8 ± 0.1 [a,b]	3.5 ± 0.3 [b]	7.8 ± 0.4 [b]	15.0 ± 0.8 [d]	7.2 ± 0.8 [c]	14.2 ± 0.8 [d]	11.3 ± 0.6 [b]
40	0.8 ± 0.1 [b]	-	4.1 ± 0.1 [c]	23.8 ± 0.4 [e]	7.1 ± 0.4 [c]	23 ± 0.4 [e]	-

Table 5.4 also gives the parameters of the Foubert model resulting from the fit of the β' peak during crystallization at a supercooling of 18.7°C. Less β' crystals were formed with an increasing PE concentration (a decreased, significant from 10% PE). Within experimental error the decrease in a was proportional to the PO amount, except for the sample with 40% PE for which the a value was significantly lower than expected from proportionality. It cannot be excluded that part of the β' signal was to be found in the preceding PE_x crystallization exotherm. The XRD data (see further below) demonstrate that these crystallization events are in fact not well separated in time. Furthermore, according to the XRD data discussed in section 5.3.2.3 it seems that the β' crystallization in the 40% PE sample slowly continues over a large time interval making definition of the DSC integration base line is rather uncertain. However, it will be demonstrated when discussing the XRD data that indeed the ultimate β' crystalline content is somewhat lower than what can be expected from proportionality. At a concentration exceeding 10% PE, the β' crystallization was also significantly slower compared to in pure PO as a function of the PE addition (K decreased). Just as seen in the results for the isothermal crystallization at 20°C in this case addition of 40% PEs did not lead to a decrease of K relative to the value obtained for the 30% PE blend. Furthermore β' crystallization started later with an increasing PE concentration as t_{ind} increased significantly for all studied concentrations. In the 40% PE blend t_{ind} was the highest, being almost three times the value of t_{ind} of pure PO. The increase of t_{ind} upon PE addition was smaller compared to that of the isothermal crystallization at 20°C which could be expected since also the increase of t_{α} was smaller for the PE-PO blends crystallized at a constant supercooling of 18.7°C.

Next to the parameters of the Foubert model, also $t_{transition}$ and ΔH_{tot} of the PE-PO blends crystallized isothermally at a constant supercooling were analyzed. The polymorphic transition started later with an increasing PE addition ($t_{transition}$ increased, significant from 10% PE). The change in $t_{transition}$ is almost equal to that of t_{ind} indicating the delayed β' crystallization is not caused by a delay in α crystallization but is due to a delay of polymorphic transition from α to β' when PEs are added. Finally, ΔH_{tot} decreased significantly compared to pure PO when adding at least 20% PE, but there was no further decrease that exceeded the error estimate if more PEs were added. However, due to the rather large errors involved, the gradual PO dilution and the potential interference of PE crystallization at high PE concentration we refrain from drawing conclusions on potential PE crystallinity differences.

From the DSC analyses it can be concluded that the main effect related to adding PEs that remains after correcting the isothermal temperature of the PE-PO blends for the difference in the degree of supercooling is the delay of polymorphic transition (increase in $t_{transition}$). The fact that this transition occurs at temperatures below

the melting temperature of the metastable α form suggests that this is a solid-solid transition rather than a melt-mediated transformation. The addition of PEs to PO in high concentrations (10-40%) probably hinders the solid-state polymorphic transition because the α crystals are physically more isolated from each other. This physical separation requires multiple, nucleation events to trigger the conversion at each separated location. This leads to a globally increased transformation time. A single nucleation event can trigger the conversion over a larger volume when α crystals are well connected, as seems to be the case for pure PO. This hypothesis was later confirmed with PLM (see section 5.3.2.4). This effect is probably enhanced by Ostwald ripening, a melt-mediated process whereby the critical size for a stable crystal increases, causing the smaller crystals to dissolve and leading to less and bigger crystals14. Due to Ostwald ripening the isolation of the PO crystals is therefore even more pronounced.

5.3.2.3. *X-ray diffraction*

The different polymorphic forms were unambiguously identified by comparing the SAXS and WAXD patterns that were simultaneously recorded during the isothermal crystallization of pure PO and PO with 20 and 40% PEs at a supercooling of 18.7°C. The mass fractions of the different polymorphs were quantitatively analyzed based on the WAXD patterns. Figure 5.4 shows the SAXS diffraction patterns of pure PO recorded at different moments during the isothermal crystallization and Figure 5.5A represents the mass fractions of α and β' as function of the isothermal time. Conform the literature the isothermal crystallization of PO at 20°C occurred in two steps[32,102–104]. Immediately after cooling, one strong first order peak at 2θ = 1.27° (d = 46.7Å) and one small third order peak at 2θ = 3.48° (d = 15.4 Å) appeared in the SAXS patterns accompanied by one peak at 2θ = 13.2° (d = 4.22 Å) in the WAXD patterns. These spacings are characteristic of the α polymorph in a 2L-stacking. The α fraction reached a maximum of about 7% (Fig. 5.5A). As deduced from the SAXS and WAXD data, the polymorphic transition to β' started after 7 min. From that moment, one strong first order peak at 2θ = 1.38° (d = 42.9 Å) and a small third order peak at 2θ = 4.18° (d = 14.1 Å) emerged in the SAXS patterns while the other peaks that were already present started to vanish. From the same moment onwards three peaks could be observed in WAXD at 2θ = 13.4° (d = 4.41 Å), 2θ = 13.9° (d = 4.27 Å) and 2θ = 15.0° (d = 3.95 Å). An isosbestic point occurred in the SAXS patterns between 9 and 14 min since all the patterns of these frames passed through one single point (Fig. 5.4). The isosbestic point indicates that the total crystal volume is constant during the polymorphic transition[104]. After 14 min approximately all α crystals were transformed to β' and extra β' crystals were formed directly from the melt. At the end of the isothermal time the mass fraction of β' crystals was circa 15% (Fig. 5.5A).

The SAXS and WAXD patterns of PO with 20% PEs were very similar to those of pure PO since only the typical PO peaks were observed and thus the PEs did not crystallize in this blend (detailed results not shown). Just as for the pure PO, immediately after cooling α peaks appeared in the SAXS and WAXD patterns. Figure 5.5B shows that the α fraction reached a maximum value of about 7%. It was clear from the SAXS and WAXD patterns that the polymorphic transition started after 9 min and in the SAXS patterns an isosbestic point was observed from 12 to 24 min after which extra β' crystals were formed directly from the melt. The fraction β' at the end of the isothermal time was approximately 13.5% (Figure 5.5B).

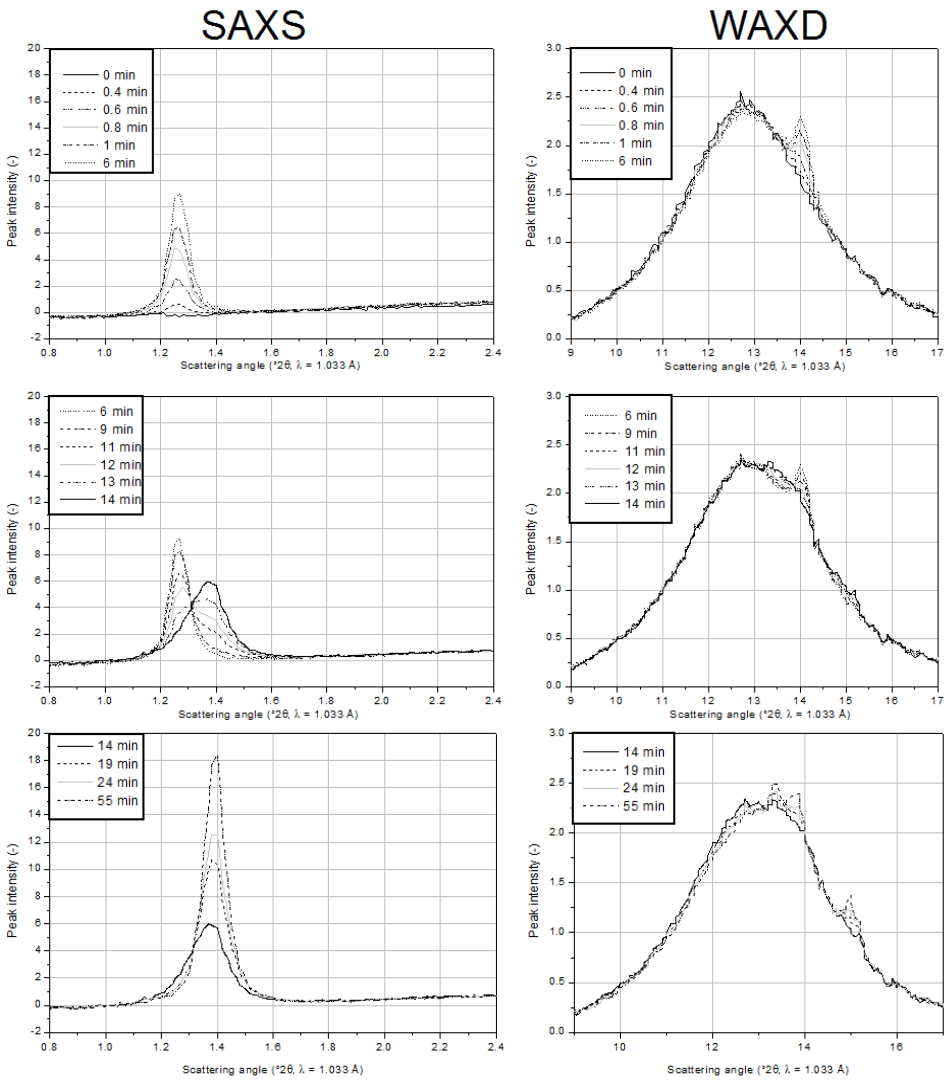

Figure 5.4. *SAXS and WAXD diffraction patterns at different times during the isothermal crystallization of pure palm oil at 20°C.*

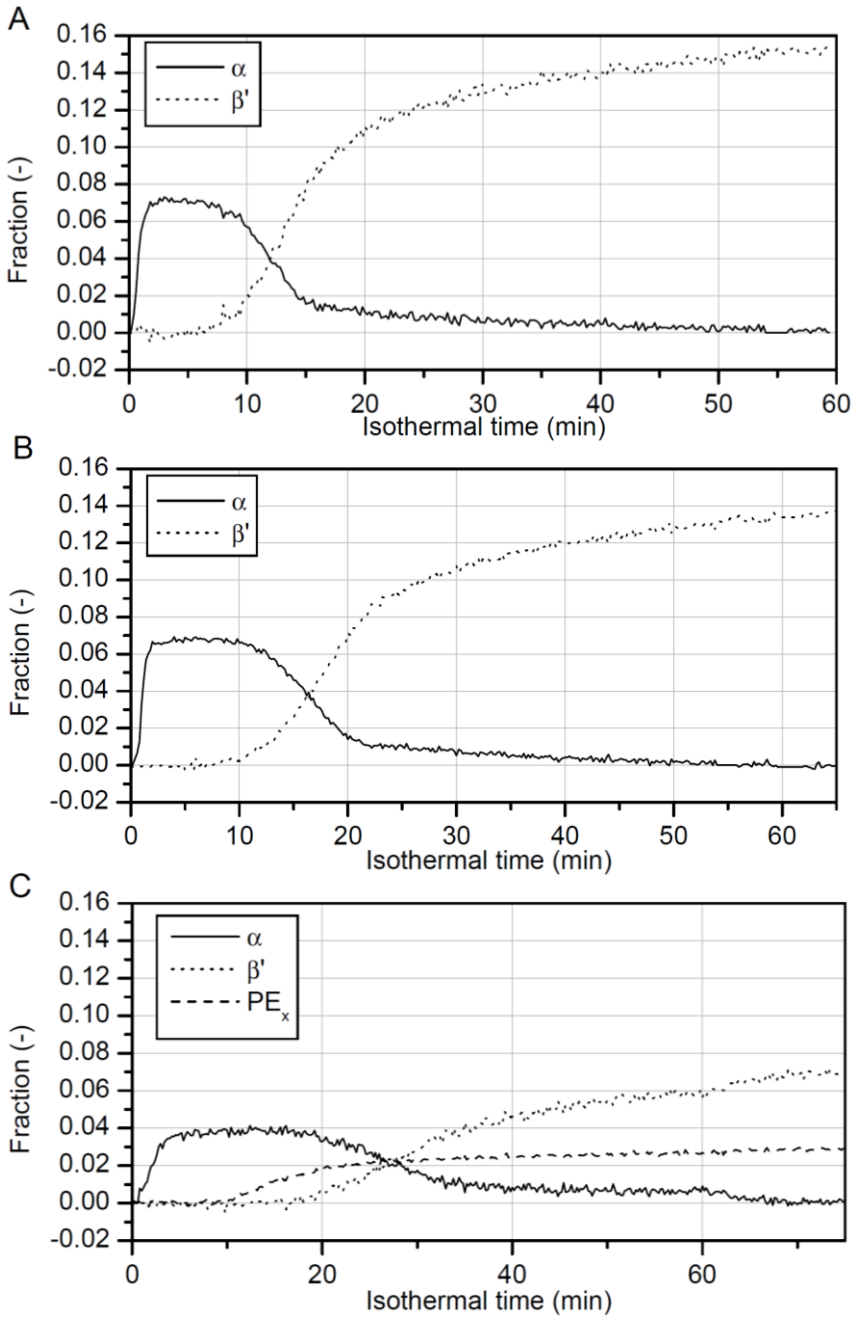

Figure 5.5. *Mass fraction of different polymorphs as measured by WAXD during isothermal crystallization at a constant degree of supercooling of 18.7°C. A: pure palm oil (PO), B: PO with 20% phytosterol esters (PEs), C: PO with 40% PEs.*

The isothermal crystallization at 18.7°C supercooling of PO with 40% PEs was different from that of pure PO and PO with 20% PEs since the PEs crystallized in this blend. Figure 5.6 shows the SAXS patterns of PO with 40% PEs recorded at different moments in time during the isothermal crystallization at a supercooling of 18.7°C and Figure 5.5C represents the mass fractions of the different polymorphic forms that occurred as a function of the isothermal time. Almost immediately after cooling typical α peaks appeared in both the SAXS and WAXD patterns. After 10 min 5 other peaks started to occur in the WAXD patterns at 2θ = 9.57° (d = 6.23 Å), 2θ = 9.80° (d = 6.06 Å), 2θ = 10.2° (d = 5.81 Å), 2θ = 12.3° (d = 4.81 Å) and 2θ = 12.9° (d = 4.61 Å). These spacings coincided with those of the structured form named PE_x as reported in chapter 3. Compared to the WAXD patterns, the PE_x peaks in the SAXS patterns at 2θ = 1.07° (d = 55.5 Å) (first order) and 2θ = 2.14° (d = 46.7 Å) (second order) were broader and had a much smaller intensity and therefore could only be clearly distinguished from about 16 min.

Since in the SAXS and WAXD patterns of PO with 40% PEs only peaks with the same spacings as the pure PO and the pure PEs occurred, it can be concluded that the PEs and PO crystallized separately from each other and that no new (compound) crystal structures were formed in this blend. Of the two ordered PE structures described in chapter 3 the PE_x structure was thus formed during isothermal crystallization of PO with 40% PEs at 18.7°C supercooling, which corresponds to a temperature of 16.3°C. This could be expected from the morphology map of heating reported in chapter 3 because 16.3°C is higher than the melting temperature of PE_Y and lower than the melting temperature of PE_x in the 40% PE blend.

Furthermore, it was confirmed that the extra peak between Peak I and Peak II in the DSC curve of PO with 40% PEs was correctly assigned to the crystallization of the PEs since the polymorphic transition of α to β' only started after PE crystallization had begun, more specifically at 19 min. However, the XRD data show that the PE crystallization was not completely finished before the α to β' conversion started, which demonstrates that these crystallization events were actually not well separated in time in the DSC crystallization curve.

Just as for pure PO and PO with 20% PE, an isosbestic point appeared in the SAXS patterns during the polymorphic transition from 20 to 45 min after which extra β' crystals were formed from the liquid phase. The occurrence of an isosbestic point in this time window indicates that the PE_x crystals do not contribute to any scattering in that angular range but that otherwise – just like for pure PO - all β' crystals are generated from existing α crystals in the initial stage. At the end of the isothermal crystallization the blend consisted of 3% PE_x and 7.5% β' crystals.

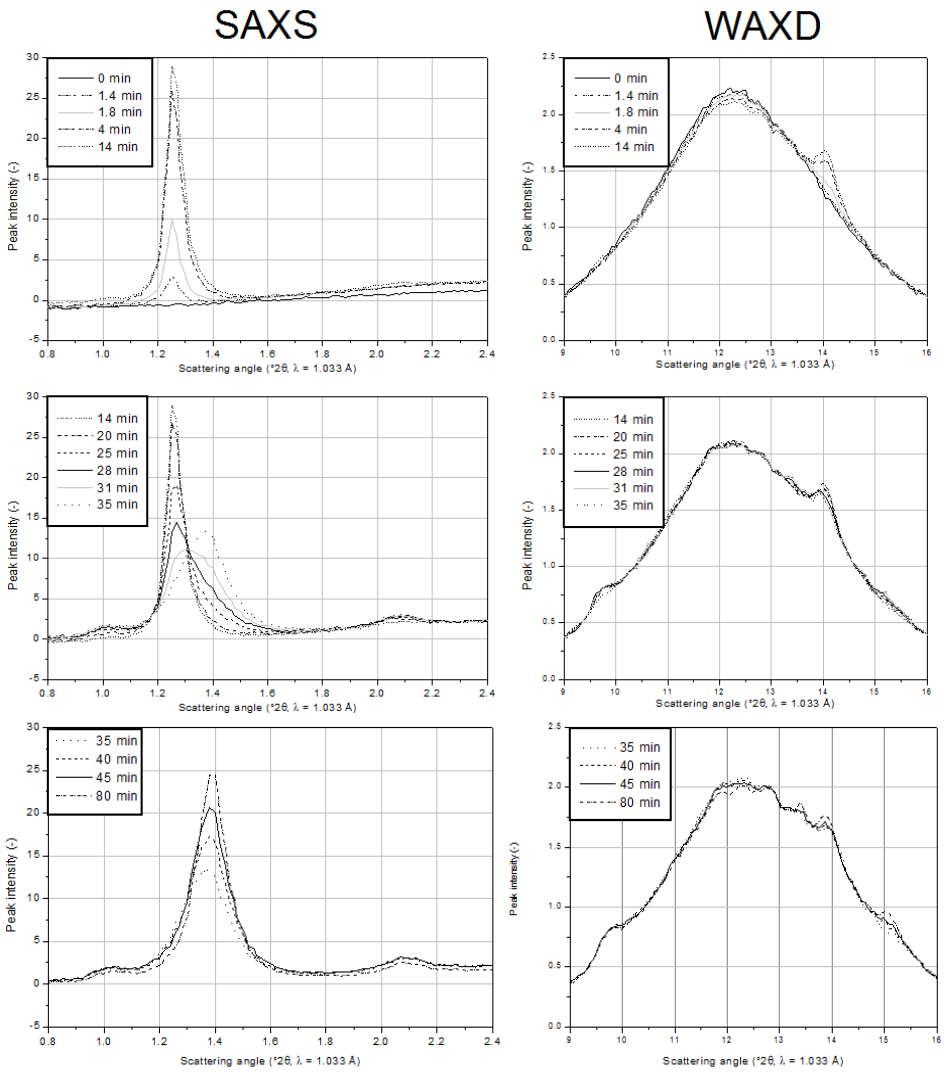

Figure 5.6. *SAXS and WAXD diffraction patterns at different times during the isothermal crystallization of palm oil with 40% PEs at 16.3°C.*

When the results of the XRD analyses are compared with those of the DSC experiments, very similar trends are observed. Both DSC and XRD results showed that the start of the α crystallization occurred immediately after cooling and was almost not delayed as a function of the PE concentration.

However the decreasing trend in the amount of α crystallization upon PE addition was in the WAXD data only visible when more than 20% PEs was added to PO while ΔH_α of PO (obtained by DSC) already decreased significantly from 20% PEs addition.

This difference is probably due to an incomplete crystallization of the samples at the end of the observed crystallization time as shown by the XRD data which resulted in an uncertain definition of the DSC integration baseline.

Concerning β' crystallization t_{ind} as measured by DSC almost equaled the start of the polymorphic transition as observed in SAXS and WAXD, except for the blend with 40% PEs where t_{ind} was higher than expected based on the WAXD data. Also a decreasing trend was observed in the amount of β' crystals formed as measured by DSC (a value of the Foubert model) as well as by XRD, although for the blend with 40% PEs the effect was larger when measured by DSC. These deviations between the DSC and the XRD data for the blend with 40% PE may both be caused by the fact that according to the XRD data the PE crystallization and the α to β' conversion were not well separated in time in the DSC crystallization curve and by the uncertain definition of the DSC integration baseline as explained before.

5.3.2.4. *Polarized light microscopy*

Figure 5.7 shows the PLM images of the lipid crystal networks of pure PO and PO with 40% PEs during isothermal crystallization at a supercooling of 18.7°C after an isothermal time of 5 min. According to the DSC and XRD results both samples only contained α crystals of PO at that moment. As can be seen in Figure 5.7 the typical network of spherulites was seen for PO[55]. The same type of spherulites were also present in the microstructure of the blend with 40% PEs but they were much smaller and also the amount was much smaller. In the blends with 10 to 30% PEs an intermediate microstructure was observed (results not shown). In the microstructure of pure PO the network of α crystals was much denser and more continuous than the microstructure of the blend with 40% PEs which only showed a weak crystal network, but physically isolated α crystals that were positioned far from each other. The increasing lack of a dense crystal network probably delays the solid-state polymorphic transition of α to β' upon an increasing PE addition.

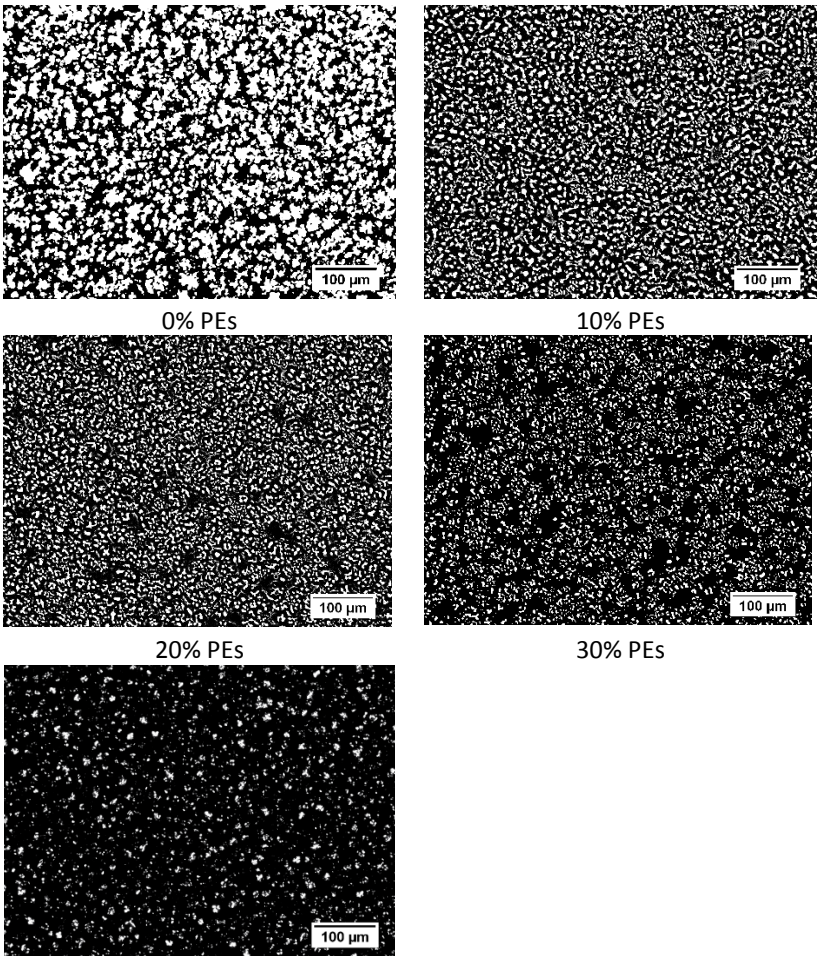

Figure 5.7. *Polarized light microscopy images of the lipid crystal networks of pure palm oil (A) and palm oil with 10%, 20%, 30% and 40% PEs (B) during isothermal crystallization at a degree of supercooling of 18.7°C after an isothermal time of 5 min. Black bar represents 100 µm.*

5.4. CONCLUSION

After correcting the isothermal crystallization temperature of the PE-PO blends for the difference in the degree of supercooling the increasing effect of PE addition on t_α had almost completely disappeared compared to the experiments without correction for the difference in the degree of supercooling. The major effect that remained was the delay of the polymorphic transition (increase in t_{ind} and $t_{transition}$). This solid-solid transformation needs to be nucleated as well and when

not well connected, each α crystal aggregate needs to nucleate on its own, which delays the global transformation process. When well connected, the transformation can travel through the network without the need for frequent primary nucleation of the solid-solid transformation. As indicated by the PLM images the α crystals were physically more isolated from each other at increasing PE concentrations.

Furthermore, it was seen that upon an increasing PE concentration less β' crystals were formed, even after correction for the difference in the degree of supercooling of the blends, although it should be noted that the crystallization of the samples was not fully completed at the end of the observed crystallization time. Of course upon PE addition the amount of PO (forming the β' crystals) that was present in the blend decreased. Furthermore, at low PE concentrations the PEs themselves did not crystallize but acted as a liquid oil, diluting the PO.

From a practical point of view, avoiding the strong delaying effects on the crystallization rate of PE-PO blends could thus be obtained by lowering the crystallization temperature in order to compensate for a difference in the degree of supercooling. However, the delay of the polymorphic transition from α to β' which also increases the necessary crystallization time still remains an issue in that case. However, at larger supercooling, the α crystalline content might increase to the extent that again a percolating network is formed, which should enhance the solid-solid transformation kinetics. Further research is needed to confirm this hypothesis.

Part III
Crystallization and melting behavior of pure phytosterol esters and their phase behavior in blends with palm oil

CHAPTER 6
NON-ISOTHERMAL CRYSTALLIZATION AND MELTING BEHAVIOR OF PURE PHYTOSTEROL ESTERS CONTAINING DIFFERENT TYPES OF FATTY ACIDS

6. NON-ISOTHERMAL CRYSTALLIZATION AND MELTING BEHAVIOR OF PURE PHYTOSTEROL ESTERS CONTAINING DIFFERENT TYPES OF FATTY ACIDS

6.1. INTRODUCTION

Several publications describe the melting behavior of different types of pure phytosterol esters (PEs)[3–8]. Most authors reported the melting temperature and melting enthalpy of the PEs except for Kuksis & Beveridge (1960)[3] who did not report enthalpy values. Next to its melting behavior, Vu et al. (2004)[5] also described the crystallization behavior of β-sitosteryl laurate. However, difficulties arise when trying to compare and use the reported data since it is unclear how the melting temperatures were extracted from the melting curves obtained with differential scanning calorimetry (DSC). Furthermore, the purity of the PEs used in the different studies is greatly divergent ranging from very high (> 95%) to rather low (50-99%) in the publication of Kuksis & Beveridge (1960)[3] and very low (8.5-40.3%) in the study of Vu et al. (2004)[5] or even not mentioned[4,6]. Finally, there is currently no X-ray based crystallographic information available on pure phytosterol esters.

The objective of this chapter was to investigate the influence of chain length and degree of unsaturation of the fatty acid esterified to β-sitosterol on the non-isothermal crystallization and melting behavior of the β-sitosteryl esters using DSC. Insight in the microstructure was obtained by using polarized light microscopy (PLM) and the crystal structure of the β-sitosteryl esters was examined for the first time with time-resolved synchrotron X-ray diffraction (XRD). β-sitosteryl esters containing different types of fatty acids (stearic (C18:0), palmitic (C16:0), lauric (C12:0), oleic (C18:1) and linoleic acid (C18:2)) were synthesized by enzymatic esterification.

6.2. MATERIALS AND METHODS

6.2.1. MATERIALS

β-sitosterol (≥ 70%) and oleic acid (≥ 90%) were purchased from Sigma Aldrich (Brondby, Denmark). Linoleic acid (97%) was obtained from TCI Europe (Zwijndrecht, Belgium) and stearic acid (97%), palmitic acid (98%) and lauric acid (99%) from Acros Organics (Geel,

Belgium). β-sitosterol and oleic acid were analyzed for their chemical composition since their purity was lower than that of the other starting materials. Table 6.1 shows the sterol composition of β-sitosterol as measured by the method described in Ryckebosch et al. (2012a)[165]. Table 6.2 reports the fatty acid composition of oleic acid as determined by the method described in Ryckebosch et al. (2012b)[166].

Table 6.1*. Sterol composition (%) of β-sitosterol (average of two measurements, the error is 0.2%).*

Sterol	
β-sitosterol	80.9
β-sitostanol	12.9
campesterol	6.2

Table 6.2. *Fatty acid composition (%) of oleic acid (average of three measurements, the error is 0.2%).*

Fatty acid	
C16:0	3.0
C18:0	4.0
C18:1	91.2
C24:1	1.7

6.2.2. ENZYMATIC SYNTHESIS OF THE B-SITOSTERYL ESTERS

The synthesis of a series of fatty acid esters of β-sitosterol was based on the method of Panpipat et al. (2013)[145]. β-sitosterol was blended with a fatty acid (C12:0, C16:0, C18:0, C18:1 or C18:2) at a mole ratio of 1.0:1.0 (mol/mol) at a concentration of 0.2M in 800 mL hexane. Immobilized *Candida antarctica* lipase A (Codexis, USA) was added to the blend in the amount of 20% (wt% of β-sitosterol).

The reaction was conducted in a 1 L closed reactor with mechanic stirrer at 50°C for 48h under continuous stirring and in the presence of 62.5% (wt% of β-sitosterol) molecular sieve (Sigma-Aldrich, Brondby, Denmark) to remove the water from the solvent. The reaction was terminated by filtering out the immobilized lipase and the molecular sieve under vacuum pressure. The residue was washed with hexane to remove any substrate or product. Five types of β-sitosteryl esters were obtained: β-sitosteryl laurate (P-laurate), β-sitosteryl palmitate (P-palmitate), β-sitosteryl stearate (P-stearate), β-sitosteryl oleate (P-oleate) and β-sitosteryl linoleate (P-linoleate).

A first, rough estimation of the yield of the esterification reaction was obtained by thin layer chromatography (TLC). Therefore 10 µl of the resulting reaction mixtures was applied to a TLC plate together with 10 µl of β-sitosterol and 10 µl of each of the fatty acids as a reference. The plates were developed with two different developing solvents: first with chloroform/methanol/water (64:10:1, v:v:v) up to half of the plate and subsequently with chloroform/methanol/acetic acid (97.5:2.5:1, v:v:v) to nearly the top of the plate. In between the two solvents and at the end the plates were dried. The visualization of the spots on the plate was done by immersing the plate shortly in a sulfuric acid solution (30% in methanol) and subsequently heating the plate at 100°C for 1 min with a blow dryer. The spots of β-sitosterol and of the β-sitosteryl esters showed a purple color, while those of the fatty acids were white. The retention factors (Rf) of β-sitosterol, the fatty acids and the β-sitosteryl esters were 0.63, 0.47 and 0.91 respectively. The reaction yield was estimated based on the relative size of the β-sitosterol spot to the β-sitosteryl ester spot. For each type of β-sitosteryl ester the reaction yield was clearly lower than 90% and was estimated to be between 40% and 60%. It was thus necessary to further purify these β-sitosteryl esters.

6.2.3. PURIFICATION OF THE B-SITOSTERYL ESTERS

The synthesized β-sitosteryl esters were purified using a low-pressure silica column. A glass column (4 cm x 40 cm) packed with 300 ml silica gel (Sigma-Aldrich, Overrijse, Belgium) dispersed in hexane was used to remove β-sitosterol and fatty acids from the β-sitosteryl esters. First 10 g of reaction product was mixed with eight spoons of silica gel in hexane at 60°C for 5 min after which the solvent was removed. The silica containing reaction product was grinded to powder and then loaded on the column. Then 1.8 L of the solvent hexane/ethyl acetate (40:1, v:v) was allowed to flow through the column and the eluent was collected in tubes of 30 ml. As tested with TLC the Rf values of β-sitosterol, the fatty acids and the β-sitosteryl esters in this solvent were 0.00, 0.00 and 0.35 respectively.

Each tube was tested for the presence of β-sitosterol, fatty acids and β-sitosteryl esters using TLC by applying 10 µl of each test tube to a TLC plate. The plates were developed as described in section 6.2.2. The presence of β-sitosterol, fatty acids and β-sitosteryl esters on the plate was visualized using a sulfuric acid solution as described in 6.2.2. The tubes containing only β-sitosteryl esters and no β-sitosterol or fatty acids were collected and the solvent was evaporated.

6.2.4. DIFFERENTIAL SCANNING CALORIMETRY

The DSC experiments were performed as described in section 3.2.3. The time-temperature program used for the saturated β-sitosteryl esters was as follows: equilibration at 120°C for 10 min to ensure complete melting and to erase the crystal memory, followed by cooling at 5°C/min to 0°C to obtain the crystallization curve, subsequently holding at 0°C for 5 min and finally heating at 5°C/min to 120°C to obtain the melting curve. The unsaturated β-sitosteryl esters were subjected to a different time-temperature program. The time-temperature program for P-oleate was equilibration at 60°C for 10 min, followed by cooling at 5°C/min to 0°C to obtain the crystallization curve and subsequently holding at 0°C for 5 min and finally heating at 5°C/min to 60°C to obtain the melting curve. P-linoleate was equilibrated at 40°C for 10 min, subsequently cooled at 5°C/min to -60°C to obtain the crystallization curve, held at -60°C for 5 min and finally heated at 5°C/min to 40°C to obtain the melting curve. Each measurement was repeated five times.

The parameters deduced from the crystallization curve using the Universal Analysis software were the onset temperature of crystallization (T_{c_onset}) and the peak maximum of the crystallization peak (T_{c_max}). T_{c_onset} was determined by the intersection of the baseline of the crystallization curve with the absolute highest tangent at the high temperature side of the crystallization peak. Concerning the melting curve four parameters were defined, being the onset temperature of melting (T_{m_onset}), the peak maximum of the melting peak (T_{m_max}), the offset temperature of melting (T_{m_offset}) and the melting enthalpy (ΔH_{melt}). T_{m_onset} was determined as the intersection of the baseline of the melting curve with the absolute highest tangent at the low temperature side of the melting curve, while T_{m_offset} was the intersection of the baseline with the absolute highest tangent at the high temperature side of the melting curve. T_{m_max} was calculated with the Universal analysis software. In the case of P-laurate two melting peaks were observed of which both T_{m_max} were determined. ΔH_{melt}, i.e. the amount of heat absorbed during melting, was calculated by integration of the melting curve using a horizontal baseline with the intersection of the baseline with the melting curve as starting point and a fixed end point of 110°C for P-stearate and P-palmitate, 90°C for P-laurate and 38°C for P-oleate and -18°C for PE-linoleate.

6.2.5. X-RAY DIFFRACTION

Time-resolved synchrotron XRD experiments were performed at DUBBLE, the Dutch-Belgian beamline (BM26) at the European Synchrotron Radiation Facility (ESRF;

Grenoble, France). For P-stearate, P-palmitate and P-linoleate, small-angle X-ray scattering (SAXS) and wide-angle X-ray diffraction (WAXD) patterns were recorded simultaneously using the same setup as described in Chapter 3 (section 3.2.4.). P-laurate and P-oleate were analyzed analogously with a wavelength of 1.033 Å, but the only difference was that the scattering angle 2θ ranged from $0.07 < 2\theta < 3.40°$ for SAXS and $7.72 < 2\theta < 28.9°$ for WAXD. About 10 mg of melted lipids were sealed into a hermetic aluminum pan (TA Instruments, Brussels, Belgium) and loaded onto a temperature-controlled sample stage (Linkam HFS 191, Tadworth, UK). The same time-temperature program was used as for the DSC measurements (section 6.2.4.). The observed SAXS and WAXD spacings were temperature dependent. The reported spacings of the different crystal structures formed during cooling are those observed at 0°C. If crystal structures only formed at lower temperatures during cooling or during heating, the spacings were read at the temperature at which they appeared which is reported in section 6.3.3.

6.2.6. POLARIZED LIGHT MICROSCOPY

The PLM experiments were performed on an Olympus BH-2 microscope (Olympus, Berchem, Belgium). A small amount of melted fat was put between two glass slides and submitted to the same time-temperature profile as described in section 6.2.4 by using a Linkam optical DSC600 hot stage (Linkam Scientific Instruments Ltd, Tadworth, UK), with a liquid nitrogen cooling system. The microscope was equipped with a ProgRes CF color camera (Jenoptik optical systems GmbH, Jena, Germany) to take pictures at regular time intervals in the ProgRes CapturePro 2.10.0.1 software (Jenoptik optical systems GmbH, Jena, Germany). No PLM images could be obtained of the P-linoleate (liquid) crystalline structure due to its low melting temperature. At temperatures below -10°C the condensation and crystallization of water in the Linkam optical stage at a temperature below -10°C blurred the images.

Just as in Kellens et al. (1992)[197] the nucleation rate was determined by counting the number of new nuclei that appeared per time unit in an observation field of 1000 by 1000 µm. As occasionally the nucleation rate increased exponentially during cooling the average nucleation rate was calculated in a temperature range of 5°C starting from the formation of the first nucleus.

The crystal growth rate was measured optically by following the increase in spherulite radius as a function of time. Since the crystal growth rate increased slightly with decreasing temperature the average crystal growth rate during the whole period of crystal growth was calculated for each sample. In case of P-oleate many crystals were

formed and therefore the crystal growth rate of P-oleate was determined for three spherulites per sample instead of for each spherulite observed.

6.3. RESULTS AND DISCUSSION

6.3.1. DIFFERENTIAL SCANNING CALORIMETRY

The crystallization and melting curves of the β-sitosteryl esters are shown in Figures 6.1A and 6.1B respectively and the parameters obtained from them are listed in Table 6.3. The crystallization curves of the saturated β-sitosteryl esters were very similar and exhibited one sharp crystallization peak with a T_{c_max} that did not differ much from T_{c_onset}. The reproducibility of the crystallization curves of the saturated β-sitosteryl esters was rather low and decreased with a decreasing fatty acid chain length (results not shown). The decreasing reproducibility with a decreasing fatty acid chain length of the β-sitosteryl esters is reflected in the increasing high standard deviations of T_{c_onset} and T_{c_max} and is related to an inefficient primary nucleation as will be shown further below by PLM. Nucleation is a stochastic process, which leads to poor reproducibility if only a few nuclei are involved that grow into rather large crystals. On the other hand it seems that, once nucleated, crystal growth proceeded rather fast as deduced from the sharpness of the exothermic transition. Occasionally the sudden, massive exothermic heat associated with crystallization led to a rise of the temperature and a temporary looping of the DSC signal to higher temperatures (data not shown)[198].

The crystallization curves of the unsaturated β-sitosteryl esters differed from those of the saturated β-sitosteryl esters and were also mutually very dissimilar. The crystallization curve of P-oleate contained one peak with a reproducible T_{c_onset} and T_{c_max}. Therefore, it is expected that the nucleation efficiency of P-oleate was higher than that of the saturated β-sitosteryl esters resulting in more and smaller crystals (confirmed by XRD and PLM). The DSC crystallization curve of P-linoleate contained one very broad and weak peak which was almost not visible resulting in a low reproducibility of T_{c_onset} and T_{c_max}.

The DSC melting curves of the saturated β-sitosteryl esters were more reproducible than the crystallization curves (results not shown) as is reflected in the smaller standard deviations (Table 6.3). This is not surprising since in contrast to crystallization, melting is rarely nucleation controlled[199]. The heating runs of the β-sitosteryl esters contained one melting peak, except for the heating run of P-laurate that contained two melting peaks,

of which the origin is explained while discussing the SAXS and WAXD results (section 6.3.3).

As expected from literature T_{m_onset} and ΔH_{melt} of the β-sitosteryl esters (Table 6.3) increased with an increasing fatty acid chain length[3–8] because a longer fatty acid chain results in stronger intermolecular interactions and a better packing[6]. On the other hand T_{m_onset} and ΔH_{melt} decreased with an increasing degree of unsaturation of the fatty acid chain and the effect was much bigger compared to that of the fatty acid chain length because the double bond in the fatty acid disturbs the crystal packing to a larger extent[6].

The very low value of ΔT of P-oleate and ΔH_{melt} of P-linoleate indicated that the crystals formed by these β-sitosteryl esters were probably not highly structured. As confirmed by XRD, indeed rather than true crystals, liquid crystals were formed in these cases, which are known to exhibit little supercooling at their formation. ΔH_{melt} of P-oleate was much higher than that of P-linoleate indicating that next to the liquid crystalline phase P-oleate also formed true crystals. This was also later confirmed by XRD (section 6.3.3).

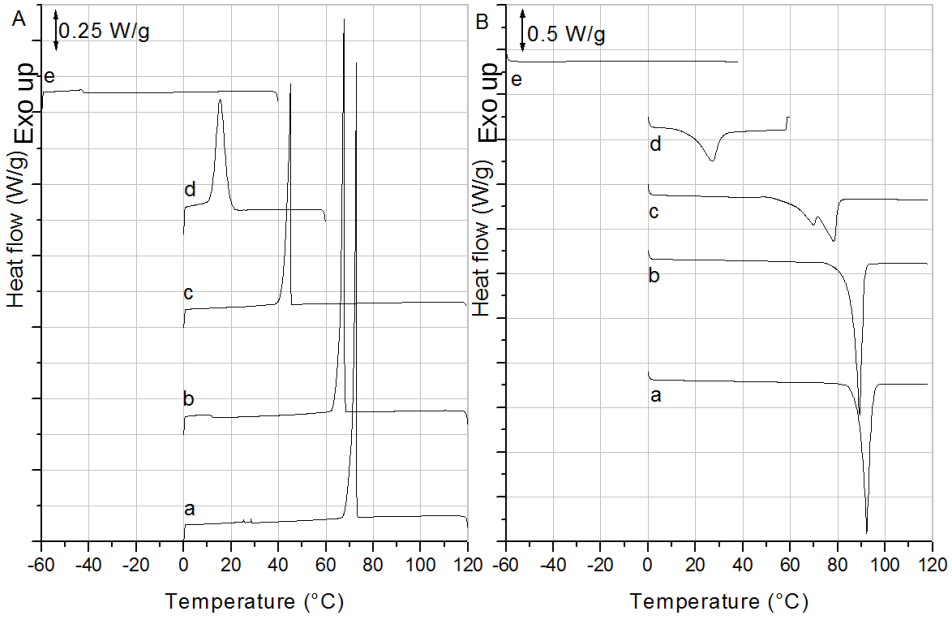

Figure 6.1. *DSC cooling (A) and heating (B) run of the β-sitosteryl esters (a: P-stearate, b: P-palmitate, c: P-laurate, d: P-oleate, e: P-linoleate).*

Table 6.3. *Onset temperature (T_{c_onset}) and peak maximum of the crystallization curve (T_{c_max}), onset temperature (T_{m_onset}), peak maximum (T_{m_max}) and offset temperature (T_{m_offset}) of the melting curve, melting enthalpy (ΔH_{melt}) and the difference between T_{c_onset} and T_{m_onset} (ΔT) of the different β-sitosteryl esters. Values show mean ± standard deviation of 5 repetitions.*

β-sitosterol ester	T_{c_onset} (°C)	T_{c_max} (°C)	T_{m_onset} (°C)	T_{m_max} (°C)	T_{m_offset} (°C)	ΔH_{melt} (J/g)	ΔT (°C)
P-stearate	73.4 ± 0.4	73.6 ± 0.6	89.5 ± 0.1	92.1 ± 0.1	94.8 ± 0.5	88.8 ± 7.2	16.1 ± 0.4
P-palmitate	65.8 ± 1.0	65.6 ± 0.9	86.0 ± 0.3	89.1 ± 0.1	91.2 ± 0.3	87.6 ± 1.1	20.2 ± 1.2
P-laurate	48.1 ± 2.8	47.3 ± 1.9	61.9 ± 3.6	69.9 ± 0.0	73.6 ± 0.1	58.9 ± 3.9	10.5 ± 1.2
				78.2 ± 0.1			
P-oleate	18.8 ± 0.2	15.2 ± 0.4	18.5 ± 2.2	27.3 ± 0.2	31.4 ± 1.7	45.1 ± 5.5	-0.9 ± 2.2
		-			34.3 ± 1.4		
P-linoleate	43.4 ± 1.4	45.1 ± 1.8	-	41.9 ± 1.8		2.3 ± 0.5	-

6.3.2. POLARIZED LIGHT MICROSCOPY

Figure 6.2 shows some images of the microstructure of the different β-sitosteryl esters. The microstructure formed by the saturated β-sitosteryl esters during cooling was very similar each containing the different features that are shown in Figure 6.2A-C at different places in the sample. During cooling only a few very large spherulites were formed as the one in P-palmitate shown in Figure 6.2A.

The growth rate of the saturated β-sitosteryl ester crystals was 50 ± 5 µm/s for P-stearate, 43 ± 6 µm/s for P-palmitate and 56 ± 15 µm/s for P-laurate. The crystal growth rates of P-stearate, P-palmitate and P-laurate were about 600, 100 and 100 times faster than that of isothermally crystallizing tristearin[17], tripalmitin[197] and trilaurin[200] respectively at a high degree of supercooling. However as in the entire observation field maximum one nucleus was observed, the nucleation rate of the saturated β-sitosteryl esters was too low to measure. Although the nucleation efficiency was low, the crystal growth rate of the saturated β-sitosteryl esters thus seemed to be very high. The combination of a low nucleation possibility and a high crystal growth rate resulted in the formation of very large crystals. The formed crystals were so large that it was only possible to see one spherulite in the observation field. As a consequence, using this setup it was not possible to determine the size of the spherulites of the saturated β-sitosteryl esters. It can only be stated that the spherulite diameter was larger than 2 mm which is the diameter of the observation field.

The hyperbolic shape of some of the spherulites such as the one shown in Figure 6.2A could be explained by the fact that it was formed relatively late and was completely swallowed by an earlier created even larger spherulite[201]. At other places in the sample (e.g. Figure 6.2B) also linear interfaces were observed between spherulites with the same size and growth rate. These were nucleated more or less simultaneously[201]. At places where no spherulites or interfaces were present, a fiber-like microstructure was observed reflecting the fiber-like arrangement of the nano-crystal aggregates in the spherulite (e.g. Figure 6.2C).

As shown in Figure 6.2D the microstructure of P-oleate was clearly different from that of the saturated β-sitosteryl esters. In this case the nucleation rate could be determined and was 1.8 ± 0.6 nuclei/mm^{2}s. The crystal growth rate was 0.49 ± 0.16 µm/s, which is approximately 100 times lower than that of the saturated β-sitosteryl esters. Due to the low crystal growth rate relative to the nucleation rate densely packed crystals with a varying size were obtained at the end of the cooling as shown in Figure 6.2D. With a spherulite diameter between 20 and 180 µm, the crystals were much smaller than those of the saturated β-sitosteryl esters.

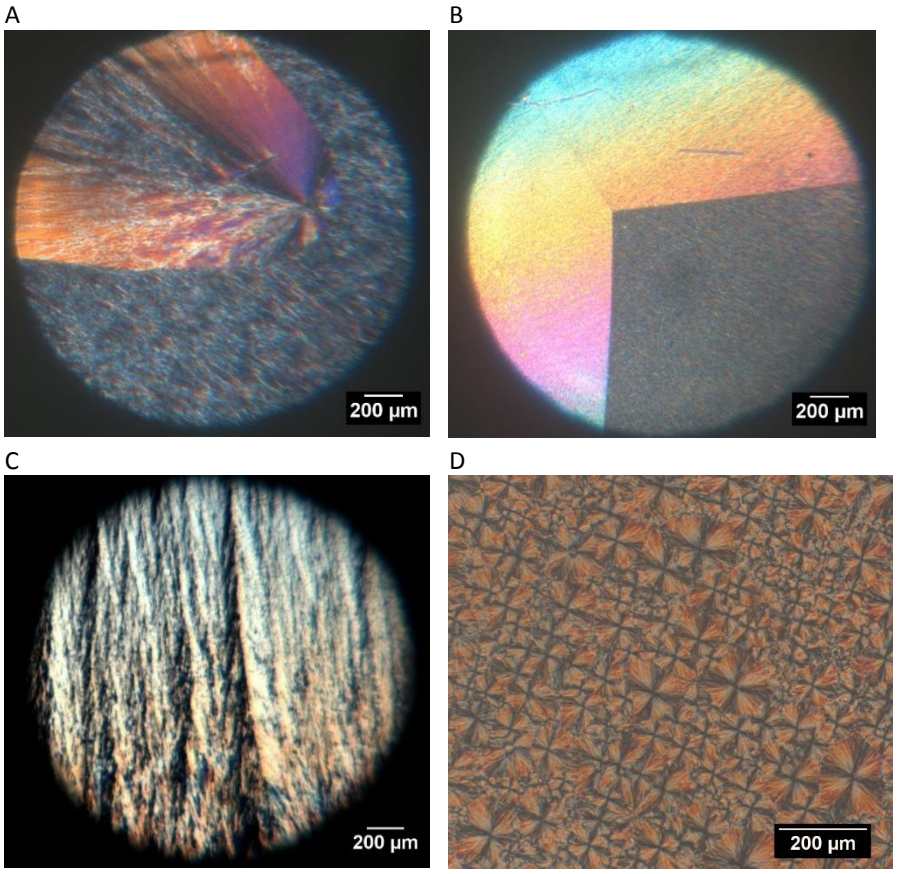

Figure 6.2. *Polarized light microscopy image of spherulites of β-sitosteryl esters at the end of the cooling (0°C). A: P-palmitate, B: P-laurate, C: P-stearate, D: P-oleate. The white scale bar represents 200 µm. Images were taken at a magnification of 40x, except for image D which was taken at a magnification of 100x.*

It was remarkable that the spherulites of the saturated as well as the unsaturated β-sitosteryl esters showed various colors such as yellow, orange, brown, light blue, green and pink. Since the microscope did not contain any type of filters, the crystal planes must have acted as a sort of filter causing destructive interference for certain wavelengths resulting in the interference colors observed through the crossed polarizers. The exact color observed at a certain position depends on many factors such as the degree of orientation of the crystal fragments in the radial direction of the spherulite nucleus, the degree of crystallinity, the distance of the position from the spherulite nucleus and the thickness of the sample[202]. The colors did further not have any importance.

During heating of the β-sitosteryl esters there was a short temperature range during which the colors faded and the image became greyish and eventually turned fully black. No other changes in the microstructures were observed.

6.3.3. X-RAY DIFFRACTION

Figures 6.3 to 6.7 show the SAXS and WAXD patterns of the different β-sitosteryl esters during cooling and heating. The SAXS and WAXD peaks that were newly formed during cooling and heating are marked according to their origin and their spacings are listed in Tables 6.4 to 6.7. The tables also indicate in which temperature range the listed spacings emerged. The temperatures at which the crystallization started as indicated in Tables 6.4 to 6.7 deviate somewhat from the values of T_{c_onset} listed in Table 6.3. The reason for this is the low reproducibility of the nucleation of the crystallization for the saturated β-sitosteryl esters, a slightly higher cooling rate (6°C/min in the XRD analysis compared to 5°C/min in the DSC analysis) due to a technical error of the Linkam device for P-oleate and the broad shape of the crystallization peak in the DSC cooling run for P-linoleate.

6.3.3.1. *Cooling*

During cooling of the saturated β-sitosteryl esters strong reflections were observed in the SAXS patterns which were (almost all) orders of the same periodicity indicating the formation of a layered crystal structure as indicated in Figures 6.3 to 6.5 and Tables 6.4 to 6.6. As many of the observed WAXD peaks were orders of the same periodicity this indicates that the ordering of the molecules into the layered crystal structure was so strong that the lamellar reflections were also visible throughout the WAXD. Moreover, these periodicity peaks were also the strongest peaks in the XRD patterns, confirming that the β-sitosteryl esters were highly ordered into the layered crystal structure. Similarly, as for the saturated β-sitosteryl esters, the SAXS and WAXD patterns of P-oleate also contained multiple orders of the same periodicity. From the XRD spacings related to the layered crystal structure it could be derived that the saturated β-sitosteryl esters and P-oleate crystallized in a bilayer structure during cooling as further discussed in section 6.3.4.

It was also examined whether the fatty acid moieties of the β-sitosteryl esters formed the same types of subcell packings as those observed in triglycerides. This was done by comparing the WAXD spacings in the XRD patterns of the β-sitosteryl esters with the typical short spacings of the aliphatic subcell packings thereby taking into account their relative intensities as far as this was allowed (see further below when discussing orientation effects). The identification of the subcell packings in the WAXD patterns was however disturbed by the presence of order peaks of the bilayer structure, often with a high intensity, at typical subcell spacings. For example the

spacing at 4.20 Å in the WAXD pattern of P-stearate could indicate a β' subcell packing, but the second typical β' peak is expected at the same spacing as the strong 16th order reflection of the bilayer structure at 3.84 Å[29]. However, the formation of a β' subcell during cooling was confirmed by the WAXD patterns during heating in which the β' peak at 3.82 Å was split off from the 16th order reflection. The reason why the β' reflection only became visible during heating is discussed into more detail in section 6.3.3.2. The situation in P-laurate was similar where the β' spacing at 4.20 Å already emerged during cooling, but the other β' spacing at 3.79 Å only became visible during heating when it was split off from the 16th order reflection. In P-palmitate the formation of the β' subcell was not confirmed as only the β' spacing at 3.77 Å was visible, while the second β' spacing coincided with the strong 14th order reflection which was not split into two peaks during cooling. The relative intensities of the β' peaks could thus not be examined. While in P-stearate and P-laurate (and possibly also in P-palmitate) a β' subcell packing was observed, the oleic acid moieties of P-oleate were packed in the α polymorph as indicated by the spacing at 4.14 Å[29]. As the hexagonal packing of the α subcell structure has a lower packing density than the orthorhombic packing of the β' subcell structure it is necessary to avoid the steric hindrance between the oleic acid chains due to the presence of the double bond. No other types of subcell packings were identified in the XRD patterns of the β-sitosteryl ester because not all required spacings were present judging relative peak intensities as considered not reliable because of orientation effects (see further below).

Of the other remaining SAXS and WAXD spacings some could be related to the ordering of the β-sitosterol moieties as they were very similar (except for a difference of 0.1 Å) to the spacings of pure β-sitosterol measured at room temperature that are reported in literature[203,204].

Another type of structure that was formed only by P-oleate and P-linoleate were liquid crystals, as indicated by the presence of one very strong SAXS peak with no corresponding WAXD peaks. During cooling P-oleate first formed a liquid crystalline phase which then transformed to a more stable crystalline phase. The formation of the liquid crystalline phase and its transformation to a truly crystalline phase could however not be distinguished in the DSC melting curve. A possible explanation for this is that the formation of the liquid crystals and the formation of the true crystals were both included in the single DSC melting peak or that the heat released by the formation of the liquid crystals was smaller than the detection limit of the DSC. During cooling of P-linoleate in SAXS one peak with a very high intensity emerged at the same spacing as for P-oleate while in WAXD no peak formation was observed. Leeson et al. (2002)[4] also reported the formation of a mesophase in P-oleate, that transformed to a more stable crystalline phase at a lower temperature and the

formation of a stable mesophase in P-linoleate, but this was not based on XRD analyses. A metastable mesophase with a very similar SAXS spacing is also formed by cholesteryl oleate[34].

Some of the spacings in the XRD patterns of the β-sitosteryl esters seemed not related to the bilayer structure, the packing of the β-sitosterol moieties, the subcell packing of the fatty acid moieties or the formation of liquid crystals. These spacings which are indicated as 'unidentified' in Figures 6.3 to 6.6 and Tables 6.4 to 6.7 could have various possible origins. First, they may be related to the packing of phytosterol moieties other than β-sitosterol as the β-sitosterol used for the synthesis of the β-sitosteryl esters also contained campesterol and β-sitostanol. The lack of the double bond in the sterol ring of β-sitostanol and especially the presence of a methyl group instead of an ethyl group in the sterol side chain of campesterol[109] could lead to a somewhat different packing of the phytosterol moieties in the crystal structure resulting in different reflections. Further research and XRD analysis of β-sitostanol and campesterol is needed to confirm this since this information is not available in literature at the moment. Furthermore, these 'unidentified' spacings may also be related to the intermolecular fatty acid – phytosterol interactions, but a profound crystallographic study, which was out of the scope of this research, is necessary to investigate this hypothesis.

Finally, it is of interest to note that rather than complete Debye-Scherrer rings, incomplete diffraction arcs were observed in the 2D SAXS and WAXD patterns of the saturated β-sitosteryl esters prior to azimuthal averaging as shown in Figure 6.8A-C. Such patterns are typical for a fiber like arrangement of the crystallites[19]. In the present case, PLM experiments demonstrated that the material crystallizes into very large spherulitic nano-crystal aggregates. The X-ray beam probes only a fragment of the spherulite far from its nucleus where a nano-crystalline bundel emanates radially from the spherulite nucleus, leading to a fiber like diffraction pattern. This effect of preferred orientation may lead to the absence or weakening of some crystalline reflections and hence a different azimuthally averaged pattern compared to when perfect powders would have been in view. Arcs in the SAXS and WAXD region with a common azimuthal orientation are crystallographically related. The arc patterns were different for the different β-sitosteryl esters. In the 2D patterns of P-palmitate pairs of arcs were observed at opposite sides of the 2D pattern indicating the X-ray beam probed the interface between two spherulites. The 2D patterns of P-laurate showed smaller arcs than those of P-stearate indicating that the P-laurate spherulite fragment was probed at a distance further away from the primary nucleus[205].

6.3.3.2. *Heating*

The various changes in the XRD patterns of the saturated β-sitosteryl esters during heating were divided into two major events. First, the intensity of some of the SAXS and WAXD peaks increased from a temperature similar to T_{m_onset} and from the same temperature more SAXS and WAXD spacings became visible. Some of these apparently new spacings were related to the packing of the β-sitosterol moieties or the packing in the bilayer structure while others could not be identified. It was also noticed that approximately from T_{m_onset} the 2D patterns left their arc like shape and converted to full circles towards the end of the melting as shown in Figure 6.8D. It is suggested that the least stable nano-crystallites (because of size or internal packing) melt and release crystal fragments from the spherulites that assume a fully random orientation. This random arrangement of the crystal fragments led to fully symmetric 2D patterns[19].

A second event in the SAXS and WAXD patterns of the saturated β-sitosteryl esters was the emerging of new peaks in a later stage during heating due to the transition to a new crystal structure. As indicated by the presence of the dimensions of the long spacings (and its higher orders in SAXS and WAXD) corresponding to the same periodicity the new crystal structure was also a bilayer. Therefore, the bilayer structure formed during cooling is referred to as bilayer 1 while the bilayer structure formed during heating is referred to as bilayer 2. The long spacings of bilayer 2 were shorter than those of bilayer 1 probably indicating that the layer to layer packing had increased while the molecule to molecule packing decreased because of thermal expansion thereby allowing a denser interdigitated layer to layer packing. In P-laurate during heating even a second structural transition occurred to yet another new crystal structure, which according to the d spacings of the stack periodicity also corresponded to a bilayer structure (bilayer 3). The layer to layer packing density in bilayer 3 was intermediate between that of bilayer 1 and bilayer 2.

Next to new order reflections related to the lamellar packing in bilayer 2 (and 3), also other new WAXD spacings emerged from the same temperature. Some of these other new WAXD spacings were very similar (except for a difference of 0.1 Å) to the spacings of pure β-sitosterol measured at room temperature that are reported in literature[203,204], while none of them were related to fatty acid subcell packings. The bilayer structures formed by the saturated β-sitosteryl esters during heating were therefore probably dominated by the packing of the β-sitosterol moieties rather than the fatty acid moieties. Furthermore, just as for bilayer 1, some of the spacings of bilayer 2 (and 3) could not be identified.

During heating of the unsaturated β-sitosteryl esters no structural changes occurred as no new peaks occurred in SAXS or WAXD (results not shown).

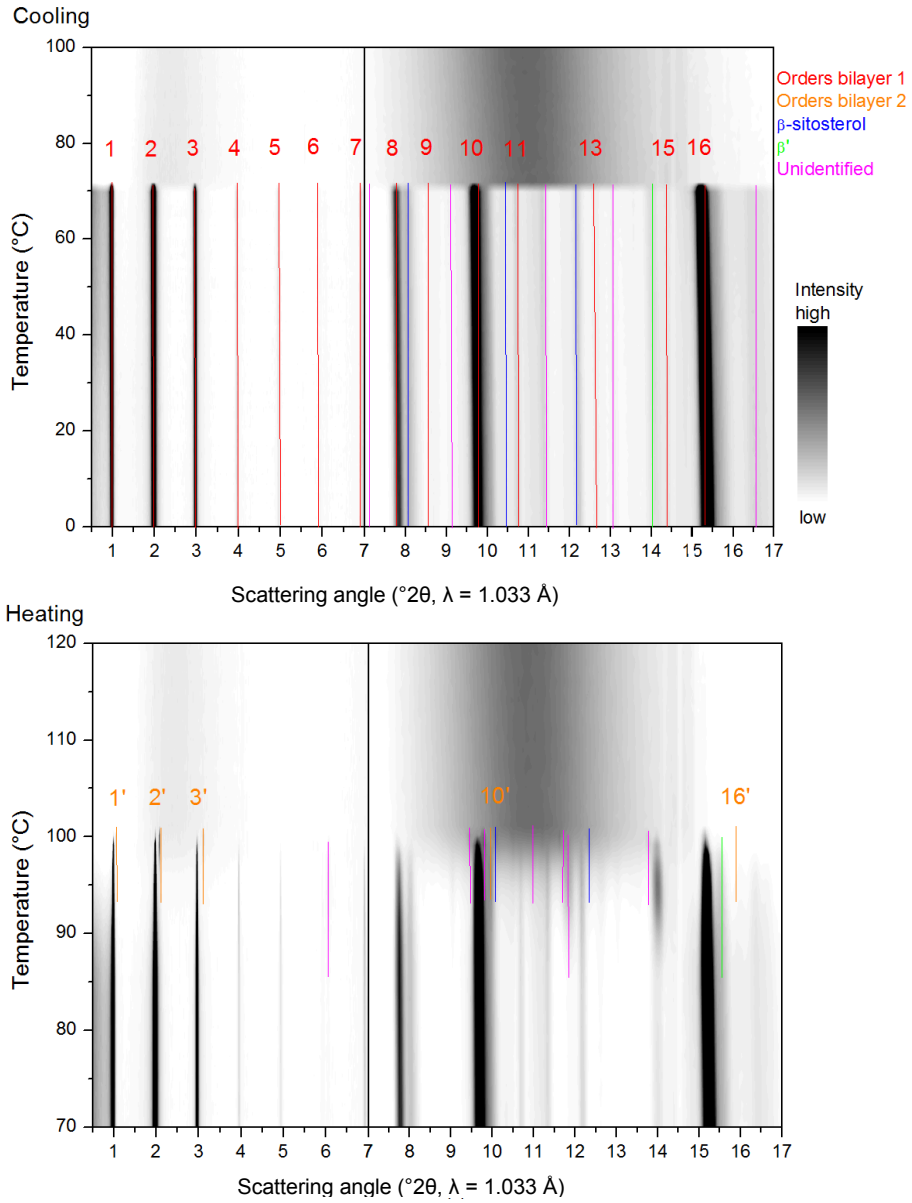

***Figure 6.3**. SAXS and WAXD data of P-stearate during cooling and heating. The legend indicates the identification of the spacings as an order reflection of bilayer 1 or bilayer 2 or as related to the packing of β-sitosterol moieties (β-sitosterol) or the β' subcell packing of the stearic acid moieties (β') or unidentified (UI).*

Table 6.4. *SAXS and WAXD spacings of new peaks appearing during cooling and heating of P-stearate with an indication if their intensity was relatively weak (w) or strong (s) and with their identification (ID) as an order reflection of bilayer 1 or bilayer 2 (with apostrophe) or as related to the packing of β-sitosterol moieties (SI) or the β' subcell packing of the stearic acid moieties (β') or unidentified (UI). The intensity of the spacings that emerged during heating was weak. λ = 1.033 Å.*

P-stearate	Cooling: from 71.8°C				Heating: 86.2-93.2°C			Heating: 93.2-100.6°C		
	2θ (°)	d (Å)	w/s	ID	2θ (°)	d (Å)	ID	2θ (°)	d (Å)	ID
SAXS	1.00	59.2	s	1				1.04	56.9	1'
	1.99	29.7	s	2				2.07	28.6	2'
	2.98	19.9	s	3				3.11	19.0	3'
	3.97	14.9	w	4						
	4.97	11.9	w	5						
	5.95	9.95	w	6						
	6.95	8.52	w	7						
	7.21	8.21	w	UI						
WAXD	7.86	7.53	s	8	6.05	9.78	UI	9.92	5.97	10'
	8.10	7.31	w	SI	11.9	4.97	UI	10.1	5.86	SI
	8.75	6.76	w	9	15.2	3.89	16	11.0	5.38	UI
	9.10	6.50	w	UI	15.5	3.82	β'	11.7	5.06	UI
	9.80	6.04	s	10				12.4	4.77	DI
	10.5	5.64	w	SI				13.9	4.26	UI
	10.7	5.53	w	11				15.9	3.72	16'
	11.4	5.19	w	UI						
	12.3	4.81	w	SI						
	12.7	4.66	w	13						
	13.1	4.52	w	UI						
	13.6	4.35	w	14						
	14.1	4.20	w	β'						
	14.4	4.11	w	15						
	15.4	3.84	s	16						
	16.6	3.57	w	UI						

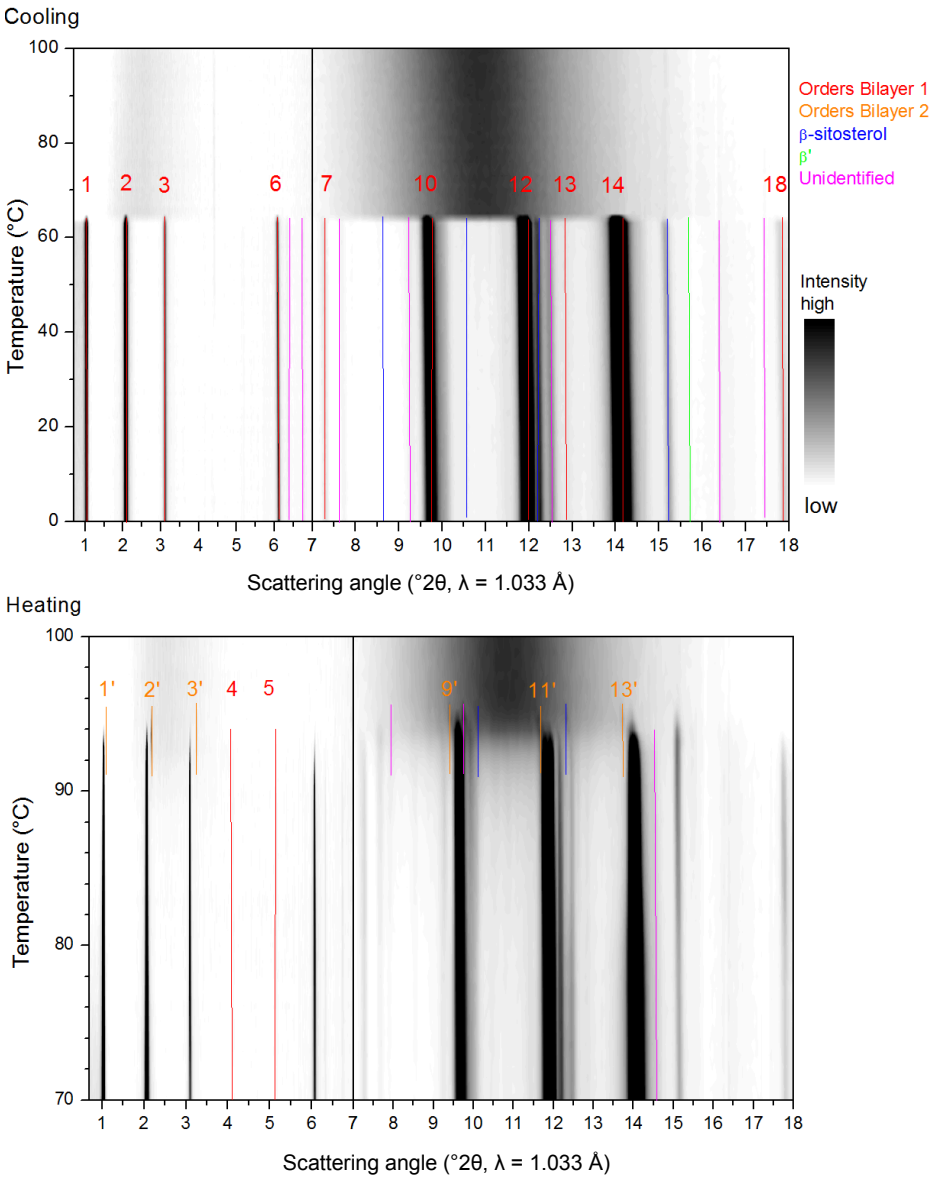

Figure 6.4. *SAXS and WAXD data of P-palmitate during cooling and heating. The legend indicates the identification of the spacings as an order reflection of bilayer 1 or bilayer 2 or as related to the packing of the β-sitosterol moieties (β-sitosterol) or the β' subcell packing of the palmitic acid moieties (β') or unidentified.*

Table 6.5. *SAXS and WAXD spacings of new peaks appearing during cooling and heating of P-palmitate with an indication if their intensity was relatively weak (w) or strong (s) and with their identification (ID) as an order reflection of bilayer 1 or bilayer 2 (with apostrophe) or as related to the packing of β-sitosterol moieties (SI) or the β' subcell packing of the palmitic acid moieties (β') or unidentified (UI). The intensity of the spacings that emerged during heating was weak. λ = 1.033 Å.*

P-palmitate	Cooling: from 64.7°C				Heating: 70.3-91.3°C			Heating: 91.3-95.6°C		
	2θ (°)	d (Å)	w/s	ID	2θ (°)	d (Å)	ID	2θ (°)	d (Å)	ID
SAXS	1.04	56.9	s	1	4.12	14.4	4	1.1	53.8	1'
	2.08	28.5	s	2	5.15	11.5	5	2.18	27.2	2'
	3.12	19.0	s	3				3.27	18.1	3'
	6.12	9.67	s	6						
	6.38	9.28	w	UI						
	6.81	8.69	w	UI						
	7.33	8.07	w	7						
WAXD	7.75	7.64	w	UI	11.8	5.02	UI	7.92	7.47	UI
	7.92	7.47	w	8	14.5	4.08	UI	9.34	6.34	9'
	8.63	6.86	w	SI				9.63	6.15	UI
	9.28	6.38	w	UI				10.1	5.86	SI
	9.75	6.07	s	10				11.6	5.10	11'
	10.5	5.64	w	SI				12.3	4.81	SI
	12	4.93	s	12				13.7	4.32	13'
	12.3	4.81	w	SI						
	12.6	4.70	w	UI						
	12.9	4.59	w	13						
	14.2	4.17	s	14						
	15.3	3.87	w	SI						
	15.7	3.77	w	β'						
	16.4	3.61	w	UI						
	17.4	3.40	w	UI						
	17.9	3.31	w	18						

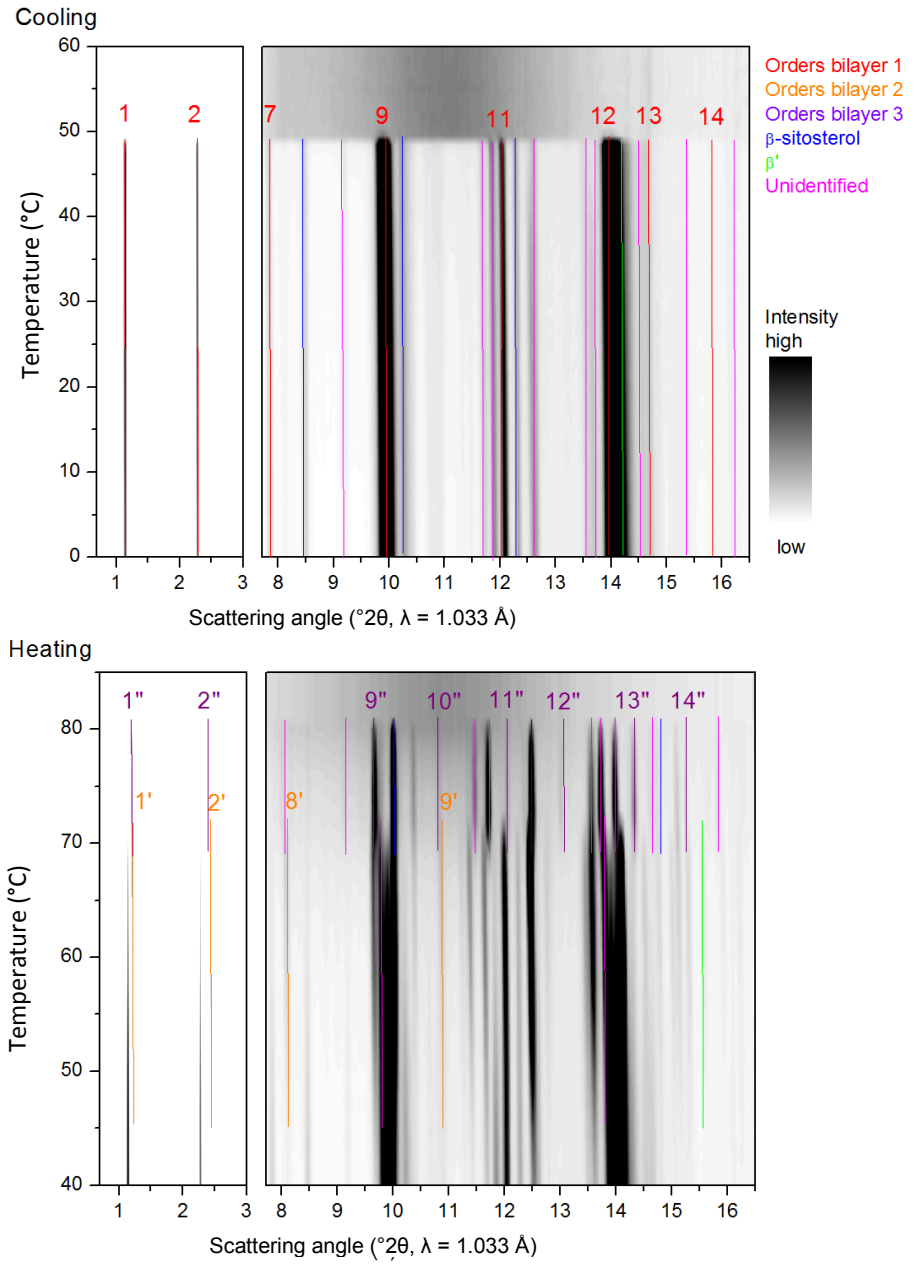

Figure 6.5. *SAXS (left) and WAXD (right) data of P-laurate during cooling and heating. The legend indicates the identification of the spacings as an order reflection of bilayer 1, bilayer 2 or bilayer 3 or as related to the packing of the β-sitosterol moieties (β-sitosterol) or the β' subcell packing of the lauric acid moieties (β') or unidentified.*

Table 6.6. *SAXS and WAXD spacings of new peaks appearing during cooling and heating of P-laurate with an indication if their intensity was relatively weak (w) or strong (s) and with their identification (ID) as an order reflection of bilayer 1, bilayer 2 (with apostrophe) or bilayer 3 (with double apostrophe) or as related to the packing of β-sitosterol moieties (SI) or the β' subcell packing of the lauric acid moieties (β') or unidentified (UI). λ = 1.033 Å.*

P-laurate	Cooling: from 47.4°C				Heating: 44.8-69.1°C				Heating: 69.1-81.0°C			
	2θ (°)	d (Å)	w/s	ID	2θ (°)	d (Å)	w/s	ID	2θ (°)	d (Å)	w/s	ID
SAXS	1.14	51.9	s	1	1.22	48.5	s	1'	1.1	53.8	s	1"
	2.28	26.0	s	2	2.44	24.3	s	2'	2.18	27.2	s	2"
WAXD	7.85	7.54	w	7	8.11	7.30	w	UI	8.06	7.34	w	UI
	8.49	6.97	w	SI	9.74	6.08	w	8'	9.13	6.48	w	UI
	9.21	6.43	w	8	9.89	5.98	s	UI	9.80	6.04	s	9"
	9.94	5.95	s	9	10.9	5.43	w	9'	10.0	5.92	s	SI
	10.2	5.80	w	SI	13.8	4.29	s	UI	10.8	5.47	w	10"
	11.7	5.06	w	UI	15.6	3.79	w	β'	11.5	5.16	w	UI
	11.9	4.97	w	UI					11.7	5.07	s	UI
	12.1	4.89	s	11					12.0	4.94	w	11"
	12.3	4.81	w	SI					12.5	4.75	s	SI
	12.6	4.70	w	UI					13.0	4.55	w	12"
	13.5	4.38	w	UI					13.6	4.37	w	UI
	13.6	4.35	w	UI					13.7	4.31	s	UI
	13.9	4.26	s	12					14.0	4.23	s	UI
	14.1	4.20	s	β'					14.3	4.14	w	13"
	14.5	4.08	w	UI					14.8	4.01	w	UI
	14.7	4.03	w	13					15.1	3.92	w	UI
	15.4	3.86	w	UI					15.3	3.88	w	14"
	15.8	3.75	w	14					15.8	3.75	w	UI
	16.2	3.66	w	UI								

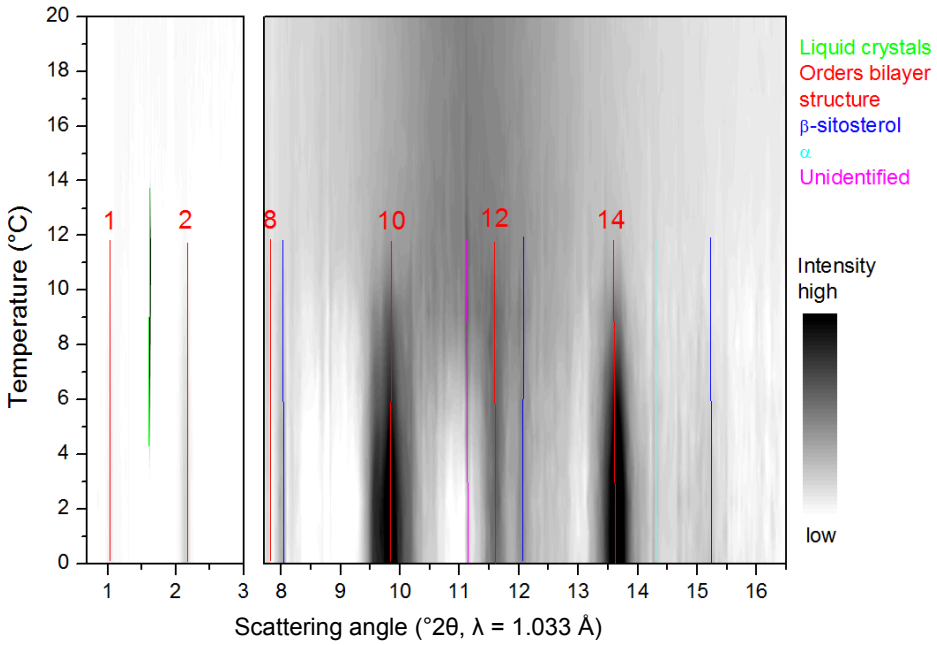

Figure 6.6. *SAXS (left) and WAXD (right) data of P-oleate during cooling. The legend indicates the identification of the spacings as an order reflection of the bilayer structure or as related to the packing of the β-sitosterol moieties (β-sitosterol), the α subcell packing of the oleic acid moieties (α) or the liquid crystals or unidentified.*

Table 6.7. *SAXS and WAXD spacings of new peaks appearing during cooling of P-oleate and P-linoleate with an indication if their intensity was relatively weak (w) or strong (s) and with their identification (ID) as an order reflection of the bilayer structure or as related to the packing of the β-sitosterol moieties (SI), the α subcell packing of the oleic acid moieties (α) or the liquid crystals (LC) or unidentified (UI). λ = 1.033 Å.*

P-oleate					P-linoleate (from -20.7°C, in SAXS)			
From 14.7°C	2θ (°)	d (Å)	w/s	ID	2θ (°)	d (Å)	w/s	ID
SAXS	1.62	36.6	s	LC	1.60	37.1	s	LC
From 11.8°C	2θ (°)	d (Å)	w/s	ID				
SAXS	1.03	57.5	w	1				
	2.14	27.7	s	2				
	3.25	18.2	w	3				
WAXD	7.89	7.50	w	8				
	8.06	7.34	w	SI				
	9.89	5.98	s	10				
	11.1	5.33	w	UI				
	11.6	5.10	m	12				
	12	4.93	w	SI				
	13.7	4.32	s	14				
	14.3	4.14	w	α				
	15.3	3.87	w	SI				

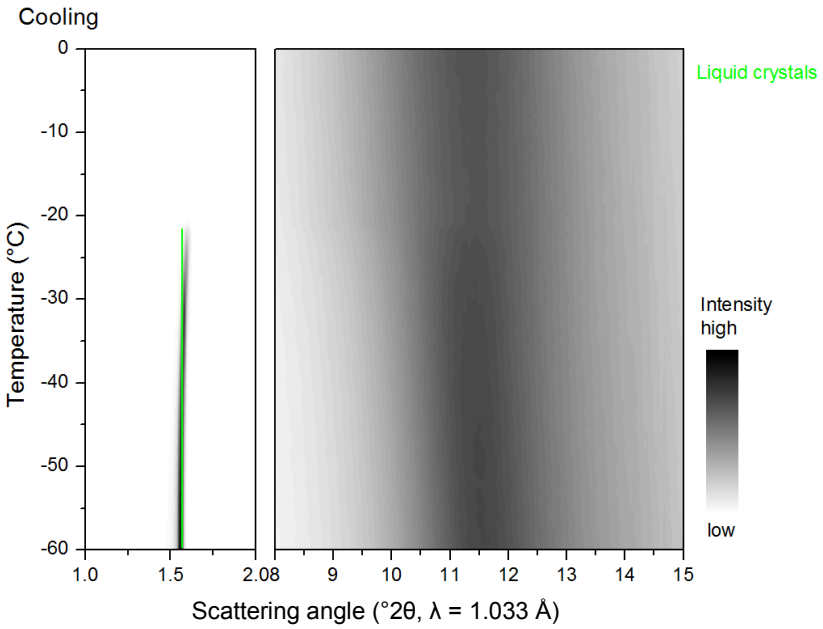

Figure 6.7. *SAXS (left) and WAXD (right) data of P-linoleate during cooling. The spacing related to the liquid crystals is marked in green.*

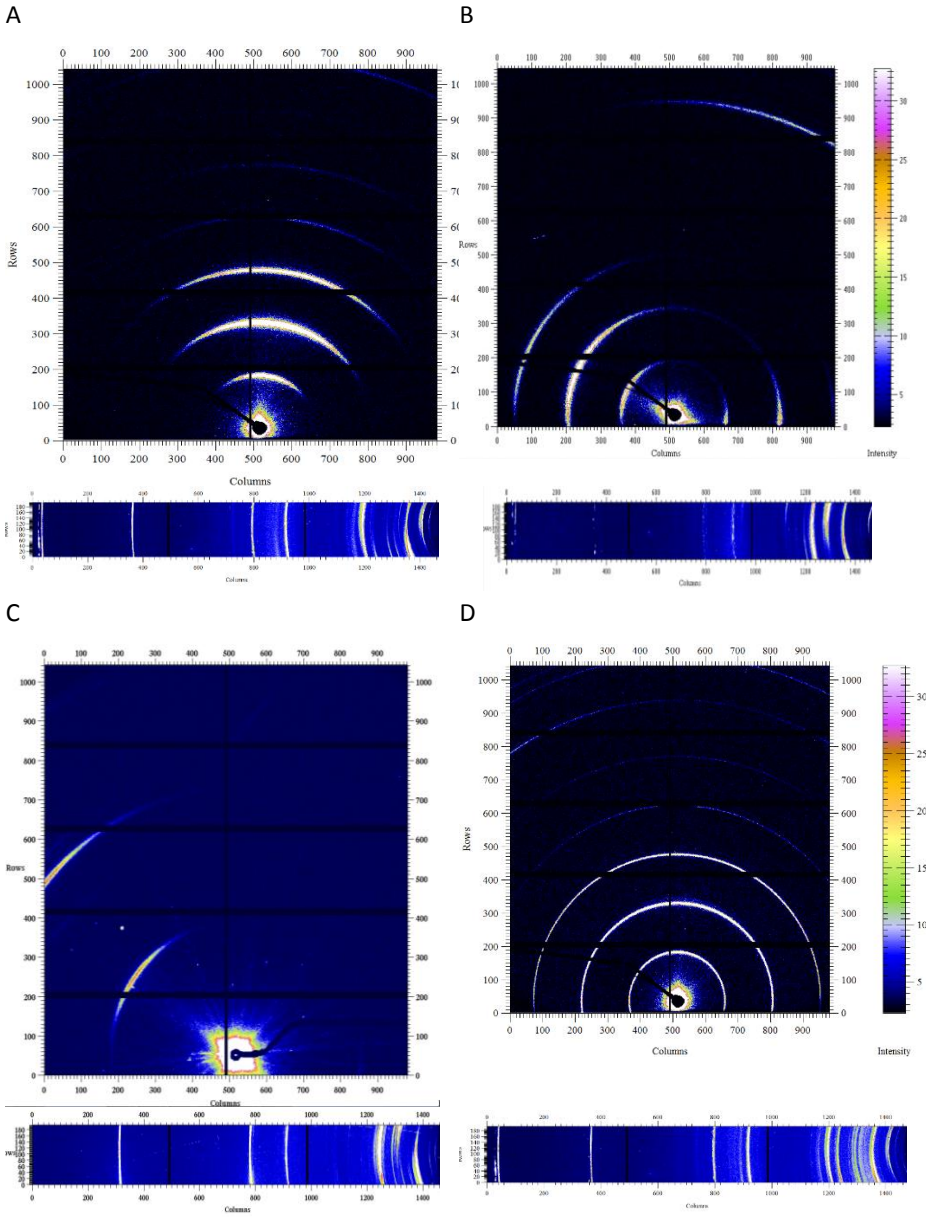

Figure 6.8. *2D patterns of the raw SAXS (above) and WAXD (below) data recorded at the end of the cooling stage (0°C) of P-stearate (A), P-palmitate (B) and P-laurate (C) and during heating of P-stearate at 93.6°C (D). The direct beam, covered by the beam stop, is visible centrally in the SAXS arcs and rings. For the WAXD patterns the direct beam is situated outside the images at the right hand side.*

6.3.4. CHARACTERIZATION OF THE BILAYER STRUCTURE

Up to now, to the best of our knowledge XRD data of PE have not been described in literature, let alone crystal structures of PE. Except for an extra ethyl group in the sterol side chain, the molecular structure of the β-sitosteryl esters in this study are the same as the analogous cholesterol esters. Therefore, it could be expected that they form similar crystal structures. Cholesteryl laurate, palmitate and stearate crystallize in a bilayer structure[34,42]. Only cholesteryl laurate is reported to sometimes form a monolayer structure when crystallizing. It could be derived from the XRD data that P-stearate, P-palmitate, P-laurate and P-oleate packed in a bilayer structure just like their analogous cholesterol esters. The presumed packing of the β-sitosteryl esters in the bilayer structure is based on the bilayer structure formed by cholesteryl esters and is presented in Figure 6.9. The β-sitosterol moiety of a β-sitosteryl ester molecule in the bilayer packing is indicated with the blue circle while the fatty acid moiety is indicated with the red box. The sterol ring system of the β-sitosterol moieties are not clearly shown in Figure 6.9 because they lie in the yz plane. Two β-sitosteryl ester molecules form the asymmetric unit of the bilayer and are arranged in an antiparallel configuration.

Based on literature it is possible to estimate the size of a β-sitosterol ester molecule. Taking into account an average bond length of 1.50 Å and an average angle of 115° between the carbon atoms in the fatty acid chain, the length of a stearic acid moiety in P-stearate would be about 20 Å[206]. Assuming that the length of the β-sitosterol moiety is the same as that of a cholesterol molecule (being 19 Å[207]), this makes the size of one P-stearate molecule about 39 Å. The bilayer thickness of the P-stearate crystals is 59.2 Å as shown by the SAXS data, which is smaller than two times the size of a P-stearate molecule, indicating that the stearic acid chains in the asymmetric unit of the bilayer interdigitate and interact with each other. This type of configuration in the bilayer also allows some space between the packed β-sitosterol moieties avoiding steric hindrance between them. With this configuration the theoretical size of the asymmetric unit of the bilayer equals 58 Å (being two times the size of a β-sitosterol moiety plus that of the stearic acid moiety), which is very similar to the experimentally observed length of the bilayer packing in the SAXS.

The same calculation can be made for the bilayer structure formed by the other β-sitosteryl esters. In section 6.3.3 it was demonstrated that the SAXS spacings of the other saturated β-sitosteryl esters were 56.9 Å for P-palmitate and 51.9 Å for P-laurate (compared to 59.2 Å for P-stearate). With a decreasing fatty acid chain length, the SAXS spacings of the β-sitosteryl esters and thus also the lamellar spacing in the bilayer decreased. The SAXS spacing of P-oleate was 57.5 Å, which is also lower than that of P-stearate. Because of an increase in the degree of unsaturation of the

fatty acid results in a decrease in the length of the fatty acid, because the double bond length is 1.37 Å and the double bond angles are 120° and 124°[208] the lamellar spacings in the bilayer structure and thus also in the SAXS spacings of P-oleate are shorter than those of P-stearate.

In general, the β-sitosterol rings of adjacent molecules are thus packed roughly parallel to each another but the ring-ring interactions are not the dominant stabilizing force in this crystal form. On the other hand, the fatty acid chains are packed in an antiparallel configuration in a specific type of subcell packing.

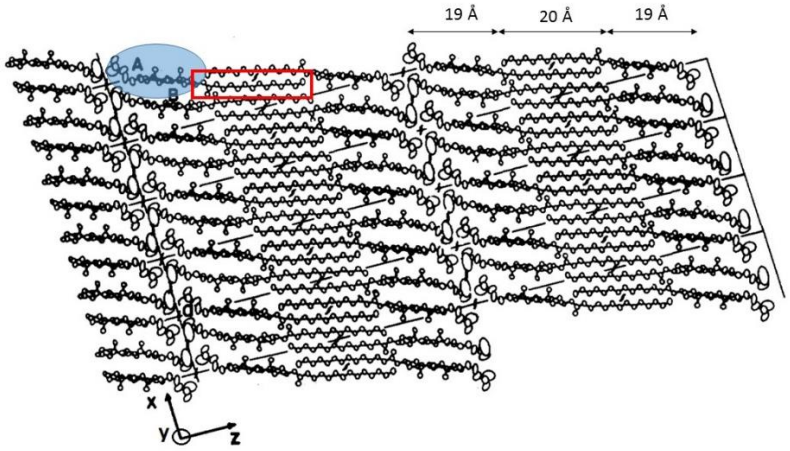

Figure 6.9. *Bilayer structure of the β-sitosteryl esters (From Ginsburg et al. 1984[34])*

6.3.5. LINK WITH CRYSTALLIZATION AND MELTING OF TRIGLYCERIDES

Some of the trends observed for the β-sitosteryl esters are similar to those of triglycerides containing fatty acids with a chain length between 12 and 18 carbon atoms. First, similar effects of fatty acid chain length and degree of unsaturation were also reported on the melting temperature and melting enthalpy of pure triglycerides[14,17]. Secondly in triglycerides the SAXS spacings depend on whether a double or triple chain length structure is formed, but within one type the SAXS spacings increase with an increasing fatty acid chain length, just as was seen for the β-sitosteryl esters[17]. Also, in β-sitosteryl ester crystals the fatty acid chains are structured in the same type of subcell packings as those that occur in triglycerides. Furthermore, similar as for the β-sitosteryl esters the limiting step for the crystallization rate in higher-melting triglycerides is the nucleation, while in lower-melting triglycerides it is the crystal growth. The nucleation efficiency of triglycerides increases with an increasing fatty acid chain length[209]. An increasing fatty acid chain length also causes a decreasing triglyceride growth rate, while in β-sitosteryl esters this had no influence.

6.4. CONCLUSION

To investigate the influence of chain length and degree of unsaturation of the fatty acid in a β-sitosteryl ester on its non-isothermal crystallization and melting behavior five different β-sitosteryl esters containing different types of fatty acids (stearic (C18:0), palmitic (C16:0), lauric (C12:0), oleic (C18:1) and linoleic acid (C18:2)) were synthesized by enzymatic esterification. The chain length as well as the degree of unsaturation of the fatty acid esterified to β-sitosterol had a great influence on the crystallization and melting behavior of the β-sitosteryl esters.

The melting temperature and melting enthalpy of the β-sitosteryl esters increased with an increasing fatty acid chain length while they decreased with an increasing degree of unsaturation of the fatty acid chain. The PLM analyses demonstrated that with an increasing degree of unsaturation the nucleation rate of the β-sitosteryl ester crystals increased, while the crystal growth rate decreased resulting in a decreasing crystal size. Since the fatty acid chain length did not affect the crystal growth rate of the β-sitosteryl esters the increasing nucleation efficiency probably resulted in smaller β-sitosteryl ester crystals with an increasing fatty acid chain length. The chain length and the degree of unsaturation of the fatty acid did not influence the morphology of the β-sitosteryl ester crystals, since the saturated β-sitosteryl esters as well as P-oleate formed spherulitic crystals.

As demonstrated by the XRD results the chain length and especially the degree of unsaturation of the fatty acid also influence the nanoscale crystal structures formed by the β-sitosteryl esters. It is hypothesized that the saturated β-sitosteryl esters and P-oleate formed a bilayer crystal structure. The SAXS spacings of the β-sitosteryl esters decreased with a decreasing fatty acid chain length and with an increasing degree of unsaturation because of a decrease in the lamellar spacings in the bilayer structure. The degree of unsaturation of the fatty acid chain in the β-sitosteryl esters greatly influenced whether or not a metastable or stable mesophase was formed and which type of subcell packing was formed by the fatty acid moieties. A β' subcell packing was observed in the crystal structure of the saturated β-sitosteryl esters, while the oleic acid moieties formed an α subcell packing in the P-oleate crystal structure.

CHAPTER 7
EFFECT OF ADDING PURE PHYTOSTEROL ESTERS CONTAINING DIFFERENT TYPES OF FATTY ACIDS ON THE 'EQUILIBRIUM' CRYSTALLIZATION BEHAVIOR OF PALM OIL

7. EFFECT OF ADDING PHYTOSTEROL ESTERS CONTAINING DIFFERENT TYPES OF FATTY ACIDS ON THE 'EQUILIBRIUM' CRYSTALLIZATION BEHAVIOR OF PALM OIL

7.1. INTRODUCTION

The objective of this chapter was to investigate the influence of the addition of different types of pure phytosterol esters PEs on the crystallization behavior of palm oil in the 'equilibrium' state (kinetically stabilized state as defined in section 4.1) to predict if PE addition gives any desired properties to the end product. The crystallization and phase behavior of the blends in the 'equilibrium' state were analyzed at various structural levels being primary crystallization, polymorphism and network formation by applying different experimental techniques including differential scanning calorimetry (DSC), X-ray diffraction (XRD) and polarized light microscopy (PLM). β-sitosterol esters containing different types of fatty acids (stearic (C18:0), palmitic (C16:0), lauric (C12:0) and oleic (C18:1) acid) were synthesized by enzymatic esterification and added to palm oil (PO) in concentrations of 0-100% with 10% intervals.

7.2. MATERIALS AND METHODS

7.2.1. MATERIALS

The same β-sitosterol, oleic acid, stearic acid, palmitic acid and lauric acid as in Chapter 6 were used in this chapter and the PO was the same as used in Chapters 3 to 5. Since their purity was lower than 97%, β-sitosterol, oleic acid and PO were analyzed for their chemical composition as described in chapters 3 (section 3.2.1) and 6 (section 6.2.1). The sterol composition of β-sitosterol is shown in Table 6.1, while the fatty acid composition of oleic acid is reported in Table 6.2. The fatty acid and triglyceride compositions of PO are shown in Tables 3.2 and 3.3 respectively.

7.2.2. ENZYMATIC SYNTHESIS OF THE B-SITOSTERYL ESTERS

The synthesis of a series of fatty acid (C12:0, C16:0, C18:0, C18:1) esters of β-sitosterol was based on the method of Panpipat, Xu, & Guo (2013) and is fully described in section 6.2.2. In this way four types of β-sitosteryl esters were obtained: β-sitosteryl laurate (P-laurate), β-sitosteryl palmitate (P-palmitate), β-sitosteryl stearate (P-stearate) and β-sitosteryl oleate (P-oleate).

7.2.3. PURIFICATION OF THE B-SITOSTERYL ESTERS

The synthesized β-sitosteryl esters were purified using a low-pressure silica column by the method described in section 6.2.3.

7.2.4. BLEND PREPARATION

For each type of β-sitosterol ester nine blends with PO were prepared with a β-sitosterol ester concentration range of 0 to 100% with composition intervals of 10%. First, the pure lipids were melted separately in an oven at a temperature of 80°C in case of P-oleate and PO, 125°C for P-laurate and 140°C for P-palmitate and P-stearate. These temperatures are chosen approximately 45°C above T_{m_offset} reported in Table 6.3. Then the melted pure lipids were blended in a conic tube and held in the oven for 30 min at the same temperature as used for melting of the β-sitosterol ester while regularly mixing with a vortex.

7.2.5. CRYSTALLIZATION TO THE 'EQUILIBRIUM' STATE

To bring the blends in the 'equilibrium' state, the samples were prepared according to the method described in section 4.2.3, except for one step. More specifically, for practical reasons, the samples were held at 10°C for 72h instead of 48h. It has been demonstrated before (see section 4.2.3) that the DSC melting enthalpy and the peak maximum of the melting curve of PO does no longer change significantly when holding at 10°C for longer than 48h.

7.2.6. MELTING PROFILE BY DIFFERENTIAL SCANNING CALORIMETRY

To obtain the melting curve of the samples after they reached the 'equilibrium' state (as described in section 7.2.5) melting curves were obtained by the method described in section 4.2.5, but with different end temperatures of the heating stage. Blends containing P-oleate were heated to 80°C, blends containing P-laurate to 120°C and P-palmitate and P-stearate containing blends to 135°C.

The different parameters that were derived from the melting curves using Universal Analysis (Version 4.5A, TA Instruments, New Castle, US) are the peak maximum (T_{m_max}) and the melting enthalpy (ΔH_{melt}). The latter is the total amount of heat released during melting and was calculated by integration of the melting curve using a horizontal baseline. The melting curves of PO and the blends of PO with P-oleate showed one peak that was integrated with a sigmoidal baseline with a fixed starting point at 15°C and an end point at 55°C. The melting curves of the blends containing P-laurate, P-palmitate and P-stearate however showed two peaks. To determine ΔH_{melt}, the melting curve was integrated with a sigmoidal baseline. The starting point for the integration was fixed at 15°C for all those blends and the end point was fixed

at 120°C for the P-stearate containing blends, 110°C for the P-palmitate containing blends and at 90°C for the P-laurate containing blends. By using a perpendicular drop at 44°C ΔH_{melt} of the individual PO and PE peaks was obtained.

7.2.7. X-RAY DIFFRACTION

XRD analyses including small angle XRD (SAXS) and wide angle XRD (WAXD) were performed on the blends of PO with 0, 20, 40, 60, 80 and 100% β-sitosterol esters after they reached the 'equilibrium state' (as described in section 7.2.5) by using the same equipment and analyzing technique as described in section 4.2.6.

7.2.8. POLARIZED LIGHT MICROSCOPY

After reaching the 'equilibrium' state (section 7.2.5) the microstructure of the blends was studied by the same method as described in section 4.2.7. Next to magnifications of 100x and 200x, in this chapter images were also taken at a magnification of 40x.

7.3. RESULTS AND DISCUSSION

7.3.1. PALM OIL

The crystallization behavior of PO in the 'equilibrium' state has already been extensively discussed in section 4.3.1. It had no significant impact on the crystallization properties that PO was tempered for 72h at 10°C instead of 48h at 10°C as in chapter 4 and therefore no detailed results are shown or discussed in this chapter. In summary it can be said that T_{m_max} of PO was 29.2 ± 0.4°C and ΔH_{melt} was 58.0 ± 1.4 J/g. Furthermore, just like after tempering for 48h at 10°C, PO had formed β' (2L) crystals according to the XRD patterns in Figure 7.1 which showed SAXS spacings at 2θ = 0.96° (d = 42.51 Å) and 2θ = 2.87° (d = 14.2 Å) and WAXD spacings at 2θ = 9.35° (d = 4.36 Å), 2θ = 9.66° (d = 4.22 Å) and 2θ = 10.5° (d = 3.90 Å). The microstructure showed needle-shaped crystals with a length of 5-7 µm which are typical for the β' polymorph[90].

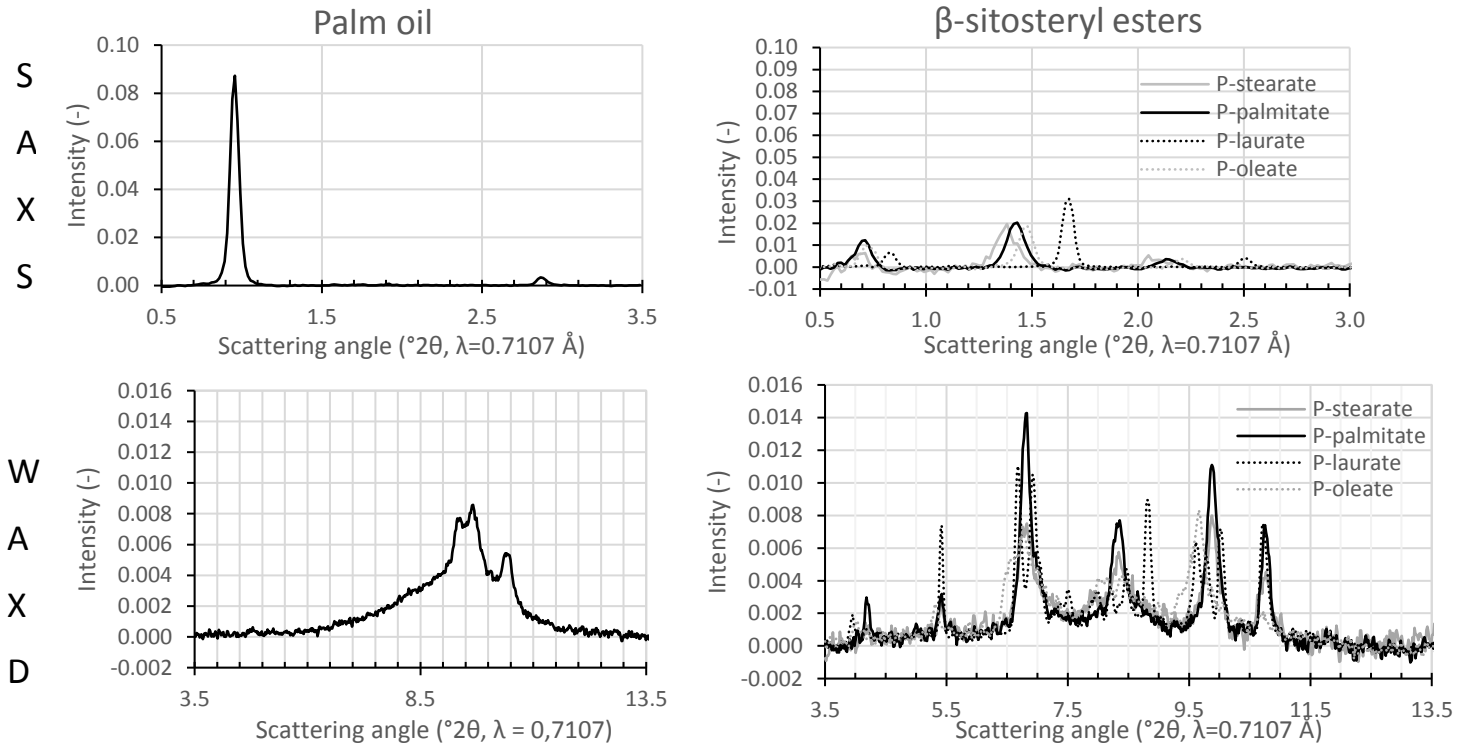

Figure 7.1. *SAXS and WAXD patterns of pure palm oil (PO) (left) and of the different types of pure β-sitosteryl esters (right) after tempering at 10°C for 72h.*

7.3.2. PURE B-SITOSTERYL ESTERS

7.3.2.1. Differential Scanning Calorimetry

The DSC melting curves of the pure β-sitosteryl esters are shown in Figure 7.2 and the parameters T_{m_max} and ΔH_{melt} in Table 7.1. The melting curves of the pure P-stearate, P-palmitate and P-oleate showed one peak, while the melting curve of P-laurate showed two peaks. The occurrence of two peaks in the melting curve of P-laurate could indicate a transition to a more stable crystal structure during heating or the presence of two different crystal structures in P-laurate in the 'equilibrium' state. As the XRD results showed that only one crystal structure, being a bilayer structure, was present in P-laurate in the 'equilibrium' state (see section 7.3.2.2), the two peaks in the melting curve of P-laurate are most probably due to a transition to a more stable crystal structure during heating. However, synchrotron XRD measurements during heating of P-laurate after it reached the 'equilibrium' state are necessary to confirm this hypothesis.

As expected from literature T_{m_max} and ΔH_{melt} of the β-sitosteryl esters increased with an increasing fatty acid chain length[3–8] because a longer fatty acid chain resulted in stronger intermolecular interactions an a better and packing[6]. On the other hand T_{m_max} and ΔH_{melt} decreased with an increasing degree of unsaturation of the fatty acid chain and the effect was much bigger compared to that of the fatty acid chain length because the double bond in the fatty acid disturbs the crystal packing to a larger extent[6].

Table 7.1. *Peak maximum (T_{m_max}) and the melting enthalpy (ΔH_{melt}) of the melting curves of the different β-sitosteryl esters after tempering at 10°C for 72h. Values show mean value ± standard deviation of 5 repetitions.*

	T_{m_max} (°C)	ΔH_{melt} (J/g)
P-stearate	93.2 ± 1.2	127.4 ± 1.7
P-palmitate	88.7 ± 0.1	121.4 ± 2.4
P-laurate	69.9 ± 0.2	88.5 ± 0.3
	78.0 ± 0.2	
P-oleate	29.9 ± 0.9	57.8 ± 1.4

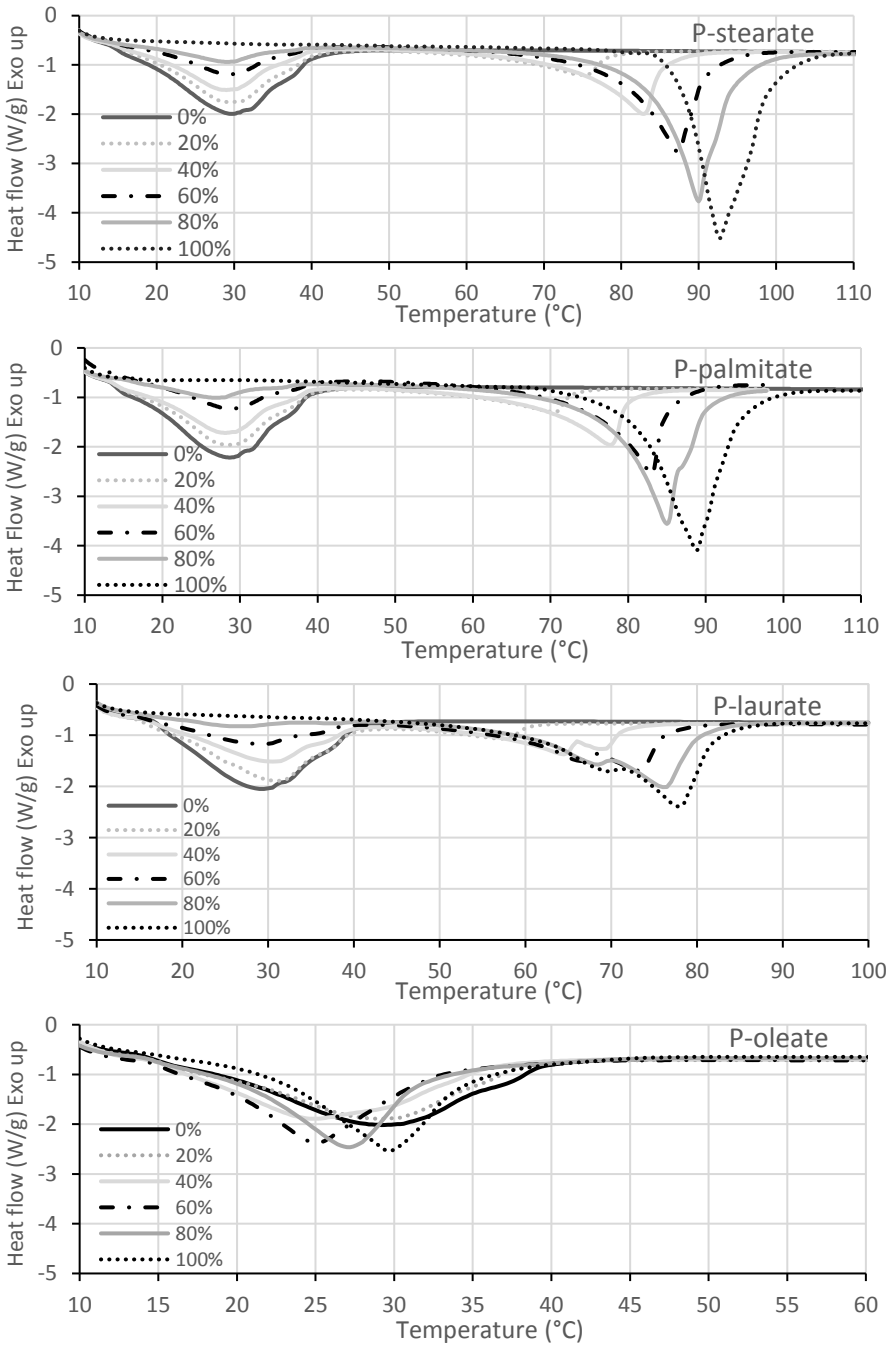

Figure 7.2. *DSC melting curves of the blends of PO with P-stearate, P-palmitate, P-laurate and P-oleate after tempering at 10°C for 72h. The different curves represent different concentrations of the β-sitosteryl esters.*

7.3.2.2. X-ray diffraction

The SAXS and WAXD patterns of the pure β-sitosteryl esters recorded after tempering at 10°C for 72h are shown in Figure 7.1. The corresponding SAXS and WAXD spacings are listed in Table 7.2.

There are a lot of similarities in the XRD patterns of the different pure β-sitosteryl esters. First in the SAXS patterns three reflections were observed which were orders of the same periodicity and indicated the formation of a layered crystal structure. As demonstrated in chapter 6 (section 6.3.4) it was derived from the SAXS spacings of the pure β-sitosteryl esters were that they formed a bilayer structure in the 'equilibrium' state. The bilayer structure is already explained in section 6.3.4. The ordering of the molecules into the bilayer structure was so strong that the lamellar reflections were also visible throughout the WAXD as many of the observed WAXD peaks were orders of the same periodicity like the SAXS reflections as indicated in Table 7.2. These order reflections were also the strongest peaks in the XRD patterns. Furthermore, the SAXS spacings of the β-sitosteryl esters increased with an increasing fatty acid chain length indicating an increase in the lamellar spacings in the bilayer structure. As indicated by the shorter SAXS spacings compared to those of P-stearate an increase in the degree of unsaturation of the fatty acid caused a decrease in the lamellar spacing in the bilayer structure because due to its double bond a P-oleate molecule is shorter than a P-stearate molecule. The WAXD pattern of P-stearate and P-palmitate contained no other peaks than those related to the periodicity of the bilayer structure.

The WAXD pattern of P-laurate contained much more peaks than that of the other β-sitosteryl esters which indicates that the P-laurate molecules were packed into the bilayer structure in a different way than the other β-sitosteryl esters. Similar as in chapter 6 it was examined whether the fatty acid moieties of the β-sitosteryl esters formed the same types of subcell packings as those observed in triglycerides by comparing the WAXD spacings in the XRD patterns of the β-sitosteryl esters with the typical short spacings of the triglyceride subcell packings, taking into account their relative intensities. For example, the WAXD peak of P-laurate at 4.11 Å could indicate that at least a part of the lauric acid moieties were packed in the α subcell packing, while the WAXD peak of P-laurate at 4.17 Å could indicate a β' subcell packing. The identification of subcell packings in the WAXD patterns of the other β-sitosteryl esters was however disturbed by the presence of order peaks of the bilayer structure, often with a high intensity, at the typical spacings of β' and α subcell packings[29].

Among the other extra peaks in the WAXD pattern of P-laurate those at 7.42 Å, 5.79 Å, 4.55 Å and 3.87 Å are typical reflections of β-sitosterol when measured at

room temperature[203,204]. Therefore, these WAXD spacings could be related to the packing of the β-sitosterol moieties in the bilayer structure.

The remaining spacings in the XRD patterns of P-laurate did not seem to be related to the bilayer structure, the packing of the β-sitosterol moieties or the subcell packing of the fatty acid moieties. These spacings which were indicated as 'unidentified' in Table7.2 and could have various possible origins. First, they may be related to the packing of phytosterol moieties other than β-sitosterol as the β-sitosterol used for the synthesis of the β-sitosteryl esters also contained campesterol and β-sitostanol. The lack of the double bond in the sterol ring of β-sitostanol and especially the presence of a methyl group instead of an ethyl group in the sterol side chain of campesterol[109] could lead to a somewhat different packing of the phytosterol moieties in the crystal structure resulting in different reflections. Further research and XRD analysis of β-sitostanol and campesterol is needed to confirm this since this information is not available in literature at the moment. Furthermore, these 'unidentified' spacings may also be related to the intermolecular lauric acid – phytosterol interactions, but a profound crystallographic study, which was out of the scope of this research, is necessary to investigate this hypothesis. Also the WAXD pattern of P-oleate contained two unidentified peaks.

***Table 7.2**. SAXS and WAXD spacings of P-stearate, P-palmitate, P-laurate and P-oleate with an indication if their intensity (I) was relatively weak (w), medium (m) or strong (s) and with their identification (ID) as an order reflection of bilayer 1 or as related to the packing of β-sitosterol moieties (SI) or the α or β' subcell packing of the lauric acid moieties or unidentified (UI).*

	P-stearate				P-palmitate				P-laurate				P-oleate			
	2θ (°)	d (Å)	I	ID	2θ (°)	d (Å)	I	ID	2θ (°)	d (Å)	I	ID	2θ (°)	d (Å)	I	ID
SAXS	0.69	58.3	m	1	0.71	56.6	m	1	0.84	47.9	w	1	0.73	55.1	m	1
	1.38	29.1	s	2	1.43	28.1	s	2	1.66	24.2	s	2	1.48	27.2	s	2
	2.07	19.4	m	3	2.2	18.3	w	3	2.52	16.0	w	3	2.2	18.3	w	3
WAXD	5.42	7.42	w	8	4.19	9.60	w	6	3.94	10.2	w	UI	4.04	9.95	w	UI
	6.83	5.89	s	10	5.42	7.42	w	8	5.42	7.42	s	SI	5.33	7.54	w	8
	8.31	4.84	m	12	6.83	5.89	s	10	6.68	6.02	s	8	6.76	5.95	s	10
	9.87	4.07	s	14	8.36	4.81	m	12	6.94	5.79	s	SI	8.15	4.93	m	12
	10.82	3.72	w	16	9.87	4.07	s	14	7.51	5.35	w	9	8.41	4.78	m	UI
					10.8	3.74	w	16	8.02	5.01	w	UI	9.68	4.15	s	14
									8.23	4.89	w	UI	10.7	3.76	w	16
									8.49	4.74	w	10				
									8.83	4.55	s	SI				
									9.65	4.17	s	β'				
									9.79	4.11	s	α				
									10.0	4.02	s	12				
									10.4	3.87	s	SI				
									10.7	3.76	s	13				

7.3.2.3. Polarized Light Microscopy

Figure 7.3 shows some PLM images of P-stearate, P-palmitate, P-laurate and P-oleate after tempering at 10°C for 72h. The crystal form of all the pure β-sitosteryl esters were spherulites of which the size depended on the fatty acid chain length and degree of unsaturation. The saturated β-sitosteryl esters formed larger spherulites than P-oleate. Among the saturated β-sitosteryl esters P-laurate formed the largest spherulites ranging from 50 up to 1200 µm. The spherulitic diameter of the P-palmitate crystals ranged from 70 to 780 µm, that of P-stearate from 150 to 260 µm and that of P-oleate from 30 to 230 µm.

Many different colors were observed in the microstructure formed by P-palmitate and P-laurate and to a lesser extent also in that formed by P-stearate. As in Chapter 6 also in this case the microscope did not contain any type of filters, the crystal planes must have acted as a sort of filter causing destructive interference for certain wavelengths resulting in the interference colors observed through the crossed polarizers[202]. The exact color observed at a certain position depends on many factors such as the degree of orientation of the crystal fragments in the radial direction of the spherulite nucleus, the degree of crystallinity, the distance of the position from the spherulite nucleus and the thickness of the sample[202]. The colors did further not have any importance.

Between the individual spherulites clear hyperbolic interfaces were visible. These hyperbolic interfaces indicate that crystallization occurred during cooling from 120°C to 10°C, so before tempering at 10°C, since hyperbolic interfaces are usually formed during a non-isothermal crystallization process[201].

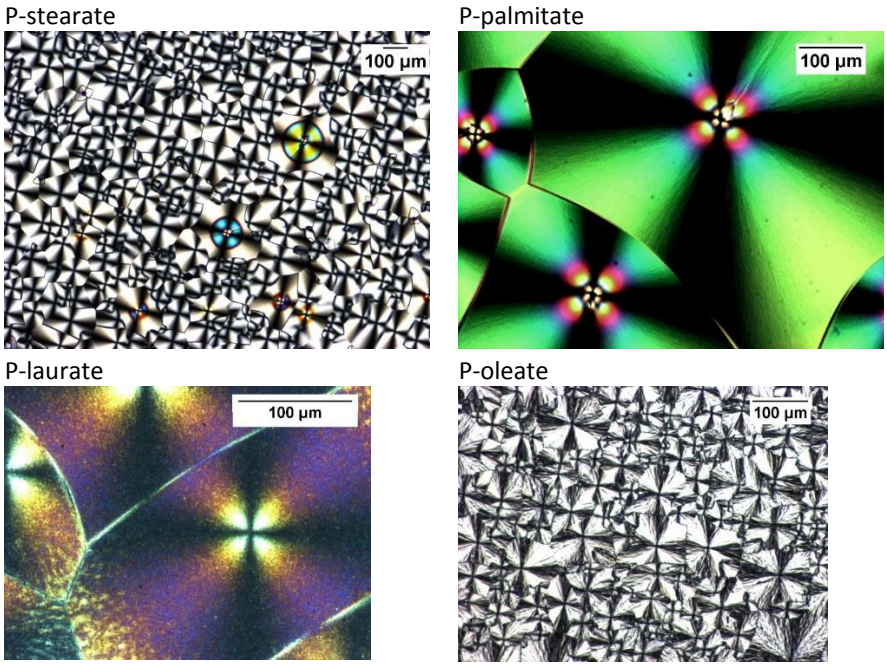

Figure 7.3. *Polarized light microscopy images of the pure β-sitosteryl esters. Black scale bar represents 100 µm. The Images were captured at a magnification of 40x for β-sitosteryl stearate (P-stearate), 100x for β-sitosteryl palmitate (P-palmitate) and β-sitosteryl oleate (P-oleate) and 200x for β-sitosteryl laurate (P-laurate).*

7.3.2.4. Link with the non-isothermal crystallization and melting behavior of the pure β-sitosteryl esters

There are some differences in the crystallization and melting behavior of the pure β-sitosteryl esters in the 'equilibrium' state as compared to their non-isothermal crystallization and melting behavior as described in chapter 6 because of the difference in the time-temperature profile they were subjected to. In chapter 6 the β-sitosteryl esters were first fully melted after which they were cooled at 5°C/min to 0°C, followed by holding at 0°C for 5 min and subsequent heating at 5°C/min until fully melted. T_{m_max} and ΔH_{melt} derived from the DSC melting curve and the long spacings of the bilayer structures formed during cooling and heating by the different types of β-sitosteryl esters as reported in chapter 6 are listed in Table 7.3. T_{m_max} of the β-sitosteryl esters in the 'equilibrium' state was higher compared to T_{m_max} of the same β-sitosteryl esters as reported in chapter 6, probably because the crystal structure of the β-sitosteryl esters in the 'equilibrium' state was more stable which led to a higher melting temperature. The only exception to this was P-laurate which had the same values for T_{m_max} in the 'equilibrium' state as reported in chapter 6,

although according to the XRD analyses a different crystal structure was formed in the 'equilibrium' state. Next to T_{m_max} also ΔH_{melt} of the β-sitosteryl esters in the 'equilibrium' state was higher compared to ΔH_{melt} reported in chapter 6, probably because in this case a longer storage time was used (72h at 10°C, compared to 5 min at 0°C in chapter 6) which caused extra crystallization in the sample.

When focusing on the XRD results it was observed that the lamellar spacings of the β-sitosteryl ester crystals in the 'equilibrium' state were the same as those observed during cooling as reported in chapter 6 since the difference was smaller than the resolution of the lab-scale XRD measurements. It is therefore concluded that the bilayer structures of the β-sitosteryl esters in the 'equilibrium' state were the same as those formed during cooling.

Finally, the crystal sizes of the different types of β-sitosteryl esters were smaller than when the same β-sitosteryl esters were cooled at 5°C/min to 0°C as described in chapter 6. As measured with a temperature probe (results not shown) the cooling rate in these sample was much higher than 5°C/min at the moment of crystallization resulting in more, but smaller crystals[14].

Table 7.3. *Average peak maximum of the melting curve (T_{m_max}) ± standard deviation (n = 5) and first order SAXS spacing of the bilayer structure formed by the different β-sitosteryl esters after cooling at 5°C/min to 0°C and during subsequent heating at 5°C/min as reported in chapter 6.*

β-sitosteryl ester	T_{m_max} (°C)	ΔH_{melt} (J/g)	d (Å) cooling
P-stearate	92.1 ± 0.1	88.8 ± 7.2	59.2
P-palmitate	89.1 ± 0.1	87.6 ± 1.1	56.9
P-laurate	69.9 ± 0.0	58.9 ± 3.9	51.9
	78.2 ± 0.1		
P-oleate	27.3 ± 0.2	45.1 ± 5.5	57.5

7.3.3. BLENDS OF PALM OIL WITH SATURATED Β-SITOSTERYL ESTERS

7.3.3.1. Differential scanning calorimetry

The melting curves of the blends of PO with P-stearate were very similar as those of the blends of PO with P-palmitate and of PO with P-laurate (Figure 7.2). The melting curves of the blends of PO with 10 to 90% P-stearate or P-palmitate or with 10 to 30% P-laurate contained two distinct melting peaks. The low-melting peak decreased and the high-melting peak increased with an increasing β-sitosteryl ester concentration. Based on T_{m_max} of pure PO and the pure β-sitosteryl esters it was

deduced that the low-melting peak (further named PO peak) corresponded to the melting of the PO part and the high-melting peak (further named PE peak) was due to the melting of the β-sitosteryl ester part. Depending on the type of β-sitosteryl ester the PE peak refers to the P-stearate, P-palmitate or P-laurate peak. The PO and PE peaks were baseline separated for the blends of PO with P-stearate or P-palmitate indicating that during heating PO was already fully melted before the β-sitosteryl ester started to melt. In the concentration range of 10% to 30% P-laurate the PO peak and the P-laurate peak were not baseline separated.

For the blends of PO with more than 30% P-laurate the situation was somewhat different. In the melting curves of the blend with 30% P-laurate the P-laurate peak had a small shoulder at the high-temperature side that became a separate peak in the melting curve of the blend with 40% P-laurate which thus contained three distinct peaks. Three melting peaks remained present in the melting curves of the blends up to a concentration of 90% P-laurate. In this concentration range the lowest-melting peak gradually decreased while the middle and highest-melting peak gradually increased with an increasing P-laurate concentration. The increase of the highest-melting peak was however larger than that of the middle-melting peak and as a result the highest-melting peak was larger than the middle-melting peak from a concentration of 50% P-laurate. Up to 50% P-laurate the lowest-melting and middle-melting peaks were not baseline separated, but from 60% P-laurate they were. The middle-melting and highest-melting peaks were never baseline separated. It is hypothesized that from a concentration of 40% P-laurate the lowest-melting peak (PO peak) corresponded to the melting of the PO fraction while the middle-melting and the highest-melting peaks (further named P-laurate peaks) were due to the melting of P-laurate. Similar as for the melting curve of the pure P-laurate, the presence of two P-laurate peaks probably indicates a transition of P-laurate molecules to a more stable crystal structure as indicated by the XRD results (see below in section 7.3.3.2).

For the blends of PO with saturated β-sitosteryl esters T_{m_max} of the PO peak and the PE peak as a function of the β-sitosteryl ester concentration is plotted in Figure 7.4. For the blends of PO with P-laurate T_{m_max} of both P-laurate peaks is shown in case P-laurate peaks were present instead of one. With an increasing β-sitosteryl ester concentration, T_{m_max} of the PO peak remained constant while T_{m_max} of the PE peak showed a logarithmic increase. Unlike the PE peaks, T_{m_max} of the PO peak remained constant with an increasing β-sitosteryl ester concentration because, the β-sitosteryl esters being present in separate crystals did not affect the PO melting. It was checked if the change in T_{m_max} of the PE peak as a function of the β-sitosteryl ester concentration can be explained by the Hildebrand equation which states that the

melting temperature of a high-melting component decreases when blending with an increasing amount of a low-melting component according to the following equation:

$$\ln X_A = -\frac{\Delta H_A}{R}\left(\frac{1}{T} - \frac{1}{T_A}\right)$$

with R being the molar gas constant, X_A the mole fraction, T_A the melting temperature and ΔH_A the molar heat of fusion of the high-melting component and T the melting temperature of the blend with X_A. The Hildebrand plot of the blends with 10 to 90% β-sitosteryl esters resulted in a linear relationship between $\ln X_A$ and $\left(\frac{1}{T} - \frac{1}{T_A}\right)$ ($R^2 > 0.99$). Furthermore, in section 7.3.3.2 it was demonstrated that in the concentration range of 20-80% β-sitosteryl esters the PO crystallized separately from and independent of the β-sitosteryl ester. The phase behavior that is represented by the phase diagrams in Figure 7.4 could thus be labelled as monotectic.

As in all the blends of PO with saturated β-sitosteryl esters T_{m_max} was much higher than body temperature this could cause a waxy or greasy mouth feeling when applying these blends in food products like for example margarines and spreads[210].

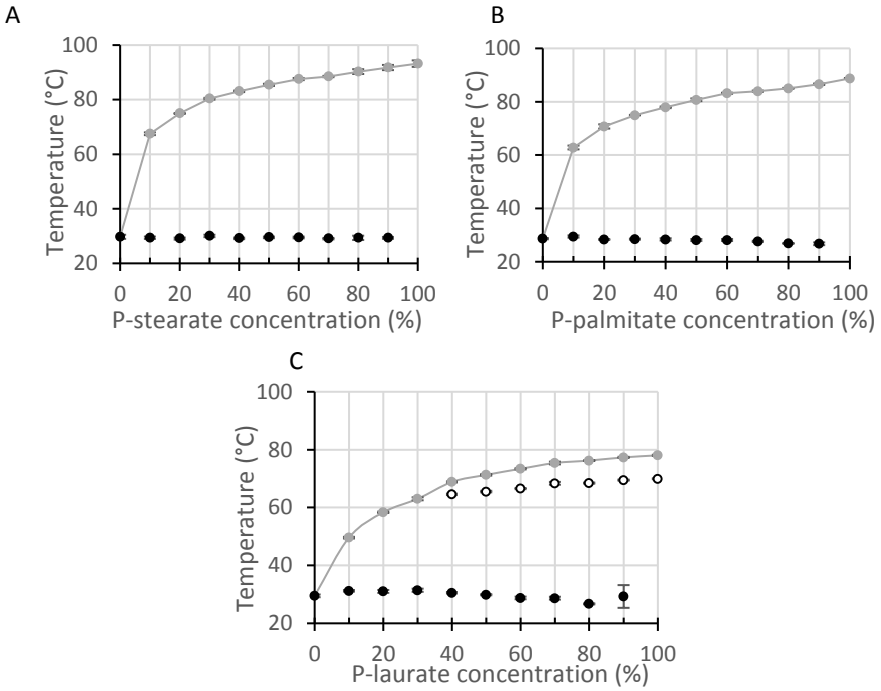

Figure 7.4. *Peak maximum of the PO peak (●) and the PE peak (●) in the DSC melting curves of the blends of PO with P-stearate (A), P-palmitate (B) and P-laurate (C) as a function of the β-sitosteryl ester concentration. The grey line represents the liquidus line of the binary system of PO and the β-sitosteryl esters. The symbol (○) in part (C) represents the peak maximum of the low-melting P-laurate peak.*

For the blends of PO with saturated β-sitosteryl esters the plots of ΔH_{melt} of the PO peak and the PE peak as a function of the β-sitosteryl ester concentration are shown in Figure 7.5. ΔH_{melt} of the P-laurate peaks in Figure 7.5.C is that of the two P-laurate peaks together. It could be observed that for each type of saturated β-sitosteryl ester ΔH_{melt} of the PO peak decreased linearly ($R^2 \geq 0.994$) with an increasing PE concentration. Moreover the decrease was proportional to the PE concentration since the experimental data were located on the black line. ΔH_{melt} of the PE peak increased as a function of the β-sitosteryl ester concentration. For all the blends of PO with the different types of saturated β-sitosteryl esters the increase in ΔH_{melt} of the PE peak was lower than expected based on the PE concentration as the experimental data were located below the grey line. The amount of PE crystallization was thus less than expected based on the PE concentration which indicates that part of the PE molecules solubilized in the liquid part of PO (palm olein). Because of partial solubilisation of the PE in liquid palm olein, the total ΔH_{melt} was lower than expected

based on the composition of the blends as the experimental data of the total ΔH_{melt} were located below the dashed line.

7.3.3.2. X-ray diffraction

The SAXS and WAXD patterns of the blends of PO with the different types of saturated β-sitosteryl esters recorded after tempering at 10°C for 72h are shown in Figures 7.6 and 7.7. In the SAXS and WAXD patterns of the blends no peaks other than the typical PO and the typical β-sitosteryl ester peaks were observed indicating no new crystal structures were formed and PO and the β-sitosteryl esters crystallized separately from each other. The only exception to this was the WAXD pattern of PO with 80% P-stearate in which no typical PO peaks could be distinguished. These typical PO peaks were probably below the detection limit in WAXD because in SAXS the PO peaks were clearly present.

Since the typical P-laurate SAXS and WAXD peaks were all observed in the blends with 20%, 40%, 60% and 80% P-laurate, the same crystalline structure of P-laurate must be present in all these blends. Therefore, the two melting peaks that occurred in the melting curves of the blends with 40% P-laurate or more and in the melting curve of pure P-laurate (section 7.3.3.1) were not due to the presence of an extra crystalline structure of P-laurate in those blends, but must be caused by a transition to a more stable crystal structure during heating as was also the case for the two peaks in the melting curve of pure P-laurate.

The sum of the peak areas of the diffraction peaks corresponding to one crystal structure is proportional to the amount of this crystal structure. The proportionality factor may however differ depending on the crystal structure, meaning that the proportions of the different crystal structures cannot be directly derived from the relative peak areas[211]. It was visually observed that with an increasing β-sitosteryl ester concentration the relative peak area of the PO peaks decreased while the relative peak area of the β-sitosteryl ester peaks increased. Therefore, it can be concluded that the amount of PO crystals decreased and the amount of the β-sitosteryl ester crystals increased with increasing concentrations of the β-sitosteryl ester. The numerical values of the areas of the PO and PE peaks are not shown since it is not recommended to draw conclusions on solubility behavior from these data as no repetitions were done for the XRD measurements.

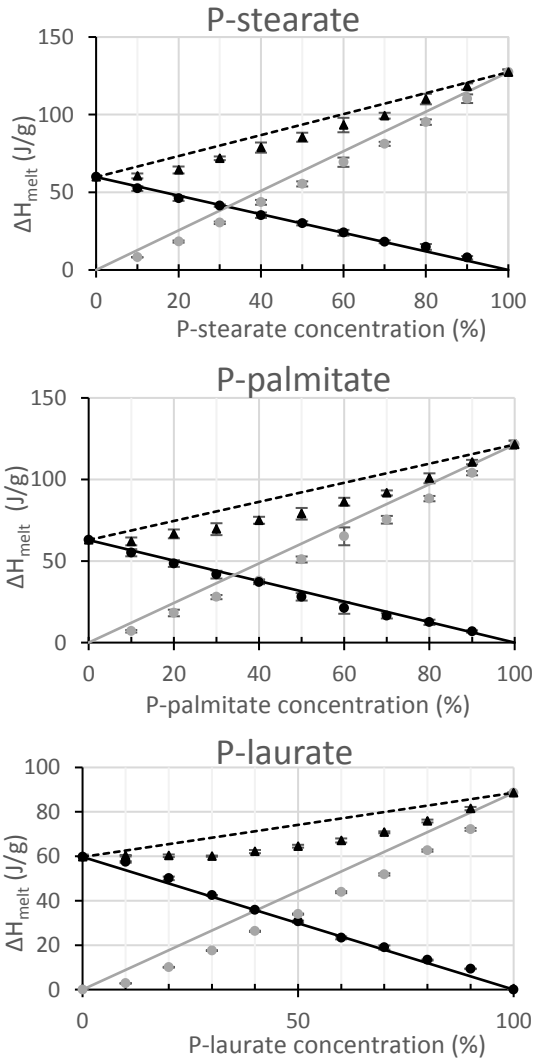

Figure 7.5. *Total melting enthalpy (ΔH_{melt}) (▲), melting enthalpy of the PO peak (●) and melting enthalpy of the β-sitosteryl ester (●) in the DSC melting curves of the blends of PO with the different types of saturated* β-sitosteryl esters *as a function of the* β-sitosteryl ester *concentration. The black solid line in the plots represents the theoretical case if ΔH_{melt} of the PO peak would decrease linearly with and proportional to an increasing PE concentration. The grey solid line represents the theoretical case if ΔH_{melt} of the PE peak would increase linearly with and proportional to an increasing PE concentration. A third line (the black dotted line) shows the theoretical value of the total ΔH_{melt} of the PE-PO blends supposing both components crystallize proportionally to their concentration.*

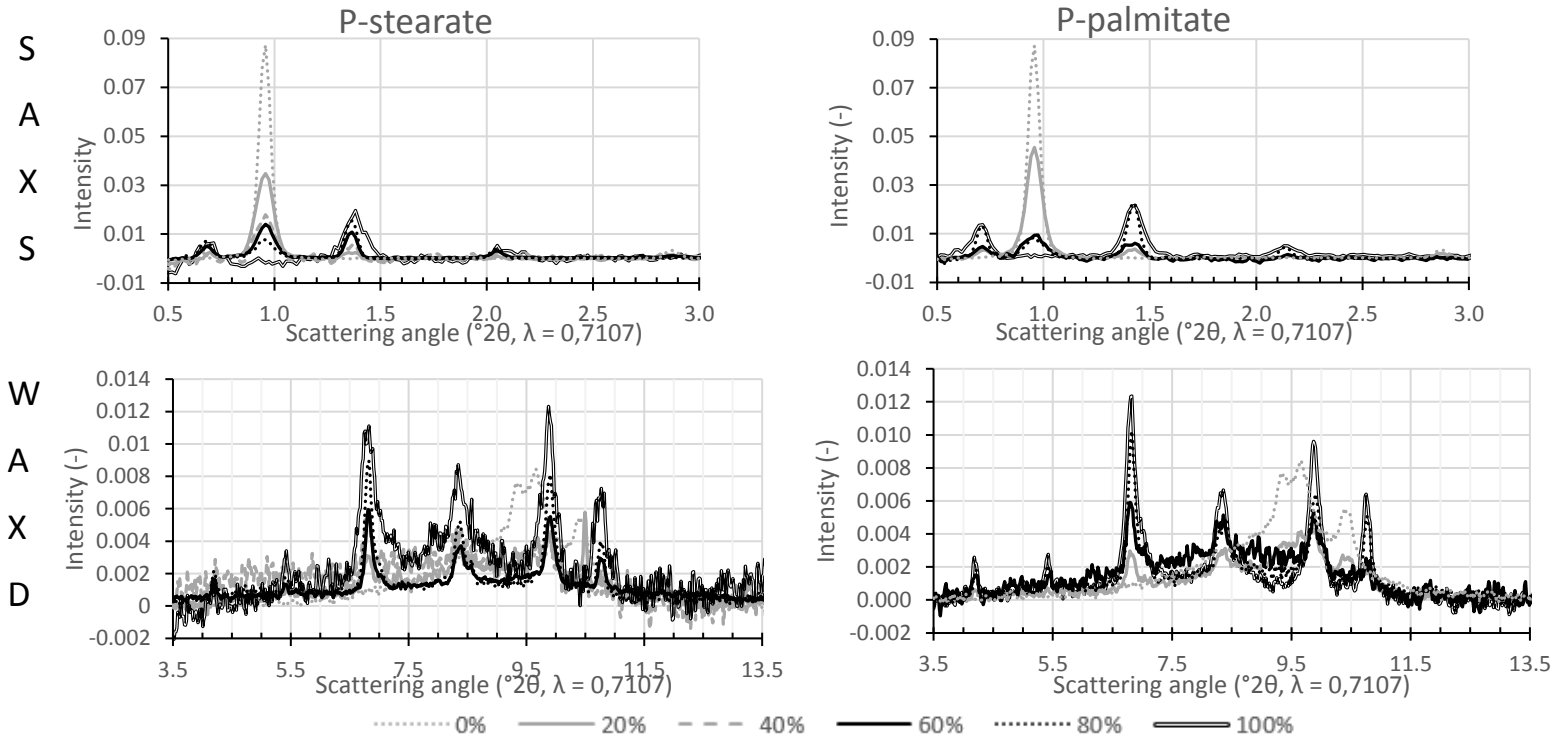

Figure 7.6. *SAXS and WAXD patterns of the blends of PO with P-stearate (left) and of the blends of PO with P-palmitate (right) after tempering at 10°C for 72h. The different curves represent different concentrations of P-stearate or P-palmitate in PO.*

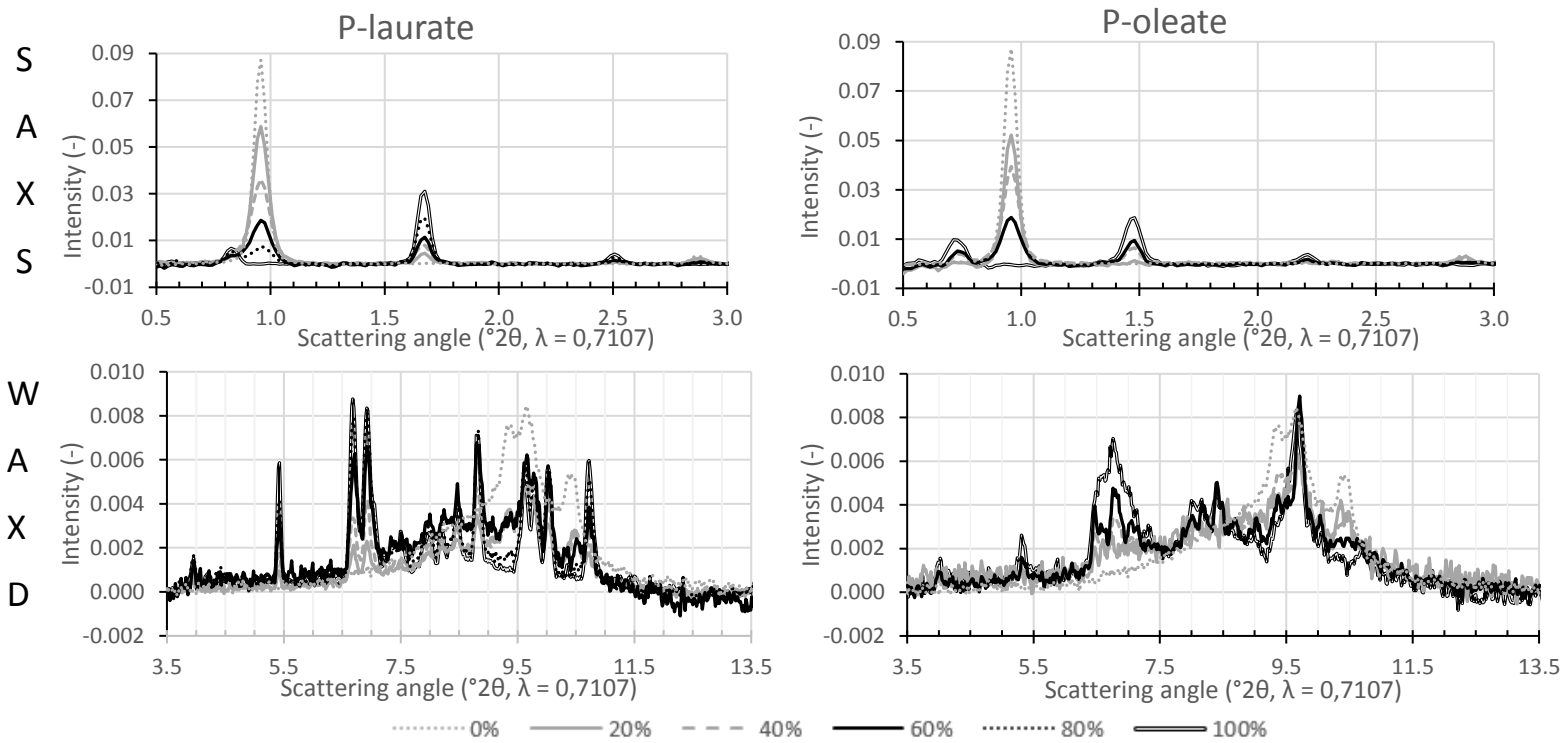

Figure 7.7. *SAXS and WAXD patterns of the blends of PO with P-laurate (left) and of the blends of PO with P-oleate (right) after tempering at 10°C for 72h. The different curves represent different concentrations of P-laurate or P-oleate in PO.*

7.3.3.3. Polarized light microscopy

Some characteristics of the images of PO with the different types of saturated β-sitosteryl esters are shown in Table 7.4, while some of the images are shown in Figure 7.8. At every concentration large (> 30 µm) spherulitic crystals of the β-sitosteryl esters were observed, except for the blend of PO with 10% P-laurate where only PO crystals were observed. These large crystals may cause a sandy mouth feeling during consumption of food products such as margarines and spreads containing this fat blend[23]. The size range of the β-sitosteryl ester spherulites shifted somewhat to larger sizes and larger size ranges with an increasing β-sitosteryl ester concentration. The largest spherulites were observed in blends with 60-90% P-laurate.

At low β-sitosteryl ester concentrations the β-sitosteryl ester spherulites had blurry edges as in the blend of PO with 30% P-laurate (Figure 7.8A). At higher β-sitosteryl ester concentrations the spherulites showed clear hyperbolic interfaces (e.g. Figure 7.8B) indicating that the spherulites were already formed during cooling of the blend to 10°C and not during the isothermal period at 10°C[212]. From 30-40% β-sitosteryl esters the spherulites were multi-colored like in the blend of PO with 70% P-stearate instead of greyscale (Figure 7.8B). The colors ranged from yellow over orange, pink, red, purple and blue to green. The different colors were caused by interference of light of different wavelengths and have no further meaning as was already explained in section 7.3.2.3.

In blends with lower P-palmitate or P-laurate concentrations needle-shaped PO crystals of about 5 µm were observed as illustrated in the image of the blend of PO with 20% P-palmitate (Figure 7.8C). In the blends of PO with P-stearate no PO crystals were observed at any P-stearate concentration. Since based on DSC and XRD it was clear that after addition of 10 to 90% P-stearate PO still crystallized separately from P-stearate, the PO crystals must be present in these blends, but probably lie underneath the P-stearate crystals and are therefore not visible in the PLM images.

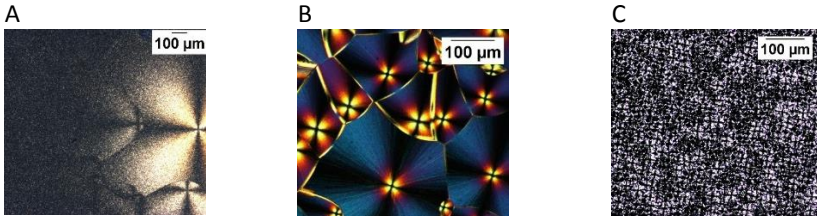

Figure 7.8. *Polarized light microscopy images of different blends of PO with saturated β-sitosteryl esters. The black scale bar represents 100 µm. The Images were captured at a magnification of 40x (A) and 100x (B and C).*

Table 7.4. *Some characteristics of the images of PO with the different types of saturated β-sitosteryl esters*

	β-sitosteryl ester concentration (%) showing…				
	PO crystals	β-sitosteryl ester crystals	Multicolored crystals	Blurry spherulite edges	Spherulite diameter in µm (at % β-sitosteryl esters)
P-stearate	Never	≥ 10%	≥ 30%	< 30%	20-43 (10%) 43-490 (> 10%)
P-palmitate	10-60%	≥ 10%	≥ 40%	< 30%	20-50 (10%) 30-270 (20-30%) 30-400 (40-50%) 40-650 (60%) 70-780 (> 60%)
P-laurate	10-50%	≥ 20%	≥ 30%	< 40%	90-750 (40-50%) 50-1200 (> 50%)
P-oleate	10-90%	≥ 20%	≥ 20%	Does not apply	16-42 (20%) 23-150 (30%) 7-25 (40-70%) 5-7 (> 70%)

7.3.4. BLENDS OF PALM OIL WITH B-SITOSTERYL OLEATE

7.3.4.1. Differential scanning calorimetry

Figure 7.2 shows the DSC melting curves of PO with addition of 0 to 100% P-oleate. These melting curves contained one peak of which T_{m_max} first decreased as a function of the P-oleate concentration up to a concentration of 50% P-oleate and then increased again with an increasing amount of P-oleate (Figure 7.9). Since at some P-oleate concentrations T_{m_max} of the blends was lower than T_{m_max} of both PO and P-oleate it can be stated that eutectic behavior occurred in the PO-P-oleate binary system[29]. The eutectic minimum was reached at 50% P-oleate with a T_{m_max} of 24.5 ± 0.1°C. ΔH_{melt} of the blends also reached a minimum, but at a concentration of 30% P-oleate (Figure 7.9).

It has been reported in literature that in binary blends of pure triglycerides the eutectic system tends to shift to a monotectic system if the difference in melting temperature of the triglycerides is high (> 20°C)[29]. A similar rule seems valid for the binary blends of PO with the β-sitosteryl esters, of course taking into account PO has a melting range instead of a melting temperature as it is not a pure lipid. The melting temperatures of the saturated β-sitosteryl esters are much higher (> 35°C) than T_{m_max} of PO, leading to the monotectic phase behavior in their binary blends. On the other hand T_{m_max} of PO is very similar to the melting temperature of pure P-oleate described in section 7.3.2.1 leading to eutectic phase behavior of their binary blends.

In the melting curves in Figure 7.2 it is clear that, just like PO, all the blends of PO with P-oleate are almost fully melted around body temperature, so no waxy mouth feeling is expected during consumption of the lipid blends[210].

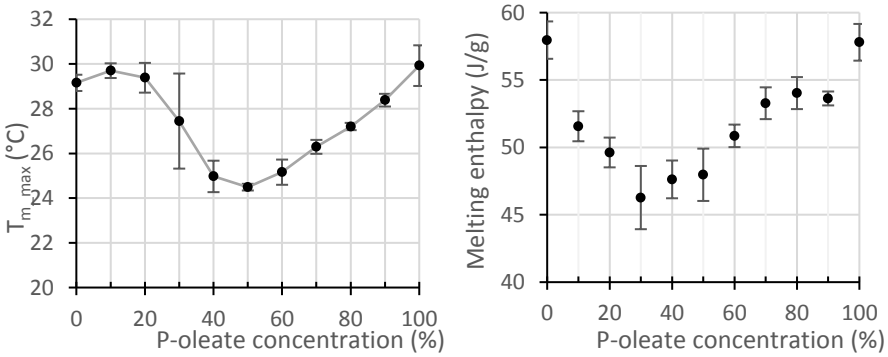

***Figure 7.9**. Peak maximum (T_{m_max}) (left) and melting enthalpy (right) of the DSC melting curves of the blends of PO with P-oleate as a function of the P-oleate concentration. The grey line in the left curve represents the liquidus line of the binary system of PO and P-oleate.*

7.3.4.2. X-ray diffraction

The SAXS (A) and WAXD (B) patterns of the blends of PO with P-oleate after tempering at 10°C for 72h are shown in Figure 7.7. It was clear that at all investigated concentrations PO and P-oleate crystallized separately from each other and no new structures were formed next to the typical PO and P-oleate structures. With an increasing P-oleate concentration the relative peak intensity of the PO peaks decreased while the relative peak intensity of the P-oleate peaks increased as was also observed for the saturated β-sitosteryl esters.

7.3.4.3. Polarized light microscopy

Figure 7.10 shows some images of the microstructure of P-oleate in blends with PO, after tempering for 72h at 10°C. Some characteristics of the images are listed in Table 7.4. In the blend with 10% P-oleate no P-oleate crystals were observed, while in the blend with 20% P-oleate bright, needle-shaped P-oleate crystals with a size of about 16 to 42 µm were observed next to the PO crystals. The largest P-oleate needle-shaped crystals were observed in the blend with 30% P-oleate and had a size of about 23 to 150 µm. From this concentration onwards the P-oleate crystals were grouped together although they did not form spherulites. It is hypothesized that up to and including 90% P-oleate the driving force for spherulitic growth, which is a secondary nucleation process, was probably too small[213]. In the blends with 40% to 90% P-oleate the needle-shaped crystals of P-oleate were smaller with a size of about 7 to 25 µm, which is not much larger than the PO crystals. From 80% P-oleate the PO crystals could not be clearly distinguished in the images anymore. In the blends with 20% to 90% P-oleate the needle-shaped P-oleate crystals were very bright and showed some orange and green colors.

Except for the blends of PO with 20% and 30% P-oleate, the blends of PO with P-oleate did not contain crystals larger than 30 µm and are therefore not expected to cause a sandy mouth feeling during consumption[23].

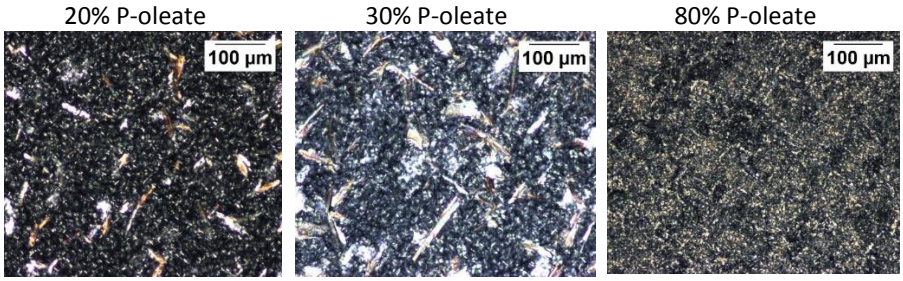

***Figure 7.10**. Polarized light microscopy images of pure P-oleate and of blends of PO with different concentrations of P-oleate. Black bar represents 100 µm.*

7.4. CONCLUSION

When focusing on the pure β-sitosteryl esters in 'equilibrium' several trends were observed concerning the effect of the chain length and the degree of unsaturation of the fatty acid esterified to β-sitosterol on their crystallization and melting behavior. T_{m_max} and ΔH_{melt} of the β-sitosteryl esters increased with an increasing fatty acid chain length, while they decreased with an increasing degree of unsaturation of the fatty acid chain. The XRD data showed that all the β-sitosteryl esters crystallized in a bilayer structure of which the lamellar spacing increased with an increasing fatty acid chain length while it decreased with an increase in the degree of unsaturation of the fatty acid. Furthermore, the WAXD pattern of P-laurate contained much more peaks than that of the other β-sitosteryl esters indicating that the P-laurate molecules were packed into the bilayer structure in a different way than the other β-sitosteryl esters. The microstructure of all the pure β-sitosteryl esters contained spherulites of which the size depended on the fatty acid chain length and degree of unsaturation.

When focusing on the blends of PO with the pure β-sitosteryl esters both the chain length and the degree of unsaturation of the fatty acid in the β-sitosteryl ester had an influence on the crystallization and phase behavior of PO after tempering at 10°C for 72h. Based on the DSC melting curves phase diagrams were constructed for the binary systems of PO with the different types of β-sitosteryl esters. As the melting temperatures of the pure saturated β-sitosteryl esters are much higher (> 35°C) than that of PO, monotectic phase behavior occurred in their binary blends. On the other hand the melting temperature of pure P-oleate was very similar to that of PO leading to eutectic phase behavior of their binary blends.

The XRD analyses demonstrated that in the blends of PO with the different types of β-sitosteryl esters, PO crystallized separately from the β-sitosteryl ester and no new

crystal structures were formed most probably as a result of the large difference in molecular shape between PO and the β-sitosteryl esters.

In the microstructure of the blends both regions with PO crystals and regions with β-sitosteryl ester crystals were observed. The PO crystals were small and needle-shaped, which is typical for the β' polymorphic form, while the β-sitosteryl esters formed large spherulites when they had a saturated fatty acid chain or small, needle-shaped crystals in case of P-oleate. In the blends with P-oleate the driving force for the arrangement of the needle-shaped crystals into spherulites was probably too small.

When applying the blends of PO with the different types of β-sitosteryl esters in food products like for example margarines and spreads a this can result in waxy or greasy mouth feeling when using saturated β-sitosteryl esters because their melting temperature is much higher than body temperature[210]. Blends of PO with saturated β-sitosteryl esters or with 20%-30% P-oleate could also result in a sandy mouth feeling because the β-sitosteryl ester crystals are larger than 30 μm[23].

GENERAL CONCLUSIONS AND PERSPECTIVES FOR FUTURE WORK

Phytosterols are plant based compounds with chemical structures similar to cholesterol. In the last two decades, phytosterols have gained much scientific and commercial interest due to their cholesterol-lowering activity. Phytosterols are esterified with fatty acids to obtain phytosterol esters (PEs) to enhance their solubility in lipid containing food products such as margarines and spreads. In this type of food products, the crystallization and melting behavior of lipids is of extreme importance because the macroscopic properties, such as spreadability, hardness, appearance and mouth feel strongly depend on it. Next to the processing conditions, the composition of the lipid phase is one of the main influencing factors for its crystallization and melting behavior. Therefore, addition of PEs to lipid containing food products may influence their crystallization and melting behavior and may thus lead to problems occurring during the production process or with the macroscopic properties of the end product. Fundamental research on this topic is however very scarce.

In this context, the objective of this PhD research was to gain in-depth knowledge on the effect of PE addition on the crystallization and melting behavior of edible fats, more specifically palm oil (PO). In a first part of this PhD research a commercially available mixture of PEs containing different types of phytosterols, esterified to different types of fatty acids was added to PO to investigate the effect of PE addition on the phase behavior of PO. In a second part pure PEs containing different types of fatty acids were synthesized by enzymatic esterification. This allowed to examine the effect of type of fatty acid on the crystallization and melting behavior of PEs in a more fundamental way. The different types of pure PEs were also added to PO to monitor the effect on the phase behavior in their blends.

In the next sections first the main conclusions about the effects of adding a commercial PE mixture on the non-isothermal (chapter 3), 'equilibrium' (chapter 4) and isothermal (chapter 5) crystallization and melting behavior of PO are summarized and a graphical overview is given in Figure 2. Thereafter results on the crystallization and melting behavior of pure PEs as such (chapter 6) and in blends with PO (chapter 7) are recapitulated and illustrated in Figure 3. Finally, some perspectives for future work are provided.

EFFECT OF ADDING A COMMERCIAL PHYTOSTEROL ESTER MIXTURE ON THE CRYSTALLIZATION AND MELTING OF PALM OIL

In chapter 3 the non-isothermal crystallization and melting behavior of a commercial PE mixture in blends with PO was studied based on differential scanning calorimetry (DSC) and time-resolved synchrotron X-ray diffraction (XRD) measurements. The time-resolved synchrotron XRD results allowed to identify two different crystal structures in the commercial PE mixture. The crystal structure designated PE_x needed a very high degree of supercooling to induce nucleation and was most likely composed of stearic and palmitic acid esterified PEs. The nature of the crystal structure designated PE_y was quite different, since it crystallized without supercooling and was liquid crystalline. PE_y is believed to predominantly contain oleic acid esterified PEs with a high tolerance for molecules of a different chemical nature, such as stearic and palmitic acid esterified PEs. In the PE-PO blends, the PEs and PO crystallized separately from each other and no new crystal structures were formed. Morphology maps were constructed showing the occurrence of the different crystal structures as a function of concentration and temperature. The morphology map of heating which could be considered as a kinetic phase diagram showed a typical eutectic behavior implying that the PEs and PO were immiscible in the solid state. These results enabled research on the impact of adding PEs to PO under industrially more relevant crystallization conditions.

In order to predict whether or not PE addition gives any desired properties to the end product, the aim of chapter 4 was to investigate the effect of PE addition on the crystallization and melting behavior of PO after it attained a kinetically stabilized state denoted as the 'equilibrium' state by tempering at 10°C for 48h. By applying many different experimental techniques including DSC, XRD, pulsed nuclear magnetic resonance, polarized light microscopy (PLM) and texture analyses it was shown that addition of the commercially available PE mixture influenced each structural level of the crystallization of PO being primary crystallization including polymorphism, network formation and textural properties. Just as in chapter 3 the PE-PO binary system in 'equilibrium' showed eutectic behavior. In case of a low PE concentration the commercial PE mixture itself did not crystallize but acted as a liquid oil diluting PO. From a concentration of 40% PEs also PE_x crystals were observed in the blends and from a concentration of 80% PEs also PE_y liquid crystals were formed. In the PE concentration range that is usually applied in industrial applications (up to 40% PEs) the PEs negatively affected the solid fat content (SFC), melting enthalpy, network structure and hardness, the latter being one of the key factors that determine the macroscopic characteristics of the food product. The crystal network structure of PO was lost after PE addition which, together with a decrease of SFC led to the drop in the hardness. When applying this commercial PE

mixture in a product, additional adaptations on the composition level will have to be made in order to compensate for the loss in hardness.

Next to the effects related to the final equilibrated structure, it was also verified whether PE addition influences the crystallization kinetics of PO. Chapter 5 investigated the isothermal crystallization behavior of PO after adding 10-40% of the commercial PE mixture at a temperature of 20°C on the one hand and at a supercooling of 18.7°C on the other hand. The DSC and time-resolved synchrotron XRD results showed that with increasing PE concentrations PO crystallization at an isothermal temperature of 20°C started later and was slower and less crystals were formed. Furthermore, a delay in the polymorphic transition of PO from α to β' was observed. When the blends were isothermally crystallized at a constant supercooling of 18.7°C, to compensate for the difference in melting temperature of the different PE-PO blends, only the delay in polymorphic transition with an increasing PE concentration remained. The solid-solid transition was delayed because the α crystals were physically more isolated from each other at increasing PE concentrations which made it necessary for the transformation to be nucleated in each α crystal aggregate on its own. From a practical point of view, avoiding the strong delaying effects of PEs on the crystallization rate of PE-PO blends could thus be obtained by lowering the crystallization temperature. However, the delay of the polymorphic transition of α to β' which also increases the necessary crystallization time then still remains an issue. Maybe at even lower temperatures and thus larger supercooling, the α crystalline content might increase to the extent that again a percolating network is formed, which could enhance the solid-solid transformation kinetics.

CRYSTALLIZATION AND MELTING BEHAVIOR OF PURE PHYTOSTEROL ESTERS AND THEIR PHASE BEHAVIOR IN BLENDS WITH PALM OIL

In chapter 6 pure PEs containing different types of fatty acids (stearic (C18:0), palmitic (C16:0), lauric (C12:0), oleic (C18:1) and linoleic acid (C18:2)) esterified to β-sitosterol were synthesized by enzymatic esterification to investigate the influence of chain length and degree of unsaturation of the esterified fatty acid on the non-isothermal crystallization and melting behavior of the pure PEs. It was found that the melting temperature and enthalpy of the β-sitosteryl esters increased with an increasing fatty acid chain length while they decreased with an increasing degree of unsaturation. The PLM analyses demonstrated that with an increasing degree of unsaturation the nucleation rate of the β-sitosteryl ester crystals increased, while the crystal growth rate decreased resulting in a decreasing crystal size. Since the fatty acid chain length did not affect the crystal growth rate of the β-sitosteryl esters the increasing nucleation efficiency probably resulted in smaller β-sitosteryl ester

crystals with an increasing fatty acid chain length. The chain length and the degree of unsaturation of the fatty acid did not influence the morphology of the β-sitosteryl ester crystals, since they all formed spherulitic crystals. Based on the synchrotron XRD results it was concluded that the saturated β-sitosteryl esters and P-oleate all formed a bilayer crystal structure of which the lamellar spacing decreased with a decreasing fatty acid chain length and with an increasing degree of unsaturation. The degree of unsaturation of the fatty acid chain in the β-sitosteryl esters also influenced the type of subcell packing of the fatty acid moieties in the bilayer structure and whether or not a metastable or stable mesophase was formed. The pure β-sitosteryl esters in 'equilibrium' as analyzed in chapter 7 generally showed the same trends concerning the effect of chain length and degree of unsaturation of the fatty acid esterified to β-sitosterol on the crystallization and melting behavior of the β-sitosteryl esters as in the non-isothermal experiments described in chapter 6.

By comparing the XRD data of the pure PEs obtained in chapter 6 with those of the commercial PE mixture obtained in chapter 3 it was clear that the XRD spacings of P-stearate and especially those of P-palmitate were very similar to those observed for PEx while the SAXS spacing of the mesophase formed by P-oleate was the same as that of PEy. The hypothesis made in chapter 3 that PEx contained mainly stearic and palmitic acid esterified to the phytosterols while oleic acid esterified PEs were the predominant PEs in PEy was thus confirmed. It is also worth noting that the melting offset temperature of the commercial PE mixture which contained some high-melting PEs such as P-stearate and P-palmitate as observed in chapter 3 was much lower than the melting temperatures of those PEs in their pure form as reported in chapter 6. The commercial PE mixture however only contains a small amount of these high-melting PEs (in total about 10%), and in combination with a high amount of liquid P-linoleate this caused the decrease in the melting temperature.

In chapter 7 the pure PEs were added to PO to monitor the effect on the 'equilibrium' crystallization and melting behavior. As the melting temperatures of the pure saturated β-sitosteryl esters were much higher than that of PO, monotectic phase behavior occurred in their binary blends. On the other hand, the melting temperature of pure P-oleate was very similar to that of PO leading to eutectic phase behavior of their binary blends. The XRD analyses demonstrated that in the blends of PO with the different types of β-sitosteryl esters, PO crystallized separately from the β-sitosteryl ester and no new crystal structures were formed most probably as a result of the large difference in molecular shape between PO and the β-sitosteryl esters. The microstructure of the blends contained both regions with PO crystals and regions with β-sitosteryl ester crystals which were large spherulites in case of the saturated β-sitosteryl esters, but needle-shaped in case of P-oleate. In the blends

with P-oleate the driving force for the arrangement of the needle-shaped crystals into spherulites was probably too small.

When applying the blends of PO with the different types of β-sitosteryl esters in food products like for example margarines and spreads this can result in a waxy or greasy mouth feel when using saturated β-sitosteryl esters because their melting temperature is much higher than body temperature. Blends of PO with saturated β-sitosteryl esters or with 20%-30% P-oleate could also result in a sandy mouth feeling because the β-sitosteryl ester crystals were larger than 30 µm.

When comparing the results of chapters 4 and 7 it is clear that the XRD spacings of P-stearate, P-palmitate and P-oleate in the 'equilibrium state' are all very similar to the XRD spacings of the PE_x crystals of the commercial PE mixture in 'equilibrium'. Although it was hypothesized in chapter 4 that the PE_y form in the 'equilibrium' state consisted of oleic acid esterified PE, the typical SAXS spacing of the PE_y liquid crystal was not detected in the XRD pattern of pure P-oleate in the 'equilibrium' state (chapter 7). In chapter 6 it was proven that P-oleate forms liquid crystals at a low supercooling which convert to true crystals at a high supercooling. When pure P-oleate was cooled to 10°C the degree of supercooling was thus high enough for the formation of true crystals, while this was not the case for the commercial PE mixture as it contains only about 30% P-oleate. Therefore after cooling to 10°C P-oleate in the commercial PE mixture was present in the form of liquid crystals.

Based on the results obtained in chapter 7 suggestions could be made for compositional adaptations of the commercial PE mixture that was used in chapter 4 to avoid loss in hardness when blending with PO. Since after tempering at 10°C for 48h P-oleate formed true crystals according to the XRD data and showed a DSC melting profile and melting enthalpy that was very similar to that of PO, it is hypothesized that PEs with a high oleic acid content may provide hardness in their pure form and when blending with PO. This is in contrast to the commercial PE mixture analyzed after tempering at 10°C for 48h which had a very low melting enthalpy and hardness, despite the high SFC, because P-oleate formed liquid crystals instead of true crystals. Moreover the DSC and PLM results in chapter 7 showed that, unlike the pure saturated PEs, P-oleate may provide hardness without giving a waxy taste due to a too high melting temperature and without leading to a sandy mouth feel because of the formation of too large crystals. However, because of the eutectic phase behavior in the blends some concentrations of P-oleate in PO might be less optimal. For certain concentrations the melting temperature and enthalpy of the blends was lower than that of pure P-oleate and pure PO, which could indicate a loss in the hardness.

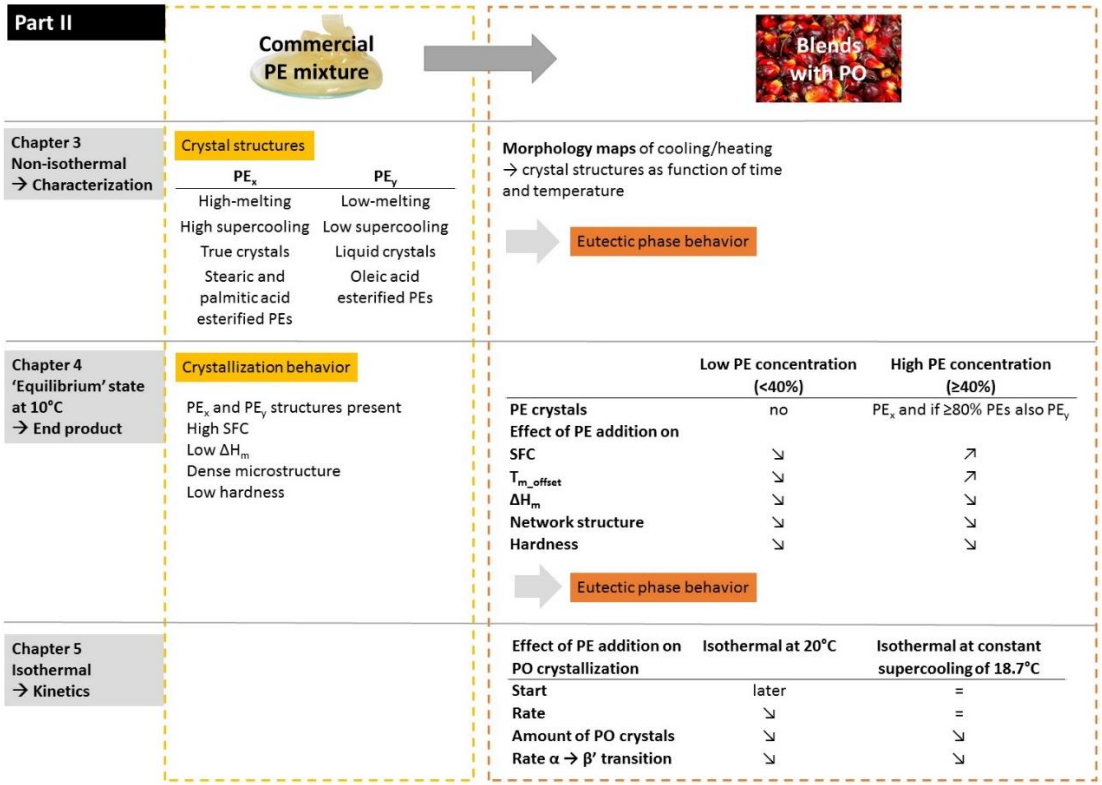

Figure 2. *Graphical overview of the main conclusions of chapter 3, 4 and 5 of this PhD study. Abbreviations PE: phytosterol ester, PO: palm oil, SFC: solid fat content, ΔH_m: melting enthalpy, T_{m_offset}: offset temperature of melting.*

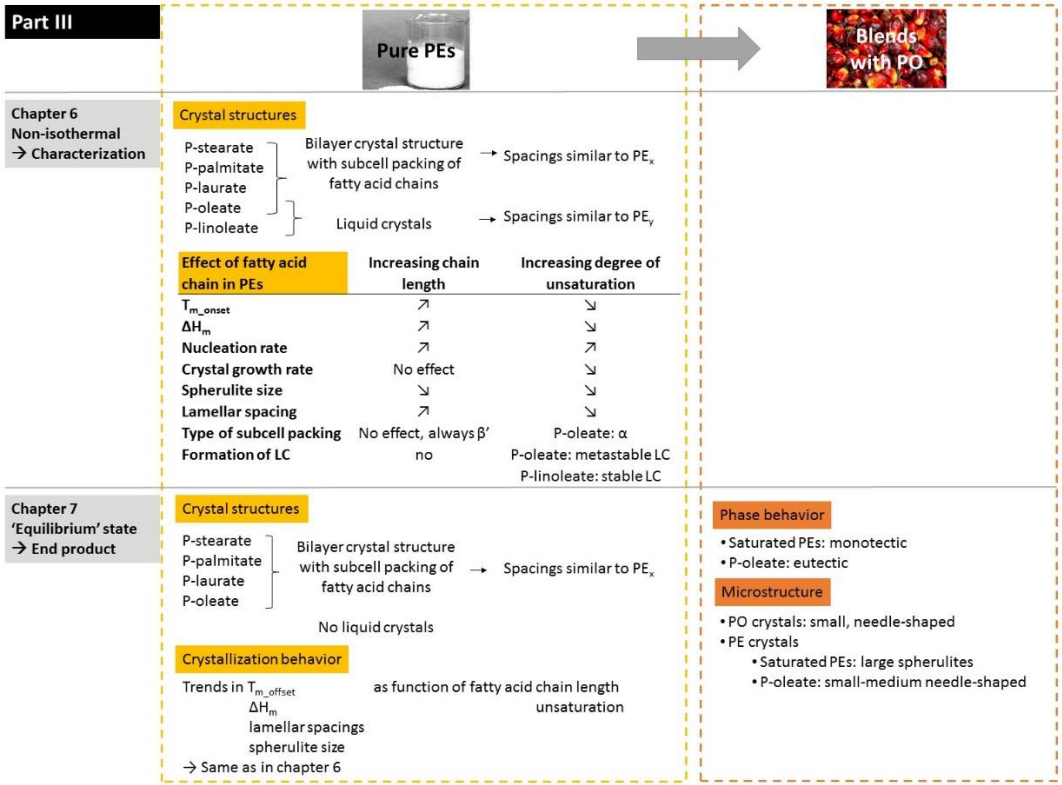

Figure 3. *Graphical overview of the main conclusions of chapter 3, 4 and 5 of this PhD study. Abbreviations PE(s): phytosterol ester(s), PO: palm oil, LC: liquid crystals, ΔH_m: melting enthalpy, T_{m_onset}: onset temperature of melting, T_{m_offset}: offset temperature of melting.*

FUTURE WORK

As this PhD research was only a first study on the effect of adding PEs on the crystallization and melting behavior of lipids many questions still remain unsolved. Based on other studies which showed that plant sterol esters have a significantly lower melting temperature than their analogous plant stanol esters, it is expected that PEs containing different types of plant sterols also have a different melting temperature. It would thus be interesting to find out how PEs are influenced by the phytosterol type regarding their crystallization and melting behavior at different levels of the crystallization hierarchy.

In chapter 7 the phase behavior of PO with different types of pure PEs (P-stearate, P-palmitate, P-laurate and P-oleate) was studied after tempering at 10°C for 48h. It would be interesting to also investigate the phase behavior of binary blends of PO with P-linoleate, which is the main PE of the commercial PE mixture used in part II of this research. As P-linoleate is expected to remain liquid after tempering at 10°C for 48h, it could be examined whether there is a simple dilution effect or interactions occur between PO and the liquid P-linoleate. These results could be compared with the phase behavior of PO when blending with a liquid triglyceride oil like for example rapeseed oil. These results could also lead to further explanations for the phase behavior observed in chapter 4 when blending PO with a commercial PE mixture containing mainly P-linoleate.

Based on the results from chapter 7 it was concluded that P-oleate may provide hardness without giving a waxy taste due to a too high melting temperature and without leading to a sandy mouth feel because of the formation of too large crystals as would be the case with high amounts of saturated PEs. Therefore it would be interesting to examine the SFC and hardness of the blends of PO with P-oleate. As these analyzing techniques require a large amount of sample it would be necessary to synthesize P-oleate on a larger scale by using a commercial fat rich in oleic acid instead of the expensive pure oleic acid. PEs with high contents of oleic acid could be obtained by a trans-esterification reaction with for example olive oil (76.5-82.5%)[214], high-oleic sunflower oil (about 80%), high-oleic soybean oil (about 82-84%) or high-oleic canola oil (about 78-84%)[73]. The crystallization and melting behavior of the synthesized PEs may then differ somewhat from that of the pure P-oleate as reported in chapter 7 due to small differences in the fatty acid profile. For example, because high-oleic sunflower oil contains approximately 10% linoleic acid and 80% oleic acid, the melting temperature and melting enthalpy of the PEs is expected to be slightly lower than that of P-oleate. On the other hand, since the percentage of saturated fatty acids in the fatty acid composition of olive oil is about

13% and of high-oleic soybean oil is about 9%, the melting temperature and enthalpy of PEs synthesized with olive oil or high-oleic soybean oil are expected to be slightly higher than that of the pure P-oleate. On that note it would be interesting to evaluate the crystallization and melting behavior of binary and ternary blends of different types of pure PEs in order to predict the crystallization and melting behavior of the PEs synthesized with commercial fats. To decide which of the commercial fats leads to the most ideal alternative commercial PE mixture it would be necessary to make blends of them with PO to study their phase behavior. Next to PO, other lipids could also serve as 'host' fat for PE addition to examine if the effect on the phase behavior would be different.

In many lipid containing food products such as margarines the lipid phase consists of lipids that are solid in room temperature like for example palm oil or its fractions and lipids that are liquid at room temperature such rapeseed oil. It would therefore be interesting to study the crystallization and melting behavior of ternary blends of PEs, PO and rapeseed oil to analyze the solubilisation behavior.

REFERENCES

(1) Frost & Sullivan. *The United States and European Market Outlook for Phytosterols and Phytostanols. The Next Revolution in the Heart Health Market.*; 2011.

(2) World Health Organisation. Global Health Observatory data: Raised cholesterol. http://www.who.int/gho/ncd/risk_factors/cholesterol_text/en/ (accessed Nov 28, 2017).

(3) Kuksis, A.; Beveridge, J. M. R. Preparation and Certain Physical Properties of Some Plant Steryl Esters. *J. Org. Chem.* **1960**, *25* (7), 1209–1219.

(4) Leeson, P.; Flöter, E. Solidification Behaviour of Binary Sitosteryl Esters Mixtures. *Food Res. Int.* **2002**, *35*, 983–991.

(5) Vu, P.-L.; Shin, J.-A.; Lim, C.-H.; Lee, K.-T. Lipase-Catalyzed Production of Phytosteryl Esters and Their Crystallization Behavior in Corn Oil. *Food Res. Int.* **2004**, *37* (2), 175–180.

(6) Panpipat, W.; Dong, M.; Xu, X.; Guo, Z. Thermal Properties and Nanodispersion Behavior of Synthesized β-Sitosteryl Acyl Esters: A Structure-Activity Relationship Study. *J. Colloid Interface Sci.* **2013**, *407* (2013), 177–186.

(7) Wester, I. Texturizing Compositions for Use in Fat Blends in Food. EP 1 011 343 B1, 1997.

(8) Khare, A. B. Steryl Ester Composition. US 2003/0068425 A1, 2002.

(9) Rodrigues, J. N.; Torres, R. P.; Mancini-Filho, J.; Gioielli, L. A. Physical and Chemical Properties of Milkfat and Phytosterol Esters Blends. *Food Res. Int.* **2007**, *40* (6), 748–755.

(10) Narine, S. S.; Marangoni, A. G. Relating Structure of Fat Crystal Networks to Mechanical Properties: A Review. *Food Res. Int.* **1999**, *32*, 227–248.

(11) Christie, W. W. *Lipid Analysis: Isolation, Separation, Identification and Structural Analysis of Lipids*, 3rd ed.; The Oily Press: Bridgwater, UK, 2003.

(12) Christie, W. W. Lipid Essentials. Structures, Occurrence, Basic Biochemistry and Function http://www.lipidhome.co.uk/lipids/lipids.html (accessed Mar 26, 2018).

(13) Peyronel, F.; Acevedo, N. N.; Marangoni, A. G. Structural and Mechanical Properties of Fats and Their Implications for Food Quality. In *Chemical Deterioration and physical instability of food and beverages*; Skibsted, L. H., Risbo, J., Andersen, M. L., Eds.; Woodhead Publishing, 2010; p 824.

(14) Foubert, I.; Dewettinck, K.; Van de Walle, D.; Dijkstra, A. J.; Quinn, P. J. Physical Properties: Structural and Physical Characteristics. In *The Lipid Handbook*; Gunstone, F. D., Harwood, J. L., Dijkstra, A. J., Eds.; CRC Press: Boca Raton, USA, 2007; pp 471–534.

(15) Patel, A. R.; Dewettinck, K. Current Update on the Influence of Minor Lipid Components , Shear and Presence of Interfaces on Fat Crystallization. *Curr. Opin. Food Sci.* **2015**, *3*, 65–70.

(16) Toro-Vázquez, J. F.; Dibildox-Alvarado, E.; Herrera-Coronado, V.; Charo-Alonso, M. A. Triacylglyceride Crystallization in Vegetable Oils: Application of Models, Measurements and Limitations. In *Crystallization and solidification properties of lipids*; Widlak, N., Hartel, R. W., Narine, S. S., Eds.; AOCS Press: Champaign, USA, 2001; pp 53–78.

(17) Himawan, C.; Starov, V. M.; Stapley, A. G. F. Thermodynamic and Kinetic Aspects of Fat Crystallization. *Adv. Colloid Interface Sci.* **2006**, *122* (1–3), 3–33.

(18) Hartel, R. W. Advances in Food Crystallization. *Annu. Rev. Food Sci. Technol.* **2013**, *4*, 277–292.

(19) Marangoni, A. G.; Acevedo, N.; Maleky, F.; Co, E.; Peyronel, F.; Mazzanti, G.; Quinn, B.; Pink, D. Structure and Functionality of Edible Fats. *Soft Matter* **2012**, *8*, 1275–1300.

(20) Sato, K.; Bayés-García, L.; Calvet, T.; Cuevas-Diarte, M. À.; Ueno, S. External Factors Affecting Polymorphic Crystallization of Lipids. *Eur. J. Lipid Sci. Technol.* **2013**, *115* (11), 1224–1238.

(21) Wu, Z.; Yang, S.; Wu, W. Shape Control of Inorganic Nanoparticles from Solution. *Nanoscale* **2016**, *8*, 1237–1259.

(22) Boistelle, R. Fundamentals of Nucleation and Crystal Growth. In *Crystallization and polymorphism of fats and fatty acids*; Garti, N., Sato, K., Eds.; Marcel Dekker: New York, USA, 1988; pp 189–226.

(23) Ribeiro, A. P. B.; Masuchi, M. H.; Miyasaki, E. K.; Domingues, M. A. F.; Stroppa, V. L. Z.; de Oliveira, G. M.; Kieckbusch, T. G. Crystallization Modifiers in Lipid Systems. *J. Food Sci. Technol.* **2015**, *52* (7), 3925–3946.

(24) Walstra, P.; Kloek, W.; van Vliet, T. Fat Crystal Networks. In *Crystallization Processes in Fats and Lipid Systems*; Garti, N., Sato, K., Eds.; Marcel Dekker: New York, USA, 2001; pp 289–328.

(25) West, A. R. *Solid State Chemistry and Its Applications*, 2nd ed.; Wiley: Chichester, UK, 2014.

(26) Sato, K. Crystallization Behaviour of Fats and Lipids — a Review. *Chem. Eng. Sci.* **2001**, *56* (7), 2255–2265.

(27) Walstra, P. Fat Crystallization. In *Food Structure and Behavior*; Blanshard, V., Lillford, P., Eds.; Academic Press: London, UK, 1987; pp 67–85.

(28) Sato, K.; Ueno, S. Molecular Interactions and Phase Behavior of Polymorphic Fats. In *Crystallization Processes in Fats and Lipid Systems*; Garti, N., Sato, K., Eds.; Marcel Dekker: New York, USA, 2001; pp 177–210.

(29) Timms, R. E. Phase Behaviour of Fats and Their Mixtures. *Prog. Lipid Res.* **1984**, *23* (1), 1–38.

(30) Idziak, S. H. J. Powder X-Ray Diffraction of Triglycerides in the Study of Polymorphism. In *Structure-Function Analysis of Edible Fats*; Marangoni, A. G., Ed.; AOCS Press: Urbana, USA, 2012; pp 79–106.

(31) Vereecken, J.; Meeussen, W.; Foubert, I.; Lesaffer, A.; Wouters, J.; Dewettinck, K. Comparing the Crystallization and Polymorphic Behaviour of Saturated and Unsaturated Monoglycerides. *Food Res. Int.* **2009**, *42* (10), 1415–1425.

(32) Verstringe, S.; Danthine, S.; Blecker, C.; Depypere, F.; Dewettinck, K. Influence of Monopalmitin on the Isothermal Crystallization Mechanism of Palm Oil. *Food Res. Int.* **2013**, *51* (1), 344–353.

(33) Craven, R. J.; Lencki, R. W. Crystallization and Polymorphism of 1 , 3-Acyl-

Palmitoyl- Rac - Glycerols. *J. Am. Oil Chem. Soc.* **2011**, *88*, 1113–1123.

(34) Ginsburg, G. S.; Atkinson, D.; Small, D. M. Physical Properties of Cholesteryl Esters. *Prog. Lipid Res.* **1984**, *23*, 135–167.

(35) Marangoni, A. G.; Narine, S. S. Identifying Key Structural Indicators of Mechanical Strength in Networks of Fat Crystals. **2002**, *35*, 957–969.

(36) Narine, S. S.; Marangoni, A. G. Microscopic and Rheological Studies of Fat Crystal Networks. *J. Cryst. Growth* **1999**, *198–199*, 1315–1319.

(37) Walstra, P. *Physical Chemistry of Foods*; Marcel Dekker: New York, USA, 2003.

(38) Danthine, S. Physicochemical and Structural Properties of Compound Dairy Fat Blends. *Food Res. Int.* **2012**, *48* (1), 187–195.

(39) Kloek, W. Mechanical Properties of Fats in Relation to Their Crystallization, Landbouwuniversiteit Wageningen, 1998.

(40) Zhang, L.; Ueno, S.; Miura, S.; Sato, K. Binary Phase Behavior of 1,3-Dipalmitoyl-2-Oleoyl-Sn-Glycerol and 1,2-Dioleoyl-3-Palmitoyl-Rac-Glycerol. *J. Am. Oil Chem. Soc.* **2007**, *84* (3), 219–227.

(41) Bouzidi, L.; Narine, S. S. Relationships between Molecular Structure and Kinetic and Thermodynamic Controls in Lipid Systems. Part II: Phase Behavior and Transformation Paths of SSS, PSS and PPS Saturated Triacylglycerols - Effect of Chain Length Mismatch. *Chem. Phys. Lipids* **2012**, *165* (1), 77–88.

(42) Dorset, D. L. Cholesteryl Esters of Saturated Fatty Acids: Cosolubility and Fractionation of Binary Mixtures. *J. Lipid Res.* **1987**, *28*, 993–1005.

(43) Kellens, M.; Meeussen, W.; Hammersley, A.; Reynaers, H. Synchrotron Radiation Investigations of the Polymorphic Transitions in Saturated Monoacid Triglycerides. Part 2: Polymorphism Study of a 50:50 Mixture of Tripalmitin and Tristearin during Crystallization and Melting. *Chemistry (Easton).* **1991**, *58*, 145–158.

(44) Takeuchi, M.; Ueno, S.; Flöter, E.; Sato, K. Binary Phase Behavior of 1 , 3-Distearoyl-2-Oleoyl-Sn-Glycerol (SOS) and 1 , 3-Distearoyl-2-Linoleoyl-Sn-Glycerol (SLS). *JAOCS, J. Am. Oil Chem. Soc.* **2002**, *79* (7), 627–632.

(45) Takeuchi, M.; Ueno, S.; Sato, K. Synchrotron Radiation SAXS / WAXS Study of Polymorph-Dependent Phase Behavior of Binary Mixtures of Saturated Monoacid Triacylglycerols. *Cryst. Growth Des.* **2003**, *3* (3), 369–374.

(46) Boodhoo, M. V; Kutek, T.; Filip, V.; Narine, S. S. The Binary Phase Behavior of 1 , 3-Dimyristoyl-2-Stearoyl- Sn -Glycerol and 1 , 2-Dimyristoyl-3-Stearoyl- Sn -Glycerol. **2008**, *154* (2008), 7–18.

(47) Zhang, L.; Ueno, S.; Sato, K.; Adlof, R. O.; List, G. R. Thermal and Structural Properties of Binary Mixtures and 1 , 2-Dioleoyl-3-Stearoyl- Sn -Glycerol (Sn -OOS). *J. Therm. Anal. Calorim.* **2009**, *98*, 105–111.

(48) Minato, A.; Ueno, S.; Smith, K.; Amemiya, Y.; Sato, K. Thermodynamic and Kinetic Study on Phase Behavior of Binary Mixtures of POP and PPO Forming Molecular Compound Systems. *J. Phys. Chem.* **1997**, *101* (18), 3498–3505.

(49) Engström, L. Triglyceride Systems Forming Molecular Compounds. *Eur. J. Lipid Sci. Technol.* **1992**, *94*, 173–181.

(50) Marangoni, A. G.; Lencki, R. W. Ternary Phase Behavior of Milk Fat Fractions. *J. Agric. Food Chem.* **1998**, *46* (10), 3879–3884.

(51) Timms, R. E. The Phase Behaviour and Polymorphism of Milk Fat, Milk Fat Fractions and Fully Hardened Milk Fat. *Leb. - Wiss. u. - Technol.* **1979**, *13*, 61–65.

(52) Lonchampt, P.; Hartel, R. W. Fat Bloom in Chocolate and Compound Coatings. *Eur. J. Lipid Sci. Technol.* **2004**, *106* (4), 241–274.

(53) Danthine, S.; Deroanne, C. Blending of Hydrogenated Low-Erucic Acid Rapeseed Oil, Low-Erucic Acid Rapeseed Oil, and Hydrogenated Palm Oil or Palm Oil in the Preparation of Shortenings. *J. Am. Oil Chem. Soc.* **2003**, *80* (11), 1069–1075.

(54) Kadivar, S.; Clercq, N. De; Mokbul, M.; Dewettinck, K. Food Science and Technology In Fl Uence of Enzymatically Produced Sun Fl Ower Oil Based Cocoa Butter Equivalents on the Phase Behavior of Cocoa Butter and Quality of Dark Chocolate. *LWT - Food Sci. Technol.* **2012**, *66* (2016), 48–55.

(55) Peyronel, F.; Marangoni, A. G. In Search of Confectionary Fat Blends Stable to Heat: Hydrogenated Palm Kernel Oil Stearin with Sorbitan Monostearate. *Food Res. Int.* **2014**, *55*, 93–102.

(56) Rigolle, A.; Van Den Abeele, K.; Foubert, I. Conventional and New Techniques to Monitor Lipid Crystallization: Fundamentals and Applications in Food, Cosmetics, and Pharmaceuticals. In *Crystallization of Lipids.*; Sato, K., Ed.; John Wiley & Sons Ltd, 2018; p 487.

(57) Marangoni, A. G.; Wesdorp, L. H. *Structure and Properties of Fat Crystal Networks*, 2nd ed.; CRC Press: Boca Raton, USA, 2013.

(58) Declerck, A.; Nelis, V.; Rimaux, T.; Dewettinck, K. Influence of Polymorphism on the Solid Fat Content Determined by FID Deconvolution. *Eur. J. Lipid Sci. Technol.* **2018**, *120*, DOI: 10.1002/ejlt.201700339.

(59) AOCS. Official Method Cd 16b-93: Solid Fat Content (SFC) by Low-Resolution Nuclear Magnetic Resonance - The Direct Method. In *Official methods and recommended practices of the American Oil Chemists' Society*; 1997.

(60) AOCS. Official Method Cd 16-81: Solid Fat Content (SFC) by Low-Resolution Nuclear Magnetic Resonance - The Indirect Method. In *Official methods and recommended practices of the American Oil Chemists' Society*; 1997.

(61) Biliaderis, C. G. Differential Scanning Calorimetry in Food Research - a Review. *Food Chem.* **1983**, *10*, 239–265.

(62) Foubert, I.; Vanrolleghem, P. A. Modelling of the Crystallization Kinetics of Fats. **2003**, *14*, 79–92.

(63) Mazzanti, G.; Guthrie, S. E.; Marangoni, A. G.; Idziak, S. H. J. Synchrotron Advances at the Frontiers of Food Physics: Studies of Edible Fats Such As Chocolate Under Shear. *Phys. Canada* **2006**, *5*, 314–320.

(64) De Graef, V.; Goderis, B.; Van Puyvelde, P.; Foubert, I.; Dewettinck, K. Development of a Rheological Method to Characterize Palm Oil Crystallizing under Shear. *Eur. J. Lipid Sci. Technol.* **2008**, *110* (6), 521–529.

(65) Sato, K.; Ueno, S.; Yano, J. Molecular Interactions and Kinetic Properties of Fats. *Prog. Lipid Res.* **1999**, *38*, 91–116.

(66) De Graef, V.; Dewettinck, K.; Verbeken, D.; Foubert, I. Rheological Behavior of Crystallizing Palm Oil. *Eur. J. Lipid Sci. Technol.* **2006**, *108* (10), 864–870.

(67) Brunello, N.; McGauley, S. E.; Marangoni, A. Mechanical Properties of Cocoa Butter in Relation to Its Crystallization Behavior and Microstructure. *LWT* -

Food Sci. Technol. **2003**, *36* (5), 525–532.

(68) Steen, L.; Fraeye, I.; Goemaere, O.; Sifre, L.; Goderis, B.; Paelinck, H.; Foubert, I. Effect of Salt and Liver/Fat Ratio on Microstructure, Emulsion Stability, Texture and Sensory Mouth Feel of Liver Paste. *Food Bioprocess Technol.* **2014**, *7* (10), 2855–2864.

(69) Mba, O. I.; Dumont, M.-J.; Ngadi, M. Palm Oil : Processing , Characterization and Utilization in the Food Industry – A Review. *Food Biosci.* **2015**, *10*, 26–41.

(70) Tan, C. P.; Nehdi, I. A. The Physicochemical Properties of Palm Oil and Its Components. In *Palm oil. Production, processing, characterization and uses*; Lai, O. M., Tan, C. P., Akoh, C. C., Eds.; AOCS Press: Ur, 2012; pp 377–392.

(71) Index Mundi. Palm Oil Production by Country in 1000 MT https://www.indexmundi.com/agriculture/?commodity=palm-oil (accessed Feb 7, 2018).

(72) Pinheiro, A. C.; Block, J. M. Palm and Palm Kernel Oil Production and Processing in Brazil. In *Palm oil. Production, processing, characterization and uses*; Lai, O.-M., Tan, C.-P., Akoh, C. C., Eds.; AOCS Press: Urbana, USA, 2012; pp 251–274.

(73) Gunstone, F. D.; Harwood, J. L. Occurrence and Characterisation of Oils and Fats. In *The Lipid Handbook*; Gunstone, F. D., Harwood, J. L., Eds.; CRC Press: Boca Raton, USA, 2007; pp 37–141.

(74) Omar, Z.; Hishamuddin, E.; Miskandar, M. S.; Hazirah, S.; Lida, N.; Ramli, M. R.; Rashid, N. A. Palm Oil: A Review. *J. Oil Palm Res.* **2015**, *27* (2), 97–106.

(75) Hashim, K.; Tahiruddin, S.; Asis, A. J. Palm and Palm Kernel Oil Production and Processing in Malaysia and Indonesia. In *Palm oil. Production, processing, characterization and uses*; Lai, O.-M., Tan, C.-P., Akoh, C. C., Eds.; AOCS Press: Urbana, USA, 2012; pp 235–250.

(76) Gibon, V. Palm Oil and Palm Kernel Oil Refining and Fractionation Technology. In *Palm oil. Production, processing, characterization and uses*; Lai, O.-M., Tan, C.-P., Akoh, C. C., Eds.; AOCS Press: Urbana, USA, 2012; pp 329–376.

(77) Vis, J. K.; Teoh, C. H.; Chandran, M. R.; Diemer, M.; Lord, S.; McIntosh, I.

Sustainable Development of Palm Oil Industry. In *Palm oil. Production, processing, characterization and uses*; Lai, O.-M., Tan, C.-P., Akoh, C. C., Eds.; 2012; pp 737–784.

(78) Roundtable on Sustainable Palm Oil. Who we are http://www.rspo.org/about/who-we-are (accessed Feb 7, 2018).

(79) Aini, I. N.; Miskandar, M. S. Utilization of Palm Oil and Palm Products in Shortenings and Margarines. *Eur. J. Lipid Sci. Technol.* **2007**, *109*, 422–432.

(80) Man, Y. B. C.; Haryati, T.; Ghazali, H. M.; Asbi, B. A. Composition and Thermal Profile of Crude Palm Oil and Its Products. *J. Am. Oil Chem. Soc.* **1999**, *76* (2), 237–242.

(81) Lida, H. M. D. N.; Sundram, K.; Siew, W. L.; Aminah, A.; Mamot, S. TAG Composition and Solid Fat Content of Palm Oil , Sunflower Oil , and Palm Kernel Olein Blends Before and After Chemical Interesterification. *J. Am. Oil Chem. Soc.* **2002**, *11*, 1137–1144.

(82) Tan, C. P.; Man, Y. B. C. Differential Scanning Calorimetric Analysis of Edible Oils : Comparison of Thermal Properties and Chemical Composition. *J. Am. Oil Chem. Soc.* **2000**, *77*, 143–155.

(83) Keys, A.; Anderson, J. T.; Grande, F. Serum Cholesterol Response to Changes in the Diet I: Iodine Value of Dietary Fat versus 2S-P. *Metab. Clinial Exp.* **1965**, *14* (7), 747–758.

(84) Hoge Gezondheidsraad. Voedingsaanbevelingen Voor België - 2016. *Brussel HGR* **2016**, Advies nr. 9285.

(85) World Health Organisation. Healthy diet http://www.who.int/mediacentre/factsheets/fs394/en/ (accessed Jan 4, 2018).

(86) Mensink, R. P. ERffects of Saturated Fatty Acids on Serum Lipids and Lipoproteins: A Systematic Review and Regression Analysis. *Geneva World Heal. Organ.* **2016**.

(87) Braipson-Danthine, S.; Gibon, V. Comparative Analysis of Triacylglycerol Composition, Melting Properties and Polymorphic Behavior of Palm Oil and Fractions. *Eur. J. Lipid Sci. Technol.* **2007**, *109* (4), 359–372.

(88) Pande, G.; Akoh, C. C.; Lai, O. M. Food Uses of Palm Oil and Its Components. In *Palm oil. Production, processing, characterization and uses*; Lai, O. M., Tan, C. P., Akoh, C. C., Eds.; AOCS Press: Urbana, USA, 2012; pp 561–586.

(89) The Council of the European Union. Council Regulation (EC) No 2991/94 of 5 December 1994 Laying down Standards for Spreadable Fats. *Off. J. Eur. Communities* **1994**, No. December, 36–41.

(90) Miskandar, M. S.; Man, Y. C.; Yusoff, M. S. A.; Rahman, R. A. Quality of Margarine: Fats Selection and Processing Parameters. *Asia Pac. J. Clin. Nutr.* **2005**, *14* (4), 387–395.

(91) Patel, A. R.; Dewettinck, K. Edible Oil Structuring: An Overview and Recent Updates. *Food Funct.* **2016**, *7*, 20–29.

(92) Naik, B.; Kumar, V. Cocoa Butter and Its Alternatives: A Reveiw. *J. Bioresour. Eng. Technol.* **2014**, *1*, 7–17.

(93) Yap, P. H.; DeMan, J. M.; DeMan, L. Polymorphism of Palm Oil and Palm Oil Products. *J. Am. Oil Chem. Soc.* **1989**, *66* (5), 693–697.

(94) Danthine, S.; Lefébure, E.; Trinh, H. N.; Blecker, C. Effect of Palm Oil Enzymatic Interesterification on Physicochemical and Structural Properties of Mixed Fat Blends. *J. Am. Oil Chem. Soc.* **2014**, *91*, 1477–1487.

(95) Chong, C. L.; Kamarudin, Z.; Lesieur, P.; Marangoni, A.; Bourgaux, C.; Ollivon, M. Thermal and Structural Behaviour of Crude Palm Oil: Crystallisation at Very Slow Cooling Rate. *Eur. J. Lipid Sci. Technol.* **2007**, *109* (4), 410–421.

(96) Verstringe, S.; Danthine, S.; Blecker, C.; Dewettinck, K. Influence of a Commercial Monoacylglycerol on the Crystallization Mechanism of Palm Oil as Compared to Its Pure Constituents. *Food Res. Int.* **2014**, *62*, 694–700.

(97) Kawamura, K. The DSC Thermal Analysis of Crystallization Behavior in Palm Oil, II. *J. Am. Oil Chem. Soc.* **1980**, *57*, 48–52.

(98) Rousseau, D.; Marangoni, A. G.; Jeffrey, K. R. The Influence of Chemical Interesterification on the Physicochemical Properties of Complex Fat Systems. 3. Rheology and Fractality of the Crystal Network. *J. Am. Oil Chem. Soc.* **1998**, *75* (11), 1633–1636.

(99) Ng, W. L.; Oh, C. H. A Kinetic Study on Isothermal Crystallization of Palm Oil

by Solid Fat Content Measurement. *J. Am. Oil Chem. Soc.* **1994**, *71* (10), 1135–1139.

(100) Ng, W. L. A Study of the Kinetics of Nucleation in a Palm Oil Melt. *JAOCS, J. Am. Oil Chem. Soc.* **1990**, *67* (11), 879–882.

(101) Tan, C. P.; Man, Y. B. C. Differential Scanning Calorimetric Analysis of Palm Oil , Palm Oil Based Products and Coconut Oil : Effects of Scanning Rate Variation. *Food Chem.* **2002**, No. 76, 89–102.

(102) Chen, C. W.; Lai, O. M.; Ghazali, H. M.; Chong, C. L. Isothermal Crystallization Kinetics of Refined Palm Oil. *J. Am. Oil Chem. Soc.* **2002**, *79* (4), 403–410.

(103) Kawamura, K. The DSC Thermal Analysis of Crystallization Behavior in Palm Oil. *J. Am. Oil Chem. Soc.* **1979**, *56*, 753–758.

(104) Fredrick, E.; Foubert, I.; De Sype, J. Van; Dewettinck, K. Influence of Monoglycerides on the Crystallization Behavior of Palm Oil. *Cryst. Growth Des.* **2008**, *8* (6), 1833–1839.

(105) Danthine, S.; Deroanne, C. Physical and Textural Characteristics of Hydrogenated Low-Erucic Acid Rapeseed Oil and Low-Erucic Acid Rapeseed Oil Blends. *JAOCS, J. Am. Oil Chem. Soc.* **2003**, *80* (2), 109–114.

(106) Braipson-Danthine, S.; Deroanne, C. Determination of Solid Fat Content (SFC) of Binary Fat Blends and Use of These Data to Predict SFC of Selected Ternary Fat Blends Containing Low-Erucic Rapeseed Oil. **2006**, *7*, 571–581.

(107) Bootello, M. A.; Hartel, R. W.; Garcés, R.; Martínez-Force, E.; Salas, J. J. Evaluation of High Oleic-High Stearic Sunflower Hard Stearins for Cocoa Butter Equivalent Formulation. *Food Chem.* **2012**, *134* (3), 1409–1417.

(108) Biswas, N.; Cheow, Y. L.; Tan, C.-P.; Siow, L. F. Blending of Palm Mid‐Fraction, Refined Bleached Deodorized Palm Kernel Oil or Palm Stearin for Cocoa Butter Alternative. *JAOCS, J. Am. Oil Chem. Soc.* **2016**, *93* (2016), 1415–1427.

(109) Piironen, V.; Lindsay, D. G.; Miettinen, T. A.; Toivo, J.; Lampi, A. Review Plant Sterols : Biosynthesis, Biological Function and Their Importance to Human Nutrition. *J. Sci. Food Agric.* **2000**, *80*, 939–966.

(110) Soupas, L.; Huikko, L.; Lampi, A.-M.; Piironen, V. Esterification Affects Phytosterol Oxidation. *Eur. J. Lipid Sci. Technol.* **2005**, *107* (2), 107–118.

(111) Nestel, P.; Cehun, M.; Pomeroy, S.; Abbey, M.; Weldon, G. Cholesterol-Lowering Effects of Plant Sterol Esters and Non-Esterified Stanols in Margarine , Butter and Low-Fat Foods. **1999**, No. 55, 1084–1090.

(112) Rossi, L.; Seijen ten Hoorn, J. W. M.; Melnikov, S. M.; Velikov, K. P. Colloidal Phytosterols: Synthesis, Characterization and Bioaccessibility. *Soft Matter* **2010**, *6* (5), 928.

(113) Wester, I.; Palmu, T.; Miettinen, T.; Gylling, H. Composition Comprising Plant Stanol Esters and the Use Thereof for Lowering the Serum Cholesterol. EP 0871451 B2, 2008.

(114) Weber, N.; Mukherjee, K. D. Plant Sterols and Steryl Esters in Functional Foods and Nutraceuticals. In *Nutraceutical and Specialty Lipids and their Co-Products*; 2006; pp 483–508.

(115) Salo, P.; Wester, I.; Hopia, A. Phytosterols. In *Lipids for Functional Foods and Nutraceuticals*; Gunstone, F. D., Ed.; The Oily Press: Bridgewater, UK, 2003; pp 183–224.

(116) Fernandes, P.; Cabral, J. M. S. Phytosterols: Applications and Recovery Methods. *Bioresour. Technol.* **2007**, *98* (12), 2335–2350.

(117) Marangoni, F.; Poli, A. Phytosterols and Cardiovascular Health. *Pharmacol. Res.* **2010**, *61* (3), 193–199.

(118) Gylling, H.; Plat, J.; Turley, S.; Ginsberg, H. N.; Ellegård, L.; Jessup, W.; Jones, P. J.; Lütjohann, D.; Maerz, W.; Masana, L.; et al. Plant Sterols and Plant Stanols in the Management of Dyslipidaemia and Prevention of Cardiovascular Disease. *Atherosclerosis* **2014**, *232*, 346–360.

(119) Ras, R. T.; Geleijnse, J. M.; Trautwein, E. A. LDL-Cholesterol-Lowering Effect of Plant Sterols and Stanols across Different Dose Ranges: A Meta-Analysis of Randomised Controlled Studies. *Br. J. Nutr.* **2014**, *112*, 214–219.

(120) Sioen, I.; Matthys, C.; Huybrechts, I.; Van Camp, J.; De Henauw, S. Consumption of Plant Sterols in Belgium: Estimated Intakes and Sources of Naturally Occurring Plant Sterols and β-Carotene. *Br. J. Nutr.* **2011**, *105* (6), 960–966.

(121) Naresh Kumar, S.; Balakrishna, a. Seasonal Variations in Fatty Acid Composition of Oil in Developing Coconut. *J. Food Qual.* **2009**, *32* (2), 158–

176.

(122) Yan, F.; Yang, H.; Li, J.; Wang, H. Optimization of Phytosterols Recovery from Soybean Oil Deodorizer Distillate. *J. Am. Oil Chem. Soc.* **2012**, *89*, 1363–1370.

(123) Kumar, M. S. S.; Mawlong, I.; Singh, D. Phytosterol Recovery from Oilseeds: Recent Advances. *J. Food Process Eng.* **2017**, 1–9.

(124) Frost & Sullivan. *Analysis of the Global Phytosterol Market*; 2013.

(125) Index Mundi. Palm oil Monthly Price https://www.indexmundi.com/commodities/?commodity=palm-oil&months=60 (accessed Mar 7, 2018).

(126) Cantrill, R. Phytosterols, phytostanols and their esters www.fao.org/fileadmin/templates/agns/pdf/jecfa/cta/69.

(127) Mäki-Arvela, P.; Martin, G.; Simakova, I.; Tokarev, A.; Wärnå, J.; Hemming, J.; Holmbom, B.; Salmi, T.; Murzin, D. Kinetics, Catalyst Deactivation and Modeling in the Hydrogenation of β-Sitosterol to β-Sitostanol over Microporous and Mesoporous Carbon Supported Pd Catalysts. *Chem. Eng. J.* **2009**, *154*, 45–51.

(128) EFSA Panel on Dietetic Products Nutrition and Allergies. Scientific Opinion on Dietary Reference Values for Fats, Including Saturated Fatty Acids, Polyunsaturated Fatty Acids, Monounsaturated Fatty Acids, Trans Fatty Acids, and Cholesterol. *EFSA Journal*. 2010, pp 1–107.

(129) Yi, J.; Knudse, T. A.; Nielsen, A.-L.; Duelund, L.; Christensen, M.; Hervella, P.; Needham, D.; Mouritsen, O. C. Inhibition of Cholesterol Transport in an Intestine Cell Model by Pine-Derived Phytosterols. *Chem. Phys. Lipids* **2016**.

(130) Ference, B. A.; Ginsberg, H. N.; Graham, I.; Ray, K. K.; Chris, J.; Bruckert, E.; Hegele, R. A.; Krauss, R. M.; Raal, F. J.; Schunkert, H.; et al. Low-Density Lipoproteins Cause Atherosclerotic Cardiovascular Disease . 1 . Evidence from Genetic , Epidemiologic , and Clinical Studies . A Consensus Statement from the European Atherosclerosis Society Consensus Panel. *Eur. Heart J.* **2018**, *38*, 2459–2472.

(131) Sioen, I.; Matthys, C.; Huybrechts, I.; Van Camp, J.; De Henauw, S. Consumption of Plant Sterols in Belgium: Consumption Patterns of Plant Sterol-Enriched Foods in Flanders, Belgium. *Br. J. Nutr.* **2011**, *105* (6), 911–

918.

(132) Brufau, G.; Angel, M.; Rafecas, M. Phytosterols: Physiologic and Metabolic Aspects Related to Cholesterol-Lowering Properties. *Nutr. Res.* **2008**, *28*, 217–225.

(133) Abumweis, S. S.; Marinangeli, C. P. F.; Frohlich, J.; Jones, P. J. H. Implementing Phytosterols Into Medical Practice as a Cholesterol-Lowering Strategy: Overview of Efficacy, Effectiveness, and Safety. *Can. J. Cardiol.* **2014**, *30*, 1225–1232.

(134) Demonty, I.; Ras, R. T.; van der Knaap, H. M. C.; Duchateau, G. S. M. J. E.; Meijer, L.; Zock, P. L.; Geleijnse, J. M.; Trautwein, E. A. Continuous Dose-Response Relationship of the LDL-Cholesterol – Lowering Effect of. *J. Nutr.* **2008**, 271–284.

(135) Katan, M. B.; Grundy, S. M.; Jones, P.; Law, M.; Miettinen, T.; Paoletti, R. Efficacy and Safety of Plant Stanols and Sterols in the Management of Blood Cholesterol Levels. *Mayo Clin. Proc.* **2003**, *78*, 965–978.

(136) Musa-veloso, K.; Poon, T. H.; Elliot, J. A.; Chung, C. Prostaglandins , Leukotrienes and Essential Fatty Acids A Comparison of the LDL-Cholesterol Lowering Efficacy of Plant Stanols and Plant Sterols over a Continuous Dose Range : Results of a Meta-Analysis of. *Prostaglandins Leukot. Essent. Fat. Acids* **2011**, *85*, 9–28.

(137) Law, M. Plant Sterol and Stanol Margarines and Health. *BMJ* **2000**, *320* (March), 861–864.

(138) Talati, R.; Sobieraj, D. M.; Makanji, S. S.; Phung, O. J.; Coleman, C. I. The Comparative Efficacy of Plant Sterols and Stanols on Serum Lipids: A Systematic Review and Meta-Analysis. *J. Am. Diet. Assoc.* **2010**, *110* (5), 719–726.

(139) Han, S.; Jiao, J.; Xu, J.; Zimmermann, D.; Actis-goretta, L.; Guan, L. Effects of Plant Stanol or Sterol- Enriched Diets on Lipid Profiles in Patients Treated with Statins: Systematic Review and Meta- Analysis. *Nat. Publ. Gr. 6*, 1–9.

(140) Harwood, J. L.; Evans, M.; Ramji, D. P.; Murphy, D. J.; Dodds, P. F. Medical and Agricultural Aspects of Lipids. In *The Lipid Handbook*; Gunstone, F. D., Harwood, J. L., Dijkstra, A. J., Eds.; CRC Press: Boca Raton, USA, 2007; pp 703–

783.

(141) Gupta, A. K.; Savopoulos, C. G.; Ahuja, J.; Hatzitolios, A. I. Role of Phytosterols in Lipid-Lowering: Current Perspectives. *QJM Mon. J. Assoc. Physicians* **2011**, *104* (4), 301–308.

(142) Willems, J. I.; Blommaert, M. A. E.; Trautwein, E. A. Results from a Post-Launch Monitoring Survey on Consumer Purchases of Foods with Added Phytosterols in Five European Countries. *FOOD Chem. Toxicol.* **2013**, *62* (2013), 48–53.

(143) Ostlund, R. E. Phytosterols in Human Nutrition. *Annu. Rev. Nutr.* **2002**, *22*, 533–549.

(144) Villeneuve, P.; Turon, F.; Caro, Y.; Escoffier, R.; Baréa, B.; Barouh, B.; Lago, R.; Piombo, G.; Pina, M. Lipase-Catalyzed Synthesis of Canola Phytosterols Oleate Esters as Cholesterol Lowering Agents. *Enzyme Microb. Technol.* **2005**, *37* (1), 150–155.

(145) Panpipat, W.; Xu, X.; Guo, Z. Improved Acylation of Phytosterols Catalyzed by Candida Antarctica Lipase A with Superior Catalytic Activity. *Biochem. Eng. J.* **2013**, *70*, 55–62.

(146) Kim, B. H.; Akoh, C. C. Modeling and Optimization of Lipase-Catalyzed Synthesis of Phytosteryl Esters of Oleic Acid by Response Surface Methodology. *Food Chem.* **2007**, *102* (1), 336–342.

(147) Robles-Manuel, S.; Barrault, J.; Valange, S. Selective Synthesis of Phytosterol Esters from Natural Sterols and Fatty Methyl Esters over Mg-Containing Solid Catalysts. *Comptes Rendus Chim.* **2011**, *14* (7–8), 656–662.

(148) Meng, X.; Pan, Q.; Yang, T. Synthesis of Phytosteryl Esters by Using Alumina-Supported Zinc Oxide (ZnO/Al2O3) from Esterification Production of Phytosterol with Fatty Acid. *J. Am. Oil Chem. Soc.* **2011**, *88* (1), 143–149.

(149) Zheng, M.-M.; Lu, Y.; Dong, L.; Guo, P.-M.; Deng, Q.-C.; Li, W.-L.; Feng, Y.-Q.; Huang, F.-H. Immobilization of Candida Rugosa Lipase on Hydrophobic/strong Cation-Exchange Functional Silica Particles for Biocatalytic Synthesis of Phytosterol Esters. *Bioresour. Technol.* **2012**, *115* (2012), 141–146.

(150) Commission of the European Communities. Commission Decision of 31

March 2004 Authorising the Placing on the Market of Yellow Fat Spreads, Milk Based Fruit Drinks, Yoghurt Type Products and Cheese Type Products with Added Phytosterols/phytostanols as Novel Foods or Novel Food Ingredients under R. *Off. J. Eur. Communities* **2004**, *105*, 49–51.

(151) Commission of the European Communities. Commission Decision of 31 March 2004 Authorising the Placing on the Market of Yellow Fat Spreads, Milk Type Products, Yoghurt Type Products, and Spicy Sauces with Added Phytosterols/phytostanols as Novel Foods or Novel Food Ingredients under Regulation (E. *Off. J. Eur. Communities* **2004**, *105*, 43–45.

(152) Commission of the European Communities. Commission Decision of 31 March 2004 Authorising the Placing on the Market of Yellow Fat Spreads, Salad Dressings, Milk Type Products, Fermented Milk Type Products, Soya Drinks and Cheese Type Products with Added Phytosterols/phytostanols as Novel Foods O. *Off. J. Eur. Communities* **2004**, *105*, 40–42.

(153) Commission of the European Communities. Commission Decision of 10 January 2008 Authorising the Placing on the Market of Rice Drinks with Added Phytosterols/phytostanols as Novel Food under Regulation (EC) No 258/97 of the European Parliament and of the Council. *Off. J. Eur. Communities* **2008**, *8*, 15–17.

(154) Commission of the European Communities. Commission Decision of 24 January 2006 Authorising the Placing on the Market of Rye Bread with Added Phytosterols/phytostanols as Novel Foods or Novel Food Ingredients under Regulation (EC) No 258/97 of the European Parliament and of the Council. *Off. J. Eur. Communities* **2006**, *31*, 21–23.

(155) European Parliament and the Council of the European Union. Regulation (EC) No 258/97 of the European Parliament and of the Council of 27 January 1997 Concerning Novel Foods and Novel Food Ingredients. *Off. J. Eur. Communities* **1997**, *43*, 1–6.

(156) Coppens, P.; da Silva, M. F.; Pettman, S. European Regulations on Nutraceuticals, Dietary Supplements and Functional Foods: A Framework Based on Safety. *Toxicology* **2006**, *221* (1), 59–74.

(157) European Commission. Commission Regulation (EU) No 686/2014 of 20 June 2014 Amending Regulations (EC) No 983/2009 and (EU) No 384/2010 as Regards the Conditions of Use of Certain Health Claims Related to the

Lowering Effect of Plant Sterols and Plant Stanols on Blood LDL-Chol. *Off. J. Eur. Communities* **2014**, *182*, 27–30.

(158) EFSA Panel on Dietetic Products Nutrition and Allergies. Scientific Opinion on the Substantiation of a Health Claim Related to 3 G/day Plant Sterols/stanols and Lowering Blood LDL-Cholesterol and Reduced Risk of (Coronary) Heart Disease pursuant to Article 19 of Regulation (EC) No 1924/2006. *EFSA* **2012**, *10* (5), 2693–2718.

(159) The European Commission. Commission Regulation (EC) No 608/2004 of 31 March 2004 Concerning the Labelling of Foods and Food Ingredients with Added Phytosterols, Phytosterol Esters, Phytostanols And/or Phytostanol Esters. *Off. J. Eur. Communities* **2004**.

(160) Vaikousi, H.; Lazaridou, A.; Biliaderis, C. G.; Zawistowski, J. Phase Transitions, Solubility, and Crystallization Kinetics of Phytosterols and Phytosterol-Oil Blends. *J. Agric. Food Chem.* **2007**, *55* (5), 1790–1798.

(161) Demirbas, A. Comparison of Transesterification Methods for Production of Biodiesel from Vegetable Oils and Fats. *Energy Convers. Manag.* **2007**, *49* (2008), 125–130.

(162) Dierking, I. *Textures of Liquid Crystals*, first edit.; Wiley-VCH: Weinheim, Germany, 2003.

(163) Guo, W.; Hamilton, J. A. Phase Behavior and Crystalline Structures of Cholesteryl Ester Mixtures: A C-13 MASNMR Study. *Biophys. J.* **1995**, *68* (6), 2376–2386.

(164) Knapp, F. F.; Nicholas, H. J. Liquid Crystalline Properties of Ergosteryl Fatty Acid Esters. *Mol. Cryst. Liq. Cryst.* **1970**, *10*, 173–186.

(165) Ryckebosch, E.; Bruneel, C.; Termote-Verhalle, R.; Goiris, K.; Muylaert, K.; Foubert, I. Nutritional Evaluation of Microalgae Oils Rich in Omega-3 Long Chain Polyunsaturated Fatty Acids as an Alternative for Fish Oil. *Food Chem.* **2012**, *160*, 393–400.

(166) Ryckebosch, E.; Muylaert, K.; Foubert, I. Optimization of an Analytical Procedure for Extraction of Lipids from Microalgae. *J. Am. Oil Chem. Soc.* **2012**, *89*, 189–198.

(167) Gommes, C. J.; Goderis, B. CONEX, a Program for Angular Calibration and

Averaging of Two-Dimensional Powder Scattering Patterns. *J. Appl. Crystallogr.* **2010**, *43* (2), 352–355.

(168) Zhou, Y.; Hartel, R. W. Phase Behavior of Model Lipid Systems: Solubility of High-Melting Fats in Low-Melting Fats. *J. Am. Oil Chem. Soc.* **2006**, *83* (6), 505–511.

(169) Sato, K.; Ueno, S.; Yano, J. Molecular Interactions and Kinetic Properties of Fats. *Prog. Lipid Res.* **1999**, *38* (1), 91–116.

(170) Abrahamsson, S.; Dahlen, B.; Löfgren, H.; Pascher, I. Lateral Packing of Hydrocarbon Chains. *Prog. Chem. Fats Other Lipids* **1978**, *16*, 125–143.

(171) Jacobsberg, B.; Ho, O. C. Studies in Palm Oil Crystallization. *J. Am. Oil Chem. Soc.* **1976**, *53*, 609–617.

(172) De Graef, V.; Foubert, I.; Smith, K. W.; Cain, F. W.; Dewettinck, K. Crystallization Behavior and Texture of Trans-Containing and Trans-Free Palm Oil Based Confectionery Fats. *J. Agric. Food Chem.* **2007**, *55* (25), 10258–10265.

(173) Abes, M.; Bouzidi, L.; Narine, S. S. Crystallization and Phase Behavior of 1, 3-Propanediol Esters (SS/MM) Binary Systems. *Chem. Phys. Lipids* **2007**, *150*, 89–108.

(174) Boodhoo, M. V; Bouzidi, L.; Narine, S. S. The Binary Phase Behavior of 1,3-Dipalmitoyl-2-Stearoyl-Sn-Glycerol and 1,2-Dipalmitoyl-3-Stearoyl-Sn-Glycerol. *Chem. Phys. Lipids* **2009**, *160*, 11–32.

(175) Vereecken, J.; Foubert, I.; Meeussen, W.; Lesaffer, A.; Dewettinck, K. Fat Structuring with Partial Acylglycerols: Effect on Solid Fat Profiles. *Eur. J. Lipid Sci. Technol.* **2009**, *111* (3), 259–272.

(176) Toro-Vazquez, J. F.; Briceño-Montelongo, M.; Dibildox-Alvarado, E.; Charó-Alonso, M.; Reyes-Hernández, J. Crystallization Kinetics of Palm Stearin in Blends with Sesame Seed Oil. *J. Am. Oil Chem. Soc.* **2000**, *77* (3), 297–310.

(177) Berghmans, H. Thermal Transitions and Gelation in Polymer Solutions. In *Calorimetry and Thermal Analysis of Polymers*; Mathot, V. B. F., Ed.; Hanser Publishers: Munich, Germany, 1995; pp 207–300.

(178) Hartel, R. W.; Kaylegian, K. E. Advances in Milk Fat Fractionation: Technology

and Applications. In *Crystallization Processes in Fats and Lipid Systems*; Garti, N., Sato, K., Eds.; Marcel Dekker: New York, USA, 2001; pp 381–428.

(179) Zeberg-mikkelsen, C. K.; Stenby, E. H. Predicting the Melting Points and the Enthalpies of Fusion of Saturated Triglycerides by a Group Contribution Method. *Fluid Phase Equilib.* **1999**, *162*, 7–17.

(180) Bouzidi, L.; Narine, S. S. Relationships between Molecular Structure and Kinetic and Thermodynamic Controls in Lipid Systems: Part III. Crystallization and Phase Behavior of 1-Palmitoyl-2,3-Stearoyl-Sn-Glycerol (PSS) and Tristearoylglycerol (SSS) Binary System. *Chem. Phys. Lipids* **2012**, *165* (1), 105–119.

(181) Latip, R. A.; Lee, Y.-Y.; Tang, T.-K.; Phuah, E.-T.; Tan, C.-P.; Lai, O.-M. Physicochemical Properties and Crystallisation Behaviour of Bakery Shortening Produced from Stearin Fraction of Palm-Based Diacyglycerol Blended with Various Vegetable Oils. *Food Chem.* **2013**, *141* (4), 3938–3946.

(182) Xu, Y.; Zhao, X.; Wang, Q.; Peng, Z.; Dong, C. Thermal Profiles, Crystallization Behaviors and Microstructure of Diacylglycerol-Enriched Palm Oil Blends with Diacylglycerol-Enriched Palm Olein. *Food Chem.* **2016**, *202*, 364–372.

(183) AOCS. Official Method Cc 3-25: Softening Point. In *Official methods and recommended practices of the American Oil Chemists' Society*; 1997.

(184) Timms, R. E. Confectionery Fats Handbook. Oily Press 2003, p 454.

(185) Moziar, C.; DeMan, J. M.; DeMan, L. Effect of Tempering on the Physical Properties of Shortening. *Can. Inst. Food Sci. Technol. J.* **1989**, *22* (3), 238–242.

(186) Martini, S.; Herrera, M. L.; Hartel, R. W. Effect of Cooling Rate on Crystallization Behavior of Milk Fat Fraction/sunflower Oil Blends. *J. Am. Oil Chem. Soc.* **2002**, *79* (11), 1055–1062.

(187) Calliauw, G.; Fredrick, E.; Gibon, V.; De Greyt, W.; Wouters, J.; Foubert, I.; Dewettinck, K. On the Fractional Crystallization of Palm Olein : Solid Solutions and Eutectic Solidification. *Food Res. Int.* **2010**, *43*, 972–981.

(188) Rodrigues, J. N.; Torres, R. P.; Mancini-Filho, J.; Gioielli, L. a. Physical and Chemical Properties of Milkfat and Phytosterol Esters Blends. *Food Res. Int.* **2007**, *40* (6), 748–755.

(189) Braipson-Danthine, S.; Deroanne, C. Influence of SFC, Microstructure and Polymorphism on Texture (Hardness) of Binary Blends of Fats Involved in the Preparation of Industrial Shortenings. *Food Res. Int.* **2004**, *37*, 941–948.

(190) Vereecken, J.; Foubert, I.; Smith, K. W.; Dewettinck, K. Relationship between Crystallization Behavior, Microstructure, and Macroscopic Properties in Trans-Containing and Trans-Free Filling Fats and Fillings. *J. Agric. Food Chem.* **2007**, *55* (19), 7793–7801.

(191) Wright, A. J.; Mcgauley, S. E.; Narine, S. S.; Willis, W. M.; Lencki, R. W.; Marangoni, A. G. Solvent Effects on the Crystallization Behavior of Milk Fat Fractions. *J. Agric. Food Chem.* **2000**, *48*, 1033–1040.

(192) Smith, K. W.; Bhaggan, K.; Talbot, G.; Malssen, K. F. Crystallization of Fats: Influence of Minor Components and Additives. *J. Am. Oil Chem. Soc.* **2011**, *88* (8), 1085–1101.

(193) Foubert, I.; Vanrolleghem, P. A.; Dewettinck, K. A Differential Scanning Calorimetry Method to Determine the Isothermal Crystallization Kinetics of Cocoa Butter. **2002**, *400* (2003), 131–142.

(194) Foubert, I.; Fredrick, E.; Vereecken, J.; Sichien, M.; Dewettinck, K. Stop-and-Return DSC Method to Study Fat Crystallization. *Thermochim. Acta* **2008**, *471*, 7–13.

(195) Daels, E.; Foubert, I.; Goderis, B. The Effect of Adding a Commercial Phytosterol Ester Mixture on the Phase Behavior of Palm Oil. *Food Res. Int.* **2017**, *100*, 841–849.

(196) Foubert, I.; Vanrolleghem, P. a; Vanhoutte, B.; Dewettinck, K. Dynamic Mathematical Model of the Crystallization Kinetics of Fats. *Food Res. Int.* **2002**, *35* (10), 945–956.

(197) Kellens, M.; Meeussen, W.; Reynaers, H. Study of the Polymorphism and the Crystallization Kinetics of Tripalmitin: A Microscopic Approach. *JAOCS, J. Am. Oil Chem. Soc.* **1992**, *69* (9), 906–911.

(198) Cabus, S.; Bogaerts, K.; Mechelen, J. Van; Smet, M.; Goderis, B. Monotropic Polymorphism in Ester-Based Phase Change Materials from Fatty Acids and 1 , 4-Butanediol. *Cryst. Growth Des.* **2013**, *13*, 3438–3446.

(199) Mei, Q. S.; Lu, K. Melting and Superheating of Crystalline Solids: From Bulk to

Nanocrystals. *Prog. Mater. Sci.* **2007**, *52*, 1175–1262.

(200) Smith, P. R.; Povey, M. J. W. The Effect of Partial Glycerides on Trilaurin Crystallization. *J. Am. Oil Chem. Soc.* **1997**, *74* (2), 169–171.

(201) Raimo, M. Growth of Spherulites : Foundation of the DSC Analysis of Solidification. *ChemTexts* **2015**, *1* (3), 1–21.

(202) Yun, J. H.; Kuboyama, K.; Chiba, T.; Ougizawa, T. Crystallization Temperature Dependence of Interference Color and Morphology in Poly(trimethylene Terephthalate) Spherulite. *Polymer (Guildf).* **2006**, *47*, 4831–4838.

(203) Christiansen, L. I.; Rantanen, J. T.; Bonsdorff, A. K. Von; Karjalainen, M. A. A Novel Method of Producing a Microcrystalline B -Sitosterol Suspension in Oil. **2002**, *15*, 261–269.

(204) Melnikov, S. M.; Seijen, J. W. M.; Bertrand, B. Can Cholesterol Absorption Be Reduced by Phytosterols and Phytostanols via a Cocrystallization Mechanism? *Chem. Phys. Lipids* **2003**, *127*, 15–33.

(205) Ueno, S.; Nishida, T.; Sato, K. Microstructures and the Polymorphic Transformation of Spherulite Crystals of Trilaurin. *Cryst. Growth Des.* **2008**, *8* (3), 2–5.

(206) Craven, B. B. M.; Detitta, G. T. Cholesteryl Myristate: Structures of the Crystalline Solid and Mesophases. *JCS Perkin II* **1975**, 814–822.

(207) Hosta-Rigau, L.; Zhang, Y.; Boon, T. M.; Postma, A.; Stadler, B. Cholesterol – a Biological Compound as a Building Block in Bionanotechnology. *Nanoscale* **2013**, *5*, 89–109.

(208) Craven, B. M.; Guerina, N. G.; Introduction, I. The Crystal Structure of Cholesteryl Oleate. *Chem. Phys. Lipids* **1979**, *29* (1979), 91–98.

(209) Zhao, J.; Reid, D. S. Thermal Studies on the Crystallization Kinetics of Triglycerides and Milkfat by DSC. *Thermochim. Acta* **1994**, *246*, 405–416.

(210) Karabulut, I.; Turan, S.; Ergin, G. Effects of Chemical Interesterification on Solid Fat Content and Slip Melting Point of Fat/oil Blends. *Eur. Food Res. Technol.* **2004**, *218* (3), 224–229.

(211) Shukat, R.; Bourgaux, C.; Relkin, P. Crystallization Behaviour of Palm Oil

Nanoemulsions Carrying Vitamin E. *J. Therm. Anal. Calorim.* **2012**, *108*, 153–161.

(212) Raimo, M. "' Kinematic '" Analysis of Growth and Coalescence of Spherulites for Predictions on Spherulitic Morphology and on the Crystallization Mechanism. *Prog. Polym. Sci.* **2007**, *32*, 597–622.

(213) Abe, H.; Kikuchi, H.; Kajiyama, T.; Hanabusa, K.; Abe, H.; Kikuchi, H.; Kajiyama, T. Morphological Studies of a (Self-Assembling Oil Gelator/liquid Crystal) Composite System. *Liq. Cryst.* **2002**, *29* (12), 1503–1508.

(214) Aranda, F.; Gomez-Alonso, S.; Rivera del Alamo, R. M.; Salvador, M. D.; Fregapane, G. Food Chemistry Triglyceride , Total and 2-Position Fatty Acid Composition of Cornicabra Virgin Olive Oil : Comparison with Other Spanish Cultivars. *Food Chem.* **2002**, *86*, 485–492.

LIST OF PUBLICATIONS

ARTICLES IN INTERNATIONALLY REVIEWED ACADEMIC JOURNALS

Daels E., Goderis B., Matton V., Foubert I. (2018). Isothermal crystallization kinetics of palm oil as influenced by addition of a commercial phytosterol ester mixture. *Journal of Agricultural and Food Chemistry*, 66 (15), 3910-3921.

Daels E., Goderis B., Steen L., Foubert I. (2018). Influence of adding a commercial phytosterol ester mixture on the 'equilibrium' crystallization behavior of palm oil. *Food Structure*, 17, 1-8.

Daels E., Foubert I., Goderis B. (2017). The effect of adding a commercial phytosterol ester mixture on the phase behavior of palm oil. *Food Research International*, 100, 841-849.

Daels E., Rigolle A., Raes K., De Block J., Foubert I. (2015). Influence of monoglycerides, polyglycerol esters, lecithin and their mixtures on the onset of non-isothermal fat crystallization is concentration dependent. *European Journal of Lipid Science and Technology*, 117 (11), 1745-1753.

Moelants K., Cardinaels R., De Greef K., Daels E., Van Buggenhout S., Van Loey A., Moldenaers P., Hendrickx M. (2014). Effect of calcium ions and pH on the structure and rheology of carrot-derived suspensions. *Food Hydrocolloids*, 36, 382-391.

MEETING ABSTRACTS, PRESENTED AT INTERNATIONAL SCIENTIFIC CONFERENCES AND SYMPOSIA, PUBLISHED OR NOT PUBLISHED IN PROCEEDINGS OR JOURNALS

Daels E., Goderis B., Foubert I. (2018). Addition of phytosterol esters to palm oil influences its ‘equilibrium’ and isothermal crystallization behavior. AOCS Annual Meeting. Minneapolis, Minnesota, 6-9 May 2018 (Oral presentation).

Daels E., Foubert I., Goderis B. (2018). Effect of adding a commercial phytosterol ester mixture on the phase behavior of palm oil. Synew. Ghent, 19-20 March 2018 (Poster presentation).

Daels E., Foubert I., Goderis B. (2017). The effect of adding a commercial phytosterol ester mixture on the phase behavior of palm oil. AOCS Annual Meeting. Orlando, 30 April - 3 May (Oral presentation).

Daels E., Goderis B., Foubert I. (2017). Isothermal crystallization kinetics of palm oil as influenced by addition of a commercial phytosterol ester mixture. Euro Fed Lipid Congress. Uppsala, 27-30 August 2017 (Oral presentation).

Daels E., Goderis B., Foubert I. (2016). Influence of the addition of a commercial phytosterol ester blend on the crystallization behavior of palm oil in the equilibrium state. Euro Fed Lipid Congress. Ghent, 18-21 September 2016 (Oral presentation).

Daels E., Rigolle A., Maertens J., Foubert I. (2014). Influence of monoglycerides, polyglycerol esters, lecithin and their mixtures on non-isothermal bulk fat crystallization. Euro Fed Lipid Congress. Montpellier, 14-17 September 2014 (Oral presentation).